J. Hydrol. Hydromech., 69, 2021, 4, 421–435
DOI: 10.2478/johh-2021-0021
ISSN 1338-4333

sciendo Journal of Hydrology and Hydromechanics

Water's path from moss to soil: A multi-methodological study on water absorption and evaporation of soil-moss combinations

Sonja M. Thielen[1, ∞], Corinna Gall[2, ∞], Martin Ebner[3], Martin Nebel[4], Thomas Scholten[2], Steffen Seitz[2, *]

[1] Invertebrate Palaeontology and Palaeoclimatology, Department of Geosciences, University of Tübingen, Schnarrenbergstr. 94-96, 72076 Tübingen, Germany.
[2] Soil Science and Geomorphology, Department of Geosciences, University of Tübingen, Rümelinstr. 19-23, 72070 Tübingen, Germany.
[3] Biogeology, Department of Geosciences, University of Tübingen, Hölderlinstr. 12, 72074 Tübingen, Germany.
[4] Nees-Institute for Biodiversity of Plants, University of Bonn, Meckenheimer Allee 170, 53115 Bonn, Germany.
[*] Corresponding author. Tel.: +49 (0)7071-29-77523. E-mail: steffen.seitz@uni-tuebingen.de
[∞] These authors contributed equally to this project and are considered co-first authors.

Abstract: Mosses are often overlooked; however, they are important for soil-atmosphere interfaces with regard to water exchange. This study investigated the influence of moss structural traits on maximum water storage capacities (WSC_{max}) and evaporation rates, and species-specific effects on water absorption and evaporation patterns in moss layers, moss-soil-interfaces and soil substrates using biocrust wetness probes. Five moss species typical for Central European temperate forests were selected: field-collected *Brachythecium rutabulum*, *Eurhynchium striatum*, *Oxyrrhynchium hians* and *Plagiomnium undulatum*; and laboratory-cultivated *Amblystegium serpens* and *Oxyrrhynchium hians*.

WSC_{max} ranged from 14.10 g g^{-1} for *Amblystegium serpens* (Lab) to 7.31 g g^{-1} for *Plagiomnium undulatum* when immersed in water, and 11.04 g g^{-1} for *Oxyrrhynchium hians* (Lab) to 7.90 g g^{-1} for *Oxyrrhynchium hians* when sprayed, due to different morphologies depending on the growing location. Structural traits such as high leaf frequencies and small leaf areas increased WSC_{max}. In terms of evaporation, leaf frequency displayed a positive correlation with evaporation, while leaf area index showed a negative correlation. Moisture alterations during watering and desiccation were largely controlled by species/substrate-specific patterns. Generally, moss cover prevented desiccation of soil surfaces and was not a barrier to infiltration. To understand water's path from moss to soil, this study made a first contribution.

Keywords: Biological soil crusts; Bryophytes; Ecohydrology; Moss structure; Moss hydrology; Rainfall interception.

INTRODUCTION

Bryophytes occur in a wide range of ecosystems, from arctic and boreal enviroments to temperate and tropical forests, drylands, and even deserts (Hedenäs, 2007; Lindo and Gonzalez, 2010; Medina et al., 2011). They often form community assemblages with other organisms such as lichens, fungi, algae, cyanobacteria and bacteria, which form what are termed biological soil crusts (biocrusts) (Belnap et al., 2016). With approximately 20000 species, they are the second biggest group of land plants, comprising mosses, liverworts and hornworts (Frey et al., 2009; Söderström et al., 2016). Moss layers fulfill crucial functional roles in a variety of ecosystems regarding water and nutrient fluxes (Bond-Lamberty et al., 2011; Cornelissen et al., 2007; Gundule et al., 2011) as well as soil physical properties (Soudzilovskaia et al., 2013). In contrast to vascular plants, mosses do not actively regulate their water content, but are poikilohydric, meaning their internal water content is in equilibrium with ambient humidity (Green and Lange, 1994). For mosses, water is primarily available via rain, dew and fog (Glime, 2017) and moss moisture is influenced by many factors, depending on the habitat as well as the species itself in regard to structure and life form (Dilks and Proctor, 1979; Oishi, 2018; Proctor, 1982; Proctor, 2000; Proctor and Tuba, 2002), i.e. the form of individual moss shoots growing together, which is considered an ecologically functional unit (Bates, 1998; Mägdefrau, 1982).

Water absorption occurs mainly via the external capillaries (ectohydric), but in some species also via internal (endohydric) movement. While the latter is achieved cell by cell or through special water conducting cells (hydroids), the ectohydric movement of water is through spaces between adjacent shoots, leaves, leaves and stems, leaves and rhizoids and capillary systems such as leaf bases, revoluted leaf margins, grooves or networks of capillary channels determined by papillae (Giordano et al., 1993; Glime, 2017). According to Schofield (1981), capillary spaces are influenced by numerous structural parameters such as leaf shape, leaf arrangement, leaf orientation, detailed leaf anatomy (e.g. surface ornamentation), branch arrangement, nature of cortical cells, and presence of rhizoids or paraphyllia. Nevertheless, there is still limited data on moss structural traits and water relations (Elumeeva et al., 2011). Overall, mosses achieve maximum water storage capacities of 108% to 2070% of their dry weight (Proctor et al., 1998), with some *Sphagnum* species even reaching over 5000% of dry weight (Wang and Bader, 2018).

Many mosses are capable of drying out without dying, which means they can endure losing all free intracellular water and recover their ordinary functions afterwards, such as photosynthesizing and growing when water is available (Proctor et al., 2007). Due to their high surface to volume ratios, rapid drying is generally facilitated (Proctor et al., 2007). Typically, moss cells are either completely turgid or desiccated, with relatively short transitions in between (Proctor et al., 2007). Factors influencing this water loss by evaporation are microclimatic conditions (Proctor, 1990), life form characteristics (Elumeeva et al., 2011; Mägdefrau and Wutz, 1951; Nakatsubo, 1994; Zotz et al., 1997) and canopy structural properties such as surface roughness, shoot density and cushion height (Goetz and Price, 2015; Rice and Schneider, 2004; Rice et al., 2001, 2018).

As an example of cushion life forms, Zotz et al. (2000) and Rice and Schneider (2004) found that evaporation rates decrease with moss cushion size.

For water balance of forest ecosystems, an intact forest floor cover such as leaf litter covers or moss layers play a crucial role (Acharya et al., 2017; Gerrits and Savenije, 2011; Mägdefrau and Wutz, 1951; Sayer, 2006). In mid- and high-latitude coniferous forests, moss layers often form at ground level (Elbert et al., 2012). As forest ecosystems have suffered from drought in recent years (Senf et al., 2020) and mosses are also increasingly threatened by global warming (He et al., 2016), it is particularly important to investigate their hydrological effects in these environments. Previous research by Price et al. (1997) in Canadian boreal forests showed that moss layers could retain 16.8 mm of water, which was approximately 21% of the precipitation input. Furthermore, Carleton and Dunham (2003) found that mosses in a boreal forest could not be fully hydrated by capillary water movement from the forest floor or dewfall, but rather from vapour from the forest floor condensing on the moss surface. Liu and She (2020) investigated a linear decrease of soil evaporation with increasing moss biomass, using moss that was previously cultivated in the laboratory. Overall, the forest floor water balance is influenced by the amounts of throughfall rain, the processes in the moss carpet, and the processes at the moss-soil interface (Price et al., 1997). However, little is known about how much water mosses release into the atmosphere and how much is transported from the soil to the moss and vice versa (Glime, 2017; Voortman et al., 2014). In particular, the influence of different moss species on water movement through moss layers into the soil has been largely disregarded in this context, but has in turn shown great effects on e.g. erosion control (Seitz et al., 2017).

With this study, we aim to shorten this knowledge gap in an interdisciplinary approach (cf. Liu and She (2020)). To do so, we examined water absorption and evaporation patterns in moss-covered soil substrates typical for a Central European temperate forest during and after watering. We hypothesize that:

1. Maximum water storage capacities (WSC_{max}) of mosses are species-specific and positively affected by their surface area.
2. Differences in the temporal dynamics of water content during watering and subsequent desiccation depend largely on the combination of moss species and the underlying soil substrates.

To test our hypotheses, we set up a greenhouse experiment with five moss species and four soil substrates, whereby artificially cultivated mosses of the same species were also included. We used biocrust wetness probes (Weber et al., 2016) for high-resolution monitoring of water content in moss layers, on the soil surface, and in a soil depth of 3 cm. Furthermore, we investigated the selected mosses in terms of their structural traits and their maximum water storage capacities.

METHODS

Moss and soil characteristics

Five moss species native to Southwest Germany (Nebel et al., 2001) differing in origin, classification and growth form were chosen for the study (Table 1). *Oxyrrhynchium hians* (Hedw.) Loeske, *Eurhynchium striatum* (Hedw.) Schimp., *Plagiomnium undulatum* (Hedw.) T.J.Kop. and *Brachythecium rutabulum* (Hedw.) Schimp. were collected in the field at different sites within the Ammer and Neckar valley. Cultures of *Amblystegium serpens* (Hedw.) Schimp. and *Oxyrrhynchium hians* were grown in a hydraulic fluid in an in vitro environment by Hummel InVitro GmbH in Stuttgart, Germany. The latter was selected a second time to study intraspecific differences between field and cultivated mosses. With regard to the position of the sporophytes, all selected mosses were pleurocarpous (side-fruited), except *P. undulatum*, which was acrocarpous (top-fruited).

Soil substrates were chosen according to common growing conditions of selected moss species and sampled from four different sites in the Schönbuch Nature Park in Southwest Germany. Sampling sites were located in the geological series of the Lower Jurassic, with shale clay, interstratified by beds of pyrite and fine grained sandstone, as well as in the Upper Triassic, where claystone with fine lime nodules and fine to coarse grained sandstone is present (Einsele and Agster, 1986). The substrates varied with regard to parent material, soil texture, and pH as well as the C/N ratio (Table 2). They were sampled from the topsoil to a depth of 10 cm and sieved by 6.3 mm. Below, we distinguish the substrates according to their geological formation: Angulatensandstein (AS), Psilonotenton (PT), Löwenstein (LS) and Trossingen (TS) (Einsele and Agster, 1986).

Greenhouse experiment

With a greenhouse experiment, we investigated water absorption patterns in moss covers and corresponding soil substrates during and after watering. To do this, we filled the substrates into infiltration boxes (40 cm × 30 cm × 15 cm) up to a height of 6.5 cm. Infiltration boxes are stainless steel containers with a triangular surface runoff gutter and an outlet on the bottom to capture percolated water. In December 2019, moss species were placed onto substrate-filled infiltration boxes, leading to 6 treatments with 2 replicates each: *P. undulatum* (Field) + PT, *O. hians* (Field) + AS, *O. hians* (Lab) + AS, *B. rutabulum* (Field) + LS, *A. serpens* (Lab) + LS, *E. striatum* + TS; yielding a total number of 12 boxes. Infiltration boxes were subsequently stored in a shady place outdoors for adaptation, until we began the greenhouse experiment in July 2020.

Table 1. Characteristics of studied moss samples.

	Amblystegium serpens	*Brachythecium rutabulum*	*Eurhynchium striatum*	*Oxyrrhynchium hians*	*Oxyrrhynchium hians*	*Plagiomnium undulatum*
Family	Amblystegiaceae	Brachytheciaceae	Brachytheciaceae	Brachytheciaceae	Brachytheciaceae	Mniaceae
Origin	Lab	Field	Field	Field	Lab	Field
Site characteristics	–	ruderalized fertile meadow	pinewood	dry hedge understore	–	flood plain
Growth form	pleurocarpous	pleurocarpous	pleurocarpous	pleurocarpous	pleurocarpous	acrocarpous
Sample site coordinates	–	Tübingen 48.544917 N 9.043309 E	Tübingen 48.546194 N 9.036407 E	Reusten 48.541665 N 8.914316 E	–	Pliezhausen 48.566723 N 9.216494 E

Table 2. Characteristics of studied soil substrates.

	AS	PT	LS	TS
Series	Lower Jurassic	Lower Jurassic	Upper Triassic	Upper Triassic
Formation	Angulatensandstein-Formation (AS)	Psilonotenton-Formation (PT)	Löwenstein-Formation (LS)	Trossingen-Formation (TS)
Parent material	sandstone	shale clay	sandstone	claystone
Soil texture	silt loam • sand: 7.00 % • silt: 67.58 % • clay: 25.68 %	silty clay loam • sand: 6.88 % • silt: 56.28 % • clay: 36.93 %	clay loam • sand: 25.02 % • silt: 42.43 % • clay: 32.60	silty clay loam • sand: 10.78 % • silt: 50.83 % • clay: 38.10 %
C/N	17.54	17.36	23.12	20.05
pH	5.8	7.0	7.0	5.6
Sample site coordinates	Tübingen 48.553054 N 9.119053 E	Tübingen 48.557425 N 9.114462 E	Tübingen 48.557527 N 9.088098 E	Tübingen 48.556036 N 9.089313

To measure water content (WC), we installed three biocrust wetness probes (BWP; UP GmbH, Cottbus, Germany) per infiltration box in different positions: in 3 cm soil depth, in the uppermost 5 mm of the soil surface and in the moss layer (Fig. 1). BWPs were specifically developed to quantify WC of soil surfaces as well as biocrusts by deriving WC from electrical conductivity measurements; they provided reliable data in several experiments under different field conditions (Gypser et al., 2017; Löbs et al., 2020; Tucker et al., 2017; Weber et al., 2016). Samples were irrigated for one hour with a sprayer (Comfort Sensitive Plant, Gardena, Ulm, Germany) with 6 L h^{-1} of water, split into 500 mL every 5 min, corresponding to a precipitation amount of 122 mm (extremely heavy rainfall event). All BWPs were installed underneath the centre of the sprayer, whereby we ensured that the BWP in the moss layer was completely encased by moss shoots. During this watering and subsequent desiccation process in the greenhouse, the electrical conductivity of the samples was logged every 10 seconds for 72 hours with the BWPs connected to a GP2 Data Logger (Delta-T Devices, Cambridge, UK). Additionally, air temperature and relative humidity (RH) in the greenhouse were monitored (Tinytag Plus 2 – TGP-4500, Gemini Data Loggers, Chichester, UK) for the same time slots. Soil WC was determined before and after watering as well as after 71 hours of desiccation applying two methods: first, we substrate inside

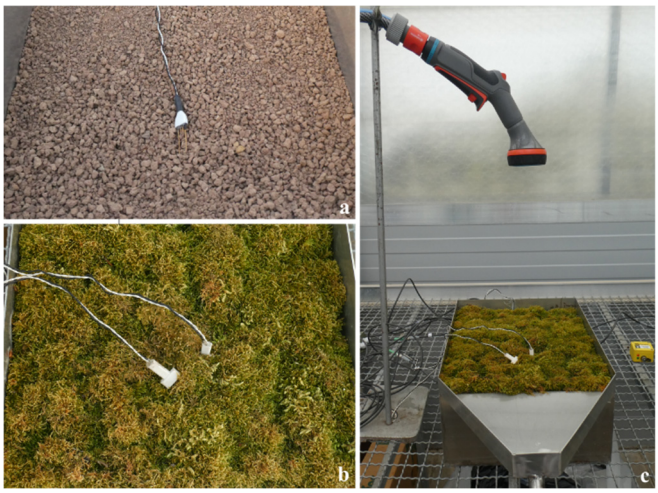

Fig. 1. Overview of the greenhouse experiment setup. a) Biocrust wetness probe (BWP) in 3 cm soil depth, b) BWP in soil surface and moss cover, c) experimental setup with moss-covered soil the infiltration box and sprayer installed at uniform height.

used a gravimetrical approach with a heavy-duty precision balance (KERN FCB 30K1, Kern & Sohn GmbH, Balingen, Germany), and second, we used a Thetaprobe ML2 in combination with a HH2 Moisture Meter (Delta-T Devices, Cambridge, UK).

To consider evaporation effects during the period of desiccation, we calculated the evaporation rate of this time span for all samples using the formula

$$E = \frac{WC_0 - WC_x}{t_x - t_0},$$

where WC_0 is the maximum gravimetric WC in the examined time period, WC_x is the gravimetric WC at time point x, and t_x and t_0 are the respective time points (Robinson et al., 2000).

Laboratory BWP calibration

To calibrate the BWP to gravimetric WC, we monitored weight loss and electrical conductivity (EC) simultaneously for all samples under laboratory conditions for at least 65 hours (average air temperature: 19.1 °C, sd = 1.2 °C; average relative humidity (RH): 45.8%, sd = 5.9%). Samples were water saturated using the immersion technique described below (in the following section). Afterwards, they were placed on a balance (Kern EW 620-3NM, Kern & Sohn GmbH, Balingen, Germany) and three BWPs were installed in each sample. Two samples were measured in parallel, using two precision balances of the same type. BWP and weight data were recorded at an interval of 10 seconds, while temperature and relative humidity were logged in 5 min intervals with Tinytag Plus 2 (see above).

During monitoring of weight loss, the scales generated individual error values, which required a filtering of data. Since the scales only measured stable values, we had irregular time intervals in the recording of weight losses. To be able to combine weight and BWP as well as RH and temperature values, we performed a linear fashion interpolation with both weight values and climate measurements.

As EC is affected by temperature, we conducted a temperature correction and derived the WC for a specific value of the BWP as described in Weber et al. (2016). According to Slatyer (1967), the formula

$$WC = \frac{(WW - DW)}{DW}$$

was used, where WC is the gravimetric WC (g g^{-1}), WW is the wet weight (g) and DW is the dry weight (g) of the soil or moss sample.

The last step of calibration included curve fitting, where we used the mean of the three BWP values and the calculated WC. We found linear relationships which can be characterized as $WC = a \cdot EC_t + b$. For non-linear relationships we used non-linear least-square regressions expressed by the equation $WC = \exp(a \cdot EC_t) \cdot b \cdot EC_t + c$, as recommended in Weber et al. (2016). Furthermore, some relationships could be better described with the equation $WC = \exp(a + b \cdot EC_t)$. While the moss samples could be dried from saturation to desiccation, soil samples did not dry out completely during the laboratory calibration. Therefore, an extrapolation of data for the calibration BWP values was necessary for the soil samples. An overview of all calibration curves is shown in Table S1 in the supporting information.

Maximum water storage capacity

For a detailed characterisation of moss species and adjunct soil substrates with regard to their maximum water storage capacity (WSC_{max}), further laboratory experiments were conducted with samples from the infiltration boxes. Therefore, we detached the mosses from the soil, dried them at 30 °C in a dehydrator (Dörrex 0075.70, Stöckli, Netstal, Switzerland) and weighed the dry samples (Mettler Toledo MS603S, Mettler Toledo, Columbus, USA). Soil samples were taken with 100 cm^3 metal core cutters from every infiltration box, dried at 105 °C in a compartment drier and weighed in dry state. Afterwards both moss species and soil substrates were saturated, using two different methods for the mosses: spray and immersion technique. For the spray technique, we moistened the mosses that had been placed in a petri plate with a spray bottle from above until samples could no longer absorb water. The excess water was removed with a pipette and volume was determined with a 25 mL measuring cylinder. By weighing the spray bottle before and after spraying we estimated the amount of water added to the mosses (in average 3.45 mm). The wet mosses were weighed again with the same balance. In contrast, with the immersion technique we moistened the mosses by submerging them in water for 5 min between two soil sieves with 52 µm mesh size on the bottom and 250 µm on the top, then drained them for 2 min, and then weighed them. We decided to use these two approaches, as we observed that some mosses were still dry on the bottom after a rainfall event, which was also described in Glime (2017). Therefore, we expected different mechanisms of water absorption in the two techniques, with the spray technique probably being more similar to the greenhouse watering process. The soil samples were placed into a tub of water until the surface was wet and afterwards we measured the wet weight. To ensure that the soil substrate remained in the core cutter during rewetting, we attached a thin water permeable fleece to the bottom of the core cutter (Blume et al., 2011).

Moss structural trait measurements

To determine the surface areas of the studied moss species, we measured the following structural traits: leaf area, leaf frequency, shoot length, length of a single component (sum of shoot length and length of attached branches), shoot density (Table 3). We determined the surface areas of the studied species using the following formula, which we adapted for our experiment following Simon (1987), Niinemets and Tobias (2014) and Niinemets and Tobias (2019):

$$A_{bryo} = L\, N_{shoot}\, \frac{A_{leaf}}{1\ cm\ shoot}$$

where A_{bryo} is moss surface area, L is the average length of a shoot with its attached branches, N_{shoot} is mean number of measured shoots, and A_{leaf} is mean leaf area. Leaf area index (LAI) was then calculated with the formula

$$LAI = \frac{A_{bryo}}{sample\ area}$$

In the first step, three circular samples with a diameter of 5.5 cm (sample area) were taken from each species. Moss samples were then dissembled into single moss shoots. Due to the very dense structure and consequent long time duration, only half of the circular area of *A. serpens* was considered. Next, detached shoots were scanned using a high definition flatbed scanner

Table 3. Species-specific average values (± standard error of the mean) of leaf area, leaf frequency, leaf area per shoot length, shoot length, length of a single component (sum of shoot length and length of attached branches), shoot density (shoot number per ground area), total surface area, leaf area index (LAI), moss cushion height, volume and density for the studied moss species.

Species	Leaf area (mm^2)	Leaf frequency (cm^{-1})	Leaf area per shoot length ($cm^2\ cm^{-1}$)	Shoot length (cm)	Length single component (cm)	Shoot density (n cm^{-2})	Total surface area (cm^2)	LAI	Cushion height (cm)	Cushion volume (cm^3)	Cushion density (g cm^{-3})
Amblystegium serpens (Lab)	0.104 ± 0.002	81.778 ± 3.929	0.085 ± 0.006	1.168 ± 0.024	1.764 ± 0.224	97.005 ± 11.786	346.204	14.572	1.322 ± 0.091	107.058 ± 10.623	0.026 ± 0.002
Brachythecium rutabulum	1.151 ± 0.035	39.333 ± 4.93	0.452 ± 0.064	3.791 ± 0.166	8.470 ± 0.286	3.031 ± 0.402	297.076	12.504	1.536 ± 0.116	139.856 ± 19.366	0.018 ± 0.001
Eurhynchium striatum	0.629 ± 0.013	91.333 ± 9.541	0.574 ± 0.06	2.018 ± 0.129	7.756 ± 0.656	2.511 ± 0.496	265.672	11.182	2.119 ± 0.092	182.071 ± 18.683	0.016 ± 0.002
Oxyrrhynchium hians	0.307 ± 0.006	69.889 ± 3.545	0.187 ± 0.008	2.524 ± 0.129	8.124 ± 0.702	4.714 ± 0.712	169.907	7.151	1.65 ± 0.13	132.174 ± 15.278	0.015 ± 0.002
Oxyrrhynchium hians (Lab)	0.393 ± 0.008	55.556 ± 2.911	0.219 ± 0.014	2.180 ± 0.092	6.198 ± 1.480	10.368 ± 2.509	333.764	14.048	1.353 ± 0.136	114.336 ± 18.998	0.022 ± 0.003
Plagiomnium undulatum	4.737 ± 0.129	20.111 ± 2.6	0.953 ± 0.121	3.004 ± 0.129	4.960 ± 0.571	3.087 ± 0.827	346.517	14.585	1.394 ± 0.08	100.778 ± 6.649	0.018 ± 0.001

(Epson Perfection V700 Photo, Suwa, Japan) and shoot numbers of all samples were counted to determine the shoot number per unit sample area. Afterwards, if sample size enabled it, 50 shoots were randomly chosen for length measurements, using ImageJ versions 1.53e and Fiji 2.1.0 (Schindelin et al., 2012; Schneider et al., 2012). Next to shoot length, we also determined the length of branches that were attached to the measured shoots. Then, from each sample three shoots were randomly selected and all leaves were carefully removed along one centimeter of the shoot. The removed leaves were put on slides and were either scanned with the flatbed scanner or a digital microscope (Keyence VHX-7000 with dual zoom lens VH-ZST, Keyence, Osaka, Japan). Leaf area was subsequently measured with ImageJ as well.

Additionally, we determined the volume of the moss cushions for all moss samples used in the WSC_{max} experiment. Therefore, we photographed all moss samples using a Nikon D5100 (Chiyoda, Japan), equipped with an AF-S DX Micro NIKKOR 40mm f/2.8G lens to identify the individual sample area with ImageJ. The height of the moss cushions was measured at four sites with a calliper and mean values were calculated for every cushion. The moss cushion density was derived from the quotient of dry weight and cushion volume.

Data analysis

All analyses were conducted with R software versions 3.6.3 and 4.0.2 (R Core Team, 2021) on the level of individual samples. To examine significant differences, we used one-way ANOVAs in combination with post-hoc Tukey's HSD tests when variables showed homogeneity of variances. In other cases, we performed post-hoc Games-Howell or Wilcoxon signed-rank tests. Previously, homoescedasticity was verified with the Levene's test. To test for differences of the means between two samples we used Welch's t-test. Significance was assessed at $p < 0.05$ in all cases.

Furthermore, we performed pairwise Pearson as well as Spearman's Rank correlation analyses to screen for relationships between WSC_{max} as well as evaporation rates of the studied samples and parameters of sample characteristics. In advance of all analyses, we used the Shapiro-Wilk Test to examine the samples for normal distribution. Additionally, generalized additive models (GAM) with restricted maximum likelihood and smoothing parameters selected by an unbiased risk estimator (UBRE) criterion were performed to assess the effect of soil substrate or moss species characteristics on WSC_{max}. Firstly, we fitted moss WSC_{max} from the spray and immersion techniques against mean shoot number, mean leaf surface area, LAI, moss cushion height as well as moss cushion density. Secondly, WSC_{max} of soil substrates were fitted against soil bulk density, sand, silt and clay contents as well as total carbon and nitrogen content.

RESULTS AND DISCUSSION

In order to discuss and answer the hypotheses presented, we first analyzed the differences in structural traits of the studied moss species and investigated their relationship with WSC_{max}. As we assumed that the temporal progression of WC in the greenhouse experiment could be explained by the structural traits of moss species, we further examined whether our samples showed similar patterns of properties in the different experiments.

Moss structural traits

A wide range of structural trait characteristics for the moss species used in this study were determined to explain moss water relations (Table 3). The average individual leaf area of the studied species ranged almost fivefold from 0.104 mm² in *A. serpens* (Lab) to 4.737 mm² in *P. undulatum*. Accordingly, average leaf area per shoot length varied elevenfold between 0.085 $cm^2\ cm^{-1}$ in *A. serpens* (Lab) to 0.953 in *P. undulatum*. Leaf frequency was the smallest in *P. undulatum* at 20.111 and ranged up to 91.333 in *E. striatum*. We found the longest shoots in *B. rutabulum* (3.79 cm on average) and the shortest shoots in *A. serpens* (Lab) (1.16 cm on average). After adding the length of attached branches to the respective shoot length, *B. rutabulum* still had the longest shoots with 8.47 cm, and *A. serpens* (Lab) had the shortest shoots with 1.764 cm. However, *A. serpens* (Lab) had the highest shoot density (97 shoots per cm^2), whereas *B. rutabulum*, *E. striatum*, *O. hians* and *P. undulatum* had much lower densities between 2.5 to 4.714 shoots per cm^2. Interestingly, shoot density of *O. hians* (Lab) was twice as high as for *O. hians* collected in nature, which might be due to missing competition with other species in a laboratory setting, as well as different light and water regimes, since moss structure is highly affected by water and light availability (Mägdefrau, 1982). This raises the question of whether field-collected *A. serpens* also has similarly high shoot densities as determined for *A. serpens* (Lab) in this study. While *A. serpens* (Lab) grew in dense and more voluminous lawns, *A. serpens* occurs more often intermingled with other species in nature. The nutrient-loving species prefers semi-shady, rather moist sites that are also preferred by many other species that are often more vigorous and thus overgrow the delicate prostrate *A. serpens* (Nebel, 2001). The dense, extensive tall lawns of *A. serpens* (Lab) therefore contradict the species' occurrence in nature and its interspersed growth with other mosses, that can be attributed to the low competitiveness of *A. serpens*.

Compared to the other five studied species, *O. hians* had a low LAI of 7.151. *B. rutabulum* and *E. striatum* were similar in their LAI of 12.504 and 11.182, respectively, and highest LAI values were determined for *A. serpens* (Lab) (14.572), *O. hians* (Lab) (14.048) and *P. undulatum* (14.585). Interestingly, *P. undulatum* and the two lab-grown mosses are very different in terms of leaf area, leaf frequency and shoot density, but all have similar LAI values. Considering the moss cushion density, *A. serpens* (Lab) was significantly denser than *E. striatum* ($p < 0.001$), *O. hians* ($p < 0.001$) and *P. undulatum* ($p < 0.01$). Furthermore, we found significant differences in regard to moss cushion density between *O. hians* (Lab) and *E. striatum* ($p < 0.01$), *O. hians* (Lab) and *O. hians* ($p < 0.05$), *B. rutabulum* and *E. striatum* ($p < 0.05$) and *E. striatum* and *P. undulatum* ($p < 0.05$).

Maximum water storage capacity

Mean values of WSC_{max} from the immersion technique (representing complete soaking) varied between 14.10 $g\ g^{-1}$ for *A. serpens* (Lab) and 7.31 $g\ g^{-1}$ for *P. undulatum*, with the difference being highly significant ($p < 0.001$) (Fig. 2 and Table S2 in the supporting information). Further significant differences were found between *E. striatum* (11.22 $g\ g^{-1}$) and *P. undulatum* as well as between *B. rutabulum* (11.80 $g\ g^{-1}$) and *P. undulatum* ($p < 0.05$). Thus, with regard to the WSC_{max}, there were strong differences between the mosses with different growth forms, but none within the group of pleurocarpous mosses. The fact

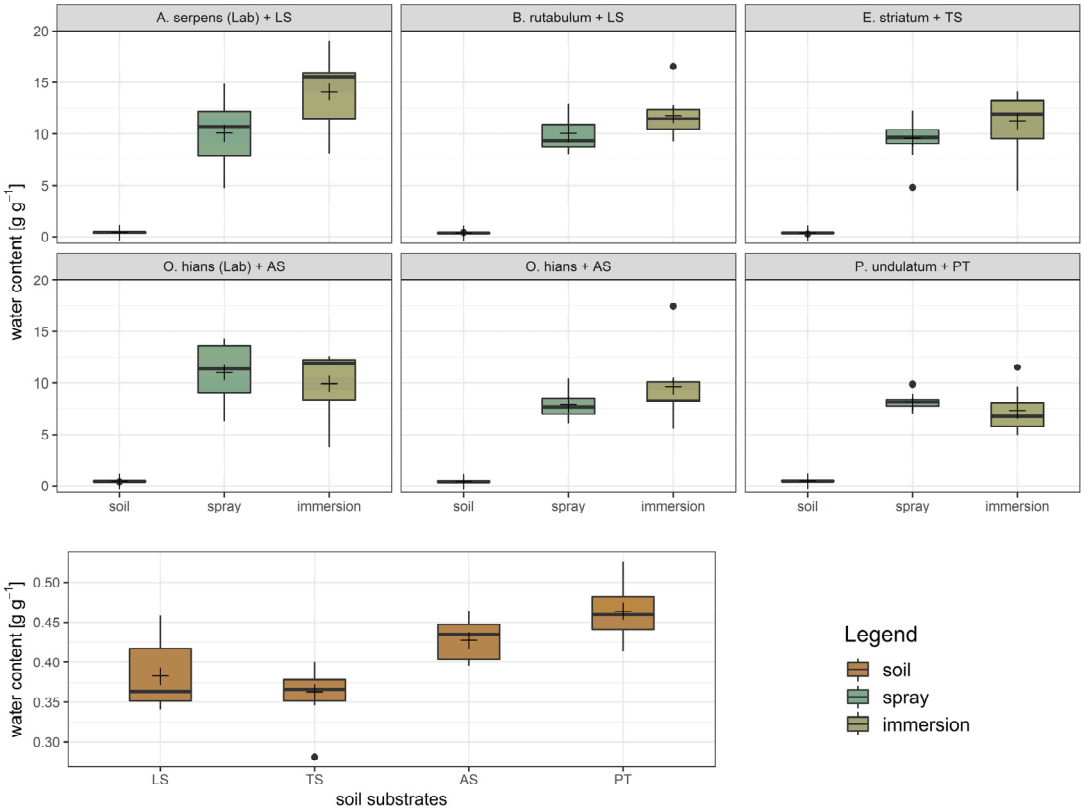

Fig. 2. Maximum water storage capacity (g g^{-1}) of treatments (moss species + soil substrate). For moss species both spray and immersion technique are illustrated. Crosses represent mean values and lines within boxplots median values. The bottom and top of the box represent the first and third quartiles, and whiskers extend up to 1.5 times the interquartile range (IQR) of the data. Outliers are defined as more than 1.5 times the IQR and are displayed as points.

that *P. undulatum* absorbed comparatively less water could be explained by its endohydric water transport, and many acrocarpous mosses are endohydric (Richardson, 1981). Since the surface of endohydric mosses comprises a water-resistant cuticle with often waxy layers (Buch, 1945; Proctor, 1979a; 1979b), water absorption through their leaves is inhibited (Glime, 2017). However, as we only measured one acrocarpous moss, this finding requires further investigation.

Although the most significant difference in WSC_{max} was shown between the visibly densest and loosest growing moss species, this relationship could not be substantiated by the surveyed traits for surface area and cushion characteristics. WSC_{max} was not affected by total surface area or LAI. Furthermore, neither height of the moss cushions, nor volume or density correlated individually with WSC_{max}. The combination of leaf area and leaf frequency seemed to have a higher influence on WSC_{max}: with a small leaf area (Spearman's correlation rho = –0.30, $p < 0.05$) and high leaf frequency (Spearman's correlation rho = 0.32, $p < 0.05$), the WSC_{max} increased. Shoot density might be another influencing factor, but due to small sample size further studies are recommended. In this context, Voortman et al. (2014) also discussed that capillary spaces between moss leaves and branches might be more relevant for water retention than those between moss shoots. For *Sphagnum* species, Bengtsson et al. (2020) also found a high influence of leaf traits on water retention.

Calculated in a GAM explaining 54.1% of the deviance, moss cushion density highly influenced WSC_{max} ($p < 0.001$), while the effects of mean leaf area ($p < 0.01$) and mean shoot density ($p < 0.05$) were smaller, but also significant. Therefore, we assume that additional parameters must be also of great importance to the WSC_{max}. Such parameters are assumed to be, for example, the capillary spaces of mosses, which are very difficult to quantify and are diverse and often complex (Proctor, 1982). According to Proctor (1982), capillary conducting systems such as spaces between overlapping leaves, between shoots, in sheathing leaf bases or amongst rhizoid tomentum and paraphyllia can be 10–100 µm large. In addition, interspaces of a few µm can be found in interstices between papillae as well as in furrows between plicae and ridges on leaves and stems (Proctor, 1982). In this context, the 3D structure of the mosses, e.g. the branching of the shoots, the shape of the leaves and the position of the leaves in relation to the stems, potentially plays an important role for capillarity of bryophytes (Giordano et al., 1993; Schofield, 1981).

In contrast to the immersion technique, the range of mean values of WSC_{max} for the spray technique, which was intended to simulate moistening of mosses by a rainfall event, was considerably smaller (Fig. 2). Here, we found a variation of 11.04 g g^{-1} for *O. hians* (Lab) to 7.90 g g^{-1} for *O. hians* from the field. However, we could not find any significant differences between species or significant correlations between the WSC_{max} and the ascertained individual moss structure parameters, and the adjunct GAM could explain 46.5% of the deviations. The greatest influence was due to moss height ($p < 0.01$), with LAI having a smaller effect ($p < 0.05$). Interestingly, the greatest difference in WSC_{max} was discovered within the same species, *O. hians*. Although they belong to the same species, *O. hians* collected in the field and *O. hians* grown in the laboratory displayed strong differences in structure. While *O. hians* grows as loose lawn in the field, the laboratory variety forms very dense moss cushions, which is also reflected in the higher shoot density

(*O. hians*: 4.714 shoots per cm^2 and *O. hians* (Lab): 10.368 shoots per cm^2), and the larger total surface area (*O. hians*: 169.907 cm^2 and *O. hians* (Lab): 333.764 cm^2). This finding indicates that the WSC_{max} of mosses is dependent on life form. In a further chain of thought, this also implies that single species can obtain more advantageous properties through laboratory cultivation, e.g. for erosion control.

Overall, we suppose that for both the immersion technique and the spray technique, the capillary spaces between moss shoots as well as between leaves and shoots are more important for WSC_{max} than surface parameters such as LAI or total surface area. Finally, it can be concluded that a further development and standardization of the spray technique is required to be able to gather more reliable data on this important moss characteristic.

Regarding the soil substrates, WSC_{max} values varied on average between 0.46 g g^{-1} for PT and 0.36 g g^{-1} for TS, which is 30 times less compared to the WSC_{max} of the mosses (Fig. 3). Within soil substrates we found highly significant differences between PT and TS, PT and LS as well as AS and TS ($p < 0.001$) and a significant difference between AS and TS ($p < 0.05$). On one hand, these differences can be explained by soil texture, as there is a negative relationship with sand content (Spearman's correlation rho = –0.62, $p < 0.001$) and a positive correlation with silt content (Spearman's correlation rho = 0.52, $p < 0.001$), while the clay content seemed to be of rather minor importance for WSC_{max} (Spearman's correlation rho = –0.40, $p < 0.01$). On the other hand, we revealed a negative correlation with bulk density (Pearson's correlation r = –0.70, $t_{39} = –5.94$, $p < 0.001$) and C/N ratio (Spearman's correlation rho = –0.62, $p < 0.001$). Additionally, we tested for a joint impact on soil WSC_{max} using a GAM with soil bulk density, sand, silt and clay contents as well as total carbon and nitrogen content as fixed effects and were able to explain 84.7% of the deviance with this model. The results also showed a high relevance of bulk soil density as well as total carbon content ($p < 0.001$), which is consistent with the results of the individually tested correlations and an influence of the clay content ($p < 0.01$). These relationships are also reported in other studies (Gong et al., 2003; Franzluebbers, 2002; Novák and Hlaváčiková, 2019; Rawls et al., 2003).

Greenhouse experiment

Watering process

Focusing on the 60 minutes of watering, we observed clear differences in WC of different moss species, regarding temporal progression as well as the level of WC achieved (Fig. 3). At the beginning of the watering, all moss species were desiccated, so that the WC initially increased until an equilibrium was reached. Moss species were classified in terms of WC in equilibrium: (a) low WC (0–5 g g^{-1}) for *A. serpens* (Lab) and *P. undulatum*, (b) medium WC (5–10 g g^{-1}) for *B. rutabulum*, *O. hians* and *O. hians* (Lab), (c) high WC (10–15 g g^{-1}) for *E. striatum*. This classification shows the possibility of distinguishing between moss species based on the BWP response.

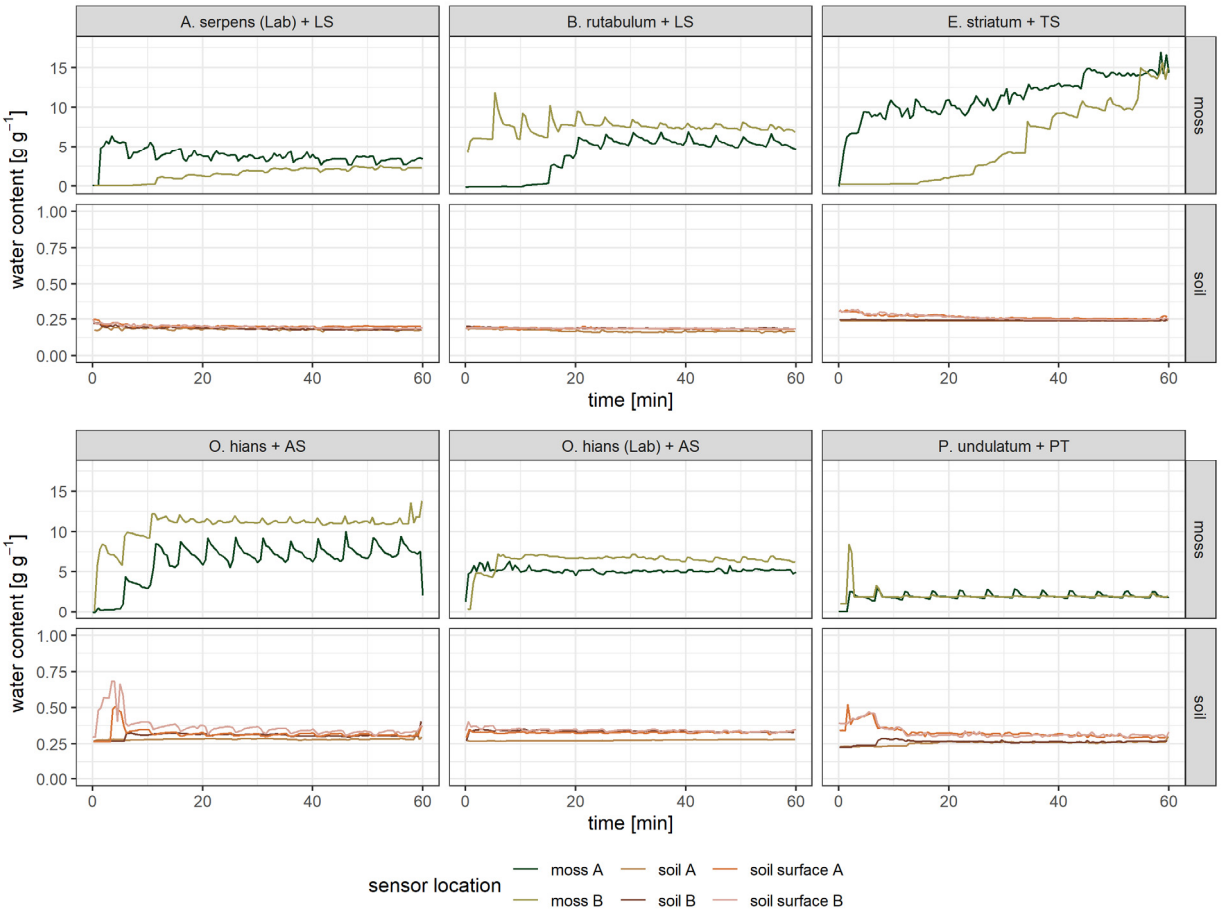

Fig. 3. Temporal progression of water content values (g g^{-1}) of treatments during watering in the greenhouse experiment. Replicate measurements are labelled with A and B for every biocrust wetness probe (BWP) location (moss cover, soil surface, 3 cm soil depth). Plotted are half-minute values.

Surprisingly, *A. serpens* (Lab) and *P. undulatum* both reached a low WC during irrigation, although they are quite different regarding their structural traits. While *A. serpens* (Lab) forms very dense moss cushions (shoot density: 97.005 ± 11.786 shoots per cm^2), *P. undulatum* is more likely to grow single shoots (shoot density: 3.087 ± 0.827 shoots per cm^2). Although *O. hians* and *O. hians* (Lab) were both assigned to medium WC, we recognized a distinct difference, with *O. hians* tending to weigh 10 g g^{-1} and *O. hians* (Lab) tending to weigh 5 g g^{-1}. Since *O. hians* (Lab) grows considerably denser than *O. hians* with a shoot density twice as high (*O. hians* (Lab) = 10.368 ± 2.509 shoots per cm^2, *O. hians* = 4.714 ± 0.712 shoots per cm^2) and a higher cushion density (*O. hians* (Lab) = 0.022 ± 0.003 shoots per cm^2, *O. hians* = 0.015 ± 0.002 shoots per cm^2), we expected that *O. hians* (Lab) would also absorb more water during watering. The fact that this expectation was not fulfilled could be attributed to *O. hians* having a comparatively high leaf frequency with small leaf area, which had already been highlighted as important factors for water absorption in previous chapters.

Furthermore, almost all moss species showed a certain variation in WC at equilibrium within replicate measurements, illustrating a great heterogeneity within species. Overall, we noticed that the variations between replicate measurements were smaller for denser moss cushions than for looser ones, with *P. undulatum* being an exception in this case. This could be attributed to the fact that denser mosses establish better contact with the sensor without forming air spaces (Löbs et al., 2020).

Some moss species demonstrated a more pronounced response to the watering pulses than others. This might also be related to denser moss cushions with less air-filled interstitial spaces (Löbs et al., 2020), as it was the case for *A. serpens* (Lab) and *O. hians* (Lab), which both form the densest cushions. To examine moss intraspecific differences regarding water absorption in detail, higher replication is necessary in future studies.

Because of the water volume applied to the samples in the greenhouse, we speculated that the moss species would reach their WSC_{max} within the watering time in the greenhouse, especially when compared with the achieved WSC_{max} using the spray technique. To go into more detail, we compared the WC values directly after watering (means of WC for all values between 60^{th} and 65^{th} minute) with the WSC_{max} determined in the lab. For most of the species the WC after watering was considerably lower than the WSC_{max}, for both spray and immersion technique. As an example, the maximum WC for *A. serpens* using the immersion technique was 5 times higher than the WC after watering (WSC_{max} (immersion) = 14.10 g g^{-1}, SE = 1.28, WC after watering = 2.63 g g^{-1}, SE = 0.02), while the spray technique showed almost a fourfold difference (WSC_{max} (spray) = 10.10 g g^{-1}, SE = 1.25). Additionally, we found an almost fivefold difference from the immersion technique, respective fourfold difference from the spray technique, and higher WSC_{max} compared to the WC after watering in *P. undulatum* (WSC_{max} (immersion) = 7.31 g g^{-1}, SE = 0.80, WSC_{max} (spray) = 8.15 g g^{-1}, SE = 0.32, WC after watering = 1.76 g g^{-1}, SE = 0.01). Based on these results, no clear patterns are discernible that would explain the different intraspecific mechanisms of water absorption comparing greenhouse and laboratory experiments. Above all, it was very surprising that especially the denser mosses, most notably the lab-grown mosses, did not absorb much water during the greenhouse experiment. In general, we can deduce that the mosses are not a barrier to infiltration in case of high precipitation rates, as also reported in Li et al. (2016). A new observation of our study is that the mosses growing on the soil do not store much of the applied water themselves, but pass it on to the soil.

Compared to the mosses, the soil substrates showed a much lower WC during the 60 minutes of watering, which is true for both the surface and 3 cm soil depth (Fig. 3). Overall, mosses adjusted their equilibrium in the range between 2.5–15.0 g g^{-1} of WC, while soil substrates varied between 0.15–0.35 g g^{-1}. The fact that mosses can absorb more water than soil substrates could be attributed to a larger surface area of mosses. Additionally, capillary effects in mosses might contribute to higher water absorption rates compared to soil substrates.

Since the soil surfaces were not completely dried out at the beginning of the experiment, they showed a relatively high starting value of WC in comparison with the later reached equilibrium. The temporal progression of WC on the soil surface started with higher values at the beginning of watering and slightly decreased over time. Regarding infiltration into the soil surface, it appeared that water had initially accumulated on the surface, causing the high WC.

When considering WC at 3 cm soil depth, temporal progression of WC was almost steady, which was also due to the already wet soil substrate at the beginning of the experiment. For two substrates (AS and PT) we observed an increase of WC during the first 10 minutes of irrigation, indicating percolation of water through the substrate. Additionally, WC tended to be lower at 3 cm soil depth than on the soil surface during irrigation. Overall, with respect to the temporal progression of WC values on soil surface and in 3 cm soil depth, we generally found substrate-specific coherences regarding the level of WC achieved.

Furthermore, we expected that the soil substrates show a similar response due to WSC_{max} in the lab and in the greenhouse experiment. However, the WC after watering in the greenhouse, which we expected to be the maximum WC reached in the greenhouse (means of WC for all values between 60^{th} and 65^{th} minute), were lower than the WSC_{max} measured in the lab, which was true for every substrate both for surface as well as in 3 cm soil depth. For example, PT achieved a WSC_{max} of 0.46 g g^{-1} and only showed a WC of 0.31 g g^{-1} on the surface and 0.27 g g^{-1} in the soil after one hour of watering in the greenhouse, which means a deviance of 32.61%. In comparison, LS reached only 50% of the WSC_{max} under *A. serpens* (Lab) (WC after watering = 0.19 g g^{-1}, WSC_{max} = 0.46 g g^{-1}) and 52% under *B. rutabulum* on the surface (WC after watering = 0.18 g g^{-1}), WC values in 3 cm soil depth were even lower (WC after watering (*A. serpens* (Lab)) = 0.18 g g^{-1}; WC after watering (*B. rutabulum*) = 0.17 g g^{-1}). Altogether, soil substrates did not show the same patterns of water absorption in the lab as in the greenhouse.

Desiccation process

During the subsequent desiccation process of 71 hours, moisture in the moss layers generally decreased, while moisture at the soil substrate surface as well as in 3 cm soil substrate depth remained at the same levels (Fig. 4). However, moss species differed in maximum WC, evaporation rates and their responses to climatic changes in the greenhouse. Sample replicates slightly differed from each other in regard to WC values, but generally showed comparable patterns. We observed the highest WC values directly after watering in *E. striatum* with a mean WC of almost 15 g g^{-1}, while mean WC of *B. rutabulum*, *O. hians* and *O. hians* (Lab) ranged between 5–10 g g^{-1}, and mean WC of *A. serpens* (Lab) and *P. undulatum* did not exceed 5 g g^{-1}. The low WC of *P. undulatum* might be related to its delicate and loose structure with a low leaf frequency and large leaf areas, and leaves that stand off the shoot. Especially

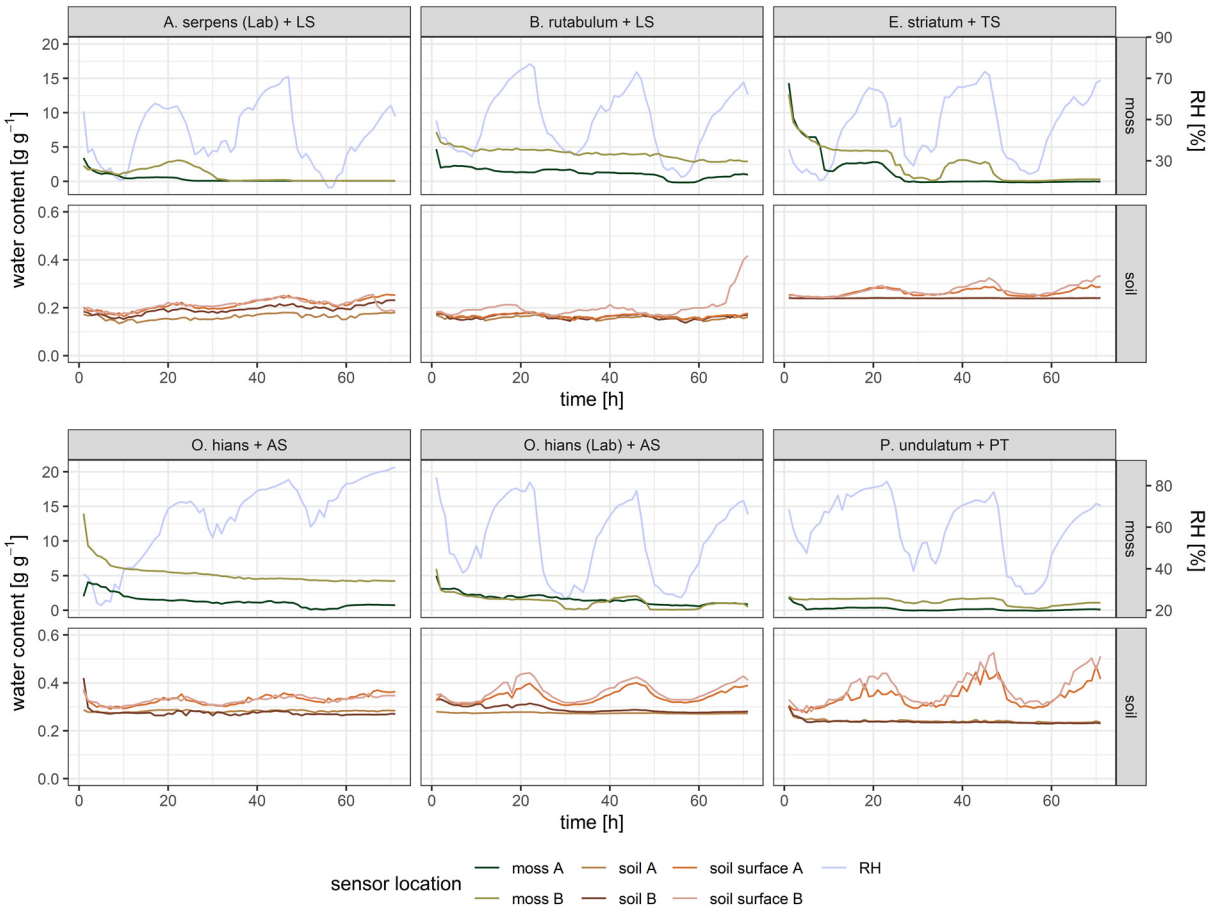

Fig. 4. Temporal progression of water content values (g g^{-1}) of treatments during 71 h of desiccation in the greenhouse experiment. Replicate measurements are labelled with A and B for every biocrust wetness probe (BWP) location (moss cover, soil surface, 3 cm soil depth). Mean temperature and mean relative humidity ± standard deviation: *Amblystegium serpens* (Lab) + Löwenstein-Formation (LS) 25.93 ± 6.13 °C, 42.67 ± 14.39%; *Brachythecium rutabulum* + Löwenstein-Formation (LS) 26.35 ± 5.38 °C, 49.45 ± 15.22%; *Eurhynchium striatum* + Trossingen-Formation (TS) 24.70 ± 5.78 °C, 46.31 ± 16.15%; *Oxyrrhynchium hians* + Angulatensandstein-Formation (AS) 20.30 ± 3.89 °C, 64.72 ± 18.45%; *Oxyrrhynchium hians* (Lab) + Angulatensandstein-Formation (AS) 23.10 ± 6.07 °C, 53.37 ± 18.38%; *Plagiomnium undulatum* + Psilonotenton-Formation (PT) 20.96 ± 4.31 °C, 59.92 ± 15.35%. Plotted are hourly values.

compared to a branched structure with high leaf frequencies and densely attached leaves, few capillary spaces for water storage are formed in *P. undulatum* (Mägdefrau and Wutz, 1951). Furthermore, leaf surfaces of mosses from the Mniaceae family often have a water-resistant cuticle, reducing their ability to absorb water via the leaves (Glime, 2017; Proctor, 2000). Additionally, we observed that leaves and stems of *P. undulatum* were twisting and curling during the desiccation process, which might result in altered measurement conditions for the sensor. Clipping the sensor to moss stems of such species as *P. undulatum*, as proposed in Leo et al. (2019), would be interesting to compare with BWP response in future studies. Nevertheless, the BWP used in this study proved to be successful in all moss species, as also confirmed in Löbs et al. (2020).

A. serpens (Lab) had dried out after 30 hours, whereas the other species generally remained moist longer than 40 hours, and did not desiccate completely during the measurement. A more stabilized, steady evaporation was observed in *B. rutabulum*, *O. hians*, *O. hians* (Lab) and *P. undulatum*. Evaporation rates calculated for the measurement period corresponded to maximum WC: *E. striatum* with the highest maximum WC after watering also had the highest evaporation rates (0.181–0.197 g h^{-1}). Evaporation rates for *P. undulatum* were considerably smaller (0.023 and 0.012 g h^{-1}). A group with slightly higher evaporation rates consisted of *A. serpens* (Lab) (0.056 and 0.03 g h^{-1}), *B. rutabulum* (0.046 and 0.055 g h^{-1}), *O. hians* (Lab) (0.057 and 0.078 g h^{-1}) and *O. hians* (0.06 and 0.093 g h^{-1}). We found a positive relationship between leaf frequency and evaporation rate (Spearman's correlation rho = 0.832, $P < 0.001$). LAI, however, correlated negatively with evaporation rate (Spearman's correlation rho = –0.78, $P < 0.001$); this was congruent with our expectations of lower evaporation rates for moss species with a high LAI, which, as a product of different structural traits, makes the formation of a multitude of capillary spaces for water storage in different hierarchical levels (leaf, shoot, and colony) more likely, overall resulting in wetter moss cushions and lower evaporation rates, as also described in Elumeeva et al. (2011).

WC in moss species showed diel fluctuations, albeit to different degrees. Desiccation periods clearly aligned with declining RH and rising temperatures in *E. striatum*, *O. hians* (Lab), and to a smaller degree in *P. undulatum*, *A. serpens* (Lab), *B. rutabulum* and *O. hians*. Comparably high RH and low temperatures contributed to the quite stable WC of *O. hians* throughout the measurement and to the fact that the moss did not dry completely. We observed slight reactions of WC towards RH changes in all samples, confirming that mosses

reacted to increasing RH and could absorb water under conditions with high RH, as also described in Löbs et al. (2020).

Climatic conditions cannot explain intraspecific variation of WC, since the replicates were measured in parallel at the same time. A possible explanation could be that moss structure at the sensor locations differed in regard to surface roughness, altering boundary layer resistance and thus resulting in different evaporation velocities (Proctor, 1982). Further experiments in a climate-controlled environment with closer control and manipulation possibilities could determine if moss reactions are species-specific.

The different soil substrates had slightly different mean WC values in 3 cm depth: LS 0.16–0.18 g g^{-1}, TS 0.24 g g^{-1}, AS 0.28 g g^{-1} and PT 0.24 g g^{-1}. In LS, a slight reaction to rising RH (due to night-day-shifts) was recognizable, and LS did not desiccate, despite high temperatures above 40 °C during the measurement period. We assume that the moss cover prevented desiccation of the substrate, but it remains unclear whether the substrate receives water from the moss cushion itself or plainly from RH. For low precipitation rates, prevention of soil evaporation from moss-dominated biocrusts was also reported in Li et al. (2016).

WC at the soil surface fluctuated diurnally depending on RH as also described in Tucker et al. (2017), especially in AS and PT and less pronounced in LS. Moreover, we found that oscillations related to RH were visible at the soil surface but not in 3 cm soil depth, which showed that fine pores at the surface were capable of adsorbing water out of the air (Agam and Berliner, 2006; Hillel, 1998). So even dense moss cushions were not completely sealing the soil surface and there was no full barrier by bryophytes. However, since the RH-induced fluctuations varied depending on the density of the moss cover, i.e. the most pronounced reactions were found in the loosest moss cover *P. undulatum*, we assume that mosses mitigate soil evaporation.

Generally, WC at the soil surface was higher than in 3 cm depth during desiccation. This could be ascribed to the fact that the soil surface had a finer texture due to clogging of the pores as an influence of splash effects (Morgan, 2005), which allows for a higher WC (Dodd and Lauenroth, 1997). A further influencing factor to explain this observation might be the initial soil WC. As we measured a high soil WC before watering, the matrix potential is reduced, resulting in a lower and less deep infiltration (Novák and Hlaváčiková, 2019).

Differences between WC values of surface and 3 cm depth depended on the substrate: for LS, the values were very similar, but especially for PT, WC values at substrate surface were higher than in 3 cm depth by a factor of 1.4 to 2.3. In AS, there was either an influence by the moss cover, or by the climatic conditions during the measurement: AS covered with *O. hians* showed a smaller difference between surface and soil WC and not very pronounced oscillations with RH. In contrast, AS covered with *O. hians* (Lab) displayed strong day-night oscillations and WC values during nights were up to 1.5-times higher in the surface than in 3 cm depth. Since RH remained above 50% after 20 hours during the measurement of AS with *O. hians*, but dropped from 75% in the nights to 25% RH during the days in the measurement of AS with *O. hians* (Lab), we cannot exclude a strong influence of these fluctuations on the different oscillation patterns in the AS measurements. To determine the effect of moss layers itself on soil substrate moistness and evaporation, an experiment with different moss species on similar substrates and control samples without moss is necessary.

CONCLUSIONS AND OUTLOOK

This study found that five moss species from Central European temperate forests can exhibit different water absorption and evaporation patterns in response to rainfall. In some cases, the target moss species also showed significant intraspecific variability in rainwater interception. With regard to our hypotheses, the following conclusions were drawn:

1. Contradictory to our hypothesis, total surface area did not affect maximum water storage capacity (WSC_{max}). Results further indicate that a combination of structural traits (high shoot density, high leaf frequency, and low leaf area) may increase WSC_{max} during immersion. Generalized additive models (GAM) revealed that cushion density also can influence WSC_{max}. A combination of different structural traits tested in a GAM showed that WSC_{max} determined using the spray technique was affected by leaf area index (LAI) and moss height. Overall, soil substrates absorbed around 30 times less water compared to mosses and an effect of bulk density, grain size distribution and total carbon content on WSC_{max} was found.

2. Both moss species and soil substrates showed species/substrate-specific patterns in regard to changes of moisture during watering as well as desiccation. Since soil substrates did not desiccate despite high temperatures, yet water content at the surface responded to relative humidity changes, we hypothesize that the moss cover prevented desiccation without sealing the soil. Because the humidity-induced fluctuations varied depending on the density of the moss cover, we further hypothesize that mosses mitigate soil evaporation. Among moss species, differences were also observed between replicates, primarily related to the moistening until an equilibrium in water content was reached, as well as in the process of desiccation. Similar WSC_{max} values (to immersion and spray) were not achieved in greenhouse experiments during watering, indicating different mechanisms of water absorption for both soil substrates and moss species, which could not be explained by clear patterns. In general, we can deduce that the mosses growing on the soil may not store much of the applied water themselves, but pass it on to the soil. Leaf frequency correlated positively with evaporation rates, while LAI showed a negative relationship with evaporation rates.

Although not explicitly mentioned in our hypotheses, the results underscore that some species can develop different morphologies due to different growing locations (field vs. laboratory). This can lead to a heterogeneous expression of the same traits and raises the question of whether beneficial traits can be conferred to individual species by laboratory cultivation, e.g. for erosion control. Thus, the interplay of individual moss structure traits appears to be very complex, such that further detailed investigations especially on the 3D structure of individual species are urgently needed. In this context, more information on moss capillary spaces would help to achieve a higher level of accuracy regarding the mechanisms of water absorption in mosses. It should be noted that the methodology also needs further improvement and the exact determination of individual species effects can be seen as non-trivial.

Considering that the methodology has proven to be sound, the full significance of the current results in this study needs to be confirmed in a larger experimental setup. Further research is required to understand the details of how different moss species and soil substrates interact regarding water absorption and evaporation. A multi-method approach to measure water content in different layers is recommended, using biocrust wetness probes as well as clip sensors for the moss cover as introduced

by Leo et al. (2019). This approach should be combined with the use of a climate-regulated greenhouse and expanded to include control samples without moss cover and large number of replicates in order to cover the existing complexity as well as possible. This complexity is also the major challenge in the investigation of "water's path from moss to soil", to the understanding of which this study has made a further contribution.

Acknowledgements. We thank Michael Sauer for his assistance and expertise during moss sample collection, Lena Grabherr and Sarah Fodor for their support in measuring moss structural parameters, Daniel Schwindt for helpful comments and Matthew Hughes for improving the language of the manuscript. We are also grateful to the Plant Ecology group of the University of Tübingen for the space provided in their greenhouse. We thank three anonymous reviewers for their constructive comments. This study was funded by the German Research Foundation (DFG SE 2767/2-1 "MesiCrust") and the Federal Ministry for Economic Affairs and Energy (AiF 19808 N).

REFERENCES

Acharya, B.S., Stebler, E., Zou, C.B., 2017. Monitoring litter interception of rainfall using leaf wetness sensor under controlled and field conditions. Hydrological Processes, 31, 240–249.

Agam, N., Berliner, P.R., 2006. Dew formation and water vapor adsorption in semi-arid environments – A review. Journal of Arid Environments, 65, 572–590.

Bates, J.W., 1998. Is 'life-form' a useful concept in bryophyte ecology? Oikos, 82, 223–237.

Belnap, J., Weber, B., Büdel, B., 2016. Biological soil crusts as an organizing principle in drylands. In: Weber, B., Büdel, B., Belnap, J. (Eds.): Biological Soil Crusts: An Organizing Principle in Drylands. Springer International Publishing, Cham, pp. 3–13.

Bengtsson, F., Granath, G., Cronberg, N., Rydin, H., 2020. Mechanisms behind species-specific water economy responses to water level drawdown in peat mosses. Annals of Botany, 126, 219–230.

Blume, H.-P., Stahr, K., Leinweber, P., 2011. Bodenkundliches Praktikum: eine Einführung in pedologisches Arbeiten für Ökologen, insbesondere Land- und Forstwirte, und für Geowissenschaftler. 3. neubearbeitete Auflage edn. Spektrum Akademischer Verlag, Heidelberg.

Bond-Lamberty, B., Gower, S.T., Amiro, B., Ewers, B.E., 2011. Measurement and modelling of bryophyte evaporation in a boreal forest chronosequence. Ecohydrology, 4, 26–35.

Buch, H.R.V., 1945. Über die Wasser- und Mineralstoffversorgung der Moose. Academic Bookstore, Helsinki.

Carleton, T., Dunham, K., 2003. Distillation in a boreal mossy forest floor. Canadian Journal of Forest Research, 33, 663–671.

Cornelissen, J.H., Lang, S.I., Soudzilovskaia, N.A., During, H.J., 2007. Comparative cryptogam ecology: a review of bryophyte and lichen traits that drive biogeochemistry. Annals of Botany, 99, 987–1001.

Dilks, T.J.K., Proctor, M.C.F., 1979. Photosynthesis, respiration and water content in bryophytes. New Phytologist, 82, 97–114.

Dodd, M.B., Lauenroth, W.K., 1997. The influence of soil texture on the soil water dynamics and vegetation structure of a shortgrass steppe ecosystem. Plant Ecology, 133, 13–28.

Einsele, G., Agster, G., 1986. Überblick zur Geologie und Morphologie des Schönbuchs. In: Einsele, G. (Ed.): Das landschaftsökologische Forschungsprojekt Naturpark Schönbuch: Wasser- und Stoffhaushalt, Bio-, Geo- und Forstwirtschaftliche Studien in Südwestdeutschland. VCH Verlagsfesellschaft, Weinheim.

Elbert, W., Weber, B., Burrows, S., Steinkamp, J., Büdel, B., Andreae, M.O., Pöschl, U., 2012. Contribution of cryptogamic covers to the global cycles of carbon and nitrogen. Nature Geoscience, 5, 459–462.

Elumeeva, T.G., Soudzilovskaia, N.A., During, H.J., Cornelissen, J.H., 2011. The importance of colony structure versus shoot morphology for the water balance of 22 subarctic bryophyte species. Journal of Vegetation Science, 22, 152–164.

Franzluebbers, A.J., 2002. Water infiltration and soil structure related to organic matter and its stratification with depth. Soil and Tillage Research, 66, 197–205.

Frey, W., Stech, M., Fischer, E., 2009. Syllabus of Plant Families - Part 3: Bryophytes and Seedless Vascular Plants. Borntraeger, Berlin, Stuttgart.

Gerrits, A.M.J., Savenije, H.H.G., 2011. Forest floor interception. In: Levia, D.F., Carlyle-Moses, D., Tanaka, T. (Eds.): Forest Hydrology and Biogeochemistry: Synthesis of Past Research and Future Directions. Springer Netherlands, Dordrecht, pp. 445–454.

Giordano, S., Colacino, C., Spagnuolo, V., Basile, A., Esposito, A., Castaldo-Cobianchi, R., 1993. Morphological adaptation to water uptake and transport in the poikilohydric moss *Tortula ruralis*. Giornale Botanico Italiano, 127, 1123–1132.

Glime, J.M., 2017. Volume 1: Physiological Ecology. Bryophyte Ecology.

Goetz, J.D., Price, J.S., 2015. Role of morphological structure and layering of Sphagnum and Tomenthypnum mosses on moss productivity and evaporation rates. Canadian Journal of Soil Science, 95, 109–124.

Gong, Y., Cao, Q., Sun, Z., 2003. The effects of soil bulk density, clay content and temperature on soil water content measurement using time-domain reflectometry. Hydrological Processes, 17, 3601–3614.

Green, T.G.A., Lange, O.L., 1994. Photosynthesis in poikilohydric plants: a comparison of lichens and bryophytes. In: Schulze, E.-D., Caldwell, M.M. (Eds.): Ecophysiology of Photosynthesis. Springer, New York, pp. 319–341.

Gundule, M.J., Deluca, T.H., Nordin, A., 2011. Bryophytes attenuate anthropogenic nitrogen inputs in boreal forests. Global Change Biology, 17, 2743–2753.

Gypser, S., Veste, M., Herppich, W., Kast, G., 2017. Linking of biological soil crust wetness and ecological performance on disturbed soils in Lower Lusatia, Germany. BES, GFÖ, NECOV, and EEF Joint Annual Meeting: Ecology across Borders. Ghent.

He, X., He, K.S., Hyvönen, J., 2016. Will bryophytes survive in a warming world? Perspectives in Plant Ecology, Evolution and Systematics, 19, 49–60.

Hedenäs, L., 2007. Global diversity patterns among pleurocarpous mosses. The Bryologist, 110, 319–331.

Hillel, D., 1998. Environmental Soil Physics: Fundamentals, Applications, and Environmental Considerations. Elsevier.

Leo, M., Lareo, A., Garcia-Saura, C., Hortal, J., Medina, N.G., 2019. BtM, a low-cost open-source datalogger to estimate the water content of nonvascular cryptogams. Journal of Visualized Experiments, 145, e58700.

Li, B., Gao, J., Wang, X., Ma, L., Cui, Q., Veste, M., 2016. Effects of biological soil crusts on water infiltration and

evaporation Yanchi Ningxia, Maowusu Desert, China. International Journal of Sediment Research, 31, 311–323.

Lindo, Z., Gonzalez, A., 2010. The bryosphere: An integral and influential component of the Earth's biosphere. Ecosystems, 13, 612–627.

Liu, D., She, D., 2020. Combined effects of moss crusts and pine needles on evaporation of carbonate-derived laterite from karst mountainous lands. Journal of Hydrology, 586, 124859.

Löbs, N., Walter, D., Barbosa, C.G.G., Brill, S., Alves, R.P., Cerqueira, G.R., de Oliveira Sá, M., de Araújo, A.C., de Oliveira, L.R., Ditas, F., Moran-Zuloaga, D., Pires Florentino, A.P., Wolff, S., Godoi, R.H.M., Kesselmeier, J., Mota de Oliveira, S., Andreae, M.O., Pöhlker, C., Weber, B. 2020. Microclimatic conditions and water content fluctuations experienced by epiphytic bryophytes in an Amazonian rain forest. Biogeosciences, 17, 5399–5416.

Mägdefrau, K., 1982. Life-forms of bryophytes. In: Smith, A.J.E. (Ed.): Bryophyte Ecology. Springer, Dordrecht.

Mägdefrau, K., Wutz, A., 1951. Die Wasserkapazität der Moos- und Flechtendecke des Waldes. Veröffentlichung des Botanischen Instituts der Forstl. Forschungsanstalt München.

Medina, N., Draper, I., Lara, F., 2011. Biogeography of mosses and allies: Does size matter? Biogeography of microscopic organisms. Is everything small everywhere? Cambridge University Press, pp. 209–233.

Morgan, R.P.C., 2005. Soil Erosion and Conservation. 3 edn. Blachwell Publishing, Oxford.

Nakatsubo, T., 1994. The effect of growth form on the evaporation in some subalpine mosses. Ecological Research, 9, 245–250.

Nebel, M., 2001. Amblystegium serpens (Hedw.) Schimp. In: Nebel, M., Philippi, G. (Eds.): Die Moose Baden-Württembergs, Band 2: Bryophytina II, Schistostegales bis Hypnobryales. Verlag Eugen Ulmer, Stuttgart, pp. 308–309.

Nebel, M., Philippi, G., Ahrens, M., Sauer, M., Schäfer-Verwimp, A., Schoepe, G., 2001. Die Moose Baden-Württembergs, Band 2: Bryophytina II, Schistostegales bis Hypnobryales. Verlag Eugen Ulmer, Stuttgart.

Niinemets, Ü., Tobias, M., 2014. Scaling light harvesting from moss "leaves" to canopies. In: Hanson, D.T., Rice, S.K. (Eds): Photosynthesis in Bryophytes and Early Land Plants. Advances in Photosynthesis and Respiration (Including Bioenergy and Related Processes). Springer, Dordrecht, pp. 151–171.

Niinemets, Ü., Tobias, M., 2019. Canopy leaf area index at its higher end: dissection of structural controls from leaf to canopy scales in bryophytes. New Phytologist, 223, 118–133.

Novák, V., Hlaváčiková, H., 2019. Applied Soil Hydrology. Springer, Heidelberg, Berlin.

Oishi, Y., 2018. Evaluation of the water-storage capacity of bryophytes along an altitudinal gradient from temperate forests to the Alpine zone. Forests, 9, 14.

Price, A.G., Dunham, K., Carleton, T., Band, L., 1997. Variability of water fluxes through the black spruce (*Picea mariana*) canopy and feather moss (*Pleurozium schreberi*) carpet in the boreal forest of Northern Manitoba. Journal of Hydrology, 196, 310–323.

Proctor, M.C.F., 1979a. Structure and eco-physiological adaptation in bryophytes. In: Bryophyte Systematics. Academic Press, London**,** pp. 479–509.

Proctor, M.C.F., 1979b. Surface wax on the leaves of some mosses. Journal of Bryology, 10, 531–538.

Proctor, M.C.F., 1982. Physiological ecology: Water relations, light and temperature responses, carbon balance. In: Smith, A.J.E. (Ed.): Bryophyte Ecology. Springer, Dordrecht.

Proctor, M.C.F., 1990. The physiological basis of bryophyte production. Botanical Journal of the Linnean Society, 104, 61–77.

Proctor, M.C.F., 2000. The bryophyte paradox: tolerance of desiccation, evasion of drought. Plant Ecology, 151, 41–49.

Proctor, M.C.F., Nagy, Z., Csintalan, Z., Takács, Z., 1998. Water-content components in bryophytes: Analysis of pressure-volume relationships. Journal of Experimental Botany, 49, 1845–1854.

Proctor, M.C.F., Oliver, M., Wood, A., Alpert, P., Stark, L., Cleavitt, N., Mishler, B., 2007. Desiccation-tolerance in bryophytes: A review. The Bryologist, 110, 595–621.

Proctor, M.C.F., Tuba, Z., 2002. Poikilohydry and homoihydry: antithesis or spectrum of possibilities? New Phytologist, 156, 327–349.

R Core Team, 2021. R: A language and environment for statistical computing. R Foundation for Statistical Computing, Vienna, Austria.

Rawls, W.J., Pachepsky, Y.A., Ritchie, J.C., Sobecki, T.M., Bloodworth, H., 2003. Effect of soil organic carbon on soil water retention. Geoderma, 116, 61–76.

Rice, S.K., Collins, D., Anderson, A.M., 2001. Functional significance of variation in bryophyte canopy structure. American Journal of Botany, 88, 1568–1576.

Rice, S.K., Gagliardi, T.A., Krasa, R.A., 2018. Canopy structure affects temperature distributions and free convection in moss shoot systems. American Journal of Botany, 105, 1499–1511.

Rice, S.K., Schneider, N., 2004. Cushion size, surface roughness, and the control of water balance and carbon flux in the cushion moss Leucobryum glaucum (Leucobryaceae). American Journal of Botany, 91, 1164–1172.

Richardson, D.H.S., 1981. The Biology of Mosses. Blackwell Scientific Publications, Oxford.

Robinson, S.A., Wasley, J., Popp, M., Lovelock, C.E., 2000. Desiccation tolerance of three moss species from continental Antarctica. Australian Journal of Plant Physiology, 27, 379–388.

Sayer, E.J., 2006. Using experimental manipulation to assess the roles of leaf litter in the functioning of forest ecosystems. Biological Reviews Cambridge Philosophical Society, 81, 1–31.

Schindelin, J., Arganda-Carreras, I., Frise, E., Kaynig, V., Longair, M., Pietzsch, T., Preibisch, S., Rueden, C., Saalfeld, S., Schmid, B., Tinevez, J.Y., White, D.J., Hartenstein, V., Eliceiri, K., Tomancak, P., Cardona, A., 2012. Fiji: an open-source platform for biological-image analysis. Nature Methods, 9, 676–682.

Schneider, C.A., Rasband, W.S., Eliceiri, K.W., 2012. NIH Image to ImageJ: 25 years of image analysis. Nature Methods, 9, 671–675.

Schofield, W.B., 1981. Ecological significance of morphological characters in the moss gametophyte. The Bryologist, 84, 149–165.

Seitz, S., Nebel, M., Goebes, P., Käppeler, K., Schmidt, K., Shi, X., Song, Z., Webber, C.L., Weber, B., Scholten, T., 2017. Bryophyte-dominated biological soil crusts mitigate soil erosion in an early successional Chinese subtropical forest. Biogeosciences, 14, 5775–5788.

Senf, C., Buras, A., Zang, C.S., Rammig, A., Seidl, R., 2020. Excess forest mortality is consistently linked to drought across Europe. Nature Communications, 11, 6200.

Simon, T., 1987. The leaf-area index of three moss species (*Tortula ruralis*, *Ceratodon purpureus*, and *Hypnum cupressiforme*). In: Pócs, T., Simon, T., Tuba, Z., Podani, J. (Eds.): IAB Conference of Bryoecology. Akadémiai Kiadó, Budapest-Vácrátót, Hungary, pp. 699–706.

Slatyer, R.O., 1967. Plant-Water Relationships. Academic Press, London, New York.

Söderström, L., Hagborg, A., von Konrat, M., Bartholomew-Began, S., Bell, D., Briscoe, L., Brown, E., Cargill, D.C., Costa, D.P., Crandall-Stotler, B.J., Cooper, E.D., Dauphin, G., Engel, J.J., Feldberg, K., Glenny, D., Gradstein, S.R., He, X., Heinrichs, J., Hentschel, J., Ilkiu-Borges, A.L., Katagiri, T., Konstantinova, N.A., Larraín, J., Long, D.G., Nebel, M., Pócs, T., Puche, F., Reiner-Drehwald, E., Renner, M.A.M., Sass-Gyarmati, A., Schäfer-Verwimp, A., Moragues, J.G.S., Stotler, R.E., Sukkharak, P., Thiers, B.M., Uribe, J., Váňa, J., Villarreal, J.C., Wigginton, M., Zhang, L., Zhu, R.-L., 2016. World checklist of hornworts and liverworts. PhytoKeys, 59, 1–828.

Soudzilovskaia, N.A., van Bodegom, P.M., Cornelissen, J.H.C., 2013. Dominant bryophyte control over high-latitude soil temperature fluctuations predicted by heat transfer traits, field moisture regime and laws of thermal insulation. Functional Ecology, 27, 1442–1454.

Tucker, C.L., McHugh, T.A., Howell, A., Gill, R., Weber, B., Belnap, J., Grote, E., Reed, S.C., 2017. The concurrent use of novel soil surface microclimate measurements to evaluate CO2 pulses in biocrusted interspaces in a cool desert ecosystem. Biogeochemistry, 135**,** 239–249.

Voortman, B.R., Bartholomeus, R.P., van Bodegom, P.M., Gooren, H., van der Zee, S.E.A.T.M., Witte, J.-P.M., 2014. Unsaturated hydraulic properties of xerophilous mosses: towards implementation of moss covered soils in hydrological models. Hydrological Processes, 28, 6251–6264.

Wang, Z., Bader, M.Y., 2018. Associations between shoot-level water relations and photosynthetic responses to water and light in 12 moss species. AoB PLANTS, 10.

Weber, B., Berkemeier, T., Ruckteschler, N., Caesar, J., Heintz, H., Ritter, H., Braß, H., Freckleton, R., 2016. Development and calibration of a novel sensor to quantify the water content of surface soils and biological soil crusts. Methods in Ecology and Evolution, 7, 14–22.

Zotz, G., Büde, B., Meyer, A., Zellner, H., Lange, O.L., 1997. Water relations and CO_2 exchange of tropical bryophytes in a Lower Montane Rain Forest in Panama. Botanica Acta, 110, 9–17.

Zotz, G., Schweikert, A., Jetz, W., Westerman, H., 2000. Water relations and carbon gain are closely related to cushion size in the moss *Grimmia pulvinata*. New Phytologist, 148, 59–67.

Received 31 March 2021
Accepted 9 June 2021

SUPPORTING INFORMATION

Table S1. Equations of calibration curves for studied soil substrates and moss species. The fit quality is assessed by the root mean square error (RMSE) and the determination coefficient (R^2) between measured and modeled water content.

Sample	Calibration equation	a	b	c	d	e	RMSE	R^2
Angulatensandstein-Formation	$y = \exp(a \cdot x) \cdot b \cdot x + c$	0.0043	$9.125e^{-07}$	0.264			0.027	0.928
Löwenstein-Formation	$y = a \cdot x + b$ (BWP < 1250 mV) $y = a \cdot x + b$ (BWP > 1250 mV)	0.00018 0.00215	0.0322 –2.437				0.002 0.016	0.990 0.954
Psilonotenton-Formation	$y = \exp(a \cdot x) \cdot b \cdot x + c$	0.0038	$2.055e^{-06}$	0.221			0.031	0.926
Trossingen-Formation	$y = \exp(a \cdot x) \cdot b \cdot x + c$	0.0065	$3.218e^{-08}$	0.238			0.010	0.990
Aamblystegium serpens (Lab)	$y = (a + b \cdot x)$	–2.555	0.0045				0.703	0.979
Brachythecium rutabulum	$y = a \cdot x + b$	0.0096	–0.401				0.229	0.996
Eurhynchium striatum	$y = a \cdot x + b$	0.0194	–0.617				0.205	0.995
Oxyrrhynchium hians	$y = a \cdot x + b$	0.0127	–0.414				0.200	0.993
Oxyrrhynchium hians (Lab)	$y = \exp(a \cdot x) \cdot b \cdot x + c$	0.0008	0.0036	–0.057			0.133	0.998
Plagiomnium undulatum	$y = a \cdot x^4 + b \cdot x^3 + c \cdot x^2 + d \cdot x + e$	$-3.141e^{-11}$	$7.996e^{-08}$	$-6.066e^{-05}$	0.0198	–0.5402	0.223	0.994

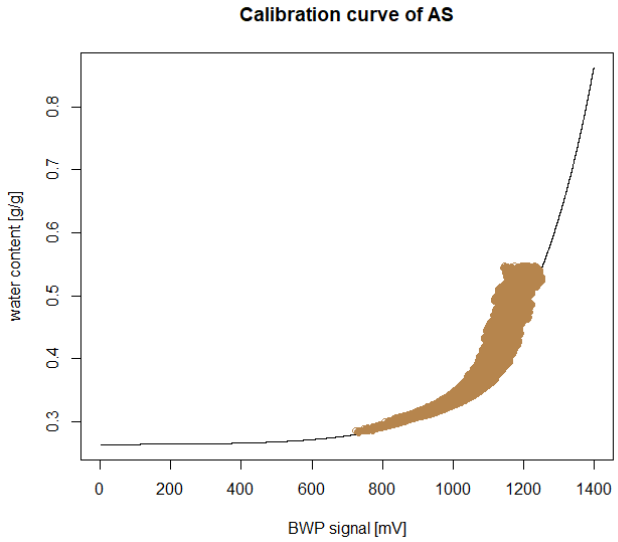
Calibration curve of AS
water content [g/g]
0.3
0.4
0.5
0.6
0.7
0.8
0
200
400
600
800
1000
1200
1400
BWP signal [mV]

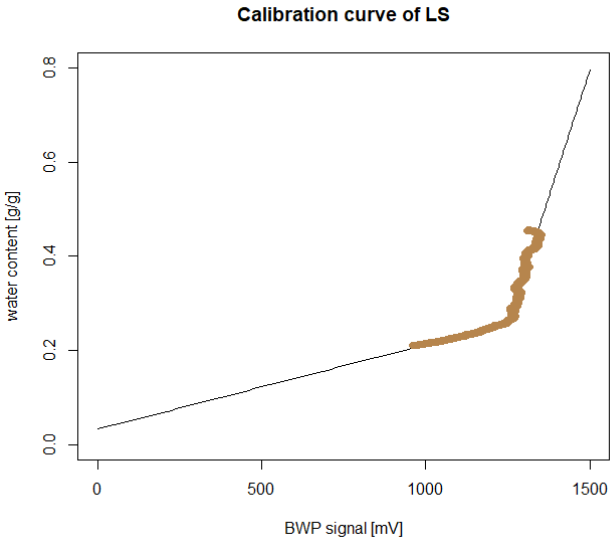
Calibration curve of LS
water content [g/g]
0.0
0.2
0.4
0.6
0.8
0
500
1000
1500
BWP signal [mV]

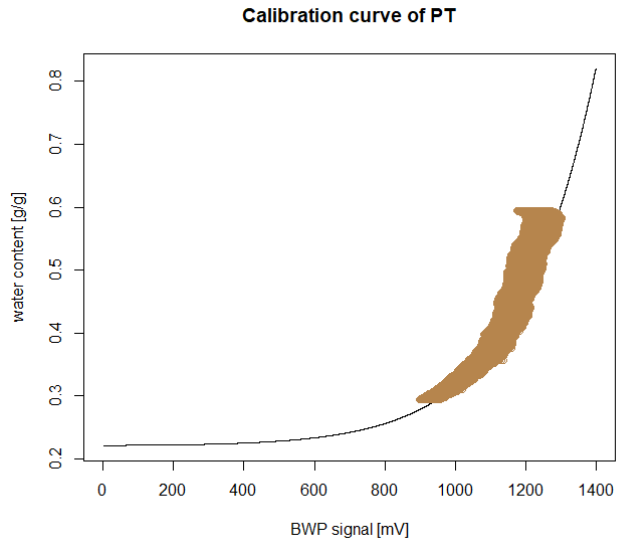
Calibration curve of PT
water content [g/g]
0.2
0.3
0.4
0.5
0.6
0.7
0.8
0
200
400
600
800
1000
1200
1400
BWP signal [mV]

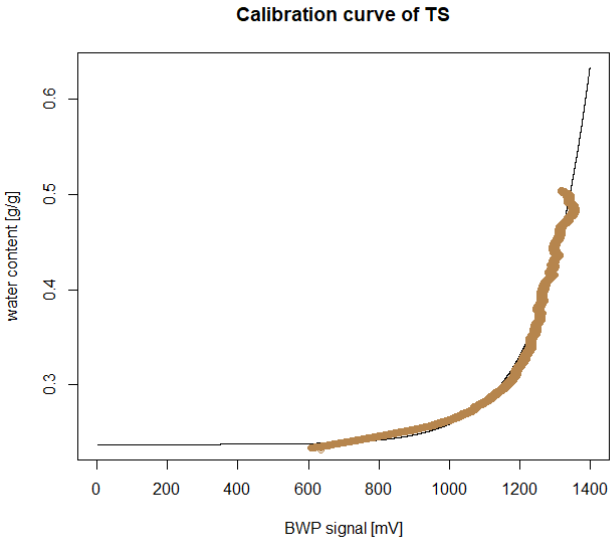
Calibration curve of TS
water content [g/g]
0.3
0.4
0.5
0.6
0
200
400
600
800
1000
1200
1400
BWP signal [mV]

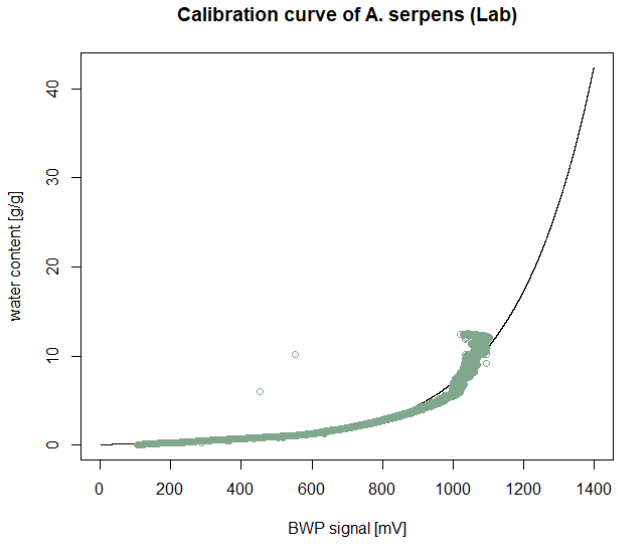
Calibration curve of A. serpens (Lab)
water content [g/g]
0
10
20
30
40
0
200
400
600
800
1000
1200
1400
BWP signal [mV]

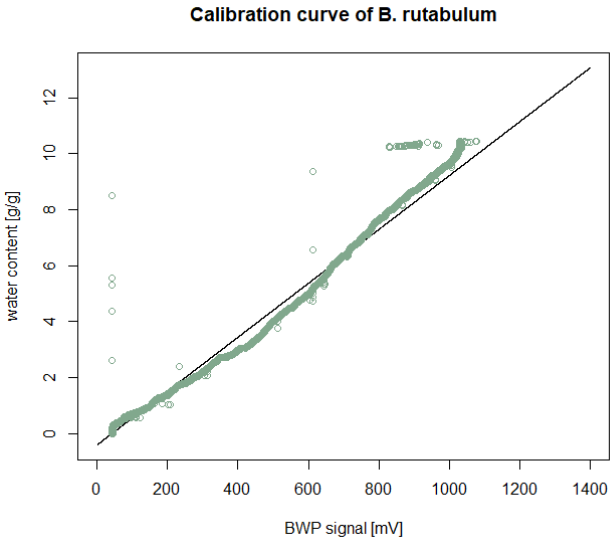
Calibration curve of B. rutabulum
water content [g/g]
0
2
4
6
8
10
12
0
200
400
600
800
1000
1200
1400
BWP signal [mV]

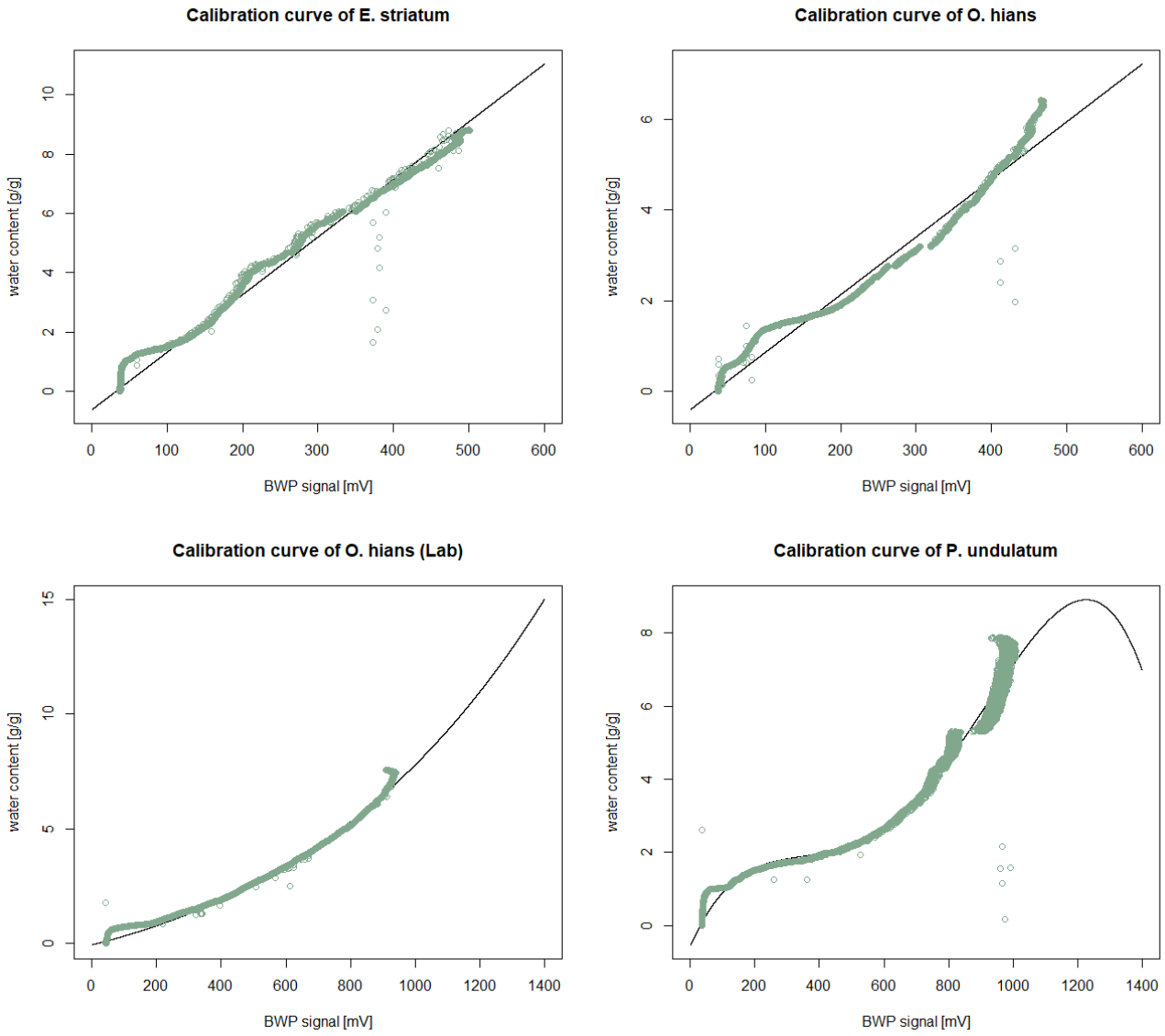

Figs. S1–S10. Plots of calibration curves for studied soil substrates and moss species. Measured water contents for soil substrates are illustrated in brown and for moss species in green.

Table S2. Maximum water storage capacity values (WSC_{max}) and sample sizes of the studied moss species for immersion and spray technique as gravimetric WSC_{max} (g g^{-1}), percentage WSC_{max} (%) and WSC_{max} per unit area (mm), ± standard error of the mean.

Moss species	Sample size	WSC_{max} immersion (g g^{-1})	WSC_{max} spray (g g^{-1})	WSC_{max} immersion (%)	WSC_{max} spray (%)	WSC_{max} immersion (mm)	WSC_{max} spray (mm)
Amblystegium serpens (Lab)	8	14.097 ± 1.28	10.082 ± 1.25	1409.668 ± 127.82	1008.176 ± 125.09	4.947 ± 0.74	3.144 ± 0.23
Brachythecium rutabulum	8	11.800 ± 0.81	10.049 ± 0.66	1179.965 ± 80.52	1004.919 ± 65.74	3.152 ± 0.31	2.712 ± 0.25
Eurhynchium striatum	17	11.223 ± 0.62	9.629 ± 0.40	1122.260 ± 61.55	962.943 ± 39.78	3.342 ± 0.21	2.820 ± 0.18
Oxyrrhynchium hians	7	9.686 ± 1.41	7.880 ± 0.57	968.598 ± 141.08	787.973 ± 56.90	2.094 ± 0.12	1.945 ± 0.09
Oxyrrhynchium hians (Lab)	7	9.934 ± 1.24	11.038 ± 1.23	993.381 ± 123.82	1103.796 ± 122.86	2.703 ± 0.32	2.448 ± 0.21
Plagiomnium undulatum	8	7.308 ± 0.80	8.146 ± 0.32	730.792 ± 79.89	814. 613 ± 31.58	1.841 ± 0.29	1.870 ± 0.13

J. Hydrol. Hydromech., 69, 2021, 4, 369–377
DOI: 10.2478/johh-2021-0022
ISSN 1338-4333

sciendo Journal of Hydrology and Hydromechanics

Water repellency decreases with increasing carbonate content and pH for different biocrust types on sand dunes

Sylvie Laureen Drahorad[1, 2*], Vincent J. M. N. L. Felde[3, 4], Ruth H. Ellerbrock[5], Anja Henss[2]

[1] Institute for Soil Science and Soil Conservation, Research Centre for BioSystems, Land Use and Nutrition (iFZ), Justus Liebig University Giessen, Giessen, Germany.
[2] Institute for Physical Chemistry, Justus Liebig University Giessen, Giessen, Germany.
[3] Department of Soil Science, University of Kassel, Witzenhausen, Germany.
[4] Institute of Soil Science, Leibniz University Hanover, Hanover, Germany.
[5] Working Group: Hydropedology, Research Area 1 "Landscape Functioning", Leibniz Centre for Agricultural Landscape Research (ZALF), Müncheberg, Germany.
[*] Corresponding author. Tel.: +49(0)641-9934522. E-mail: Sylvie.Drahorad@phys.chemie.uni-giessen.de

Abstract: Biocrusts are biological communities that occupy the soil surface, accumulate organic matter and mineral particles and hence strongly affect the properties of the soils they cover. Moreover, by affecting water repellency, biocrusts may cause a preferential infiltration of rainwater, with a high impact on the formation of local water pathways, especially for sand dunes. The aim of this study is to shed light on the connections between water repellency and pH, carbonate and organic matter content in two dune ecosystems with different biocrust types. For this, we used contact angle measurements, gas volumetric carbonate determination and organic matter characterization via FT-IR and TOF-SIMS. In both ecosystems, moss-dominated biocrusts showed higher water repellency and higher amounts of organic matter compared to algal or cyanobacterial biocrusts. Surprisingly, the biocrusts of the two dune systems did not show differences in organic matter composition or organic coatings of the mineral grains. Biocrusts on the more acidic dunes showed a significantly higher level of water repellency as compared to higher carbonate containing dunes. We conclude that the driving factor for the increase in water repellency between cyanobacterial and moss-dominated biocrusts within one study site is the content of organic matter. However, when comparing the different study sites, we found that higher amounts of carbonate reduced biocrust water repellency.

Keywords: Organic matter composition; Surface characteristics; TOF-SIMS; Biocrust; Carbonate content; Water repellency.

INTRODUCTION

Water repellency (WR) is an important factor for surface and subsurface water redistribution, plant growth and aggregate stability, as well as soil erosion (Doerr et al., 2000; Zheng et al., 2016). While WR can occur on a variety of soil types and textures, it affects soils with a high content of sand particles (like dune soils) to a higher degree than soils with a fine texture (González-Peñaloza et al., 2013; Woche et al., 2005). Especially the amount and composition of mineral particles and organic matter (OM) affect the extent and persistence of WR. The effect of texture on WR can be explained by the specific surface area (SSA) of the mineral particles, which increases with decreasing particle size. Hence, for the coating of fine-grained soil particles, a higher amount of hydrophobic OM is needed as compared to coarser particles (González-Peñaloza et al., 2013). Assuming the same amount of hydrophobic OM, this relation causes a decrease in WR with decreasing particle size (Woche et al., 2005; Zheng et al., 2016). Consequently, the addition of smaller particles like clay and silt decreased WR and texture is the most predictive factor influencing WR (McKissock et al., 2000). Additionally, the application of lime also affects WR via two mechanis. First, the input of fine particles increases the SSA and secondly because it increases the decomposition of hydrophobic compounds by bacteria due to the creation of more favorable environmental conditions (Roper, 2005). Most studies show a positive correlation of WR and the amount of OM with a non-linear increase in WR with increasing OM content (Leelamanie and Karube, 2009; Vogelmann et al., 2013; Woche et al., 2005). OM consists of fresh plant tissues, plant waxes and a high number of amphiphilic compounds like fatty acids. These compounds can form OM coatings (Graber et al., 2009; Morley et al., 2005). If OM components are mixed with mineral particles, the WR increases only slightly while a coating of particles with OM results in more intense WR (Bisdom et al., 1993).

However, WR is a highly dynamic soil property. For example, WR increases with decreasing water content (Dekker and Ritsema, 1994) while under laboratory conditions WR decreases with increasing soil pH (Diehl et al., 2010). For Mediterranean soils, the persistence of WR in the field was found to decrease with increasing pH value (Mataix-Solera et al., 2007; Zavala et al., 2009).

Biocrusts cover soils as part of early ecological succession or as permanent soil cover in semiarid and in humid climates including sand dunes around the world (Belnap, 2006; Nierop et al., 2001; Tighe et al., 2012). Biocrusts consist of cyanobacteria, algae, lichens, bacteria, fungi and mosses in different ratios depending on climate and successional stage. During growth, these organisms influence the soil pH, accumulate carbon, nitrogen (Chamizo et al., 2012; Lichner et al., 2018) and other elements (Beraldi-Campesi et al., 2009), stabilize the soil surface and change the soil structure (Felde et al., 2014) of the upper soil layer at millimeter scale. Since biocrust formation changes the properties of the very soil surface, it also affects WR and hydraulic conductivity of the soil surface (Gypser et al. 2016; Tighe et al., 2012). In most studies, bi-

ocrusts show only subcritical WR values, including studies on biocrusts in the Negev (Gypser et al., 2016; Keck et al., 2016; Kidron and Büdel, 2014). The semi-arid northwestern Negev provides unique growing conditions for biocrust organisms, as the sand dunes are part of a nature protection area and the ecosystem has a high input of dust (Littmann and Schulz, 2008) and moisture via dew (Jacobs et al., 2000). The geological material is enriched in carbonates, has an alkaline pH and biocrust growth is rather fast (Kidron et al., 2020). In contrast to this, biocrusts from the humid Sekule site in Slovakia show strong WR on carbonate-free dunes with an acidic pH-value (Lichner et al., 2012). This effect increased with ongoing biocrust development and increasing amounts of OM (Drahorad et al., 2013b; Drahorad et al., 2020). Until now, studies comparing the WR and correlated soil properties of biocrusts in contrasting ecosystems are missing. We compared biocrusts of the Negev dunes (Israel) and at Sekule (Slovakia) to test the hypothesis that higher pH values (as induced by higher carbonate contents) are correlated with lower levels of WR in biocrusts. To check this, we correlated contact angle (CA) data with pH values. Moreover, as earlier studies did show that an increase in WR correlates with an increase in OM but does not relate to OM characteristics at the Sekule site, we hypothesized that the same effect will be visible for biocrusts of the Negev. To test this, we compared data on OM amounts of two biocrust types at each study site and characterized the OM at the Negev site using Fourier transform infrared spectrometry (FT-IR). Moreover, organic coatings may play a major role in WR of biocrusts. We use Time of Flight Secondary Ion Mass Spectrometry (TOF-SIMS) as powerful tool for the characterization of environmental samples to show the surface characteristics of biocrust-associated mineral grains (Arenas-Lago et al., 2016; Cliff et al., 2002). As the biocrusts at Sekule developed under humid climate conditions, we hypothesize a higher OM accumulation in these biocrusts as compared to biocrusts of the Negev (Israel), which in turn may be accompanied by a thicker organic coating of mineral grains.

MATERIAL AND METHODS

The first study site is located at Sekule (southwestern Slovakia) with a mean annual precipitation of 550 mm and carbonate-free inland sand dunes as parent material. Because of sand mining for building purposes, an artificial glade arose, where biocrusts cover the sandy soils. The biocrusts at freshly disturbed areas are thin, algae- and cyanobacteria-dominated crusts while thick, moss-dominated crust cover the soil at less disturbed areas. For a detailed description of the forest glade side and the occurring biocrust species, see Lichner et al. (2013). The second study site is located in the Negev dunes (Israel) 25 km north of Nizzana and 12 km south of the town of Yevul and is characterized by a mean annual precipitation of approx. 170 mm and carbonate containing sand as parent material. Biocrusts stabilize the dunes with thin cyanobacterial crusts at the south-exposed slopes and thicker, moss-dominated crusts dominate at the wetter, north-exposed dune slopes. For a detailed description of biocrust OM composition and occurring cyanobacterial species see Drahorad et al. (2013a) and Hagemann et al. (2015).

Sampling of biocrusts and underlying soil

At both study sites, we sampled biocrusts in two depths, including algae-and cyanobacterial-dominated biocrusts at freshly disturbed areas in Sekule and the southexposed slopes in the Negev and moss-dominated biocrusts at less disturbed areas in Sekule and northexposed dune slopes in the Negev. Sampling included three depths: i) the topcrust (TC; 0–2 mm) ii) the underlying subcrust (SC; 2–20 mm) and iii) the topsoil (TS; 20–100 mm). We analyzed soil texture, carbonate content, pH and CA on these samples. In addition, we used the Water Drop Penetration Time (WDPT) test for the description of actual repellency on intact in-situ biocrusts (only for the TC). For the characterization of OM of Negev biocrusts we used the TC and SC samples of cyanobacterial- and moss-dominated biocrusts, to allow a good comparability with existing results of the same biocrust types at Sekule site. To test the hypothesis of changes in the organic coatings of mineral biocrust particles, we isolated particles from moss-dominated biocrusts of the two study sites. These TCs are characterized via ToF-SIMS. We concentrated on these samples as moss-dominated biocrusts showed the highest WR. Therefore, we expect to find the highest differences in coating thickness and composition for mineral particles between the two study sites.

Sample treatment and analysis

The content of sand particles and finer (i.e. silt and clay) particles (2000–63 µm and < 63 µm, respectively) was classified based on wet sieving according to ISO 11277. All samples were dried at 105°C and sieved (2 mm) and an aliquot was finely ground (0.05 mm) for the measurement of total carbon (C) and total nitrogen (N) by dry combustion (Vario EL CNS analyzer). For the Negev samples, the carbonate content was analyzed gas-volumetrically using a Scheibler apparatus according to ISO 10963. For the Negev, this includes mainly calcium carbonates and to a lesser extent, magnesium carbonates (Rozenstein et al., 2014). The amount of total organic carbon (TOC) was calculated as the difference between carbonate content and total carbon. The pH value was measured in a 1:5 water extract.

For the Negev samples, we included an **OM characterization via FT-IR.** For recording FT-IR spectra, we used 1 mg of ground, desiccated soil (< 0.5 mm) mixed with 80 mg of potassium bromide and dried over night over silicagel in an exsiccator (Ellerbrock et al., 1999). The mixture was pressed into a pellet by applying a pressure of 980.7 MPa for 10 min. Infrared absorbance spectra of OM were collected in the wave number range of 4,000–400 cm^{-1} with 16 scans per spectrum. The spectra were smoothed (boxcar moving average algorithm, factor 45) and corrected for baseline shifts using WIN-IR Pro 3.4 software (Digilab, Massachusetts, USA). For a detailed description on FT-IR spectra of the Sekule samples see Drahorad et al. (2020).

Water repellency (WR) measurements included water drop penetration time (WDPT) test. It is the fastest in-situ method for assessing the persistence of the actual WR of the undisturbed biocrusts. A drop of distilled water (approx. 50 µL) is placed on the soil surface and the time that it takes for complete surface penetration is recorded. Since water only enters the soil if the contact angle between water and soil is less than 90°, the WDPT test is a measure of the time required until the contact angle reaches values below 90° and thus, of the persistence of WR rather than its intensity (Iovino et al., 2018; Letey et al., 2000). We use the terms ´actual WR` for field-moist samples in natural position and ´potential WR` as the maximum possible WR for samples that were dried by 105 °C, according to Dekker and Ritsema (1994).

A second method that we used for the analysis of WR was the measurement of the contact angle via the Wilhelmy Plate Method (WPM). The WPM allows the determination of the advancing and receding contact angle and is theoretically suited

to measure contact angles between 0° and 180° (Bachmann et al., 2003). Briefly, we used disturbed samples (< 2 mm) to create a thin layer of soil particles on a glass slide using double-sided adhesive tape. When present, aggregates were gently crushed in a mortar. Despite the coarse texture of the samples, we decided not to grind them in order to avoid the breaking of sand grains, which would have resulted in the creation of new surfaces that likely cause an underestimation of the CA. We measured the advancing contact angle with five repeated measurements for each sample, using a dynamic contact angle tensiometer (DCAT11, Dataphysics, Filderstadt, Germany).

It should be noted that one possible source of error that can lead to the overestimation of CA for the Sekule samples may have been the coarse texture and the fact that samples were not ground prior to CA analysis. While the Negev samples contained more fine particles, which are likely to have covered the complete adhesive tape, this was not the case for the Sekule samples. Containing fewer silt and clay-sized mineral particles, it may have been the case that some spots on the adhesive tape between larger sand grains were exposed to the water, which may have led to an overestimation of the CA for this sample.

For **surface characterization and the description of mineral grain coatings**, we analyzed single sand grains by using Time of Flight Secondary Ion Mass Spectrometry (ToF-SIMS). Therefore, we isolated mineral grains of moss-dominated biocrusts via density separation in deionized water and transferred them on an adhesive copper tape. The ToF-SIMS measurements were performed with a TOF.SIMS M6 instrument (ION-TOF GmbH, Muenster, Germany) equipped with a 30 keV Bi-cluster primary ion gun, as well as with a gas cluster ion beam (GCIB) and a dual source column (DSC) for sputtering. All analyses were carried out with Bi^{3+} primary ions, with a cycle time of 75 µs (imaging mode) or 120 µs (spectrometry mode) in positive and negative ion mode. Charge compensation was done with low energetic electrons. Mass spectra were recorded using the spectrometry mode on an analysis area of 500 x 500 µm^2 keeping a dose density limit of 10^{12} ions cm^{-2}. A mass resolution of FWHM m/Δm > 3500 at m/z 29.00 (CHO^+) in positive ion mode and m/Δm > 1800 at m/z 26.00 (CN^-) in negative ion mode was achieved. The signals H^{2+}, CH^{3+} (15.02 u), Na^+ (22.99 u), K^+ (38.96 u), $C_3H_5^+$ (41.04 u), $C_3H_7^+$ (43.05 u) in positive ion mode and H_2^- (2.01 u), C^- (12.01 u), C_2^- (24.00 u), C_3^- (36.00 u), PO^{2-} (62,97 u) in negative ion mode were used for internal mass calibration. Surface analysis of the soil particles turned out to be challenging due to their heterogeneous surface properties and the particulate character of the sample system. In addition, the topography of the particles has a significant impact on mass resolution of the obtained spectra. Therefore, five regions of each sample set were analyzed in spectrometry mode for comparison. The corresponding mass images were used to set regions of interest (ROI), which were defined by a threshold of 10%–90% pixel intensity of the total ion image to select the particle areas. By normalization to the total ion signal intensity, we minimized the topographic effect not only on the mass resolution but also on the signal intensity and enabled a comparison of selected mass signals. The mass images shown in Fig. 4 were recorded in imaging mode with delayed extraction for good mass and good lateral resolution (Henss et al., 2018). For the images, areas of 500 x 500 µm^2 with 1024 x 1024 pixels were scanned. More detailed information on SIMS measurements can be found elsewhere (Vickermann and Gilmore, 2009). Data analysis was performed with the "SurfaceLab 7.1.1" software (ION-TOF GmbH).

Data management and statistics included the calculation of significant differences between the measured biocrust parameters on a level of significance of 5%, using a 1-way ANOVA. As the data-set was too small for a MANOVA including biocrust depths, types and sampling areas as single fixed factors, we reclassified these samples in 12 equal factors, allowing the calculation of a 1-way ANOVA. Post Hoc Scheffé test was used, as the data set was unbalanced. Pearson´s correlation coefficient was used to describe correlations (Statistica 14).

RESULTS AND DISCUSSION

The TC samples at different sampling sites show significant differences in pH, carbonate content, texture and CA ($p < 0.001$) (Table 1). Interestingly, TC samples of the same biocrust type show comparable contents of TOC and N at the two study sites (Table 1 and Figure 1). This is surprising, as the humid ecosystem in Sekule should in general favor higher biomass accumulation due to higher amounts of annual precipitation. With increasing annual precipitation and available moisture, biocrust biomass increases (Kidron et al., 2014; Lichner et al., 2018).

Table 1. Basic biocrust and soil characteristics at Sekule (Slovakia) and Negev dunes (Israel) in three sampling depths (TC 0–2 mm; SC 2–20 mm; TS 20–100 mm; n = 7/6/4 for Sekule and n = 3 for Negev dunes). Particle size distribution by wet sieving (n = 4 Sekule, n = 3 Negev). All values are means, standard deviation in parenthesis. Different upper case letters denote significant differences between sampling depths within the same biocrust type at each sampling site, different lower case letters denote significant differences between biocrust types at the same sampling depth and sampling site and different numbers denote significant differences between comparable biocrusts types at different sampling sites.

						sand particles			fine particles
Area	type	depth	pH	Carbonates	N	2000–630 µm	630–200 µm	200–63 µm	< 63 µm
				[weight-%]	[%]	[%]			
Sekule	algae	TC	4.8 (±0.1)^{A,a,1}	0.0^{A,a,1}	0.04 (±0.01)^{A,a,1}	0.01 (±0.02)^{A,a,1}	32.43 (±10.84)^{A,a,1}	57.42 (±9.93)^{A,a,1}	3.01 (±0.32)^{A,a,1}
		SC	4.9 (±0.1)^{A,b,1}	0.0^{A,a,1}	0.02 (±0.01)^{A,b,1}	0.01 (±0.01)^{A,a,1}	32.35 (±8.17)^{A,a,1}	61.89 (±7.67)^{A,a,1}	3.10 (±0.85)^{A,a,1}
		TS	4.9 (±0.1)^{A,b,1}	0.0^{A,a,1}	0.01 (±0.00)^{A,b,1}	0.02 (±0.02)^{A,a,1}	29.07 (±2.30)^{A,a,1}	65.15 (±3.81)^{A,a,1}	3.31 (±0.77)^{A,a,1}
	moss	TC	4.4 (±0.1)^{A,a,1}	0.0^{A,a,1}	0.09 (±0.02)^{B,a,1}	0.00 (±0.00)^{A,a,1}	28.39 (±9.31)^{A,a,1}	44.69 (±8.19)^{A,a,1}	4.69 (±1.29)^{A,a,1}
		SC	4.6 (±0.1)^{A,b,1}	0.0^{A,a,1}	0.03 (±0.01)^{A,b,2}	0.03 (±0.01)^{A,a,1}	34.75 (±15.22)^{A,a,1}	50.28 (±16.36)^{A,a,1}	3.93 (±0.35)^{A,a,1}
		TS	4.8 (±0.1)^{B,b,1}	0.0^{A,a,1}	0.01 (±0.00)^{A,b,2}	0.03 (±0.03)^{A,a,1}	37.16 (±13.46)^{A,a,1}	51.38 (±15.98)^{A,a,1}	3.68 (±1.23)^{A,a,1}
Negev	cyano	TC	7.4 (±0.1)^{A,b,2}	2.6 (±0.2)^{A,a,2}	0.03 (±0.01)^{A,a,1}	4.61 (±1.15)^{A,a,2}	58.56 (±2.40)^{A,a,2}	33.83 (±2.68)^{A,b,2}	10.13 (±1.42)^{A,a,1}
		SC	8.0 (±0.4)^{A,b,2}	1.7 (±0.2)^{A,a,2}	0.01 (±0.00)^{A,b,1}	3.33 (±0.67)^{A,a,2}	56.57 (±3.93)^{A,a,2}	37.00 (±3.85)^{A,b,2}	5.75 (±0.74)^{A,a,1}
		TS	8.4 (±0.3)^{B,b,2}	1.0 (±0.2)^{A,a,2}	0.01 (±0.00)^{A,b,1}	2.34 (±0.60)^{A,a,2}	58.08 (±1.80)^{A,a,2}	36.27 (±1.66)^{A,a,2}	5.76 (±2.36)^{A,a,1}
	moss	TC	7.1 (±0.2)^{A,b,2}	7.3 (±1.1)^{A,b,2}	0.10 (±0.02)^{B,a,1}	3.30 (±0.82)^{A,a,2}	57.97 (±3.68)^{A,a,2}	34.05 (±3.37)^{A,a,2}	26.92 (±2.09)^{B,b,2}
		SC	7.6 (±0.2)^{A,b,2}	5.4 (±2.2)^{A,b,2}	0.04 (±0.01)^{A,b,2}	4.08 (±1.42)^{A,a,2}	54.28 (±1.65)^{A,a,1}	37.70 (±2.91)^{A,a,2}	14.94 (±2.38)^{A,b,2}
		TS	8.0 (±0.2)^{B,b,2}	4.2 (±0.5)^{B,b,2}	0.02 (±0.01)^{A,b,2}	2.96 (±0.79)^{A,a,2}	57.65 (±2.34)^{A,a,1}	35.71 (±1.78)^{A,a,2}	11.44 (±4.36)^{A,a,2}

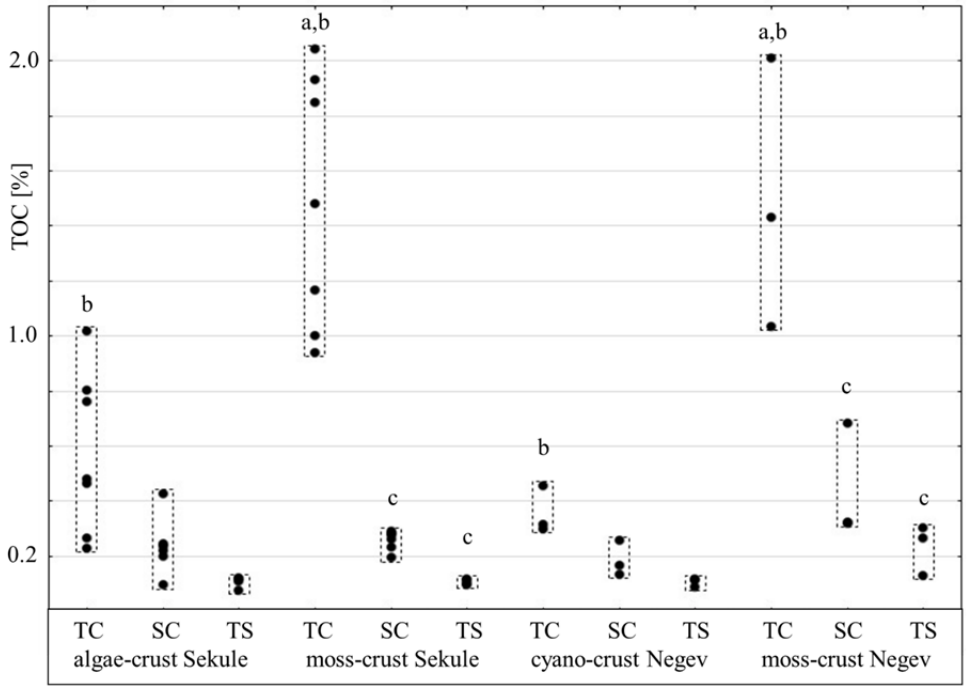

Fig. 1. Variability plot showing the total organic carbon (TOC) of two biocrust types (algae/cyano; moss) in three sampling depths (TC 0–2 mm; SC 2–20 mm; TS 20–100 mm) in Sekule and the Negev. Letters indicate a significant difference ($p < 0.05$) between sampling depths within the same biocrust type (a), a significant difference between the biocrust types at the same sampling depth and sampling site (b) or a significant difference between comparable biocrusts types at different sampling sites (c).

We therefore assume that the available moisture is lower in Sekule, as water infiltrates fast and the biocrusts dry rapidly due to the high content of sand sized particles (> 95%). In contrast, higher amounts of fine sized particles (Table 1) increase the water holding capacity and wetness duration, likely favoring a higher biomass build-up in cyanobacterial Negev biocrusts (Kidron et al., 2009).

Total organic carbon and pH-values of biocrusts

The TCs show lower pH values as compared to SC and TS samples (with the exception of the TC of the algae biocrust at Sekule). This is in accordance with findings for biocrust-covered soils located in humid regions of eastern Germany (pH decrease from 4.8 to 4.2) or in semiarid regions within the Negev (pH decrease from 8.6 to 7.6) (Fischer et al., 2010; Keck et al., 2016). The biocrust samples from both sites, Negev and Sekule, show a decrease in pH from the cyanobacterial/algae biocrust to the moss-dominated biocrust. This trend was also found for a development from algae to moss-dominated biocrusts in the Netherlands (pH decrease from 4.8 to 4.2) (Nierop et al., 2001).

The accumulation of TOC is significantly higher in the TC of moss-dominated biocrusts at both sites as compared to the SC and TS underneath and as compared to the algae- or cyanobacterial-dominated biocrust (Figure 1). For Sekule, the two examined biocrust types represent an early and a late successional development stage, respectively. As late successional biocrusts show higher gross photosynthesis than early successional biocrusts, that can induce higher overall TOC accumulation in these biocrust (Miralles et al., 2018).

Organic matter characterization of Negev dune biocrust

FT-IR was used to describe the OM of the biocrusts at the Negev site as already done in an earlier work for the biocrusts of Sekule (Drahorad et al., 2020). The FT-IR spectra are characterized by the same bands as the previously recorded for data on biocrusts in Sekule (Figure 2). This included the bands relevant for the WR of soils at the wavenumbers at 2925 cm^{-1} + 2858 cm^{-1} (aliphatic C-H) and 1635 cm^{-1} (C=O, aromatics) (Ellerbrock et al., 2005). This similarity in the spectra is in accordance with FT-IR data of biocrusts sampled in humid climate (Fischer et al., 2013). Nierop et al. (2001) did show a comparable pattern of polysaccharides in marine algae, soil algal mats and moss-covered dune sand. In general, bacterial vs. fungal materials show the same pattern in ^{13}C NMR-spectra with high proportions of alkyl-C structures and polysaccharides (Kögel-Knabner, 2002). NMR-spectra of biocrusts from the Negev and eastern Germany showed similar OM composition and also similarities to cell spectra of algae (Fischer et al., 2013). More studies on the OM composition are needed to reveal general (i.e. global) patterns. Nevertheless, for the comparison between Negev and Sekule biocrusts we assume that the biocrust OM composition is not the relevant driver for differences in WR.

Differences in the FT-IR spectra were pronounced for the bands 1085 and 1033 cm^{-1} (polysaccharides, silicates and clay minerals) showing a double peak for Negev biocrusts compared to Sekule biocrusts. This reflects the higher amount of fine particles and therefore likely higher clay mineral content in these samples. Moreover, the second difference between the spectra are bands near 1430 and 875 cm^{-1}, which are characteristic for carbonates (Smidt et al., 2002). For the Negev biocrusts, the reduction in absorbance of the spectrum at 875 cm^{-1} in the order cyanobacterial TC>cyanobacterial SC>moss TC >moss SC is in line with the carbonate concentrations determined (Table 1). The results demonstrate that FT-IR can also be used for carbonate concentration measurements in biocrusts as already shown for other carbonate-containing soils (Tatzber et al., 2007).

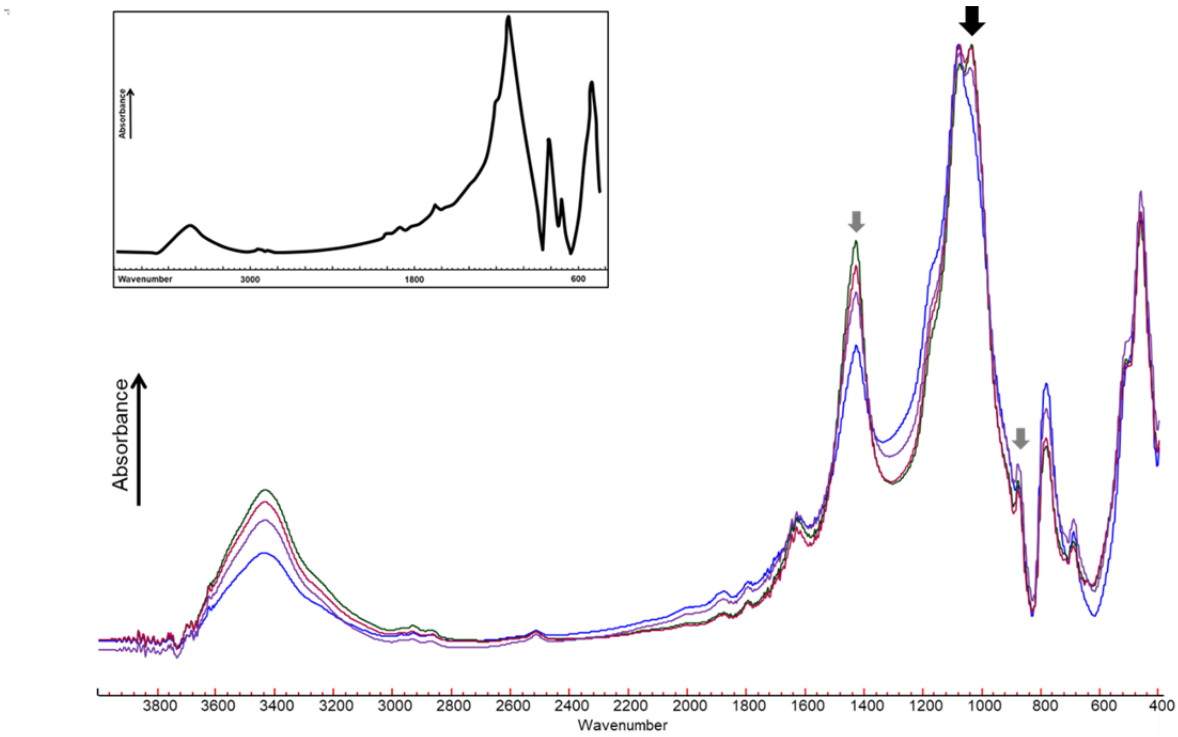

Fig. 2. FT-IR spectra of cyanobacterial and moss-dominated biocrust of the Negev (green = cyanobacterial topcrust; red = cyanobacterial subcrust; violet = moss-dominated topcrust; blue = moss-dominated subcrust). Insert for comparison: mean FT-IR spectra of algae and moss top- and subcrusts at Sekule, original data see: Drahorad et al., 2020). Arrows indicate differences in FT-IR spectra with bands indicating higher clay content (black arrow) and bands indicating the occurrence of calcium carbonate (grey arrows).

Table 2. Intensity of water repellency (contact angle) in the examined biocrusts at Sekule (Slovakia) and Negev dunes (Israel) in three sampling depths (TC 0–2 mm; SC 2–20 mm; TS 20–100 mm; n = 7/6/4 for Sekule and n = 3 for Negev) and persistence of water repellency (actual repellency) of the undisturbed biocrusts in situ (n = 10). Different upper case letters denote significant differences between sampling depths within the same biocrust type at each sampling site, different lower case letters denote significant differences between different biocrust types at the same sampling depth and sampling site and numbers denote significant differences between comparable biocrusts types at different sampling sites.

Area	crust type	depth	contact angle [°]	actual repellency / WDPT [s]
Sekule	algae	TC	111.75 (±11.92)^{A,a,1}	very hydrophilic 0 (±0)
		SC	109.90 (±10.29)^{A,a,1}	–
		TS	88.39 (±7.26)^{B,a,1}	–
	moss	TC	135.01 (±8.99)^{A,b,1}	moderately hydrophobic 294 (±14)
		SC	113.63 (±4.37)^{B,a,1}	–
		TS	93.54 (±4.24)^{C,a,1}	–
Negev	cyano	TC	29.07 (±2.87)^{A,a,2}	very hydrophilic 0(±0)
		SC	27.43 (±13.65)^{A,a,2}	–
		TS	29.40 (±6.50)^{A,a,2}	–
	moss	TC	86.70 (±11.75)^{A,b,2}	very hydrophilic 0(±0)
		SC	62.50 (±11.08)^{A,b,2}	–
		TS	38.77 (±9.55)^{B,a,2}	–

Actual repellency and intensity of WR of biocrusts

The WDPT of the undisturbed biocrust in-situ shows that only one biocrust is moderately hydrophobic (Table 2). Early biocrusts on Sekule sand and biocrust growing on carbonate containing sands of the Negev do not show an actual WR persistence. These values are below WR values of sandy soil surfaces under various European pine forests (< 433 s) (Iovino et al., 2018) and below the actual repellency found on non-calcareous sand dunes in the Netherlands (600–3600 s) (Dekker et al., 2001). Compared to these rather low values of the actual repellency, the CA data shows a moderate to very strong potential WR resistance for algae biocrusts at Sekule study site. Two treatment effects explain this difference. First, the concept of potential WR includes drying of samples and the potential WR of soil samples increases with increasing drying temperature (Dekker et al., 2001; Diehl et al., 2009). Moreover, the disturbance itself during sampling has a profound influence. Graber et al. (2006) identified strong differences of WR between disturbed and undisturbed samples in sandy soils. They hypothesized that the reason for these changes relate to differences in surface roughness, pore size distribution, pore connectivity, bulk density and changes in the distribution and orientation of the substances that are responsible for repellency. Moreover,

even very thin layers of fine particles covering biocrusts changes the WR on the surface (Cania et al., 2020; Fischer et al., 2010). For example, sand burial of moss-dominated biocrusts in the Tengger desert was reported to decrease WR (Jia et al., 2020). These results show the importance of the biocrust surface structure and the in-situ integration in the ecosystem for real field site WR. Therefore, measurements of intact biocrusts are relevant for the evaluation of water flow pathways in biocrust covered ecosystems.

In contrast to the actual repellency determined by WDPT, the intensity of WR shows CA of above 100° for both biocrust types at Sekule and CA up to almost 90° for the moss-dominated biocrust of the Negev. Here, differences between crust types are most obvious. While the values for all depths of the cyanobacterial biocrust of the Negev do not show any differences, for the moss-crust a clear increase from 38.77° to 62.50° and finally 86.70° can be observed from TS to SC and finally to TC. Different CA between the different sampling depths, which show the effect of OM accumulation by the crust organisms, are obvious for all but the cyanobacterial crust from the Negev. The fact that differences between crust types in Sekule are very low (and in fact are only significant in the case of the TC vs. TS in the moss-dominated biocrust) may be indicative for the effect of texture and pH at this study site. Soils below the Sekule biocrusts have a coarser texture and a more acidic pH compared to the Negev soils.

Relation between WR, TOC and pH value of biocrusts

In both ecosystems, algae- or cyanobacterial-dominated biocrusts show lower TOC content and CA than moss-dominated biocrusts. This trend is in line with earlier studies on WR of biocrusts. As biocrusts develop, their thickness and the amount of OM increase as well, and so does their WR (Drahorad et al, 2020; Gypser et al., 2016; Lichner et al., 2018). For both study sites, TOC and CA are highly correlated (r = 0.81 Sekule and r = 0.83 Negev). This confirms part one of our hypothesis on OM dynamics, namely that an increase in biocrust OM induces an increase in WR. Plotting the complete data set confirms visually that the Sekule biocrusts show higher WR for samples with a similar TOC content compared to Negev biocrusts (Figure 3). Therefore, we assume that within each study site, the differences in WR result from a higher overall amount of OM in the moss-dominated biocrusts as compared to the algal-/cyanobacterial crusts. This effect may be stronger at the Sekule site, as Wang et al. (2010) found that soil organic carbon affected WR stronger in soils that were classified as repellent, while texture and pH had a higher impact on WR in wettable/non-repellent soils.

Based on the conclusion that an increasing OM content is inducing a higher WR for biocrusts at the same study site but that OM amount or composition do not explain the differences between the study sites, two effects may explain the differences in the WR. First, the biocrusts at the Negev reveal a higher pH value than the biocrusts in Sekule and pH and CA show a strong negative correlation (r = –0.76 Sekule and r = –0.73 Negev). Studies on WR and pH on semiarid alkaline soils showed lower persistence of WR compared to acidic soils (Mataix-Solera et al., 2007). In their meta-analysis, Zheng et al. (2016) also reported a negative correlation between pH and WR, while soil organic carbon generally correlates positively with WR.

Deprotonation of surface sites and the changes in OM confirmation are the mechanisms that explain the effect of pH changes on WR (Diehl et al., 2010; Doerr et al., 2000). Doerr et al. (2000) state that this effect is strong enough to explain all

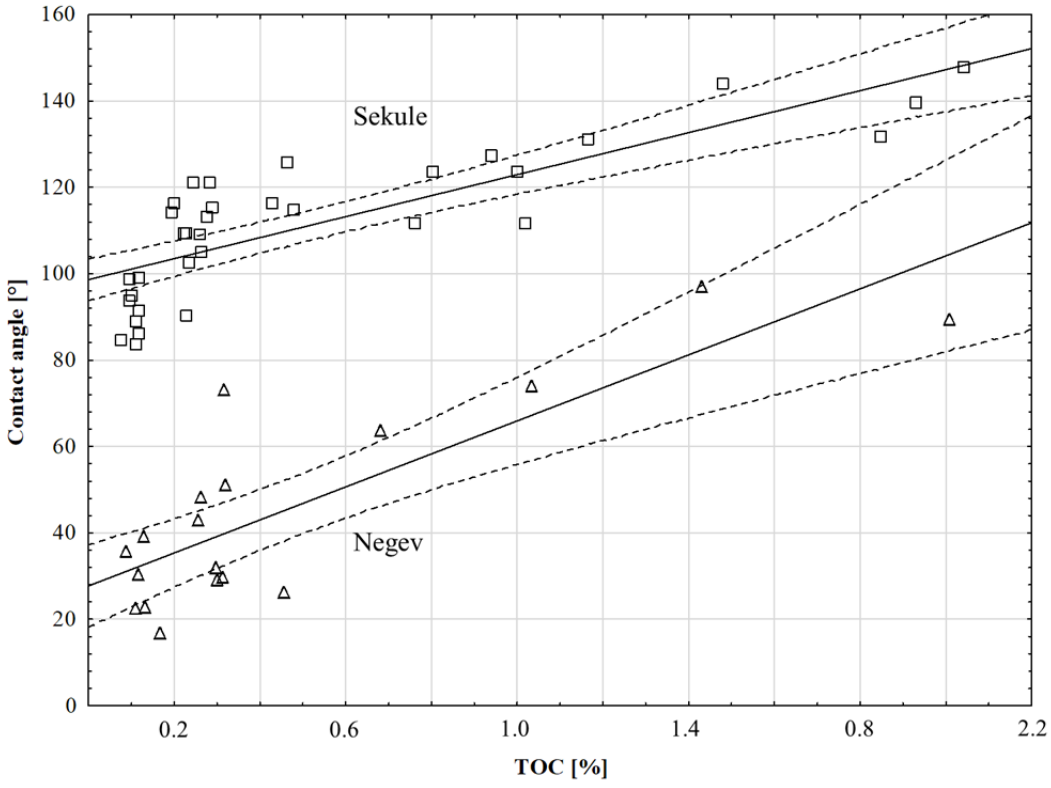

Fig. 3. Correlation between contact angle and amount of total organic carbon (TOC) for all samples at the study site Sekule (Slovakia; n = 34) and the Negev (Israel; n = 18). Dashed lines showing the regression bands (level of confidence 0.95).

changes in WR. We doubt this for the examined biocrusts as the changes between the study sites are very strong. As the correlation between H^+-concentration and TOC is very high (r = 0.75 / r = 0.91, Sekule/ Negev), it is not possible to separate the effect pH has on the detected WR. Nevertheless, at the Negev site, the amount of carbonates has a higher correlation with CA (r = 0.81) than the pH (r = –0.62). This indicates that the amount of carbonates has a higher effect on WR than the pH value. In our opinion, this highlights the more relevant second variable influencing the differences in WR between the study sites, namely texture. The Negev biocrusts are composed of a high amount of finer particles compared to Sekule biocrusts. In general, WR decreases with particle size (González-Peñaloza et al., 2013). In this study, the dunes at Sekule show significantly higher amounts of coarse and middle-sized sand grains, while the Negev biocrusts show significantly higher amounts of fine sized sand grains, fine particles (< 63µm) and carbonates (Table 1). First results on the particle size distribution of the fine fraction < 63µm show around 5% clay and up to 20% silt within this fraction (unpublished data). This material mix reduces WR effectively as shown by McKissock et al. (2000). Moreover, Harper et al. (2000) did show that more TOC was needed to induce WR in soils that have clay contents above 5%. In addition, the Negev biocrusts contain up to 7.3 (±1.1) weight-% carbonates (Table 1). This may have a direct effect on WR as well, as addition of powdered lime effectively reduced WR in soils during remediation trials (Roper, 2005).

Surface characterization of mineral particles separated from moss-dominated biocrust

No significant difference in the composition of organic fragments can be found in the mass spectra from Sekule and Negev (Figure 4). But for the inorganic compounds an increased intensity of Ca^+, Si^+, Mg^+ and Fe^+ was found for the sample from the Negev site. The higher detected amounts of Mg^+ and Fe^+ may have an influence on WR. Harper et al. (2000) found that these minerals reduce WR in soil samples. Moreover, in the Negev samples a higher content of $CaPO_3^-$ was detected in the negative ion mode. The higher Ca^+ and $CaPO_3^-$ signal intensity refers to an increased amount of Ca and most likely of $CaCO_3$ for the Negev sample. Unfortunately, carbonate fragments cannot be assigned specifically as there is an overlap of CO^-/Si^- and CO_3^-/SiO_2^-. Due to the sample roughness, the mass resolution is not sufficient to differentiate between these overlapping peaks. Nonetheless, the SiO_2^- signal is also significantly increased for the Negev sample, which is certainly due to the signal overlap of CO_3^- and SiO_2^-. This is supported by the higher C content of the Negev biocrust samples (Table 1) and accounts for a higher fraction of carbonate-bound C in the sample from the Negev site. Figure 4 shows exemplary mass images of particles from both sites in positive and negative ion mode. Beside the particular structure, the overlay of different mass signals shows clearly the heterogeneous composition of the surface layer. It can be seen that the organic fragments represented by CN^- and $C_3H_3O^+$ are only found in certain areas and hence, the sand grains are not completely covered by OM.

CONCLUSIONS

We compared the WR of two biocrusts types on carbonate-free and carbonate-containing sand dunes and examined the effect of OM, pH and carbonate content on WR. We conclude that the driving factor for the increase in WR within the individual sampling sites is the OM content and not the OM composition. However, this is only true for comparisons within one site, but not among sites. The high differences in potential WR between the study sites is related neither to OM amount, nor to changes in OM composition or organic coating characteristics. The most relevant factors explaining the lower WR in biocrusts of the Negev are the higher amounts of carbonates and the related higher pH values. Moreover, the Negev biocrusts show higher amounts of fine particles that are likely to reduce WR as well. As carbonates are destructed during the texture analysis, further studies are needed to identify the textural effect that carbonates may have on biocrusts' WR by increasing the amount of fine particles. This could be done by comparing the effect of siliceous vs. carbonate mineral particles of the silt fraction on the WR of different soils.

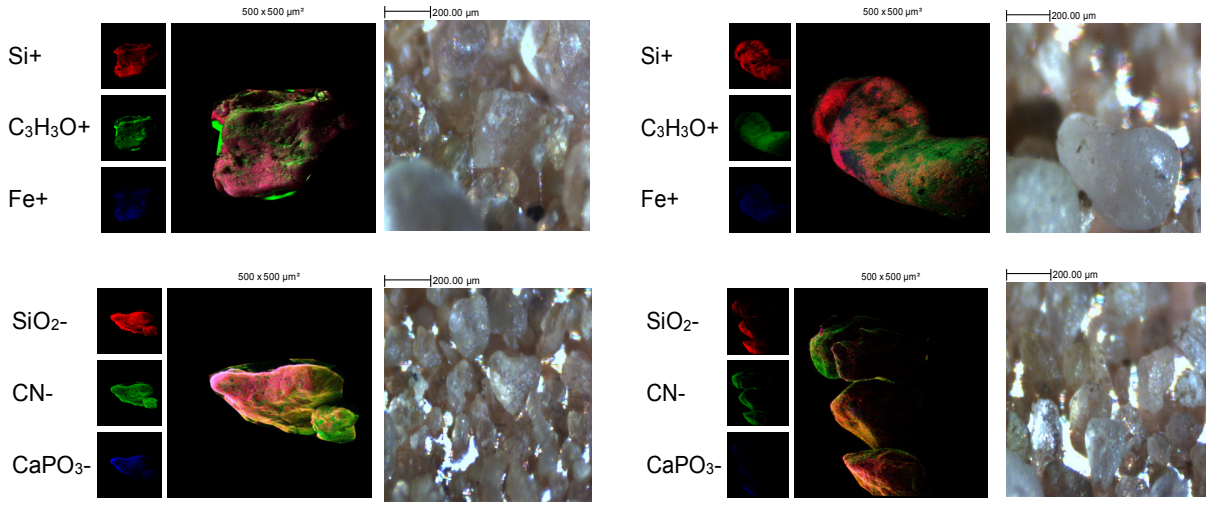

Fig. 4. Images of TC mineral particles from moss-dominated biocrusts (Negev site = left; Sekule site = right) show an overlay of the Si^+, $C_3H_3O^+$ and Fe^+ signal in positive ion mode and SiO_2^-, CN^- and $CaPO_3^-$ signals in the negative ion mode. The visualizations show the heterogeneous surface composition of the particles and proof that the organic crust (represented by $C_3H_3O^+$ and CN^- in green) is not covering the complete particle.

Acknowledgements. For partial funding, we thank the DFG (FE 218/14-1). Likewise, we are grateful for logistical support by S. Berkowicz (Hebrew University of Jerusalem) and L. Lichner (Slovak Academy of Sciences). In addition, we thank D. Steckenmesser, F. Jehn, E. Schneidenwind and E. Müller for the support during field and lab work.

REFERENCES

Arenas-Lago, D., Andrade, M.L., Vega, F.A., Singh, B.R., 2016. TOF-SIMS and FE-SEM/EDS to verify the heavy metal fractionation in serpentinite quarry soils. Catena, 136, 30–43.

Bachmann, J., Woche, S.K., Goebel, M.O., Kirkham, M.B., Horton, R., 2003. Extended methodology for determining wetting properties of porous media. Water Resour. Res., 39, 12, 1353.

Belnap, J., 2006. The potential roles of biological soil crusts in dryland hydrologic cycles. Hydrol. Process., 20. 15, 3159–3178.

Beraldi-Campesi, H., Hartnett, H. E., Anbar, A., Gordon, G. W., Garcia-Pichel, F., 2009. Effect of biological soil crusts on soil elemental concentrations: implications for biogeochemistry and as traceable biosignatures of ancient life on land. Geobiology, 7, 3, 348–359.

Bisdom, E., Dekker, L.W., Schoute, J., 1993. Water repellency of sieve fractions from sandy soils and relationships with organic material and soil structure. In: Brussaard, L., Kooistra, M.J.(Eds.): Soil Structure/Soil Biota Interrelationships. International Workshop on Methods of Research on Soil Structure/Soil Biota Interrelationsships, held at the International Agricultural Centre, Wageningen, the Netherlands, 1991. Elsevier, Amsterdam, pp. 105–118.

Cania, B., Vestergaard, G., Kublik, S., Köhne, J.M., Fischer, T., Albert, A., Winkler, B., Schloter, M., Schulz, S., 2020. Biological soil crusts from different soil substrates harbor distinct bacterial groups with the potential to produce exopolysaccharides and lipopolysaccharides. Microb. Ecol., 79, 2, 326–341.

Chamizo, S., Cantón, Y., Miralles, I., Domingo, F., 2012. Biological soil crust development affects physicochemical characteristics of soil surface in semiarid ecosystems. Soil Biol. Biochem., 49, 96–105.

Cliff, J.B., Gaspar, D.J., Bottomley, P.J., Myrold, D.D., 2002. Exploration of inorganic C and N assimilation by soil microbes with time-of-flight secondary ion mass spectrometry. Appl. Environ. Microbiol., 68, 8, 4067–4073.

Dekker, L.W., Doerr, S.H., Oostindie, K., Ziogas, A.K., Ritsema, C.J., 2001. Water repellency and critical soil water content in a dune sand. Soil Sci. Soc. Am. J., 65, 6, 1667–1674.

Dekker, L.W., Ritsema, C.J., 1994. How water moves in a water repellent sandy soil: 1. Potential and actual water repellency. Water Resour. Res., 30, 9, 2507–2517.

Diehl, D., Bayer, J.V., Woche, S.K., Bryant, R., Doerr, S.H., Schaumann, G.E., 2010. Reaction of soil water repellency to artificially induced changes in soil pH. Geoderma, 158, 3–4, 375–384.

Diehl, D., Ellerbrock, R.H., Schaumann, G.E., 2009. Influence of drying conditions on wettability and DRIFT spectroscopic C-H band of soil samples. Eur. J. Soil. Sci., 60, 4, 557–566.

Doerr, S.H., Shakesby, R.A., Walsh, R., 2000. Soil water repellency: its causes, characteristics and hydro-geomorphological significance. Earth-Science Rev., 51, 1–4, 33–65.

Drahorad, S., Felix-Henningsen, P., Eckhardt, K.-U., Leinweber, P., 2013a. Spatial carbon and nitrogen distribution and organic matter characteristics of biological soil crusts in the Negev desert (Israel) along a rainfall gradient. J. Arid Environ., 94, 18–26.

Drahorad, S., Steckenmesser, D., Felix-Henningsen, P., Lichner, Ľ., Rodný, M., 2013b. Ongoing succession of biological soil crusts increases water repellency — a case study on Arenosols in Sekule, Slovakia. Biologia, 68, 6, 1089–1093.

Drahorad, S.L., Jehn, F.U., Ellerbrock, R.H., Siemens, J., Felix-Henningsen, P., 2020. Soil organic matter content and its aliphatic character define the hydrophobicity of biocrusts in different successional stages. Ecohydrol., 13, 6, e2232.

Ellerbrock, R.H., Hoehn, A., Rogasik, J., 1999. Functional analysis of soil organic matter as affected by long-term manurial treatment. Eur. J. Soil. Sci., 50, 65–71.

Ellerbrock, R.H., Gerke, H.H., Bachmann, J., Goebel, M.-O., 2005. Composition of organic matter fractions for explaining wettability of three forest soils. Soil Sci. Soc. Am. J., 69, 1, 57.

Felde, V.J.M.N.L., Peth, S., Uteau-Puschmann, D., Drahorad, S., Felix-Henningsen, P., 2014. Soil microstructure as an under-explored feature of biological soil crust hydrological properties: case study from the NW Negev Desert. Biodivers. Conserv., 23, 7, 1687–1708.

Fischer, T., Veste, M., Schaaf, W., Dümig, A., Kögel-Knabner, I., Wiehe, W., Bens, O., Hüttl, R.F., 2010. Initial pedogenesis in a topsoil crust 3 years after construction of an artificial catchment in Brandenburg, NE Germany. Biogeochem., 101, 1–3, 165–176.

Fischer, T., Yair, A., Veste, M., Geppert, H., 2013. Hydraulic properties of biological soil crusts on sand dunes studied by 13C-CP/MAS-NMR: A comparison between an arid and a temperate site. Catena, 110, 155–160.

González-Peñaloza, F.A., Zavala, L.M., Jordán, A., Bellinfante, N., Bárcenas-Moreno, G., Mataix-Solera, J., Granged, A.J., Granja-Martins, F.M., Neto-Paixão, H.M., 2013. Water repellency as conditioned by particle size and drying in hydrophobized sand. Geoderma, 209–210, 31–40.

Graber, E.R., Ben-Arie, O., Wallach, R., 2006. Effect of sample disturbance on soil water repellency determination in sandy soils. Geoderma, 136, 1–2, 11–19.

Graber, E.R., Tagger, S., Wallach, R., 2009. Role of divalent fatty acid salts in soil water repellency. Soil Sci. Soc. Am. J., 73, 2, 541–549.

Gypser, S., Veste, M., Fischer, T., Lange, P., 2016. Infiltration and water retention of biological soil crusts on reclaimed soils of former open-cast lignite mining sites in Brandenburg, north-east Germany. J. Hydrol. Hydromech., 64, 1, 1–11.

Hagemann, M., Henneberg, M., Felde, V.J.M.N.L., Drahorad, S.L., Berkowicz, S.M., Felix-Henningsen, P., Kaplan, A., 2015. Cyanobacterial diversity in biological soil crusts along a precipitation gradient, Northwest Negev Desert, Israel. Microb. Ecol., 70, 1, 219–230.

Harper, R.J., McKissock, I., Gilkes, R.J., Carter, D.J., Blackwell, P.S., 2000. A multivariate framework for interpreting the effects of soil properties, soil management and landuse on water repellency. J. Hydrol., 231, 371–383.

Henss, A., Otto, S.-K., Schaepe, K., Pauksch, L., Lips, K.S., Rohnke, M., 2018. High resolution imaging and 3D analysis of Ag nanoparticles in cells with ToF-SIMS and delayed extraction. Biointerphases, 13, 3, 03B410.

Iovino, M., Pekárová, P., Hallett, P. D., Pekár, J., Lichner, Ľ., Mataix-Solera, J., Alagna, V., Walsh, R., Raffan, A., Schacht, K., Rodný, M., 2018. Extent and persistence of soil water repellency induced by pines in different geographic

regions. J. Hydrol. Hydromech., 66, 4, 360–368.
Jacobs, A.F., Heusinkveld, B.G., Berkowicz, S.M., 2000. Dew measurements along a longitudinal sand dune transect, Negev Desert, Israel. Int. J. Biometeorol., 43, 4, 184–190.
Jia, R., Gao, Y., Liu, L., Yang, H., Zhao, Y., 2020. Effect of sand burial on the subcritical water repellency of a dominant moss crust in a revegetated area of the Tengger Desert, Northern China. J. Hydrol. Hydromech., 68, 3, 279–284.
Keck, H., Felde, V.J.M.N.L., Drahorad, S.L., Felix-Henningsen, P., 2016. Biological soil crusts cause subcritical water repellency in a sand dune ecosystem located along a rainfall gradient in the NW Negev desert, Israel. J. Hydrol. Hydromech., 64, 2, 133–140.
Kidron, G.J., Büdel, B., 2014. Contrasting hydrological response of coastal and desert biocrusts. Hydrol. Process., 28, 2, 361–371.
Kidron, G.J., Vonshak, A., Abeliovich, A., 2009. Microbiotic crusts as biomarkers for surface stability and wetness duration in the Negev Desert. Earth Surf. Process. Landforms, 34, 12, 1594–1604.
Kidron, G.J., Xiao, B., Benenson, I., 2020. Data variability or paradigm shift? Slow versus fast recovery of biological soil crusts-a review. Sci. Total Environ., 721, 137683.
Kögel-Knabner, I., 2002. The macromolecular organic composition of plant and microbial residues as inputs to soil organic matter. Soil Biol. Biochem., 34, 2, 139–162.
Leelamanie, D.A.L., Karube, J., 2009. Effects of hydrophobic and hydrophilic organic matter on the water repellency of model sandy soils. Soil Sci. Plant Nutri., 55, 4, 462–467.
Letey, J., Carrillo, M.L.K., Pang, X.P., 2000. Approaches to characterize the degree of water repellency. Journal of Hydrology, 231, 61–65.
Lichner, L., Felde, V.J., Büdel, B., Leue, M., Gerke, H.H., Ellerbrock, R.H., Kollár, J., Rodný, M., Šurda, P., Fodor, N., Sándor, R., 2018. Effect of vegetation and its succession on water repellency in sandy soils. Ecohydrol., 11, 6, e1991.
Lichner, L., Hallett, P.D., Drongová, Z., Czachor, H., Kovacik, L., Mataix-Solera, J., Homolák, M., 2013. Algae influence the hydrophysical parameters of a sandy soil. Catena, 108, 58–68.
Lichner, Ľ., Holko, L., Zhukova, N., Schacht, K., Rajkai, K., Fodor, N., Sándor, R., 2012. Plants and biological soil crust influence the hydrophysical parameters and water flow in an aeolian sandy soil. J. Hydrol. Hydromech., 60, 4, 309–318.
Littmann, T., Schultz, A., 2008. Atmospheric input of nutrient elements and dust into the sand dune field of the northwestern Negev. In: Breckle, S.-W., Yair, A., Veste, M. (Eds.): Arid Dune Ecosystems. Springer, Berlin, Heidelberg, pp. 271–284.
Mataix-Solera, J., Arcenegui, V., Guerrero, C., Mayoral, A.M., Morales, J., González, J., García-Orenes, F., Gómez, I., 2007. Water repellency under different plant species in a calcareous forest soil in a semiarid Mediterranean environment. Hydrol. Process., 21, 17, 2300–2309.
McKissock, I., Walker, E., Gilkes, R., Carter, D., 2000. The influence of clay type on reduction of water repellency by applied clays: a review of some West Australian work. J. Hydrol., 231–232, 323–332.
Miralles, I., Ladrón de Guevara, M., Chamizo, S., Rodríguez-Caballero, E., Ortega, R., van Wesemael, B., Cantón, Y., 2018. Soil CO_2 exchange controlled by the interaction of biocrust successional stage and environmental variables in two semiarid ecosystems. Soil Biol. Biochem., 124, 11–23.
Morley, C.P., Mainwaring, K.A., Doerr, S.H., Douglas, P., Llewellyn, C.T., Dekker, L.W., 2005. Organic compounds at different depths in a sandy soil and their role in water repellency. Soil Res., 43, 3, 239.
Nierop, K.G., van Lagen, B., Buurman, P., 2001. Composition of plant tissues and soil organic matter in the first stages of a vegetation succession. Geoderma, 100, 1–2, 1–24.
Roper, M.M., 2005. Managing soils to enhance the potential for bioremediation of water repellency. Soil Res., 43, 7, 803.
Rozenstein, O., Zaady, E., Katra, I., Karnieli, A., Adamowski, J., Yizhaq, H., 2014. The effect of sand grain size on the development of cyanobacterial biocrusts. Aeol. Research, 15, 217–226.
Smidt, E, Lechner, P., Schwanninger, M., Haberhauer, G., Gerzabek, M. H., 2002. Characterization of Waste Organic Matter by FT-IR Spectroscopy: Application in Waste Science. Appl. Spectrosc., AS 56, 9, 1170–1175.
Tatzber, M., Stemmer, M., Spiegel, H., Katzlberger, C., Haberhauer, G., Gerzabek, M.H., 2007. An alternative method to measure carbonate in soils by FT-IR spectroscopy. Environ. Chem. Lett., 5, 1, 9–12.
Tighe, M., Haling, R.E., Flavel, R.J., Young, I.M., 2012. Ecological succession, hydrology and carbon acquisition of biological soil crusts measured at the micro-scale. PloS One, 7, 10, e48565.
Vickerman, J.S., Gilmore, I.S., (Eds.), 2009. Surface Analysis-Principal Techniques. 2nd Ed. John Wiley and Sons.
Vogelmann, E.S., Reichert, J.M., Prevedello, J., Consensa, C., Oliveira, A., Awe, G.O., Mataix-Solera, J., 2013. Threshold water content beyond which hydrophobic soils become hydrophilic: The role of soil texture and organic matter content. Geoderma, 209–210, 177–187.
Wang, X.Y., Zhao, Y., Horn, R., 2010. Soil wettability as affected by soil characteristics and land use. Pedosphere, 20, 1, 43–54.
Woche, S.K., Goebel, M.-O., Kirkham, M.B., Horton, R., van der Ploeg, R.R., Bachmann, J., 2005. Contact angle of soils as affected by depth, texture, and land management. Euro. J. Soil Sci., 56, 2, 239–251.
Zavala, L.M., González, F.A., Jordán, A., 2009. Intensity and persistence of water repellency in relation to vegetation types and soil parameters in Mediterranean SW Spain. Geoderma, 152, 3–4, 361–374.
Zheng, W., Morris, E.K., Lehmann, A., Rillig, M.C., 2016. Interplay of soil water repellency, soil aggregation and organic carbon. A meta-analysis. Geoderma, 283, 39–47.

Received 30 March 2021
Accepted 13 July 2021

J. Hydrol. Hydromech., 69, 2021, 4, 456–466
DOI: 10.2478/johh-2021-0023
ISSN 1338-4333

sciendo Journal of Hydrology and Hydromechanics

Relation of influencing variables and weather conditions on rainfall partitioning by birch and pine trees

Katarina Zabret[1, 2], Mojca Šraj[1*]

[1] University of Ljubljana, Faculty of Civil and Geodetic Engineering, Jamova 2, 1000 Ljubljana, Slovenia.
[2] Institute for Water of the Republic of Slovenia, Einspielerjeva 6, 1000 Ljubljana, Slovenia.
[*] Corresponding author. Tel.: +386 1 4768 684. E-mail: mojca.sraj@fgg.uni-lj.si

Abstract: General weather conditions may have a strong influence on the individual elements of the hydrological cycle, an important part of which is rainfall interception. The influence of general weather conditions on this process was analysed, evaluating separately the influence of various variables on throughfall, stemflow, and rainfall interception for a wet (2014), a dry (2015), and an average (2016) year. The analysed data were measured for the case of birch and pine trees at a study site in the city of Ljubljana, Slovenia. The relationship between the components of rainfall partitioning and the influential variables for the selected years was estimated using two statistical models, namely boosted regression trees and random forest. The results of both implemented models complemented each other well, as both indicated the rainfall amount and the number of raindrops as the most influential variables. During the wet year 2014 rainfall duration seems to play an important role, correlating with the previously observed influence of the variables during the wetter leafless period. Similarly, during the dry year 2015, rainfall intensity had a significant influence on rainfall partitioning by the birch tree, again corresponding to the influences observed during the drier leafed period.

Keywords: Throughfall; Stemflow; Rainfall interception; Rainfall microstructure; Boosted regression trees; Random forest.

INTRODUCTION

The hydrological cycle is altering due to climate change, as differences in global redistribution of precipitation and variations in seasonal precipitation patterns are observed (Inglezakis et al., 2016). This results in a significant reduction of precipitation in some parts of the world, while major variations in the timing and amount of precipitation per dry and wet season are expected elsewhere (Peng et al., 2021). The pronounced differences between the wet and dry periods significantly alter the water yield and the local water balance, the ecosystem services, the water availability for vegetation, leading to changed occurrences of floods and droughts (Bezak and Mikoš, 2014; Hungate and Hampton, 2012; Xu et al., 2020).

In the context of climate change, the relationship between the water balance and vegetation in dry and wet periods is increasingly recognized. In this aspect, various influences of different vegetation systems were studied. Vegetation is an important component, determining the ecosystem services, which were recognised to help mitigate the intensity of extremely dry and wet conditions expected in the future (Peng et al., 2021). An important contribution to the ecosystem services is also presented by the forest ecosystem affecting the global carbon budget. The different response of a forest ecosystem in wet and dry periods was analysed by Xiao et al. (2020), who concluded that in the dry season the precipitation generated significantly positive effects to the cumulative CO_2 emissions, while the soil respiration rate was mainly influenced by the fine root biomass regardless the season. An analysis of historical data from the tree rings was performed by Gao et al. (2020), who observed that the growth of trees was improved by wetness, suggesting that tree growth is more sensitive to wetness than the forest coverage. Wetter conditions may, on the contrary, reduce the carbon flux and evapotranspiration in steppe ecosystems, for which Hao et al. (2008) reported that both timing and frequency of rainfall events during the growing season significantly alter the capacity of steppe vegetation to uptake CO_2.

Forest ecosystems and trees in general also significantly influence the hydrological cycle through the process of rainfall interception (Dohnal et al., 2014; Klamerus-Iwan et al., 2020; Xu et al., 2013). Precipitation reaching the vegetation surface is distributed among the intercepted rainfall, which is captured by the canopy and eventually evaporates back into to the atmosphere, throughfall, which is described as the precipitation reaching the ground by dripping from the canopy or falling directly to the ground through the gaps in the foliage, and stemflow, presenting the water flowing to the ground down the branches and stems (Levia and Germer, 2015; Sadeghi et al., 2020; Staelens et al., 2008; Xiao et al., 2000; Yue et al., 2021; Zabret et al., 2018). Rainfall interception is influenced by vegetation and meteorological characteristics. Vegetation characteristics considered are mainly tree characteristics, such as the tree height and surface area (e.g., projected tree canopy), smoothness and absorbance of the bark, leaf area index, canopy coverage, and canopy storage capacity (Dohnal et al., 2014; Klamerus-Iwan et al., 2020; Xu et al., 2013; Zabret, 2013). According to the differences among the tree species, the different response of rainfall partitioning was analysed (Honda et al., 2014; Schooling and Carlyle-Moses, 2015). As characteristics of some tree species (e.g., deciduous trees) are substantially influenced by the phenoseasons (presence and absence of leaves in the tree canopy), the rainfall partitioning in leafed and leafless period has also been frequently studied, mainly in relation to the meteorological conditions (Brasil et al., 2020; Levia and Germer, 2015; Mużyło et al., 2012; Su et al., 2019; Zabret et al., 2018). Meteorological characteristics on the contrary explain the characteristics of rainfall events, for example the

rainfall amount, duration and intensity, air temperature and humidity, vapour pressure deficit and wind conditions (Andre et al., 2008; Staelens et al., 2008; Zabret and Šraj, 2019a). Although meteorological conditions are significantly associated with dry and wet periods, which influence the hydrological cycle, the influence of these two water-related conditions has been so far overlooked in the analysis of rainfall interception.

Rainfall interception is an important part of the hydrological cycle and is, due to the inclusion of trees, also one of the ecosystem services. The response of rainfall interception according to various influencing variables, type of rainfall events, and phenoseasons has been analysed; however, the process of rainfall interception associated with dry and wet periods has been neglected so far. As numerous researchers have observed the relationship between wet and dry periods and vegetation response to various natural processes, the main objective of the presented analysis is to investigate a possible influence of general weather conditions (e.g., wet and dry periods) on throughfall, stemflow, and rainfall interception. Extreme weather events are becoming more frequent due to climate change and the differences in water balance between dry and wet periods are increasing. As a result, the connections between climate variables and individual interception processes as well as the processes of the hydrological cycle are also different. There are not many studies with data sets long enough to capture wet and dry periods, therefore this is one of the important advantages of this study. Two statistical methods, namely boosted regression trees and random forest, were used to evaluate the influence of meteorological variables on rainfall partitioning components during wet, dry, and average years. Such statistical methods are seldom used for analysis of rainfall interception data, although the application of such methods can give us a new, different insight into the data and the connections between them. Additionally, the study of different tree species is very important in the field of interception, as these results cannot be generalized.

MATERIAL AND METHODS

Study site

The study site is located in the outskirt of the city of Ljubljana, Slovenia (46.04° N, 14.49° E). The area has typical sub-alpine climate with well-defined seasons and is characterized by Temperate oceanic climate (Cfb) according to the Köppen Climate Classification. The long-term analysis of the meteorological data was prepared taking into account the data collected at the Ljubljana Bežigrad meteorological station between years 1986 and 2016 (ARSO, 2020). The average air temperature for the area was equal to 10.5 °C. Generally, the lowest temperatures are observed during January (–0.1 °C on average), while the warmest is July (20.8 °C on average). The average long-term air temperature in winter was 0.8 °C, in spring and autumn 10.7 °C, and in summer 19.9 °C. The average amount of rainfall delivered per year in the analysed period was 1355 mm. The driest year was observed to be 2011, characterized by 998 mm of rainfall, while the wettest year was 2014, delivering 1851 mm of rainfall in total. The most rainfall is in general delivered during the autumn months (around 30% of total yearly rainfall), while winter is the driest period, also because snow precipitation is observed instead of rainfall in the colder part of the year.

The study plot is part of a small urban park, located between educational and business buildings. The research plot itself spans over 600 m^2 and is covered with regularly mowed grass. In its western part there are two separated groups of trees, while in the east side there is a clearing. One group of trees in the southern part consists of birch trees (*Betula pendula* Roth.), which are on average 15.7 m high and have a total projected crown area of 17.9 m^2 and a diameter at breast height of 17.9 cm. Their branches grow upwards, and its bark is smooth and thin with a bark storage capacity estimated to be 0.7 mm (Zabret and Šraj, 2021). Birch is a deciduous tree species with distinct phenoseasons, which were determined according to the observations of the tree canopy at the field and complemented with leaf area index (LAI) measurements, using LAI-2200c Plant Canopy Analyzer (LI-COR). In general, the leafless phenoseason was observed between October and April, when LAI was on average 0.8 and the canopy storage capacity was 1.1 mm. The leafed phenoseason was observed between April and October, when LAI was equal to 2.6 and the canopy storage capacity increased to 3.5 mm. The group of the trees on the northern part of the plot are pine trees (*Pinus nigra* Arnold). They are on average 12.6 m high, have an average diameter at breast height of 19 cm, and a total projected crown area of 22.7 m^2. The bark surface is rough, the bark itself is thick and more absorbent with an estimated storage capacity of 3.5 mm. The branches are inclined downwards. As pine is a coniferous tree species, phenoseasons are not influencing the canopy characteristics to such an extent as in the case of birch trees. However, LAI in winter is 3.4 and the canopy storage capacity was estimated to be 2.7 mm, while in the summer time, LAI is 4.3 and the canopy storage capacity 2.9 mm.

Measurements

The components of rainfall partitioning have been measured at the study plot since the beginning of 2014 (Zabret and Šraj, 2021; Zabret et al., 2018). Measurements of throughfall and stemflow were performed under both groups of trees, while rainfall in the open was measured on the clearing at the study plot and at the nearby rooftop (Zabret, 2013; Zabret and Šraj 2019a; Zabret and Šraj, 2021). Values of other meteorological characteristics (wind speed and direction, air temperature and humidity) were obtained from the Ljubljana Bežigrad meteorological station (ARSO, 2020), which is because of its location representative for the whole Ljubljana basin (Nadbath, 2008).

Measurements of throughfall were performed both automatically and manually. Under each group of trees there were two fixed steel trough gauges (0.75 m^2) positioned from the tree trunk towards the edge of the canopy. One was equipped with a tipping bucket flow gauge (Unidata 6506G, 50 mL/tip) and a data logger (Onset HOBO Event), while the other one was connected to 10 L and 50 L polyethylene containers, which were manually emptied after each event. Under each group of trees there were also 10 funnel-type gauges (78.5 cm^2, 1-L capacity), manually emptied after each event and occasionally moved under the trees to capture the spatial variability of throughfall. These collectors were moved after every 20 events in a random pattern under the canopy. Throughfall values used in the analysis were determined as the weighted average according to all the collectors' area used.

Stemflow was measured per one tree from each group. The halved rubber collar was spirally wrapped around the tree trunk and attached with silicone and nails. In case of a pine tree the water was collected in a manually read 1-L container at the bottom of the tree, which was emptied at the same time as the throughfall collectors. In case of a birch tree, the stemflow was automatically recorded, as the hose from the collar was connected to a tipping bucket flow gauge (Onset RG2-M, 0.2 mm/tip) and a data logger (Onset HOBO Event).

Rainfall was measured at two locations, at the clearing approximately 10 m from the nearest tree canopy and at the nearby rooftop, approximately 45 m from the treetops. Rainfall at the clearing was measured with a tipping bucket rain gauge (Onset RG2-M, 0.2 mm/tip), connected to the data logger (Onset HOBO Event). Rainfall on the rooftop was measured with a disdrometer (OTT Parsivel), enabling also measurements of rainfall microstructure, i.e. raindrop diameter, raindrop velocity, and the number of raindrops. The measuring area of the disdrometer is 54 cm^2 and the measured data are allocated to one of the 32 drop diameter classes (ranging from 0.312 mm to 24.5 mm) and 32 velocity classes (ranging from 0.05 m/s to 20.8 m/s). The drop diameters smaller than 0.312 mm were assigned to the smallest drop diameter class, as they are outside the device's measurement range. The recorded time series data from the rain gauge and the disdrometer were used to identify the rainfall events (separated with at least a 4-hour dry period) and their characteristics (duration and intensity). The 4-hour dry period was selected to divide the events based on the observations of the rainfall and throughfall dynamics at the field, as during the wetter time of the year throughfall lasted for quite some time after the cessation of the rainfall. Shorter rainfall interruptions were captured as part of the defined events. The dry period was defined with an accuracy of 0.2 mm of rainfall (equal to the volume of the rain gauge tipping bucket).

The tree characteristics were determined in individual surveys. The photographs of the trees were taken at a required distance to avoid deformation of proportions and were used to determine the tree height, the area of the projected canopy, and the branch inclination. The diameter at breast height was calculated from the measured perimeter of the stem. The bark storage capacity was determined from the bark samples, extracted using a steel hole puncher, according to the procedure described by Perez-Harguindeguy et al. (2013). Phenoseasons were determined based on the regular measurements of LAI, performed with LAI-2200c Plant Canopy Analyzer (LI-COR) following the protocol for isolated trees (Li-COR, 2015). The canopy storage capacity was calculated from the observed rainfall and throughfall data according to the Leyton graphical method (Leyton et al., 1967).

Data analysis

Measured data of rainfall precipitation (P), throughfall (TF), and stemflow (SF), collected in years 2014, 2015, and 2016, were used in the analysis. Based on these data, the third component of rainfall partitioning, i.e. rainfall interception (I), was calculated for each event:

$$I = P - TF - SF \quad (1)$$

In the selected period, 413 rainfall events were observed in total, but not all of them were included in the analysis. Snow and sleet events were excluded in the initial phase, while during the further preparation of the data, the events without complete time series on rainfall, throughfall, and stemflow due to clogging of the measurement equipment were also excluded. Therefore 365 rainfall events were taken into account in the analysis, capturing 86% of the total rainfall, delivered in the analysed period. Additionally, the disdrometer was not operational due to a software error for a longer time period during 2015. Therefore, rainfall microstructure data were not included in the analysis for this year.

For the selected rainfall events, the influence of the variables describing general weather conditions was evaluated using two similar statistical methods, namely general boosted regression trees (BRT) and random forest (RF). Both models are based on the method of the regression trees, however the way of upgrading them differs for each method. Two methods were selected for the analysis as a combination of several methods allows the verification of the results of an individual method and enables a broader interpretation of the results. The regression tree model is designed by repeating the divisions of the influential variables and by adapting a simple prediction model for the target variable within each division. The result of the division process is shown graphically with a decision or regression tree (Loh, 2011; Zabret et al., 2018). As a target variable, throughfall (TF), stemflow (SF), and rainfall interception (I) were set. Each model was run six times per observed year (namely, 2014, 2015, and 2016), once per each target variable, taking into account all influential variables and also the variables without data on the rainfall microstructure due to the longer period without available data (year 2015 was excluded). The influential variables included in the analysis (Table 1) were the total rainfall amount per event (P_a), the average rainfall event intensity (P_i), the total duration of the rainfall event (P_d), the average air temperature (T), and the vapour pressure deficit (VPD) during an event, the average wind speed (W_s) and the direction (W_d) per event, the dry period duration before a rainfall event ($DryP$), the time when an event occurred, namely during the day, the night, or both (DN), the phenoseason ($Feno$), the average raindrop diameter ($DropD$), the velocity ($DropV$) per event, the median volume diameter of an event's raindrops (MVD), and the number of raindrops delivered per event ($DropNr$).

Table 1. Influential variables included in the analysis.

Variable	Abbreviation	Unit
Rainfall amount per event	P_a	mm
Average rainfall event intensity per event	P_i	mm/h
Total duration of the rainfall event	P_d	h
Average air temperature during the event	T	°C
Average vapour pressure deficit during the event	VPD	kPa
Average wind speed during the event	W_s	m/s
Average wind direction during the event	W_d	°
Dry period duration before the rainfall event	$DryP$	h
Time when the event occurred, namely during the day, the night, or both	DN	–
Phenoseason	$Feno$	–
Average raindrops diameter of the drops, observed during the event	$DropD$	mm
Average raindrops velocity of the drops, observed during the event	$DropV$	m/s
Median volume diameter of an event's raindrops	MVD	mm
Number of raindrops delivered per event	$DropNr$	–

The BRT method combines two algorithms, regression trees and boosting (Elith et al., 2008), which improve the efficiency of an individual model and provide a better understanding of the results with additional factors. Boosting is based on the assumption that the average of many raw predictions, which are upgraded after every single repetition, will result in a better final model. The sequential approach of the step-by-step meth-

od iteratively adjusts and improves the model based on a set of training data (Elith et al., 2008). Due to the larger number of model runs, it is also possible to estimate the impact of an individual variable on the design of the model and thus on the target variable. Friedman (2001) presented an equation that can be used to estimate the relative influence (RI) of each variable included in the BRT model. The RI is based on how many times a variable has been selected in the model to divide the regression tree. The number of selections is weighted by the square of the model improvement rate as a result of each split and expressed as an average with respect to all generated regression trees (Friedman and Meulman, 2003). The RI is adjusted so that the sum of the RI values of all considered variables equals 100, making the higher values directly indicating a greater influence of the variable.

The BRT models were implemented using the "gbm" package (Ridgeway, 2020) in R software (R core team, 2020). In the initial phase we determined the arguments of the model, using 75% of the whole data set for training and 25% of the data for testing of the model, implementing 50 iterations for each set of the arguments and calculating the RMSE value of predictions from all iterations. When adjusting the model, various number of regression trees (15000, 1500, and 500) and values of the shrinkage parameter (0.001, 0.01, 0.05) were applied. According to the results, the final BRT models were estimated, taking into account the Gaussian distribution, 1500 trees, a shrinkage parameter of 0.01, and 5 cross-validation folds.

Random Forest (RF) is an ensemble-learning algorithm, which merges the concepts of regression trees and bagging (Breiman, 2001). Bagging is a procedure enabling growing of regression trees from different subsets in order to avoid highly correlated predictors. This algorithm relies on random selection of trees to describe the reliable relationship between the target and the influential variables. Cases are randomly selected from a data set, a random sample is used to design an individual regression tree, and predictions are formed for the remaining cases. The model repeats this process several times. Randomness is additionally ensured by imposing different randomly selected sets of influential variables on each division. This is possible due to random and repeated selection of individual target values and influential variables (Breiman, 2001). For each variable the variable importance measure is also estimated (Breiman et al., 2018). The variable importance gives the total decrease in node impurities from splitting on the variable, averaged over all trees. In case of regression, as presented here, it is measured by the residual sum of squares.

The RF models were built in R software (R core team, 2020), using package "RandomForest" (Breiman et al., 2018). In the first phase of the model establishment, we divided the data set into a training (75%) and test (25%) set. The model arguments were selected one by one, applying numerous iterations for each of the 30 models. For the number of variables randomly sampled as candidates at each split (mtry), the values between 10 and 40 were tested, using the "tune" function. The maximum number of terminal nodes of the trees (maxnode) was applied for the values between 5 and 30, while the number of the trees to grow (n.trees) was tested for values between 250 and 5000. For these two arguments the best value was selected according to the RMSE and R^2 values of the iteration results.

RESULTS

The analysed data on rainfall partitioning were collected during the years 2014, 2015, and 2016. These years were hydrologically quite distinct, as according to the long-term average annual precipitation, 2014 was recognised as a wet, 2015 as a dry, and 2016 as an average year. During 2014 we registered 167 events, delivering 1575 mm of rainfall. For this year, the total rainfall amount (1841 mm) was 36% larger than the average long-term yearly rainfall amount of 1355 mm measured at the Ljubljana-Bežigrad meteorological station. On the contrary, in 2015, we recorded 85 events, delivering 931 mm of rainfall. The total delivered rainfall (1106 mm) was 18% smaller than the long-term average rainfall amount per year (1355 mm). Furthermore, the year 2016 was similar to an average one, as we observed 113 rainfall events delivering 1139 mm of rainfall. Through the entire year, 1317 mm of rainfall was measured, which is comparable to a long-term average precipitation of 1355 mm at the Ljubljana-Bežigrad meteorological station. Although during the dry year 2014 the largest number of the rainfall events were recorded, they on average delivered the smallest amount of rainfall per event (9.4 mm) and on average lasted for the shortest time (5.7 h), but were on average the most intense (2.1 mm/h) (Figure 1). The average rainfall intensity and duration of rainfall events during the years 2015 and 2016 were similar (average intensity of 1.4 mm/h and 1.5 mm/h, respectively and average duration of 8.0 h and 8.1 h, respectively); however, the events in the dry year 2015 delivered on average more rainfall (11.0 mm) than the events in the average year 2016 (10.1 mm per event on average).

Comparing the climate conditions in the considered years only slight differences were observed for the wind characteristics, vapour pressure deficit, and air temperature. However, a noticeably shorter dry period between the events was observed in the wet year 2014 (40 h on average) comparing to the years 2015 and 2016 (58 h and 56 h, respectively). The rainfall events characteristics in the considered years also differ according to the rainfall microstructure. The size of the rainfall drops was significantly different ($p < 0.001$) during the wet year 2014 comparing to the years 2015 and 2016, as in the year 2014 an average raindrop diameter was equal to 0.85 mm and *MVD* was equal to 1.79 mm, while during the years 2015 and 2016 the drop diameter on average accounted to 0.67 mm and 0.62 mm and *MVD* to 1.51 and 1.44 mm, respectively. However, the larger raindrops resulted in the smaller number of drops per event, as the lowest number of raindrops was on average detected in the wet year 2014 (Figure 1).

The values of rainfall partitioning components were quite similar for the years 2014 and 2016, while some deviations are observed for the values measured in 2015, when higher values of throughfall and stemflow proportions according to the rainfall in the open were observed (Figure 2). In general, over all three observed years, throughfall under the birch tree was on average equal to 53% (± 34%), average stemflow was 1.2% (± 2.5%), and average rainfall interception was 46% (± 35%). Throughfall under the pine tree was on average lower than under the birch tree, resulting in 27% (± 26%) of rainfall in the open, while stemflow accounted for only 0.03% (± 0.10%) and the rainfall interception by the pine tree on average presented 73% (± 26%) of rainfall in the open.

Influence of the rainfall event characteristics on throughfall

Both of the applied models, namely BRT and RF, indicate that throughfall under the birch trees is influenced by the larger number of variables than throughfall under the pine trees, regardless the year (Figure 3). Throughfall (TF) under the birch trees in the wet year 2014 was the most dependent on the rainfall amount (P_a) and intensity (P_i), rainfall duration (P_d), and the average vapour pressure deficit (*VPD*) during the rainfall

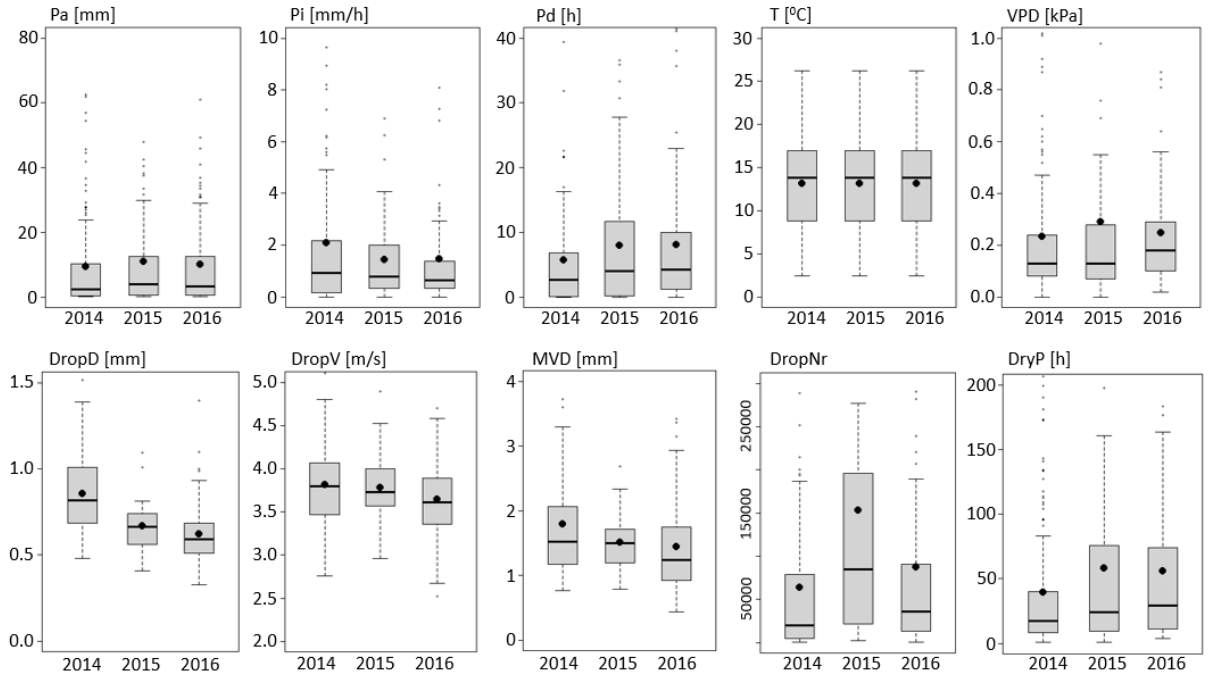

Fig. 1. Boxplots of considered rainfall event characteristics for each analysed year.

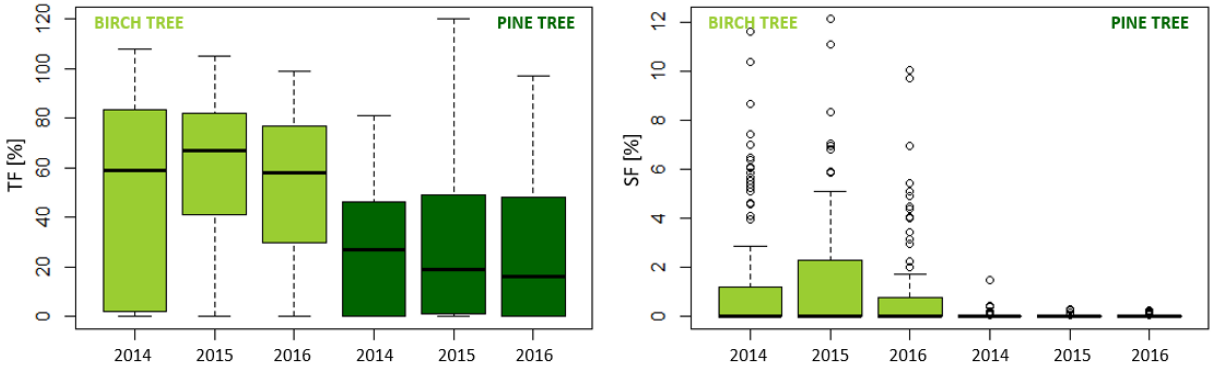

Fig. 2. Measured throughfall (TF) and stemflow (SF) by birch and pine trees per rainfall event according to the observed year.

event (Figure 3). Rainfall amount and intensity demonstrated between 18% and 20% of relative influence (RI) each by both applied methods, while RI for the first four most influential variables exceeded 60% in total. However, when taking into account also the variables describing the rainfall microstructure, the number of raindrops (*DropNr*) became the most influencing variable, indicating the amount of throughfall by birch in the wet year 2014.

For the throughfall under the birch trees during the dry year 2015, both models assigned a similar relative influence of almost 30% to rainfall intensity, indicating this variable as the most significant in addition to the rainfall amount. The BRT model also recognized air temperature and vapour pressure deficit as the influential variables with RI of 10%, while the random forest model assigned more than 8% of RI to rainfall duration and wind speed (W_s) (Figure 3).

The data collected during the average year 2016 showed a significant influence of the rainfall amount only, as it represented almost 40% of RI according to the BRT model and more than half of the total RI expressed by RF model. More than 9% of RI was assigned also to wind speed and vapour pressure deficit according to the BRT method and to air temperature and wind speed according to the RF model. In case of data for 2016, the inclusion of rainfall microstructure variables does not affect the order of the influencing factors (Figure 3). As the most influencing variable, the rainfall amount is still recognised by both applied models, however the second most influencing variable, having a similar value of RI, is the number of raindrops. In this case both variables together represent 45% and 60% of RI according to the BRT and RF model, respectively.

The number of influencing variables according to the dominant value of the relative influence in the case of throughfall under the pine tree is more straightforward (Figure 3). Rainfall amount was recognized to be the most influencing variable regardless the year, with an average RI between 43% (RF for 2014) and 82% (RF for 2016). Both models also recognized the influence of rainfall intensity and duration on throughfall by pine trees in 2014, while in 2015, more than 8% of RI was assigned to wind speed. In 2016, in addition to the rainfall duration air temperature was the second most influencing variable with RI larger than 5%. None of the rainfall microstructure variables exceeded more than 6% of RI, regardless the applied model or the year observed in case of throughfall under the pine trees.

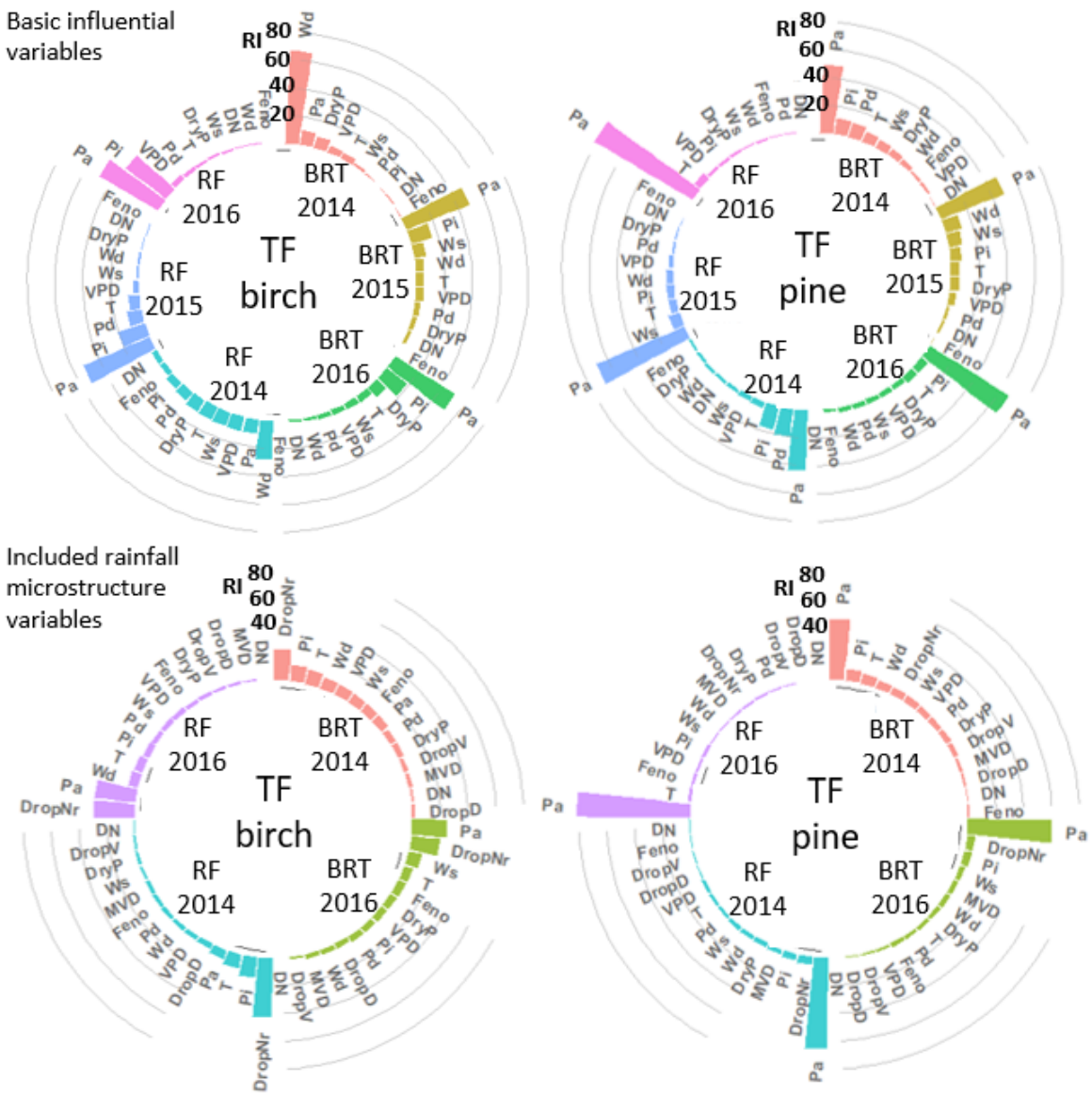

Fig. 3. Relative influence (RI) of the considered variables for throughfall (TF) by the birch and pine trees according to the observed years, evaluated by the boosted regression trees (BRT) and random forest (RF) models.

Influence of the rainfall event characteristics on stemflow

Similarly as throughfall, stemflow is in general the most influenced by the rainfall amount (Figure 4). Stemflow (SF) by the birch tree was the most characterized by the rainfall amount regardless the year as the RI for this variable ranged between 35% (RF, year 2014) and 61% (RF, year 2015). Stemflow by the birch tree in the wet year 2014 and the average year 2016 was also highly influenced by the rainfall duration, which had the second highest RI in both years, regardless the model used.

On the contrary, in the dry year 2015 stemflow by the birch tree was affected by a larger number of variables (Figure 4). The BRT model indicated that in addition to the rainfall amount, stemflow by the birch tree is also influenced by rainfall intensity, wind speed, vapour pressure deficit, and rainfall duration, as RI for all mentioned variables was larger than 9% (Figure 4). However, according to the RF model, the value of RI higher than 10% was estimated for the dry period duration and air temperature.

When taking into account also the rainfall microstructure characteristics, the rainfall amount is still one of the most influencing variables, combined with the number of raindrops. Stemflow in the wet year 2014 is still the most influenced by the rainfall amount, while the number of raindrops and *MVD* were also recognized as more influential. However, for stemflow in 2016, the number of raindrops together with the rainfall amount and duration were recognized as the variables with the highest RI (together accounting for 59% according to the BRT and 82% according to the RF model).

The amount of stemflow by the birch trees was similarly influenced during the years 2014 and 2016, however for the pine trees similarities can be observed between the years 2015 and 2016 (Figure 4). Stemflow by the pine trees during 2014 was the most influenced by wind direction, followed by the rainfall amount. In case of the BRT model these two variables resulted in RI of 77%, while in case of the RF model, the influencing variables with RI of more than 10% are also vapour pressure deficit, wind speed, and air temperature.

When also including the rainfall microstructure variables, the influence of wind direction is minimized, as rainfall amount, duration, and the number of raindrops in combination with *MVD* (estimated by the BRT model) and air temperature

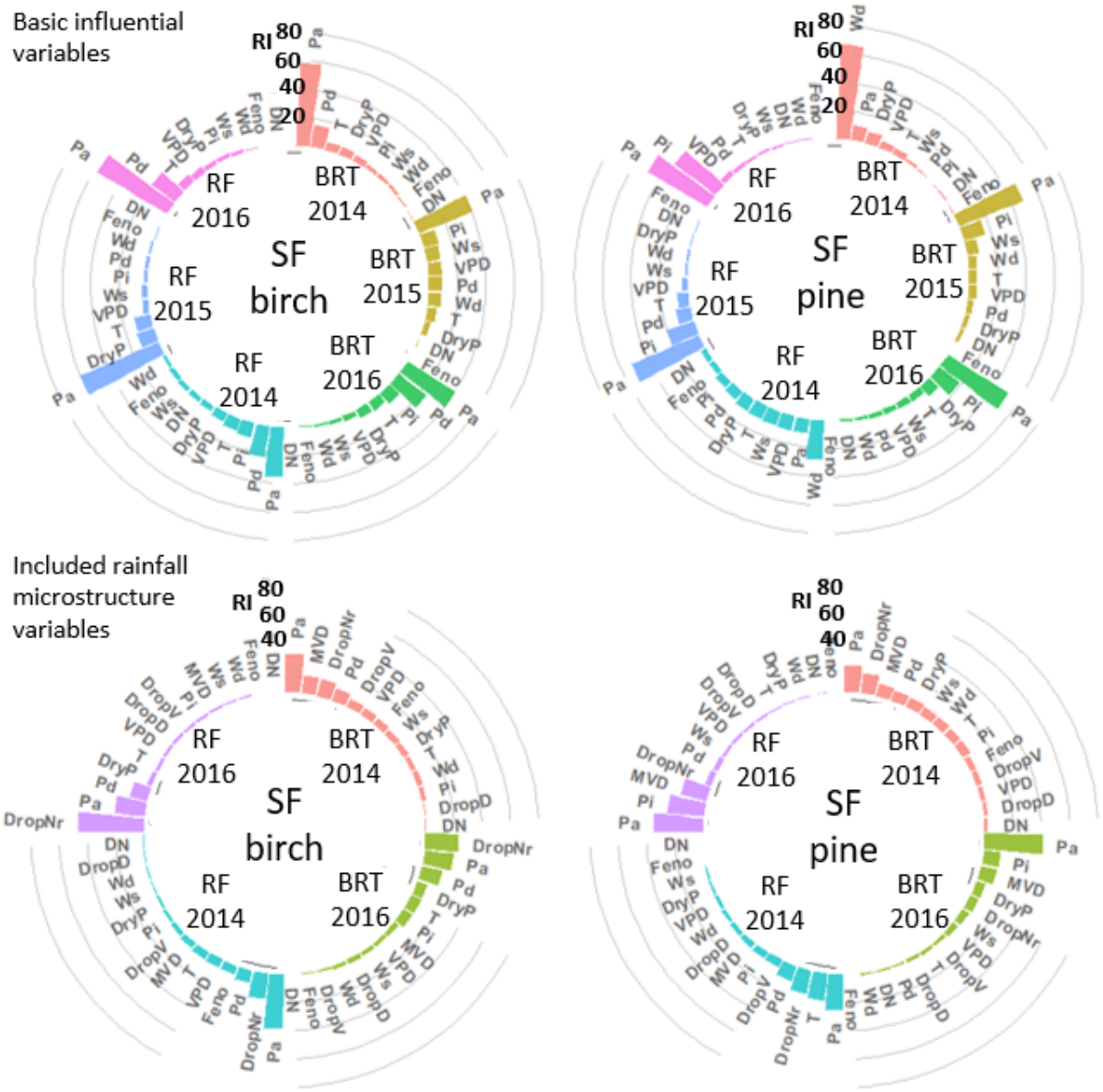

Fig. 4. Relative influence (RI) of the considered variables for stemflow (SF) by the birch and pine trees according to the observed years, evaluated by the boosted regression trees (BRT) and random forest (RF) models.

(estimated by the RF model) resulted in RI higher than 50%. Stemflow by the pine trees in 2015 and 2016 is significantly influenced by the rainfall amount and intensity, as regardless the model or the year, these two variables present between 64% and 85% of RI. The substantial influence of the rainfall amount and intensity is also retained when introducing the rainfall microstructure influence. In this case, as the second most influencing variable with RI larger than 10% both models recognised *MVD*.

Influence of rainfall event characteristics on rainfall interception

Rainfall interception (I) is calculated as the difference between the measured values, i.e. rainfall amount in the open, throughfall, and stemflow (Eq. 1). Therefore, as the amount of throughfall is much larger than stemflow, this is the value that mainly determines the proportion of intercepted rainfall, resulting in similarly evaluated influencing variables as throughfall (Figure 3).

Rainfall interception by birch and pine trees is the most influenced by the rainfall amount, which has the highest values of RI according to both models. In case of the birch trees the values of RI for the amount of rainfall ranged between 22% and 63%, while in case of the pine trees they were even higher, ranging from 47% to 83%. Comparing these values to RI estimated for throughfall, the values were a bit larger in case of the birch trees, while for the pine trees they were kept in a similar range.

Rainfall interception of the birch trees was in the wet year 2014 also significantly influenced by the rainfall duration and intensity, while in the dry year 2015 it was mainly influenced by rainfall intensity and in the average year 2016 by vapour pressure deficit (according to the BRT model) and air temperature (according to the RF model). In case of the pine trees the results were also very similar to the ones for the throughfall; in 2015 and 2016 only the rainfall amount played a significant role in the process of rainfall interception, while in the wet year 2014 also rainfall intensity and duration demonstrated RI values larger than 10% (Figure 5).

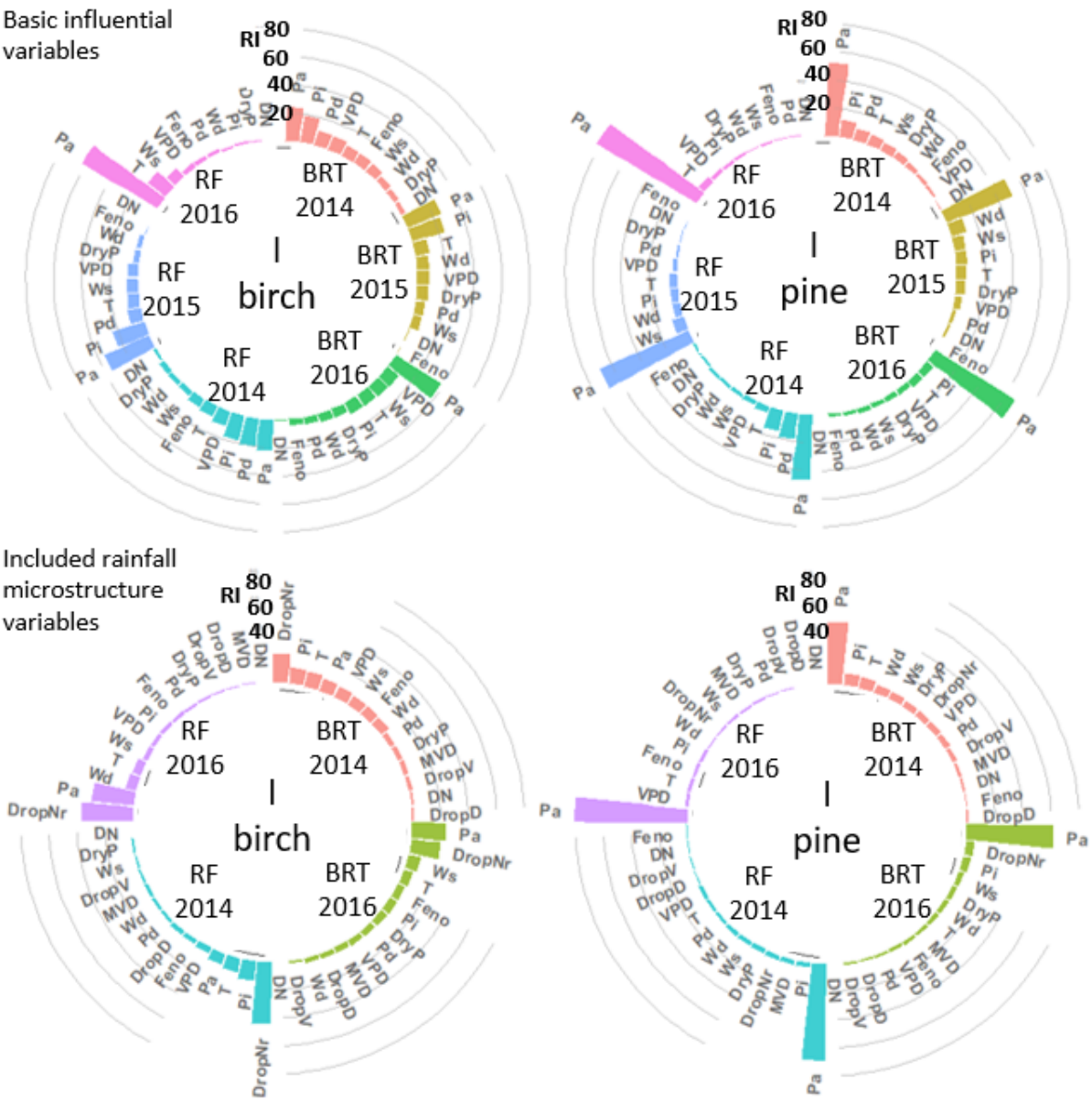

Fig. 5. Relative influence (RI) of the considered variables for rainfall interception (I) by the birch and pine trees according to the observed years, evaluated by the boosted regression trees (BRT) and random forest (RF) models.

The results of both applied models considering also the rainfall microstructure are also similar to the results of throughfall data analysis (Figure 3). In case of the birch trees, the number of drops was recognised as a variable with the highest influence among the newly introduced variables, while in case of the pine trees for none of these variables the estimated RI exceeded 6% (Figure 5).

DISCUSSION

Although the two methods are very similar as they are both based on the principle of regression trees, there is one main difference if we consider the method associated with the regression trees (boosting and bagging). This is also reflected in the estimation of the most influential variables and their RI values. A comparison of the results by the two models shows that in general, the RI values of the variables estimated by the RF model are higher than those estimated by the BRT model (Figures 3–5). Therefore, the number of the variables for which the RI value exceeds the threshold value is larger when taking into account results of the BRT instead of the RF model. Thus, the combined analysis of the two methods allows for a more comprehensive evaluation of the results, as the RF model indicates the most influencing variables, while the BRT model highlights also the other possible variables with meaningful influence.

The results demonstrate that throughfall, stemflow, and rainfall interception by birch and pine trees were the most influenced by the amount of rainfall, which has been repeatedly recognized as the factor most influencing the rainfall partitioning components in general also in other studies (e.g., Levia and Germer, 2015; Staelens et al., 2008; Su et al., 2019; Zabret et al., 2018). In case of both considered tree species, rainfall duration seems to play an important role mainly during the wet year 2014, while rainfall intensity had a significant influence on rainfall partitioning by birch trees during the dry year 2015. This observation seems to correlate well with the results presented by Mużyło et al. (2012), who observed a significant influence of rainfall duration on throughfall in a deciduous forest, especially during the leafless season. The leafless season is usually characterized by more precipitation and generally

wetter months, which may be equivalent to the hydrologically wetter year of 2014, in which a more pronounced influence of rainfall duration was observed in this study (Figures 3–5).

As the wetter year 2014 can be correlated with the wetter leafless phenoseason, the drier year 2015 is expected to be associated with the drier leafed period. Therefore, the influence of rainfall intensity on rainfall partitioning in the drier year 2015 is initially unexpected. Rainfall intensity was actually recognized as one of the most influential variables in previous studies, but its effect was observed for winter throughfall (Xiao et al., 2000), rainfall interception in the leafless period (Zabret et al., 2018), and rainfall interception in a wet year (Zabret and Šraj, 2019b). However, for a beech tree, Staelens et al. (2008) reported significant influence of rainfall intensity on stemflow, especially during the leafed period resulting in a decrease in the stemflow amount due to splashing of droplets intercepted by the canopy and forming throughfall instead of stemflow. Additionally, a more evident influence of rainfall intensity was estimated by both applied models for birch rather than for pine trees (Figures 3–5). A different influence of rainfall intensity on tree species with distinct vegetation properties was already observed in other analyses (e.g., Sadeghi et al., 2020; Siegert and Levia, 2014; Zabret et al., 2018). Birch trees have a smoother bark surface and more flexible leaves compared to the rougher and more absorbent bark of pine trees and its compact needles, therefore the process of splashing of intercepted droplets may be more intense in the canopy of the birch trees.

The relative influence, estimated by the BRT and RF models, shows that throughfall under the birch trees is determined by a larger number of influencing variables. In addition to the rainfall amount, duration, and intensity, also air temperature and vapour pressure deficit (*VPD*) were assigned with values of RI larger than 8%. Air temperature and *VPD* are closely connected to the season of the year, corresponding also to the phenoseasons, and are especially significant for a deciduous birch trees (Zabret et al., 2018). Therefore, the significant RI values of air temperature and *VPD* may indirectly indicate the influence of phenoseasons on throughfall by birch, which is larger in the leafless period, characterized by lower air temperature and lower *VPD* values (Andre et al., 2008; Brasil et al., 2020; Mużyło et al., 2012; Šraj et al., 2008; Zabret and Šraj, 2018; Zabret et al., 2021). However, the relation between the influence of phenoseasons and meteorological variables on rainfall partitioning has already been recognized as a very complex one (e.g., Andre et al., 2008; Mużyło et al., 2012; Zabret and Šraj, 2021). When analysing the influence of air temperature and *VPD* on throughfall by the birch tree, the results are similar among the years (Figure 6). Throughfall is in general decreasing with increasing air temperature, which was observed also by Staelens et al. (2008). Warmer months of the year are also characterized with a fully leafed canopy, also decreasing the throughfall, while a higher air temperature increases the evaporation, which may also lead to a decrease in throughfall (Šraj et al., 2008; Xiao et al., 2000). However, the response of

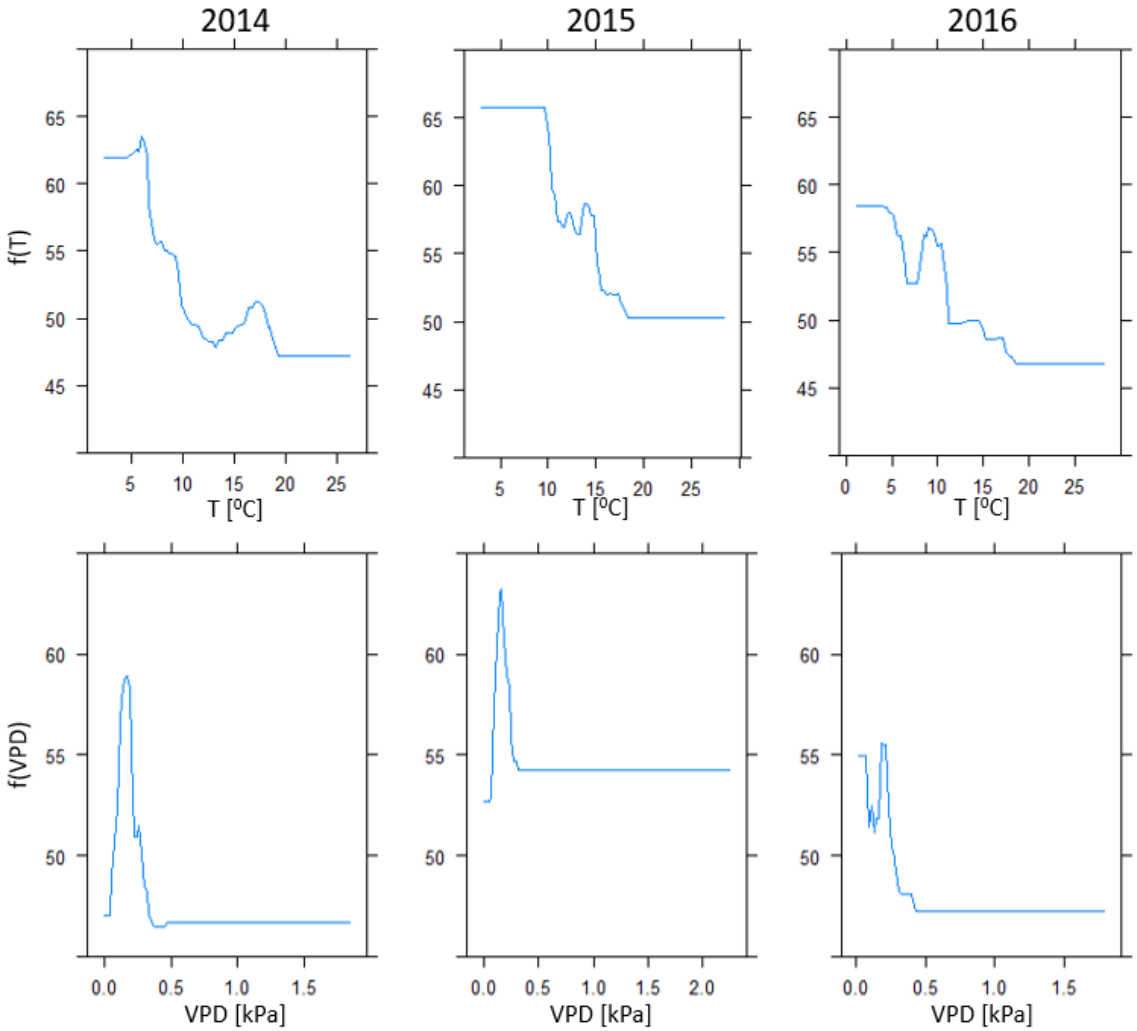

Fig. 6. Partial dependence plots of the influence of air temperature (*T*) and vapour pressure deficit (*VPD*) on throughfall (TF) by birch trees during the considered years.

throughfall according the *VPD* values is similar for the years 2014 and 2015, as lower *VPD* up to 1.5 kPa increases throughfall under the birch tree, while larger values of *VPD* decrease the amount of throughfall (Figure 6). The data collected in 2016 show a bit different response of throughfall according to the *VPD* values up to 2 kPa, while larger *VPD* values decrease throughfall under birch trees as well.

Pine tree's stemflow was influenced by more variables compared to throughfall. In addition to the rainfall amount, which mainly determines stemflow under both tree species, rainfall intensity and rainfall duration also had an important influence on stemflow under the pine and birch trees, respectively. The significance of rainfall duration on stemflow by the birch tree was also recognised in the analysis of the stemflow response (Zabret and Šraj, 2021), as well as in the analysis of predicting the stemflow of a birch tree using the regression trees (Zabret et al., 2018). Although rainfall intensity was recognised as a less influential variable in the case of throughfall under the pine trees, it seems to have a larger influence on its stemflow. Results of both implemented models (BRT and RF) indicate RI values larger than 15% for rainfall intensity in the years 2015 and 2016 (Figure 4). This is consistent with the results of the BRT model applied to stemflow data of a leafed phenoseason (Zabret et al., 2018), which also indicates some similarities in meteorological influences during the leafed phenoseason and the drier hydrological year.

Introduction of variables specifying the rainfall microstructure into the analysis expressed significant influence of the number of rain drops on throughfall and rainfall interception by the birch trees. The number of raindrops as well as the mean volume diameter (*MVD*) were estimated to have considerable influence on stemflow in case of both considered tree species. However, no influence of these variables on throughfall under the pine trees was observed, as throughfall under the pine trees was still the most influenced by the amount of rainfall, which provided more than half of the RI according to the other considered variables. A more noticeable influence of rainfall microstructure on throughfall by birch than by pine trees was also confirmed in previous study (Zabret et al., 2018), in which a similar comparison of data with BRT models per phenoseason showed the influence of *MVD* on throughfall by pine trees only in the leafless season, while the number of raindrops had a significant role in regulating throughfall under the birch trees regardless the phenoseason. This might be connected to the distinct characteristics of the foliage of the considered tree species, i.e. leaves of the birch trees and needles of the pine trees. The different interaction of needles and leaves to the rain drops and their characteristics has been already reported by other researchers (e.g., Holder, 2013; Nanko et al., 2016; Zabret et al., 2017; Zabret et al., 2018).

CONCLUSIONS

The rainfall partitioning process is part of the hydrological cycle, for which changes are expected due to more pronounced precipitation patterns, resulting in more intense wet and dry periods. Accordingly, the influence of meteorological factors on throughfall, stemflow, and rainfall interception during a wet, a dry, and an average year was analysed. Two similar statistical methods based on the regression tree approach were applied, namely boosted regression trees and random forest. The comparison of the results showed that the methods are complementary, since the BRT model indicates numerous variables with relevant influence and the RF model highlights the variables with the highest influence.

The variables with the highest influence expressed by both models were the rainfall amount and the number of raindrops. The comparison of the influential variables indicates to some extent the correlation between the wet period and the leafless season, as well as between the dry period and the leafed season. For example, rainfall duration had a high relative influence on rainfall partitioning by both tree species mainly in the wet year 2014, while researchers already reported its influence in the leafless season. Stemflow by birch trees was also strongly influenced by air temperature and vapour pressure deficit, which are dependent on the season of the year, which is also consistent with the phenoseason. However, the results of the models also indicate significant differences in the response of the two tree species. The influence of rainfall intensity, the number of raindrops, and the median volume diameter was more pronounced in the case of the birch trees, while it was negligible in the case of the pine trees. This observation coincides with the conclusions of previous studies, i.e. that raindrops behave differently when interacting with needles or leaves.

The presented analysis mainly confirms all previous observations made by other researchers about the different influences on the rainfall partitioning process by distinct tree species. However, a new insight into the impact of wet and dry period is presented, indicating that during a longer wet period the trees behave similarly as in the leafless period and during the longer dry period the rainfall interception process is similar as that in the leafed period. Nevertheless, additional analysis, taking into account multiple wet and dry periods as well as data for these periods for other tree species and other locations with different microclimatic characteristics, should be implemented in order to understand this aspect in more detail.

Acknowledgements. The work was founded by the Slovenian Research Agency (ARRS) through research program P2-0180.

REFERENCES

Andre, F., Jonard, M., Ponette, Q., 2008. Influence of species and rain event characteristics on stemflow volume in a temperate mixed oak–beech stand. Hydrol. Process., 22, 4455–4466.

ARSO, 2020. Measurements archive. http://www.meteo.si/met/sl/archive/ (Accessed 5 May 2021).

Bezak, N., Mikoš, M., 2014. Estimation of design floods using univariate and multivariate flood frequency approach with regard to one wet year. Acta hydrotechnica, 27, 103–117.

Brasil, J.B., de Andrade, E.M., de Queiroz Palácio, H.A., dos Santos, J.C.N., Medeiros, P.H.A., 2020. Temporal variability of throughfall as a function of the canopy development stage: from seasonal to intra-event scale. Hydrol. Sci. J., 65, 1640–1651.

Breiman, L., 2001. Random Forests. Mach. Learn., 45, 5–32.

Breiman, L., Cutler, A., Liaw, A., Wiener, M., 2018. Package 'RandomForest'. https://cran.r-project.org/web/packages/randomForest/randomForest.pdf (Accessed 25 March 2021)

Dohnal, M., Černý, T., Votrubová, J., Tesař, M., 2014. Rainfall interception and spatial variability of throughfall in spruce stand. J. Hydrol. Hydromech., 62, 277–284.

Elith, J., Leathwick, J.R., Hastie, T., 2008. A working guide to boosted regression trees. J. Anim. Ecol., 77, 802–813.

Friedman, J.H., 2001. Greedy function approximation: a gradient boosting machine. Ann. Stat., 29, 1189–1232.

Friedman, J.H., Meulman, J.J., 2003. Multiple additive regression trees with application in epidemiology. Stat. Med., 22, 1365–1381.

Gao, S., Zhou, T., Yi, C., Shi, P., Fang, W., Liu, R., Liang, E., Camarero, J.J., 2020. Asymmetric impacts of dryness and wetness on tree growth and forest coverage. Agr. Forest. Meteorol., 288–289, 107980.

Hao, Y., Wang, Y., Mei, X., Huang, X., Cui, X., Zhou, X., Niu, H., 2008. CO_2, H_2O and energy exchange of an Inner Mongolia steppe ecosystem during a dry and wet year. Acta Oecologica, 33, 133–143.

Holder, C.D., 2013. Effects of leaf hydrophobicity and water droplet retention on canopy storage capacity. Ecohydrology, 6, 483–490.

Honda, E.A., Mendonça, A.H., Durigan, G., 2014. Factors affecting the stemflow of trees in the Brazilian Cerrado. Ecohydrology, 8, 1351–1362.

Hungate, B., Hampton, H., 2012. Valuing ecosystems for climate. Nat. Clim. Change, 2, 151–152.

Inglezakis, V.J., Poulopoulos, S.G., Arkhangelsky, E., Zorpas, A.A., Menegaki, A.N., 2016. Aquatic environment. In: Poulopoulos, S., Inglezakis, V. (Eds.): Environment and Development: Basic Principles, Human Activities, and Environmental Implications. Elsevier, pp. 137–212.

Klamerus-Iwan A., Link T.E., Keim R.F., Van Stan, J.T., 2020. Storage and routing of precipitation through canopies. In: Van Stan, J T., Gutmann, E., Friesen, J. (Eds.): Precipitation Partitioning by Vegetation: A Global Synthesis. Springer Nature, Berlin, Germany, pp. 17–34.

Levia, D.F., Germer, S., 2015. A review of stemflow generation dynamics and stemflow-environment interactions in forests and shrublands. Rev. Geophys., 53, 673–714.

Leyton, L., Reynolds, E.R.C., Thompson, F.B., 1967. Rainfall interception in forest and moorland. In: Sopper, W.E., Lull, H.W. (Eds.): Forest Hydrology. Pergamon, Oxford, pp. 163–178.

Loh, W., 2011. Classification and regression trees. Data Min. Knowl. Disc., 1, 14–23.

Mużyło, A., Llorens, P., Domingo, F., 2012. Rainfall partitioning in a deciduous forest plot in leafed and leafless periods. Ecohydrology, 5, 759–767.

Nadbath, M., 2008. Meteorological station Ljubljana Bežigrad. Naše okolje 15, 1. (In Slovenian.)

Nanko, K., Hudson, S.A., Levia, D.F., 2016. Differences in throughfall drop size distributions in the presence and absence of foliage. Hydrolog. Sci. J., 61, 620–627.

Peng, Y., Chen, L., Tian, J., Sun, B., Jiang, C., Lu, Y., Shang, J., 2021. Ecosystem services help alleviate the intensity of dryness/wetness. Global Ecol. Conser., 27, e01581.

Perez-Harguindeguy, N., Diaz, S., Garnier, E. et al. 2013. New handbook for standardized measurement of plant functional traits worldwide. Aust. J. Bot., 61, 167–234

R core team, 2020. R: A language and environment for statistical computing. R Foundation for Statistical Computing, Vienna, Austria. http://www.R-project.org/ (Accessed 20 August 2020)

Ridgeway, G., 2020. Generalized Boosted Regression Models. https://cran.r-project.org/web/packages/gbm/gbm.pdf (Accessed 10 August 2020)

Sadeghi, S.M.M., Gordon, D.A., Van Stan, J.T., 2020. A global synthesis of throughfall and stemflow hydrometeorology. In: Van Stan, J T., Gutmann, E., Friesen, J. (Eds.): Precipitation Partitioning by Vegetation: A Global Synthesis. Springer Nature, Berlin, Germany, pp. 49–70.

Schooling, J.T., Carlyle-Moses, D.E., 2015. The influence of rainfall depth class and deciduous tree traits on stemflow production in an urban park. Urban Ecosyst., 18, 1261–1284.

Siegert, C.M., Levia, D.F., 2014. Seasonal and meteorological effects on differential stemflow funneling ratios for two deciduous tree species. J. Hydrol., 519, 446–454.

Staelens, J., De Schrijver, A., Verheyen, K., Verhoest, N.E.C., 2008. Rainfall partitioning into throughfall, stemflow, and interception within a single beech (*Fagus sylvatica* L.) canopy: influence of foliation, rain event characteristics, and meteorology. Hydrol. Process., 22, 33–45.

Su, L., Xie, Z., Xu, W., Zhao, C., 2019. Variability of throughfall quantity in a mixed evergreen-deciduous broadleaved forest in central China. J. Hydrol. Hydromech., 67, 225–231.

Šraj, M., Brilly, M., Mikoš, M., 2008. Rainfall interception by two deciduous Mediterranean forests of contrasting stature in Slovenia. Agr. Forest. Meteorol., 148, 121–134.

Xiao, Q., McPherson, E.G., Ustin, S.L., Grismer, M.E., Simpson, J.R., 2000. Winter rainfall interception by two mature open-grown trees in Davis, California. Hydrol. Process., 14, 763–784.

Xu, Z., Feng, Z., Zhao, C., Zheng, J., Yang, J., Tian, F., Peng, H., Wang, C., Peng, S., Sher, H., 2013. The canopy rainfall interception in actual and potential distribution of Qinghai spruce (*Picea crassifolia*) forest. J. Hydrol. Hydromech., 61, 64–72.

Xu, L., Cao, G., Wang, Y., Hao, J., Wang, Y., Yu, P., Liu, Z., Xiong, W., Wang, X., 2020. Components of stand water balance of a larch plantation after thinning during the extremely wet and dry years in the Loess Plateau, China. Global Eco. Conser., 24, e01307.

Yue, K., De Frenne, P., Fornara, D.A., Van Meerbeek, K., Li, W., Peng, X., Ni, X., Peng, Y., Wu, F., Yang, Y., Peñuelas, J., 2021. Global patterns and drivers of rainfall partitioning by trees and shrubs. Glob. Change. Biol., 27, 3350–3357.

Zabret, K., 2013. The influence of tree characteristics on rainfall interception. Acta Hydrotech., 26, 99–116. (In Slovenian.)

Zabret, K., Rakovec, J., Mikoš, M., Šraj, M., 2017. Influence of raindrop size distribution on throughfall dynamics under pine and birch trees at the rainfall event level. Atmosphere, 8, 240.

Zabret, K., Rakovec, J., Šraj, M., 2018. Influence of meteorological variables on rainfall partitioning for deciduous and coniferous tree species in urban area. J. Hydrol., 558, 29–41.

Zabret, K., Šraj, M., 2019a. Evaluating the influence of rain event characteristics on rainfall interception by urban trees using multiple correspondence analysis. Water, 11, 2659.

Zabret, K., Šraj, M., 2019b. Rainfall interception by urban trees and their impact on potential surface runoff. Clean Soil, Air, Water, 47, 8, 1800327.

Zabret, K., Šraj, M., 2021. How characteristics of a rainfall event and the meteorological conditions determine the development of stemflow: A case study of a birch tree. Front. Front. For. Glob. Change, 4, 663100.

Received 28 May 2021
Accepted 5 August 2021

J. Hydrol. Hydromech., 69, 2021, 4, 467–474
DOI: 10.2478/johh-2021-0024
ISSN 1338-4333

sciendo Journal of Hydrology and Hydromechanics

Effects of slow and fast pyrolysis biochar on N_2O emissions and water availability of two soils with high water-filled pore space

Eugene Balashov[1*], Natalya Buchkina[1], Vladimir Šimanský[2], Ján Horák[3]

[1] Department of Soil Physics, Physical Chemistry and Biophysics, Agrophysical Research Institute, Grazhdansky pr. 14, 195220 St. Petersburg, Russia.
[2] Department of Soil Science, Institute of Agronomic Sciences, Faculty of Agrobiology and Food Resources, Slovak University of Agriculture, Tr. A. Hlinku 2, 94901 Nitra, Slovakia.
[3] Institute of Landscape Engineering, Faculty of Horticulture and Landscape Engineering, Slovak University of Agriculture, Hospodárska 7, 94976 Nitra, Slovakia.
[*] Corresponding author. E-mail: eugene_balashov@mail.ru

Abstract: Biochars, depending on the types of feedstocks and technological conditions of pyrolysis, can vary significantly in their properties and, therefore, it is difficult to predict biochar-induced effects on nitrous oxide (N_2O) emissions from various soils, their physical properties and water availability. The objectives of this study were (1) to quantify effects of slow pyrolysis biochar (BC) and fast pyrolysis biochar (PYRO) on physical and hydro-physical properties of sandy soil (Haplic Arenosol) and clayey loam soil (Gleyic Fluvisol), and (2) to assess corresponding N_2O emissions from these two soils. The study included a 63-day long laboratory investigation. Two doses of BC or PYRO (15 t ha^{-1} and 30 t ha^{-1}) were applied to the soils in combination or without nitrogen fertilizer (NH_4NO_3, 90 kg N ha^{-1}). The obtained results have shown a significant decrease in the bulk density of sandy soil after it was amended with either rate of BC or PYRO. Water retention capacity of the soils in all the treatments with BC or PYRO increased considerably although no changes was found in the soil water-filled pore space (WFPS) which was higher than 60%. BC was increasing N_2O emission rates from the sandy soil treated with N fertilizer, and reducing N_2O emission rates from the clayey loam soil treated with N fertilizer. PYRO was more efficient and was reducing N_2O emissions from both fertilized soils, but for the sandy soil the reduction was statistically significant only at higher dose (30 t ha^{-1}) of the biochar.

Keywords: Biochar; Sandy soil; Clayey loam soil; Bulk density; Water retention capacity; N_2O emission.

INTRODUCTION

Biochar is a carbon-rich, aromatic material produced by slow or fast pyrolysis of different organic wastes at high temperatures (up to 900 °C) in oxygen free or limited oxygen environment (Das et al., 2021; Kuppusamy et al., 2016; Lehmann et al., 2011; Lei and Zhang, 2013). Because of high chemical stability, biochar has a great potential to enhance atmospheric carbon sequestration (Laird et al., 2008; Lehmann et al., 2006). Soil amendments such as biochar, composts or their mixtures can decrease soil bulk density (Abd El-Mageed et al., 2021; Hardie et al., 2014), improve soil structure (Ajayi and Horn, 2016; Juriga et al., 2021), increase soil pH (Horák, 2015) cation exchange capacity (Igaz et al., 2018; Jien and Wang, 2013), soil N availability (Haider et al., 2017; Van Zwieten et al., 2010), organic carbon content (Ajayi and Horn, 2016; Šrank and Šimanský, 2020), soil porosity (Blanco-Canqui, 2017; Githinji, 2014), available water content (Głąb et al., 2016; Ibrahim et al., 2013) and saturated hydraulic conductivity (Jien and Wang, 2013; Toková et al., 2020).

Syakila and Kroeze (2011) reported that agricultural N_2O emission in 2006 reached 23–31% of the global emissions with the main source being nitrogen fertilizer and manure application to soils. Temperature, water-filled pore space (WFPS), O_2 concentration, pH, available soil organic carbon content (Dobbie and Smith, 2003; Wrage et al., 2001), mineral nitrogen content (Buchkina et al., 2012; Horák et al., 2019) affect microbial processes of nitrification and denitrification which are pathways of N_2O production in soils (Lee et al., 2009; Wrage et al., 2001).

Biochars produced under different conditions can have different physical (bulk density, porosity), physico-chemical (pH, CEC, BET surface area, oxygenated functional groups) and chemical (total carbon, nitrogen, hydrogen content) properties which, in due course, can have positive, neutral or negative effect on soil properties (Das et al., 2021; Liao et al., 2021; Novak et al., 2009; Rajapaksha et al., 2014) and crop yields (Murtaza et al., 2021). According to Bruun et al. (2012), application of fast pyrolysis biochar (produced from wheat straw) resulted in immobilization of soil N (43%) during the 65-day incubation, while application of slow pyrolysis biochar led to net N mineralization (7%) in soil. Application of biochar can be considered as one of the useful ways of mitigating N_2O emissions from soils (Buchkina et al., 2019; Horák et al., 2017; Ippolito et al., 2012; Rizhiya et al., 2019; Wang et al., 2013; Zhang et al., 2021). Biochar-induced improvement of soil physical and hydro-physical properties may mitigate microbial process of denitrification, which is the main process of N_2O production in soils (Wrage et al., 2001). Nevertheless, several studies have shown that biochar could stimulate N_2O emissions from soils under dry (Saarnio et al., 2013) and anaerobic conditions (Yanai et al., 2007) or had no effect on N_2O emissions (Karhu et al., 2011). According to Cayuela et al. (2013), there are four possible explanations for reduced N_2O emissions from soils after biochar application: binding of N_2O with metal ions (Fe, Cu) on the biochar surface; adsorption of organic substances by biochar and lower availability of this substances for microorganisms; liming effect of biochar resulting in an increase of soil pH and in a decrease of denitrification; improvement of soil aeration.

Fast and slow pyrolysis biochars can demonstrate different effects on N_2O emissions from soils with different texture. Stewart et al. (2013) reported that the fast pyrolysis biochar (from oak pellets, 550 °C) caused several times higher N_2O emission from a coarse-textured soil than from a fine-textured soil. Slow pyrolysis is usually carried out at temperatures lower than 600 °C. Therefore, slow pyrolysis biochars, in comparison with fast pyrolysis biochars, often demonstrated higher porosity, higher content of nutrients and organic substrates, and, as a result, greater ability to mitigate N_2O emissions from soils (Das et al., 2021; Kuppusamy et al., 2016). So, up to date, mechanisms and reasons of biochar different effects on nitrogen transformation and relevant N_2O emissions from soils are still obscure.

The objectives of the study were: (1) to quantify the effects of slow and fast pyrolysis biochar on physical and hydrophysical properties of sandy and clayey loam soils, and (2) to assess the corresponding changes in N_2O emissions from both soils.

MATERIALS AND METHODS

The effect of two doses of slow pyrolysis biochar (BC) and fast pyrolysis biochar (PYRO) on N_2O emissions from two soils with different texture, their physical and hydro-physical properties was studied in a laboratory experiment. The soils of the experiment were classified as Haplic Arenosol (sandy soil) and Gleyic Fluvisol (clayey loam soil) according to WRB (2014). Disturbed field moist soil samples for the laboratory experiment were collected from the upper 0–20 cm layer of agricultural plots with Haplic Arenosol located in Rišňovce (N48° 21.788', E17° 54.685') and with Gleyic Fluvisol located in Janikovce (N48° 6.933', E18° 07.031'). The sandy soil contained 924 g kg^{-1} of sand, 53 g kg^{-1} of silt, and 5 g kg^{-1} of clay while the clayey loam soil contained 288 g kg^{-1} of sand, 417 g kg^{-1} of silt and 295 g kg^{-1} of clay. Soil organic carbon (SOC) content in the sandy soil ranged from 2.95 to 3.19 g C kg^{-1} soil while in the clayey loam soil – from 5.86 to 6.20 g C kg^{-1} soil. Values of pH (KCl) were equal to 6.83 and 6.25 for sandy soil and clayey loam soil, respectively.

BC was produced at a temperature of 500–600 °C in a Pyreg reactor, while PYRO was produced at a temperature of 900 °C in a Spanner Re2 wood power plant. PYRO and BC had particle diameters of ≤1 mm and ≤3 mm, respectively. The treatments investigated in the study are shown in Table 1.

For the experiment air-dried soil (120–125 g, dry weight) was mixed with the biochars or/and the nitrogen fertilizer according to the treatments and moistened to a field capacity. The field capacity of the soils was equal to 50–55% of their full saturation. The moistened soil was inserted into steel cores (95 cm^{-3}). A 63-day incubation of the soil cores was carried out at a room temperature. The cores were regularly weighed and moistened to maintain the moisture content in both soils equal to 50–55% of full saturation in all the studied treatments. The full saturation of the soils (% of weight) with all the treatments was measured. For the sandy soil it was: 50% (control), 54% (15 t ha^{-1} of BC or PYRO) and 58% (30 t ha^{-1} of BC or PYRO) while for the clayey loam soil it was: 62% (control), 64% (15 t ha^{-1} of BC or PYRO), 66% (30 t ha^{-1} of BC or PYRO). The laboratory experiment was carried out in six replicates.

To measure N_2O emissions, the soil cores were inserted into plastic vessels (1000 cm^3) with airtight lids equipped with sealed rubber septums. At every air sampling occassion the plastic vessels were sealed for 20 minutes and air samples were collected from the headspaces with a syringe and transferred to pre-evacuated 12-ml glass vials (Labco Exetainer, Lampeter, UK). The same technique was used earlier in other experiments (Buchkina et al., 2019). The collected air samples were analyzed for N_2O concentration using a gas chromatograph (GC-2010 Plus, Shimadzu) equipped with a ^{63}Ni electron capture detector (ECD). The gas chromatograph (GC) was calibrated using two certified standard gas mixtures (N_2O and N_2) in the expected concentration range. Analytical conditions of the GC were: carrier gas (Helium, 30 ml min^{-1}) and detector temperature: 330 °C for ECD.

Concentration of mineral nitrogen (in $N\text{-}NO_3^-$ form) in the soil samples was determined by an extraction technique proposed by Yuen and Pollard (1954) using a spectrometer (SP-870 PLUS, Metertech Inc.) at wavelengths of 410 and 420 nm, respectively. Soil pH (at 1:2.5 ratio of soil to 1M KCI solution) was measured using pH meter (HI 9017 Microprocessor Benchtop, HANNA instruments). Water-filled pore space (WFPS), or a volume of soil pores filled with water as a percent of total soil porosity, was calculated using the data on the soil moisture content (% of weight) and soil bulk density measured at the last day of the incubation experiment.

Statistical assessment of the experimental results was carried out on the basis of the calculated means, standard deviations, and 95% confidence intervals. Spearman's rank correlation coefficients (Spearman, 1904) were used to assess the strength of associations between the sets of soil parameters in all the treatments at $P \leq 0.05$. One-way analysis of variance (ANOVA, available at https://www.socscistatistics.com) was applied to evaluate the significance of differences between means of normally distributed data. Mann-Whitney U test (Mann and Whitney, 1947) was applied to assess the significance of differences in means (at $P \leq 0.05$) if the distribution was not normal according to the Shapiro-Wilk test (Shapiro and Wilk, 1965). Calculation procedure is available at https://scistatcalc.blogspot.com/2013/10/shapiro-wilk-test-calculator.html.

Table 1. The investigated treatments of the experiment.

No. of treatment	Description
C	control (soils without biochars and nitrogen fertilizer)
F	soil with ammonium nitrate (NH_4NO_3) fertilizer (90 kg N ha^{-1})
15 BC	soil with 15 t ha^{-1} of BC
15	soil with 15 t ha^{-1} of PYRO
15 BC F	soil with 15 t ha^{-1} of BC + NH_4NO_3 (90 kg N ha^{-1})
15 PYRO F	soil with 15 t ha^{-1} of PYRO + NH_4NO_3 (90 kg N ha^{-1})
30 BC	soil with 30 t ha^{-1} of BC
30 PYRO	soil with 30 t ha^{-1} of PYRO
30 BC F	soil with 30 t ha^{-1} of BC + NH_4NO_3 (90 kg N ha^{-1})
30 PYRO F	with 30 t ha^{-1} of PYRO + NH_4NO_3 (90 kg N ha^{-1})

RESULTS AND DISCUSSION

Physicochemical properties of biochars

Different pyrolysis conditions resulted in different physicochemical properties of the two biochars used in the study (Table 2). BC, the slow pyrolysis biochar, had higher organic carbon content compared to PYRO, the fast pyrolysis biochar. According to Keiluwert et al. (2010), slow pyrolysis contributes to a higher conversion of non-aromatic organic matter into aromatic carbon. The higher specific surface area of PYRO is in correlation with the biochar particle size: fast pyrolysis resulted in significant disintegration of the feedstock material and PYRO had a dust-like structure, while BC inherited some of the feedstock structure and consisted of bigger particles.

The H/C, O/C, and (O+N)/C atomic ratios are usually used as indicators of aromaticity and polarity of biochars (Das et al., 2021). BC was more carbonized and had higher number of aromatic compounds than PYRO. Based on the higher values of O/C and (O+N)/C of PYRO, it can be assumed that fast pyrolysis biochar had a greater number of oxygen-containing polar groups (carboxylic, phenolic, hydroxylic), which could contribute to its higher affinity to water, better water adsorption and retention (Das et al., 2021; Ren et al., 2016).

Soil bulk density and water retention capacity

Incorporation of biochars into soils often leads to a decrease in their bulk density (Abd El-Mageed et al., 2021; Hardie et al., 2014). A degree of biochar-induced decrease in soil bulk density depends on soil texture and biochar application dose (Murtaza et al., 2021). In the conducted experiment the biochars application affected the bulk density of the coarse-textured soil more than that of heavy-textured soil. The data on the bulk densities of the two soils studied in the experiment with all the treatments are presented in Fig. 1 and Fig. 2.

Bulk density of the sandy soil was reduced significantly due to application of both doses of BC or PYRO in comparison to the control treatment. Application of 15 t ha^{-1} of PYRO to sandy soil with or without N-fertilizer resulted in considerably lower soil bulk density compared to similar treatments with BC ($P <$ 0.05). Marginal differences were found in the bulk density of the sandy soil with various treatments after application of the higher dose (30 t ha^{-1}) of biochar irrespective of the biochar type.

Very negligible changes in the clayey loam soil bulk density were found under any of the studied treatments of the experiment in comparison to the control treatment. Therefore, both biochars were more effective in decreasing the bulk density of the sandy soil than the clayey loam soil. This might be attributed to the higher content of fine clay particles of the latter soil.

Figures 3 and 4 show the water retention curves of the two soils treated with two doses of BC or PYRO. The readily available water content is being held by soils in the range of water potentials from –5 to –300 kPa (the latter is the water potential of the first signs of plant wilting) and can be assessed using the water retention curves. The obtained results for the control treatments indicate that water retention capacity corresponding to the readily available water was significantly lower in the sandy soil in comparison to the clayey loam soil (at $P < 0.001$). Incorporation of either dose of BC or PYRO to the sandy soil significantly increased its water retention capacity (at $P < 0.05$). The increase after PYRO application was significantly higher ($P < 0.05$) than after BC application for both doses of the

Table 2. Properties of biochars used in the laboratory experiment.

Biochar	Specific surface area, m^2 g^{-1}	Oxygen (O), %	Hydrogen (H), %	Carbon (C), %	Nitrogen (N), %	O:C molar ratio	H:C molar ratio	(O+N)/C	pH KCl
PYRO	258	16.25	1.63	58.7	0.29	0.21	0.33	0.28	10.4
BC	123	6.20	0.63	76.7	0.64	0.06	0.10	0.09	9.1

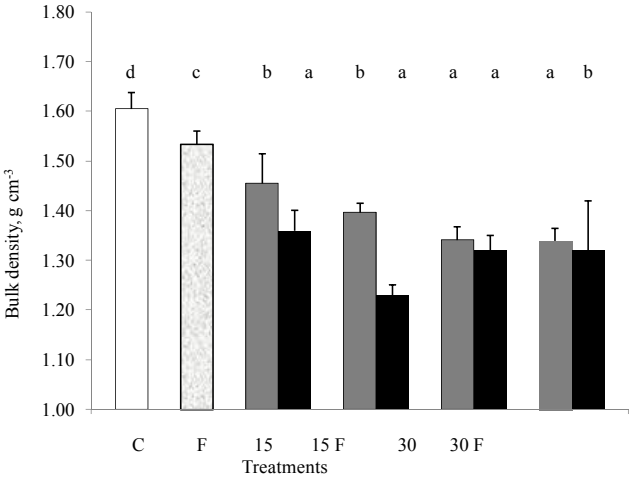

Fig. 1. Bulk density of the sandy soil with different treatments. Bars show the 95% confidence intervals. Different letters indicate the significance of differences (at $P < 0.05$) according to one-way ANOVA. C – control; F – 90 kg N ha^{-1}; 15 BC PYRO – 15 t ha^{-1} of BC or PYRO; 15 BC PYRO F – 15 t ha^{-1} of BC or PYRO with 90 kg N ha^{-1}; 30 BC PYRO – 30 t ha^{-1} of BC or PYRO; 30 BC PYRO F – 30 t ha^{-1} of BC or PYRO with 90 kg N ha^{-1}.

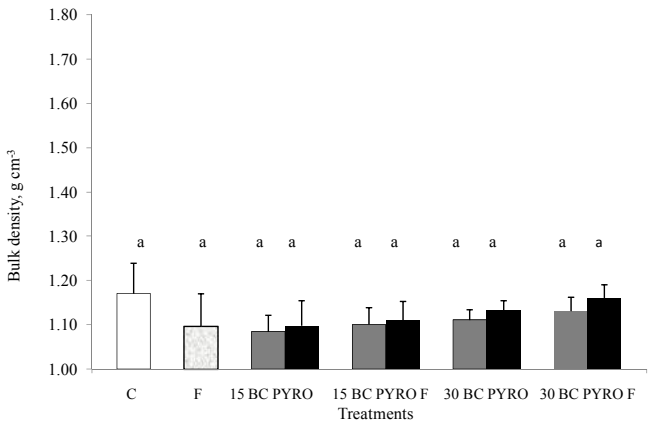

Fig. 2. Bulk density of the clayey loam soil with different treatments. Bars show the 95% confidence intervals. Different letters indicate the significance of differences (at $P < 0.05$) between treatments according to one-way ANOVA. C – control; F – 90 kg N ha^{-1}; 15 BC PYRO – 15 t ha^{-1} of BC or PYRO; 15 BC PYRO F – 15 t ha^{-1} of BC or PYRO with 90 kg N ha^{-1}; 30 BC PYRO – 30 t ha^{-1} of BC or PYRO; 30 BC PYRO F – 30 t ha^{-1} of BC or PYRO with 90 kg N ha^{-1}.

biochars (Fig. 3). There was no significant difference in the water retention capacity of the sandy soil between the treatments with two doses of BC while application of PYRO resulted in a significant difference in water retention capacity between the treatments with 15 and 30 t ha^{-1}.

Greater specific surface area of PYRO and higher number of polar groups on the biochar surface could be the reason for higher water retention capacity of the sandy soil amended with this type of biochar (Ren et al., 2016).

Particle diameter of PYRO (up to 1 mm) was smaller than particle diameter of BC (up to 3 mm). Therefore, incorporation of PYRO to the sandy soil at the dose of 30 t ha^{-1} led to a two-fold decrease in the volume of capillary macro- and meso-pores (the intervals of water potentials between –5 kPa and –55 kPa) compared to that after application of 15 t ha^{-1} of PYRO. At the same time, the incorporation of either dose of BC did not cause similar changes in the volume of macro- and meso-pores of this soil.

Incorporation of both doses of PYRO or BC into the clayey loam soil also resulted in a significant (at $P < 0.05$) increase in the soil water retention capacity, compared to the control treatment (Fig. 4). The higher was the dose of either biochar, the higher was the water retention capacity (at $P \leq 0.05$) of the clayey loam soil in the range of water potentials from –5 to –300 kPa.

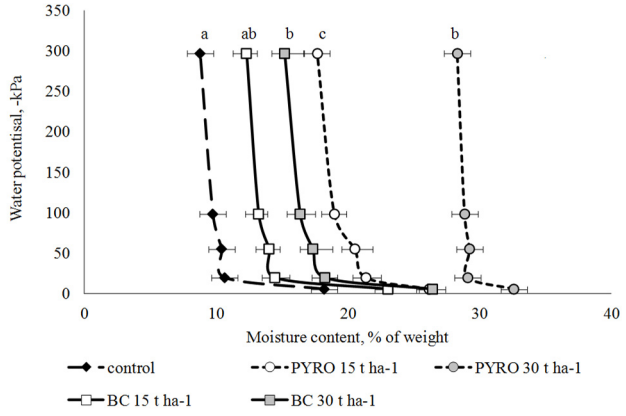

Fig. 3. Water retention curves of the sandy soil with different treatments. Bars show the 95% confidence intervals. Different letters indicate the significance of differences according to one-way ANOVA (at $P < 0.05$).

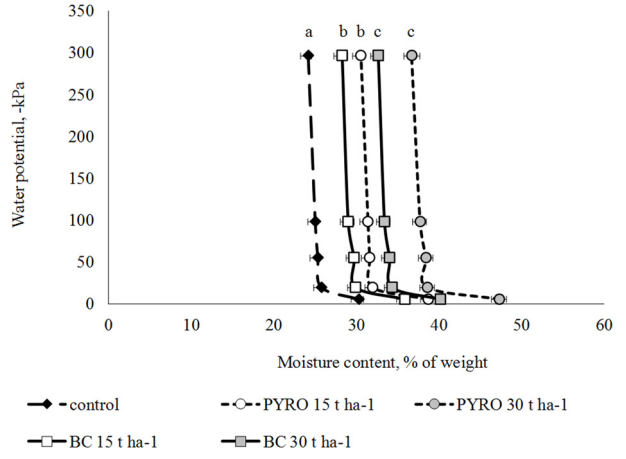

Fig. 4. Water retention curves of the clayey loam soil with different treatments. Bars show the 95% confidence intervals. Different letters indicate the significance of differences according to one-way ANOVA (at $P < 0.05$).

The difference in water retention capacity of clayey loam soil amended with 15 t ha^{-1} of either biochar was not statistically significant, as well as there was no difference in water retention capacity of the soil amended with 30 t ha^{-1} of BC or PYRO.

In the studies of N_2O emission from soils, WFPS is being often used as an important indicator of soil conditions favorable for microbial processes of nitrification or denitrification. These conditions are observed in soils at WFPS being lower than 60% (mainly aerobic conditions) and higher than 60% (mainly anaerobic conditions), respectively (Dobbie and Smith, 2003; Wrage et al., 2001). The data on the WFPS (%) of the studied soils are given in Table 3. During the experiment, the WFPS of the sandy soil was higher than 60% in all the treatments including control and control + N-fertilizer. Incorporation of BC or PYRO in two studied doses did not result in any significant increase of WFPS in the sandy soil compared to control treatment. WFPS of the sandy soil was considerably higher after application of 15 t ha^{-1} of BC than 15 t ha^{-1} of PYRO. There were negligible differences in WFPS between treatments with 30 t ha^{-1} of BC and PYRO.

In the clayey loam soil, values of WFPS were also higher than 60%. Application of BC or PYRO did not significantly change WFPS of this soil compared to the control treatment. Application of 30 t ha^{-1} of PYRO resulted in significantly (at $P < 0.001$) higher values of WFPS compared to the treatments with 30 t ha^{-1} of BC. As the WFPS values during the experiment were always higher than 60% (anaerobic conditions) in both soils under all the studied treatments, microbial process of denitrification was likely to be the main pathway of N_2O formation in these soils (Dobbie and Smith, 2003).

Table 3. Average values of WFPS, %, (mean ± 95% confidence interval) for the sandy and clayey loam soils with different treatments. Letters a, b and c, d show significant differences among values of WFPS in sandy soil and clayey loam soil, respectively, by one-way ANOVA (at $P < 0.05$).

Treatment	Sandy soil	Clayey loam soil
Control	64.4± 3.9a	79.0±6.5c
Control + N-fertilizer	61.9±2.7a	71.4±7.6c
15 t ha^{-1} of BC	69.4±5.5a	66.4±4.4d
15 t ha^{-1} of BC + N-fertilizer	64.6±3.1a	73.1±6.7c
30 t ha^{-1} of BC	59.4±4.8a	67.4±3.1d
30 t ha^{-1} of BC + N-fertilizer	58.1±4.8b	71.9±4.4c
15 t ha^{-1} of PYRO	61.0±4.0a	72.9± 4.4c
15 t ha^{-1} of PYRO + N-fertilizer	57.1±3.0b	72.3±4.3c
30 t ha^{-1} of PYRO	62.7±3.6a	78.2±3.1c
30 t ha^{-1} of PYRO + N-fertilizer	66.0±5.5a	83.1±4.2c

N_2O emissions and soil mineral nitrogen

N_2O emission rates from the soils with different treatments are shown on Fig. 5 and 6 while the average values of N_2O emission rates – in Table 4. There was a very high variability of N_2O emissions from both soils under all the studied treatments during the entire period of the experiment and, for this reason, some differences in N_2O emission rates, which were found during the experiment, were not statistically significant. Still, the obtained results provide a good possibility to see the main directions of the changes in N_2O emission rates, related to the biochars application to fertilized and unfertilized soils of different texture.

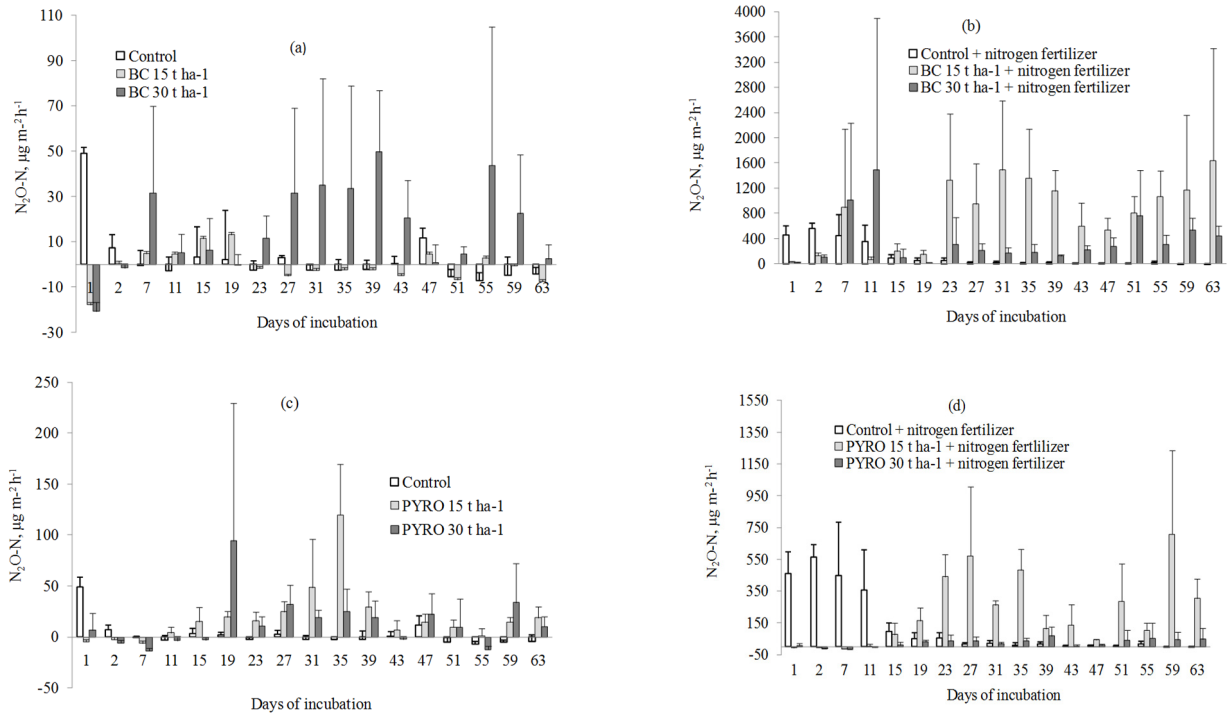

Fig. 5. N_2O emission rates for the sandy soil with BC application (a and b) and with PYRO application (c and d). Bars show the 95% confidence intervals.

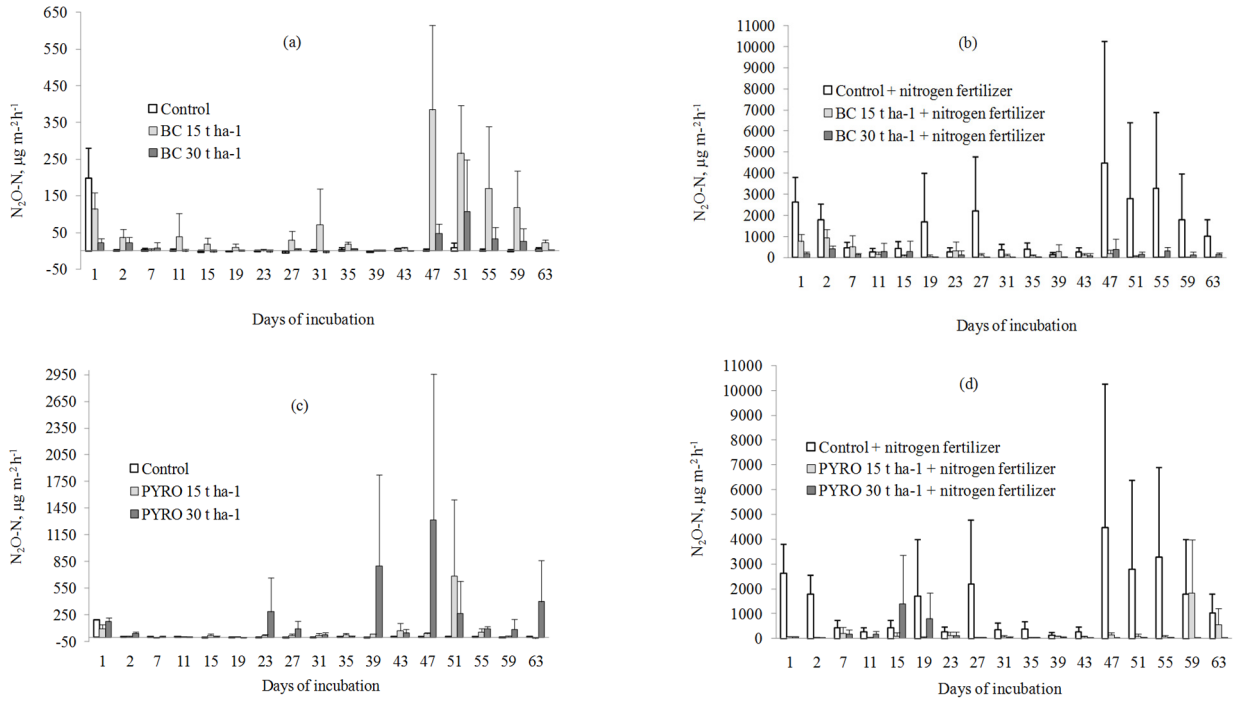

Fig. 6. N_2O emission rates for the clayey loam soil with BC application (a and b) and with PYRO application (c and d). Bars show 95% confidence intervals.

The rate of N_2O emission from the control soils was not very high and the reason for that was, presumably, the very low N-content in the soils. Despite of the six-fold difference in the numbers, the difference in N_2O emission rates between control treatments of the sandy soil and the clayey loam soil was not statistically significant due to the high variability of the flux. Application of the biochars to the unfertilized soils either did not significantly change the rate of N_2O emission (for the sandy soil: treatments 15 t ha^{-1} of BC, 30 t ha^{-1} of PYRO; for the clayey loam soil treatment 30 t ha^{-1} of BC) or significantly increased it (for the sandy soil: treatments 30 t ha^{-1} of BC or 15 t ha^{-1} of PYRO; for the clayey loam soil: treatments 15 t ha^{-1} of BC and 30 t ha^{-1} of PYRO). Nitrogen content in the biochars could be the main reasons for N_2O flux increase in the circumstances when the soil water content was kept at the same level throughout the experiment.

Application of N-fertilizer (90 kg N ha^{-1}) to both soils resulted in a significant increase in the rate of N_2O emission and

Table 4. Average values of N_2O emission rates (μg m^{-2} h^{-1}) for the sandy and clayey loam soils with different treatments (means ± 95% confidence intervals). Different letters indicate the significance of differences according to one-way ANOVA within each column (at $P < 0.05$).

Treatment	Sandy soil	Clayey loam soil
Control	2.4±6.1a	12.3±22.8a
Control + N-fertilizer	124.5±92.5c	1423.5±617.4d
15 t ha^{-1} of BC	–0.6±3.5ab	76.6±55.1b
15 t ha^{-1} of BC + N-fertilizer	797.5±255.3e	219.9±127.3c
30 t ha^{-1} of BC	16.3±9.0b	15.4±13.4a
30 t ha^{-1} of BC + N-fertilizer	368.1±185.3d	159.5±63.5c
15 t ha^{-1} of PYRO	19.3±3.9b	66.4±77.4ab
15 t ha^{-1} of PYRO + N-fertilizer	216.0±104.9cd	208.7±207.9bc
30 t ha^{-1} of PYRO	14.2±12.0ab	216.3±166.5b
30 t ha^{-1} of PYRO + N-fertilizer	24.5±11.3b	175.5±173.8bc

Table 5. Average N-NO_3^- content (mg kg^{-1} of soil) for the sandy and clayey loam soils with different treatments (means ± 95% confidence interval). Different letters indicate the significance of differences according to one-way ANOVA within each column (at $P < 0.05$).

Treatment	Sandy soil	Clayey loam soil
Control	0.10±0.01a	0.10±0.01c
Control + N-fertilizer	1.0±0.8a	40.3±16.3d
15 t ha^{-1} of BC	0.4±0.3a	2.3±3.8c
15 t ha^{-1} of BC + N-fertilizer	12.6±6.7b	24.4±23.5d
30 t ha^{-1} of BC	0.9±0.8a	2.2±2.0c
30 t ha^{-1} of BC + N-fertilizer	9.9±3.7b	13.2±3.2d
15 t ha^{-1} of PYRO	1.2±0.6b	2.8±2.3c
15 t ha^{-1} of PYRO + N-fertilizer	24.8±5.0b	55.6±9.8d
30 t ha^{-1} of PYRO	1.5±0.6b	12.8±8.4d
30 t ha^{-1} of PYRO + N-fertilizer	0.5±0.3a	24.0±23.1d

the increase was significantly higher for the clayey loam soil compared to the sandy soil (at $P < 0.05$). Application of N-fertilizer also resulted in an increase of N-NO_3^- content in both soils (Table 5) and that was the main reason of the increased N_2O emission rates from the fertilized soils of the experiment compared to the control. Another factor that could affect N_2O emission rate from the soils was WFPS but values of WFPS were about the same for different treatments of the same soil (>60%) and therefore had about the same effect on N_2O emissions independent of the treatment, providing conditions suitable for the process of denitrification. Combination of high values of WFPS and high N-content are the main factors promoting processes of denitrification, which is the main source of N_2O in wet soils.

Application of BC to the fertilized sandy soil resulted in a significant increase of N_2O emission rates for both doses of the biochar while application of the same biochar to the fertilized clayey loam soil resulted in significant decrease of N_2O emission rates compared to the control + fertilizer treatment. In general, BC application did not help to mitigate N_2O emissions from N-fertilized sandy soil at WFPS >60% and even was most likely to increase the N_2O flux. At the same time, BC application to the fertilized clayey loam soil was effective in reducing N_2O emission rates compared to the fertilized treatment with no BC at WFPS >60%.

PYRO was reducing N_2O emission rates from both fertilized soils. For the sandy soil, the 5-fold reduction was statistically significant only for the higher rate of PYRO, while for the clayey loam soil N_2O emission rates were 6–9 times lower and the reduction was statistically significant for both rates.

It was shown earlier that biochars can influence the process of microbial denitrification through the improvement of soil aeration and lower mineral nitrogen utilization by denitrifying microorganisms, but that was not the case in the conducted experiment where the WFPS of the studied soils was kept at quite a high level and N_2O emissions were studied in the conditions of no water deficiency.

According to Liao et al. (2021), biochars with the larger specific surface area decrease soil N_2O emission by affecting the diversity, abundance, and composition of total bacteria and N_2O-producing microbial communities. That could be the reason of more pronounced N_2O emission rate reduction from both fertilized soils after PYRO application.

The obtained experimental results indicate a high efficiency of the biochars to mitigate N_2O emissions from the N-fertilized clayey loam soil but not from the N-fertilized sandy soil.

When the mean N_2O emission rates from all the treatments with BC or PYRO and mineral fertilizer were analyzed together, the Spearman's rank correlation coefficients did not distinguish any significant relationship between N_2O emissions and WFPS for either soil studied in the experiment; showed a significant (at $P < 0.01$) relationship with N-NO_3^- content for the sandy soil but not for the clayey loam soil at WFPS higher than 60%.

CONCLUSIONS

The results of the study have shown that application of BC and PYRO resulted in a significant reduction in bulk density of the sandy soil but not the clayey loam soil. Addition of BC or PYRO increased water retention capacity of the two soils used in the study. However, incorporation of BC or PYRO was not affecting the soils' water-filled pore space, which was > 60% for all the studied treatments.

BC did not significantly reduce N_2O emission rates from the N-fertilized sandy soil and was even increasing the flux. In the N-fertilized clayey loam soil BC was more efficient and significantly reduced N_2O emission rate at WFPS >60%.

The mitigating effect of PYRO application on N_2O emission rate was less pronounced in the sandy soil, where only the higher dose of the biochar was successfully reducing the flux from the N-fertilized soil. In the clayey loam soil N_2O emission rates were significantly reduced by PYRO at both rates.

Acknowledgements. This research was funded by the SCIENTIFIC GRANT AGENCY, grant number VEGA 1/0116/21, the CULTURAL AND EDUCATIONAL GRANT AGENCY, grant number KEGA 019SPU–4/2020 and the Operational Program Integrated Infrastructure within the project "Sustainable smart farming systems, taking into account the future challenges 313011W112, cofinanced by the European Regional Development Fund. The authors are very thankful to Drs. J. Leifeld and R. Hüppi (Agroscope, Switzerland) for the provision of the biochars and their properties for the experiment. Dr. N.P. Buchkina was partly working according to the scientific topic of the Agrophysical Research Institute.

Conflicts of interest. The authors declare no conflict of interest.

REFERENCES

Abd El-Mageed, T.A., Abdelkhalik, A., Abd El-Mageed, S.A., Semida, W.M., 2021. Co-composted poultry litter biochar enhanced soil quality and eggplant productivity under different irrigation regimes. Journal of Soil Science and Plant Nutrition. https://doi.org/10.1007/s42729-021-00490-4

Ajayi, A.E., Horn, R., 2016. Modification of chemical and hydrophysical properties of two texturally differentiated soils due to varying magnitudes of added biochar. Soil and Tillage Research, 164, 34–44.

Blanco-Canqui, H., 2017. Biochar and soil physical properties. Soil Science Society of America Journal, 81, 4, 687–711.

Bruun, E.W., Ambus, P., Egsgaard, H., Hauggaard-Nielsen, H., 2012. Effects of slow and fast pyrolysis biochar on soil C and N turnover dynamics. Soil Biology and Biochemistry, 46, 73–79.

Buchkina, N., Rizhiya, E., Balashov, E., 2012. N_2O emission from a loamy sand Spodosol as related to soil fertility and N-fertilizer application for barley and cabbage. Arch. Agron. Soil Sci., 58, S141–S146.

Buchkina, N.P., Hüppi, R., Leifeld, J., 2019. Biochar and short-term N_2O and CO_2 emission from plant residue-amended soil with different fertilisation history. Zemdirbyste-Agriculture, 106, 2, 99–106.

Cayuela, M.L., Zwieten, L.V., Singh, B.P., Jeffery, S., Roig, A., Sánchez-Monedero, M.A., 2013. Biochar's role in mitigating soil nitrous oxide emissions: a review and metaanalysis. Agric. Ecosyst. Environ., 191, 5–16.

Das, S.K., Ghosh, G.K., Avasthe, R.K., Sinha, K., 2021. Compositional heterogeneity of different biochar: Effect of pyrolysis temperature and feedstocks. Journal of Environmental Management, 278, 111501.

Dobbie, K.E., Smith, K.A., 2003. Nitrous oxide emission factors for agricultural soils in Great Britain: The impact of soil water-filled pore space and other controlling variables. Global Change Biol., 9, 204–218.

Githinji, L., 2014. Effect of biochar application rate on soil physical and hydraulic properties of a sandy loam. Archives of Agronomy and Soil Science, 60, 4, 457–470.

Głąb, T., Palmowska, J., Zaleski, T., Gondek, K., 2016. Effect of biochar application on soil hydrological properties and physical quality of sandy soil. Geoderma, 281, 11–20.

Haider, G., Steffens, D., Moser, G., Müller, C., Kammann, C.I., 2017. Biochar reduced nitrate leaching and improved soil moisture content without yield improvements in a four-year field study. Agriculture, Ecosystems & Environment, 237, 80–94.

Hardie, M., Clothier, B., Bound, S., Oliver, G., Close, D., 2014. Does biochar influence soil physical properties and soil water. Plant Soil, 376, 347–361.

Horák, J., 2015. Testing biochar as a possible way to ameliorate slightly acidic soil at the research field located in the Danubian lowland. Acta Horticulturae et Regiotecturae, 18, 1, 20.

Horák, J., Kondrlová, E., Igaz, D., Šimanský, V., Felber, R., Lukac, M., Balashov, E., Rizhiya, E., Buchkina, N., Jankowski, M., 2017. Biochar and biochar with N-fertilizer affect soil N_2O emission in Haplic Luvisol. Biologia, 72, 9, 995–1001.

Horák, J., Balashov, E., Šimanský, V., Igaz, D., Buchkina, N., Aydin, E., Bárek, V., Drgoňová, K., 2019. Effects of conventional moldboard and reduced tillage on seasonal variations of direct CO_2 and N_2O emissions from a loam Haplic Luvisol. Biologia, 74, 767–782.

Igaz, D., Šimanský, V., Horák, J., Kondrlová, E., Domanová, J., Rodný, M., Buchkina, N.P., 2018. Can a single dose of biochar affect selected soil physical and chemical characteristics? Journal of Hydrology and Hydromechanics, 66, 4, 421–428.

Ibrahim, H.M., Al-Wabel, M.I., Usman, A.R., Al-Omran, A., 2013. Effect of Conocarpus biochar application on the hydraulic properties of a sandy loam soil. Soil Science, 178, 4, 165–173.

Ippolito, J.A., Laird, D.A., Busscher, W.J., 2012. Environmental benefits of biochar. Journal of Environmental Quality, 41, 4, 967–972.

Jien, S.H., Wang, C.S., 2013. Effects of biochar on soil properties and erosion potential in a highly weathered soil. Catena, 110, 225–233.

Juriga, M., Aydın, E., Horák, J., Chlpík, J., Rizhiya, E.Y., Buchkina, N.P., Balashov, E.V., Šimanský, V., 2021. The importance of initial application and reapplication of biochar in the context of soil structure improvement. Journal of Hydrology and Hydromechanics, 69, 1, 87–97.

Karhu, K., Mattila, T., Bergström, I., Regina, K., 2011. Biochar addition to agricultural soil increased CH_4 uptake and water holding capacity – Results from a short-term pilot field study. Agriculture, Ecosystems & Environment, 140, 1–2, 309–313.

Keiluweit, M., Nico, P.S., Johnson, M.G., Kleber, M., 2010. Dynamic molecular structure of plant biomass-derived black carbon (biochar). Environmental Science & Technology, 44, 4, 1247–1253.

Kuppusamy, S., Thavamani, P., Megharaj, M., Venkateswarlu, K., Naidu, R., 2016. Agronomic and remedial benefits and risks of applying biochar to soil: current knowledge and future research directions. Environment International, 87, 1–12.

Laird, D.A., 2008. The charcoal vision: a win–win–win scenario for simultaneously producing bioenergy, permanently sequestering carbon, while improving soil and water quality. Agronomy Journal, 100, 1, 178–181.

Lee, J., Hopmans, J.W., van Kessel, C., King, A.P., Evatt, K.J., Louie, D., Rolston, D.E., Six, J., 2009. Tillage and seasonal emissions of CO_2, N_2O and NO across a seed bed and at the

field scale in a Mediterranean climate. Agric. Ecosyst. Environ., 129, 378–390.

Lehmann, J., Gaunt, J., Rondon, M., 2006. Bio-char sequestration in terrestrial ecosystems – a review. Mitigation and Adaptation Strategies for Global Change, 11, 2, 403–427.

Lehmann, J., Rillig, M.C., Thies, J., Masiello, C.A., Hockaday, W. C., Crowley, D., 2011. Biochar effects on soil biota – a review. Soil Biology and Biochemistry, 43, 9, 1812–1836.

Lei, O., Zhang, R., 2013. Effects of biochars derived from different feedstocks and pyrolysis temperatures on soil physical and hydraulic properties. Journal of Soils and Sediments, 13, 9, 1561–1572.

Liao, J., Hu, A., Zhao, Z., Liu, X., Jiang, C., Zhang, Z., 2021. Biochar with large specific surface area recruits N_2O-reducing microbes and mitigate N_2O emission. Soil Biology and Biochemistry, 156, 108212.

Mann, H.B., Whitney, D.R., 1947. On a test of whether one of two random variables is stochastically larger than the other. The Annals of Mathematical Statistics, 18, 1, 50–60.

Murtaza, G., Ahmed, Z., Usman, M., Tariq, W., Ullah, Z., Shareef, M., Iqbal, H., Waqas, M., Tariq, A., Wu, Y., Zhang, Z., Ditta, A., 2021. Biochar induced modifications in soil properties and its impacts on crop growth and production. Journal of Plant Nutrition, 44, 11, 1677–1691.

Novak, J.M., Lima, I., Xing, B., Gaskin, J.W., Steiner, C., Das, K.C., Ahmedna, M., Rehrah, D., Watts, D.W, Busscher, W.J., Schomberg., H., 2009. Characterization of designer biochar produced at different temperatures and their effects on a loamy sand. Annals of Environmental Science, 3, 195–206.

Rajapaksha, A.U., Vithanage, M., Zhang, M., Ahmad, M., Mohan, D., Chang, S.X., Ok, Y.S., 2014. Pyrolysis condition affected sulfamethazine sorption by tea waste biochars. Bioresource Technology, 166, 303–308.

Ren, X., Sun, H., Wang, F., Cao, F., 2016. The changes in biochar properties and sorption capacities after being cultured with wheat for 3 months. Chemosphere, 144, 2257–2263.

Rizhiya, E.Y., Mukhina, I.M., Balashov, E.V., Šimanský, V., Buchkina, N.P., 2019. Effect of biochar on N_2O emission, crop yield and properties of Stagnic Luvisol in a field experiment. Zemdirbyste-Agriculture, 106, 4, 297–306.

Saarnio, S., Heimonen, K., Kettunen, R., 2013. Biochar addition indirectly affects N2O emissions via soil moisture and plant N uptake. Soil Biology and Biochemistry, 58, 99–106.

Shapiro, S.S., Wilk, M.B., 1965. An analysis of variance test for normality (complete samples). Biometrika, 52, 3/4, 591–611.

Spearman, C., 1904. ”General intelligence,” objectively determined and measured. The American Journal of Physiology, 15, 2, 201–292.

Stewart, C.E., Zheng, J., Botte, J., Cotrufo, M.F., 2013. Co-generated fast pyrolysis biochar mitigates green-house gas emissions and increases carbon sequestration in temperate soils. GCB-Bioenergy, 5, 2, 153–164.

Syakila, A., Kroeze, C., 2011. The global nitrous oxide budget revisited. Greenhouse Gas Measur. Manag., 1, 17–26.

Šrank, D., Šimanský, V., 2020. Differences in soil organic matter and humus of sandy soil after application of biochar substrates and combination of biochar substrates with mineral fertilizers. Acta Fytotechnica et Zootechnica, 23, 3, 117–124.

Toková, L., Igaz, D., Horák, J., Aydin, E., 2020. Effect of biochar application and re-application on soil bulk density, porosity, saturated hydraulic conductivity, water content and soil water availability in a silty loam Haplic Luvisol. Agronomy, 10, 7, 1005.

Van Zwieten, L., Kimber, S., Morris, S., Chan, K.Y., Downie, A., Rust, J., Cowie, A., 2010. Effects of biochar from slow pyrolysis of papermill waste on agronomic performance and soil fertility. Plant and Soil, 327, 1, 235–246.

Wang, Z., Zheng, H., Luo, Y., Deng, X., Herbert, S., Xing, B., 2013. Characterization and influence of biochars on nitrous oxide emission from agricultural soil. Environmental Pollution, 174, 289–296.

WRB, 2014. World reference base for soil resources. World Soil Resources Reports, No. 106, FAO, 189 p.

Wrage, N., Velthof, G.L., van Beusichem, M.L., Oenema, O., 2001. Role of nitrifier denitrification in the production of nitrous oxide. Soil Biol. Biochem., 33, 1723–1732.

Yanai, Y., Toyota, K., Okazaki, M., 2007. Effects of charcoal addition on N_2O emissions from soil resulting from rewetting air-dried soil in short-term laboratory experiments. Soil Science and Plant Nutrition, 53, 2, 181–188.

Yuen, S.H., Pollard, A.G., 1954. Determination of nitrogen in agricultural materials by the Nessler reagent. II. Microdeterminations in plant tissue and in soil extracts. J. Sci. Food Agric., 5, 364–369.

Zhang, Q., Wu, Z., Zhang, X., Duan, P., Shen, H., Gunina, A., Yan, Z., Xiong, Z., 2021. Biochar amendment mitigated N_2O emissions from paddy field during the wheat growing season. Environmental Pollution, 281, 117026.

Received 31 May 2021
Accepted 4 August 2021

J. Hydrol. Hydromech., 69, 2021, 4, 436–446
DOI: 10.2478/johh-2021-0025
ISSN 1338-4333

sciendo Journal of Hydrology and Hydromechanics

Effect of mature spruce forest on canopy interception in subalpine conditions during three growing seasons

Martin Jančo[1], Pavel Mezei[2,3], Andrej Kvas[4], Michal Danko[1], Patrik Sleziak[1], Jozef Minďáš[5], Jaroslav Škvarenina[4*]

[1] Institute of Hydrology, Slovak Academy of Sciences, Dúbravská cesta 9, 841 04 Bratislava, Slovakia.
[2] Institute of Forest Ecology, Slovak Academy of Sciences, Štúrova 2, 960 53 Zvolen, Slovakia.
[3] Department of Forest Protection, Faculty of Forestry, Technical University in Zvolen, T.G. Masaryka 24, 960 01 Zvolen, Slovakia.
[4] Department of Natural Environment, Faculty of Forestry, Technical University in Zvolen, T.G. Masaryka 24, 960 01 Zvolen, Slovakia.
[5] Ecological & Forestry Research Agency EFRA, Medený hámor 11, 974 01 Banská Bystrica, Slovakia.
[*] Corresponding author. Tel.: +421 455 206 209. E-mail: skvarenina@tuzvo.sk

Abstract: The interception process in subalpine Norway spruce stands plays an important role in the distribution of throughfall. The natural mountain spruce forest where our measurements of throughfall and gross precipitation were carried out, is located on the tree line at an elevation of 1,420 m a.s.l. in the Western Tatra Mountains (Slovakia, Central Europe). This paper presents an evaluation of the interception process in a natural mature spruce stand during the growing season from May to October in 2018–2020. We also analyzed the daily precipitation events within each growing season and assigned to them individual synoptic types. The amount and distribution of precipitation during the growing season plays an important role in the precipitation-interception process, which confirming the evaluation of individual synoptic situations. During the monitored growing seasons, precipitation was normal (2018), sub-normal (2019) and above-normal (2020) in comparison with long-term precipitation (1988–2017). We recorded the highest precipitation in the normal and above-normal precipitation years during the north-eastern cyclonic synoptic situation (NEc). During these two periods, interception showed the lowest values in the dripping zone at the crown periphery, while in the precipitation sub-normal period (2019), the lowest interception was reached by the canopy gap. In the central crown zone near the stem, interception reached the highest value in each growing season. In the evaluated vegetation periods, interception reached values in the range of 19.6–24.1% of gross precipitation total in the canopy gap, 8.3–22.2% in the dripping zone at the crown periphery and 45.7–51.6% in the central crown zone near the stem. These regimes are expected to change in the Western Tatra Mts., as they have been affected by windstorms and insect outbreaks in recent decades. Under disturbance regimes, changes in interception as well as vegetation, at least for some period of time, are unavoidable.

Keywords: Precipitation; Interception; Synoptic types; Norway spruce (*Picea abies* L. Karst.); Growing season.

INTRODUCTION

In the conditions of the Western Carpathians, atmospheric precipitation is almost the only income component of the water balance (Minďáš, 2003). Forest canopies standing up in the air impede precipitation from reaching the ground. A portion of precipitation is inevitably intercepted by the canopy (canopy interception), flows along the stem to the ground surface (stemflow), drips from the foliage and branches or passes through canopy openings to the ground (throughfall), or is further intercepted by ground plants or the forest floor (litter interception). These processes cause a reduction in precipitation quantity and a redistribution of precipitation towards the soil (Arnell, 2002; Chang, 2013; Klamerus-Iwan et al., 2020; Sadeghi et al., 2020; Střelcová et al., 2006). The water regime of forest stands is also determined by the precipitation conditions of a given locality as well as by the properties of soils. Out of the many properties of a stand, the amount and distribution of the assimilation area is the most important factor for affecting the water balance in an ecosystem. Indeed, it determines the amount of transpiration as well as the retention of precipitation on the surface, i.e. interception (Bruijnzeel, 2004; Landsberg and Waring, 2014; Pypker et al., 2011; Shelton, 2009; Zabret et al., 2018). Interception is the process in which part of the rainwater is used or retained on the surface of trees or plants. This water neither infiltrates into the soil nor drains in the form of surface runoff. Therefore, the amount of intercepted precipitation that returns to the atmosphere upon evaporation is often referred to as interception loss (Dohnal et al., 2014; Gregersen et al., 2007; Llorens and Gallart, 2000; Šraj et al., 2008; Ward and Trimble, 2003).

From the point of view of the water balance, the interception of precipitation in spruce stands is quite significant. However, its magnitude varies in an orographically and vertically divided area. Interception plays a significant negative role in spruce forests at lower altitudes. By contrast, in mountain locations, the interception process of liquid precipitation changes due to occult precipitation from fog and interception may be perceived very differently, from a significantly negative item of the water balance of stands up to a positive item, depending on the local conditions (Bartík et al., 2016; Chroust, 1997; Kantor, 1981; Krečmer, 1973; Krečmer et al., 1981; Valtýni, 1986).

The topic of interception losses in forest hydrology has long received considerable attention. Nevertheless, we do not yet have enough reliable quantitative data, particularly from specific mountain habitats. One such habitat consists of climax mountain spruce trees growing in extreme mountain climate conditions below the tree line (Minďáš et al., 2018; Šípek et al.,

2020). Mountain spruce forests perform a number of important ecosystem services in the country (e.g. snow accumulation, protection against avalanches and soil erosion, a headwater function) as stated by, for instance, Fleischer et al. (2017), Holko et al. (2021), Pichler et al. (2010) and Seidl et al. (2019). The long-distance transport of air pollution and acid deposition from the 1970s through the 1990s in many mountain massifs, particularly in Western and Central Europe, caused a decline in natural mountain spruces (e.g Fazekašová et al., 2016; Minďáš and Škvarenina, 1995; Oulehle et al., 2013; Rehfuess, 1985; Vacek et al., 2015). The onset of climate change, accompanied by natural hazards such as extreme temperatures, drought, storms and the consequent calamities of bark beetles, has instigated thelarge-scale decline of fragile mountain spruces (Grodzki et al., 2006; Hroššo et al., 2020; Mezei et al., 2017; Seidl et al., 2011). Many recent works have also pointed to changes in the basic hydrological and ecological functions of affected areas (Bartík et al., 2019; Bernsteinová et al., 2015; Černohous et al., 2018; Gömöryová et al., 2017; Homolák et al., 2020; Hotový and Jeníček, 2020; Iovino et al., 2018; Jeníček et al. 2017; Lichner et al. 2020; Švihla et al., 2016). Due to the aforementioned reasons, it has become necessary to examine in detail the water balance of mountain spruces, including with regard to canopy interception.

The present research was conducted in a natural mountain Norway spruce (*Picea abies* L. Karst.) forest in the Western Tatra Mountains (Slovakia). It was designed to: (i) examine estimation of spruce canopy interception including the description of its small-scale spatial variability; (ii) determine the interception losses of spruce stands based on data from three consecutive growing seasons with different precipitation amounts (average, dry, wet) and determine the impact of atmospheric synoptic types on gross precipitation; and (iii) analyze the spatial and temporal variability of throughfall in the three growing seasons and to compare these values with those published for spruce ecosystems with similar ecological conditions.

MATERIAL AND METHODS

Study site

The Červenec study site is situated in a mature (climax) spruce stand in the Jalovecká valley in the Western Tatra Mts. (latitude 49.183617°N, longitude 19.641944°E, altitude 1,420 m a.s.l.) (Fig. 1.). This valley is characterized with its quaternary glacial terrain modelling. The whole research plot is located within a geologic boundary between the Crystallinic and Mesozoic zones in the Inner Western Carpathians. The predominant crystalline rocks are granodiorites and rules covered with cambisol podsoles and accompanied with lithosols and rankers. From the Mesozoic rocks, the dominant types include calcites and dolomites with developed cambisol rendzinas (Bartík et al., 2014, 2016; Holko et al., 2020). This part of the Western Tatras belongs to the cold climatic region, the cold mountain and very wet district (Lapin et al., 2002). The annual average air temperature at Červenec is 3.0 °C and long-term annual precipitation is 1,450 mm (Danáčová et al., 2019).

The main vegetation cover of the study plots comprises forest ecosystems, predominantly following forest types: *Sorbeto-Piceetum* (9410 Acidophilous spruce forests (*Vaccinio-Piceetea*)); *Cembreto-Piceetum* (9420 Alpine *Larix decidua* and *Pinus cembra* forests); above the timberline (4070 Bushes with *Pinus mugo*) (Hančinský, 1972; Stanová and Valachovič, 2002).

The predominant tree species is Norway spruce (*Picea abies* L. Karst.), accounting for 100% of the tree species coverage. Sites characterized by loosened canopy and the understorey include rowan (*Sorbus aucuparia* L.), raspberry brushes (*Rubus ideaus* L.), bilberry (*Vaccinium myrtillus* L.) and natural spruce regeneration. The plot has a south-east exposition with a slope of 20°–33° and an area of about 0.3 ha. In the over-130-year-old stand the average tree height is 26.8 m, the average stem diameter at breast heigh is 40.5 cm and the stocking density, at about 0.6, is low (Oreňák et al., 2013).

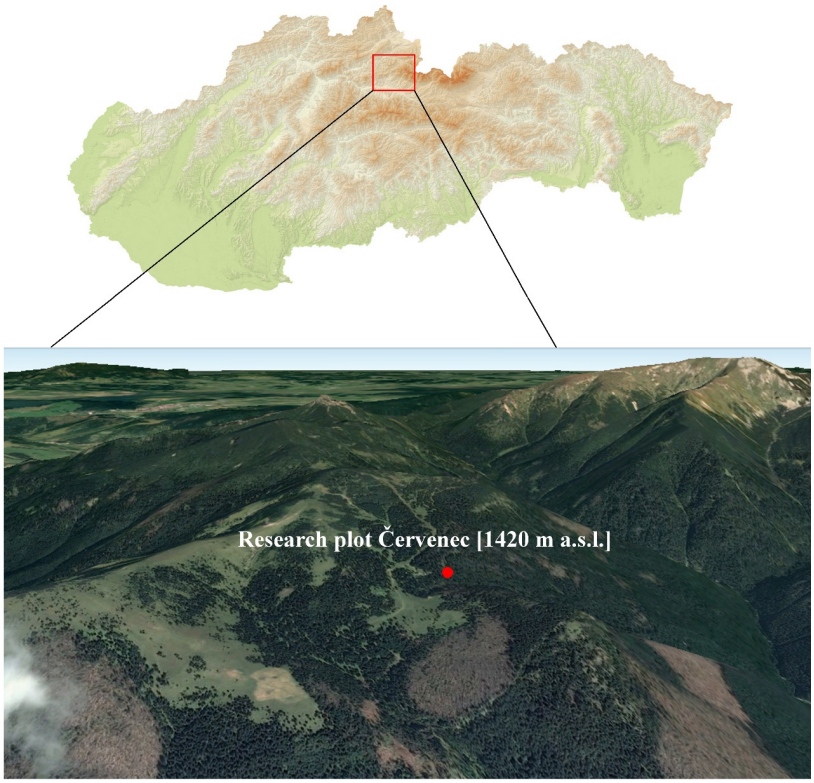

Fig. 1. Research plot Červenec.

Precipitation measurements

The amount of precipitation was recorded in the growing seasons of 2018–2020. The growing season in these areas begins in early May and concludes around the end of October, depending on the weather conditions. The data were sampled in approximately two-week intervals, as the research plot is rather remote. Water precipitation was collected in ten standard Czechoslovak rain gauges METRA (an orifice area of 500 cm^2 (Fig. 2.). The primary categorization of the measurements of precipitation was in an open area vs. in the forest stand. Daily precipitation totals were recorded by means of automatic weighing rain gauge TRwS 504 with an orifice area of 500 cm^2, we based our evaluation of synoptic situation on this metric. One standard METRA rain gauge was located on an open area, situated at a sufficient distance from the forest stand to limit or eliminate the influence of the surrounding standing trees on the amount of precipitation as a result of the air flow. Due to the structure of the forest stand, the rain gauges were installed in the canopy gap (GAP), in the dripping zone at the crown periphery (CROWN) and in the central crown zone near the stem (STEM) (Fig. 2.). In the forest, three METRA rain gauges were located in each of these three localities. We considered this research design sufficient for preliminary research on canopy interception in mountain forest, mainly due to rough terrain and accessibility regarding periodical measurements.

The canopy gap was characterized as an unconnected area by trees or their branches in a stand without trees with an area of about 20–30 m^2. Rain gauges were placed in the middle of this space. The dripping zone at the crown periphery represented precipitation, which was caught in the surface parts of the crown and dripped into the sub-canopy space after canopy saturation. In the central crown zone near the stem, rain gauges were located near the stem (Bartík et al., 2016; Dohnal et al., 2014; Minďáš et al., 2018; Oreňák et al., 2013).

Data analysis

In the period from 1 May to 31 October in years 2018, 2019 and 2020, each day was assigned the appropriate type of synoptic situation (Slovak Hydrometeorological Institute, 2021) and, in the case of precipitation on a given day,the appropriate precipitation total as well.Atmospheric circulation was characterized by the synoptic types according to Ballon et al. (1964) and Brádka et al. (1961), updated by Racko (1996), which are extensively used in synoptic and climatological practice in the Czech and Slovak republics. Czech and Slovak types are basically a modification of the catalogue of Hess and Brezowsky (1977) to optimally suit the conditions in the former Czechoslovakia (Beranova and Huth, 2005). The Czech and Slovak catalogue consists of 28 types, leaving no days unclassified. For the list of types see Table 1. Similarly, the synoptic types were applied to characterize pollutant concentrations in precipitation (Fišák and Tesař, 2015; Fišák et al., 2004).

The recorded totals of throughfall in individual measurements were first expressed as the arithmetic mean for each locality in the stand. Interception loss (I_L)in mm was calculated as the difference between gross precipitation (P_G) and throughfall (T_F)using the following equation:

$$I_L = P_G - T_F \quad (1)$$

The interception ratio (I) in % was then calculated as follows:

$$I = \left(\frac{I_L}{P_G} \right) \times 100 \quad (2)$$

All analyses and plot displays were performed using Statgraphics Centurion 16, Statistica 12 and Microsoft Excel 2016

Fig. 2. Throughfall measurements in the mature spruce forest in the research plot Červenec: in the canopy gap „GAP“ (A), in the dripping zone at the crown periphery „CROWN“ (B) and in the central crown zone near the stem „STEM“ (C).

software. When comparing the equality of the mean of the two dependent samples, we first needed to ascertain whether the data (interception in %) showed a normal distribution. To determine whether the data came from a normal distribution, we used the Shapiro–Wilk test. If the p-value ≥0.05, the data showed a normal distribution, while if the p-value <0.05 the data did not come from a normal distribution. If the compared samples showed a normal distribution, we used Student's paired t-test. If the distribution of one of the compared samples was not normal, we used the non-parametric Wilcoxon paired test. The level of significance (α) in the test was set at 95% in all cases, so if the p-value ≤0.05, we were able to state that the difference between the individual samples was statistically significant.

We used correlation and regression analysis to determine the dependence of interception losses in the stand (mm) on gross precipitation. The statistical significance of the linear relationship between the samples was tested with analysis of variance at a 95% confidence level. If p-value ≤0.05, the relationship was not significant.

RESULTS AND DISCUSSION

Evaluation of synoptic situations and precipitation totals

The occurrence of precipitation in individual synoptic types is presented in Table 1. For an illustration of the occurrence of individual synoptic types during the monitored periods in 2018–2020, the absolute frequency of these types is also given in Table 1 (column 1 (days)).

Table 1. Frequency of synoptic types (ST) in days, gross precipitation total (P_G) and percentage contribution (PC) of each synoptic situation to the precipitation total of the months May–October in the years 2018, 2019 and 2020.

	2018			2019			2020		
Synoptic types	ST (days)	PG (mm)	PC (%)	ST (days)	PG (mm)	PC (%)	ST (days)	PG (mm)	PC (%)
B	21	83.2	10.7	22	17.1	28.5	17	90.5	8.8
Bp	20	119.7	15.5	24	86.7	14.1	5	72.0	7.0
C	4	28.2	3.6	5	112.2	18.3	6	105.1	10.3
Cv	11	26.9	3.5	2	7.8	1.3	19	155.6	15.2
NWc	13	131.5	17.0	1	5.8	0.9	3	72.7	7.1
NEc	17	288.4	37.3	7	10.0	1.6	12	247.3	24.2
Nc	2	23.7	3.1	10	26.5	4.3	3	33.3	3.3
Wc				3	6.2	1.0	7	48.5	4.7
Wcs				7	33.8	5.5	5	31.0	3.0
SWc1				3	5.2	0.8	8	41.9	4.1
SWc2				7	38.6	6.3	4	2.2	0.2
SWc3							2	24.4	2.4
SEc	10	32.2	4.2	3	11.9	1.9	5	15.7	1.5
Ec				3	0.2	0.0	3	4.7	0.5
Vfz				3	19.1	3.1	2	20.2	2.0
A	2	0.0	0.0	7	10.6	1.7	9	0.2	0.0
Ap1				8	31.6	5.1	7	9.2	0.9
Ap2	13	4.7	0.6	7	1.8	0.3	8	4.2	0.4
Ap3				5	0.5	0.1			
NWa	8	0.9	0.1	13	8.9	1.4	11	5.2	0.5
NEa	13	8.7	1.1	1	0.1	0.0	9	6.3	0.6
Wa	2	1.4	0.2	7	3.0	0.5	8	0.7	0,1
Wal	20	6.3	0.8		0.0	0.0	14	18.6	1.8
Sa	11	0.2	0.0	16	0.5	0.1	3	0.1	0.0
SEa	1	2.4	0.3	7	16.6	2.7	3	11.4	1.1
SWa	7	0.3	0.0	10	0.8	0.1	6	2.6	0.3
Ea	9	15.2	2.0	3	0.5	0.1	5	0.0	0,0
Sume of type c	98	733.7	94.8	100	539.1	87.8	101	965.0	94.3
Sume of type a	86	40.1	5.2	84	74.9	12.2	83	58.6	5.7
Sume of c+a	184	773.8	100.0	184	614.0	100.0	184	1023.6	100.0

Synoptic situations: **Wc**, west cyclonic; **Wcs**, west cyclonic with southern pathway; **Wa**, west anticyclonic; **Wal**, west anticyclonic of summer type; **NWc**, north-west cyclonic; **NWa**, north-west anticyclonic; **Nc**, north cyclonic; **NEc**, north-east cyclonic; **NEa**, north-east anticyclonic; **Ec**, east cyclonic; **Ea**, east anticyclonic; **SEc**, south-east cyclonic; **SEa**, south-east anticyclonic; **Sa**, south anticyclonic; **SWc1**, south-west cyclonic of the 1st type; **SWc2**, south-west cyclonic of the 2nd type; **SWc3**, south-west cyclonic of the 3rd type; **SWa**, south-west anticyclonic; **B**, trough over Central Europe; **Bp**, travelling trough; **Vfz**, entry of the frontal zone; **C**, cyclone over Central Europe; **Cv**, upper cyclone; **A**, anticyclone over Central Europe; **Ap1**, travelling anticyclone of the 1st type; **Ap2**, travelling anticyclone of the 2nd type; **Ap3**, travelling anticyclone of the 3rd type

Year 2018: a so-called normal/average year (102% of the long-term precipitation average for May–October). Almost 95% of the precipitation from May to October 2018 fell in cyclonic weather types. The highest total precipitation fell on days with the synoptic situation of NEc, namely 288 mm, representing 37% of the total in the observed period. In the NEc situation, the highest daily total (129 mm) recorded in 2018 fell on 18 July. Subsequently, large amounts of precipitation fell in NWc 132 mm (17%), Bp 120 mm (16%) and B 83 mm (11%). Types C, Cv SEc and Nc contributed only marginally (3–4%). The anticyclonic types, Ea, NWa and Wal, altogether contributed about 4% to the total precipitation.

Year 2019: a relatively dry year (85% of the long-term precipitation average for May–October). Precipitation in 2019 fell in the following proportion: 88% for cyclonic types and 12% for anticyclone types of weather situations. During the period with synoptic situations B, almost 175 mm, representing 29% of the total in the observed period. Then there were the following situations C 112 mm (18%) and Bp 87 mm (14%), together SWc 44 mm (7%) and Wcs 34 mm (5.5%), and other cyclonic types were below 5%. The highest daily total (64.2 mm) fell on 22 May in situation C. This situation C cyclone over Central Europe lasted for five days from 19 to 23 May, during which a total of 132 mm fell, representing about 21% of the precipitation in the observed period. In 2019, in comparison with the other years evaluated, there was more precipitation even in anticyclonic synoptic situations, mostly precipitation of a storm nature. The types Ap (together) accounted for about 34 mm (5%), SEa for about 17 mm (3%) and A for 11 mm (2%).

Year 2020: an above-normal year of precipitation (135% of the long-term precipitation average for the months of May–October). In this year, cyclonic synoptic types predominated (94% of the precipitation total), while anticyclonic types accounted for only 6%. As in 2018, the synoptic type NEc contributed the most to the total, with a total of 247 mm (24%). The highest daily total precipitation (77 mm) was reached again in the NEc situation on 30 September. It is worth mentioning that the second-highest daily total (64 mm) was reached in the same synoptic situation NEc on 22 June. Synoptic types (Cv 156 mm, 15%; C 105 mm (10%) also accounted for a more significant share of the total, so in summary, situations C and Cv represented up to 25% of the total. Regarding the othercyclonic types, B and Bp should be mentioned, as they collectively contributed to a total of about 160 mm (15%). Out of the rest of the types, only the anticyclonic situations Wal and Ap contributed above 1% of the total.

The Western Tatras, as a massive mountain range, form the north-western edge wall for precipitation-bearing western, northern and partly also north-eastern cyclonic situations. Compared to the other parts of Slovakia (Petrovič, 1972), the character of precipitation hereis different. Indeed, in other regions of Slovakia, the most precipitation was brought by synoptic situations with a western and north-western flow (Bp, Wc, NWc and SWc). In the study area, the largest amount of precipitation wasobserved in the north-eastern cyclonic situation (NEc) in 2018 and 2020. As mentioned by Krečmer (1973), the mountain locality Šerlich (elevation 960 m a.s.l.) in the Orlické Mountains also classified the NEc type as the rainiest. The Orlické Mountains are located on the north-eastern border of the Czech Republic and Poland, where the geographical effects of air flow and movement of active frontal and air masses manifest similarly to those on the edge of the Western Tatras. A similar opinion was expressed by Konček and Orlicz (1974) for the Polish side of the Western Tatras, when they analyzed the summer precipitation conditions of the mountain obsevatory at Kasper Peak (elevation 1987 m a.s.l.). In addition to the synoptic situation of NEc in the summer rain totals, the situation of Nc predominates. Compared to other, southern parts, the south-western cyclonic situations (SWc1 to SWc3) bringgreater precipitation to the marginal northern parts of our territory only sporadically (Polčák and Mészáros, 2018).

Comparison of interception in individual zones of stand measurement during growing seasons (2018–2020)

The amount of precipitation had a significant effect on the values of interception during the analyzed growing seasons of 2018, 2019 and 2020. The distribution of sub-canopy precipitation within the natural spruce stand with reduced stocking density showed considerable heterogeneity. The recorded values of interception during vegetation periods fluctuated considerably. In the canopy gap, we recorded interception values of the gross precipitation total in the range of 4.4–40.0% in the growing season of 2018, 7.0–39.3% in 2019 and 13.3–32.3% in 2020 (Fig. 3.). Furthermore, in the canopy gap, there were two situations in the growing season of 2019 and one situation in the growing season of 2020 when the measured precipitation total in the stand exceeded the gross precipitation. These situations could have been caused by the influence of the wind, which transported precipitation captured in the canopy space into the area of the canopy gap.

In the dripping zone at the crown periphery, we recorded the highest variability of interception. One of the factors influencing values of interception during the vegetation period is the occurrence of occult precipitation (Holko et al., 2009; Krečmer, 1973; Minďáš et al., 2018; Vorčák et al., 2009). This effect was most pronounced in the studied locality, when we recorded five cases in all evaluated periods with the throughfall exceeding the gross precipitation. High levels of throughfall always occurred at the beginning of each growing season during a two-week period: for example, on 21 May 2020 we recorded up to 42.9% higher throughfall than gross precipitation (Fig. 3.). We also registered significantly higher throughfall on 28 July 2018 at the highest recorded two-week gross precipitation total (232.4 mm) of all three evaluated periods. In addition, occult precipitation by its interaction reduces canopy storage capacity. The range of interception values in the dripping zone at the crown periphery ranged from –17.9 to 53.7% in the growing season of 2018, from –17.3 to 64.3% in 2019 and from –42.9 to 56.7% in 2020 (Fig. 3.). Out of 12 measurements in the dripping zone at the crown periphery, Bartík et al. (2016) reported up to 8 times higher throughfall than gross precipitation in a living spruce stand at this locality during the growing season of 2014. In a spruce forest in the Orlické Mountains (960 m a.s.l.) in the growing seasons 1962–1966 during individual months, Krečmer (1968) reported a significant variability of interception, ranging from an improvement of throughfall by 28.0% up to the canopy interception of 25.0%. Fojt and Krečmer (1975) reported an enrichment of 15% by occult precipitation at the same locality during the growing season (6 months). Kantor (1981) reported a negative interception of 2.0% in the growing season of 1978 during rainfall events with the occurrence of fog. In research conducted in North America, Lovett et al. (1982) reported enrichment with rainwater of 450 mm per year (20% of the annual gross precipitation) at an elevation above 1,200 m a.s.l. in a Douglas fir stand (*Pseudotsuga menziesii*), while Harr et al. (1982) reported an improvement of 880 mm (30% of the annual gross precipitation) in Oregon, also at an elevation above 1,200 m a.s.l. in Douglas fir forests.

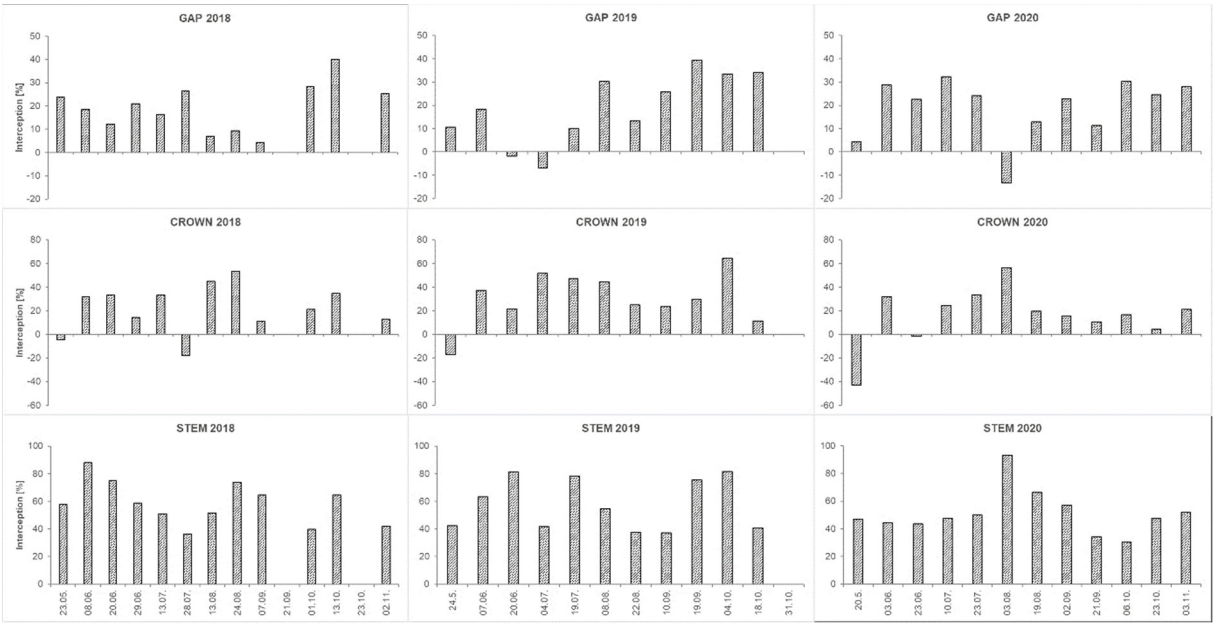

Fig. 3. Interception (%) in the canopy gap (GAP), in the dripping zone at the crown periphery (CROWN) and in the central crown zone near the stem (STEM) during the growing seasons of 2018–2020.

In the central crown zone near the stem, interception reached the highest values in most cases. In this locality, which is not identical with the stemflow, the lowest amount of precipitation was able to penetrate due to the shape of the growing branches. In the growing seasons, we recorded interception in the range of 36.2–87.8% in 2018, 37.1–81.7% in 2019 and 30.5–93.3% in 2020 (Fig. 3.).

The calculated sums of throughfall (mm), interception losses (mm), interception (%) and gross precipitation (mm) during the evaluated periods are given in Table 2. The canopy gap reached a total interception loss of 163.7 mm (21.2% of the gross precipitation total) in 2018, 120.5 mm (19.6%) in 2019 and 246.4 mm (24.1%) in 2020. The dripping zone at the crown periphery reached a total interception loss of 64.1 mm (8.3% of the gross precipitation total) in 2018, 136.4 mm (22.2%) in 2019 and 156.3 mm (15.3%) in 2020. The central crown zone near the stem reached a total interception loss of 395.2 mm (51.1% of the gross precipitation total) in 2018, 300.9 mm (49.0%) in 2019 and 467.8 mm (45.7%) in 2020. When comparing individual localities, we recorded the lowest interception losses in the growing seasons of 2018 and 2020 in the following order: the dripping zone at the crown periphery > canopy gap > the central crown zone near the stem. An exception was the poorest precipitation period of 2019, when we recorded the lowest interception in the following order: the canopy gap > the dripping zone at the crown periphery > the central crown zone near the stem. This could have been caused either by two recorded situations, when the throughfall reached higher values than the gross precipitation, or by very warm weather, especially in the period June–October. The year 2019 was the warmest in Europe since at least 1980, with the warmest period being June–August (European Centre for Medium-Range Weather Forecasts and Copernicus Climate Change Service, 2020). The warm growing season was also manifested by the highest values of interception in the dripping zone at the crown periphery in comparison with the growing seasons 2018 and 2020. Regarding this study site in the living forest during the growing seasons of 2007–2011, Oreňák et al. (2013) reported that average interception was 27.0% in the canopy gap, 20% in the dripping zone at the crown periphery and 63% in the central crown zone near the stem. Also concerning this study site in the living forest during the growing seasons of 2012–2015, Jančo et al. (2017) reported that average interception was 10.1% in the canopy gap, 1.6% in the dripping zone at the crown periphery and 70.6% in the central crown zone near the stem. Regrettably, both of the living stands used in the past with which we compared our results are now dead. Expressing interception as the average of these three localities (GAP, CROWN, STEM) during each evaluated growing season, interception reached 26.8% in 2018, 30.3% in 2019 and 28.3% in 2020. These interception values obtained in spruce forest support numerous previous findings from Europe and North America that average coniferous forest interception ranges from 25.0 to 35.0% of the gross precipitation total (Robinson and Ward, 2017) Furthermore, the values of average interception obtained here correspond to the results of other authors, who have reported values in the range of 23.0–38.0% for older spruce stands (e.g. Grelle et al., 1997; Grunicke et al., 2020; Halmová et al., 2006; Kofroňová et al., 2021; Tužinský, 2004; Viville et al., 1993).

We statistically compared the interception data (%) calculated from each measurement at individual localities in the stand in each evaluated growing season (Fig. 4). A statistical evaluation of the results is given in Table 3. Based on the completed Student's paired t-test and the nonparametric Wilcoxon paired test, a statistically significant difference was not confirmed in all growing seasons between the canopy gap and the dripping zone at the crown periphery. However, when comparing the central crown zone near the stem with these two localities, we were able to see a significant difference (bold values in Table 3) in all cases.

Relationship between interception loss in individual zones of stand measurement and gross precipitation

The expressed linear regression of the calculated values of the interception loss (mm) on the amount of gross precipitation at the measured localities in the stand (GAP, CROWN, STEM) are shown in Figs. 5, 6 and 7. Above the graphs are the linear regression equation, the coefficient of determination (R^2), Pearson's correlation coefficient (R) and p-value, informing us

Table 2. Precipitation total and interception (mm, %) in the growing seasons of 2018–2020.

Position of rain gauges	Growing season		
	2018	**2019**	**2020**
Canopy gap	Throughfall [mm]		
	610.1	493.5	777.2
	Interception [mm, %]		
	163.7 21.2	120.5 19.6	246.4 24.1
Dripping zone at the crown periphery	Throughfall [mm]		
	709.7	477.6	867.3
	Interception [mm, %]		
	64.1 8.3	136.4 22.2	156.3 15.3
Central crown zone near the stem	Throughfall [mm]		
	378.6	313.1	555.8
	Interception [mm, %]		
	395.2 51.1	300.9 49.0	467.8 45.7
Open area	Gross precipitation [mm]		
	773.8	614.0	1023.6

Table 3. Statistical characteristics of interception (%).

	Count	Average	Standard deviation	Coeff. of variation	Minimum	Maximum	Range	Shapiro–Wilk p-value
GAP 2018	12	19.4	10.21	52.61	4.4	40.0	35.6	**0.8752**
CROWN 2018	12	22.4	20.43	91.29	–17.9	53.7	71.6	**0.7529**
STEM 2018	12	58.6	15.60	26.64	36.1	87.8	51.7	**0.8792**
GAP 2019	11	18.8	15.22	80.97	–7.0	39.3	46.3	**0.6239**
CROWN 2019	11	30.8	22.17	71.89	–17.3	64.3	81.6	**0.7255**
STEM 2019	11	57.6	18.78	32.61	37.1	81.7	44.6	0.0352
GAP 2020	12	19.0	13.20	69.33	–13.3	32.3	45.6	0.0292
CROWN 2020	12	15.9	23.86	150.20	–42.9	56.7	99.6	**0.1668**
STEM 2020	12	50.7	16.54	32.63	30.5	93.3	62.8	0.0450

p* - result of Shapiro–Wilk test (bold value means, that the data come from normal distributions)

Locality	p-value	Locality	p-value	Locality	p-value
GAP 18 vs. CROWN 18*	0.6978	GAP 19 vs. CROWN 19*	0.1562	GAP 20 vs. CROWN 20**	0.2721
GAP 18 vs. STEM 18*	**0.0001**	GAP 19 vs. STEM 19**	**0.0033**	GAP 20 vs. STEM 20**	**0.0022**
CROWN 18 vs. STEM 18*	**0.0000**	CROWN 19 vs. STEM19**	**0.0044**	CROWN 20 vs. STEM 20**	**0.0022**

*Student´s paired test, ** Wilcoxon paired test (bold values define statistically significant differences $p \leq 0.05$)

whether a statistically significant difference was confirmed between the correlation of interception loss and gross precipitation. Bold values represent a statistically significant difference. The Pearson's correlation coefficient was most significant in the central crown zone near the stem, indicating a relatively strong relationship between the variables, followed by the canopy gap, indicating a moderately strong relationship between the variables as well. The least significant of the three was the dripping zone at the crown periphery, indicating a relatively weak relationship between the variables. The R-squared statistic (coefficient of determination) indicated that the fitted model explained 88.8% of the variability in interception loss in the central crown zone near the stem, 87.6% of the variability in interception loss in the canopy gap and 1.2% of the variability in interception loss in the dripping zone at the crown periphery out of the gross precipitation. A statistically significant difference in correlation was confirmed in the canopy gap and in the central crown zone near the stem. It follows that in the central crown zone near the stem, interception losses were most affected by the gross precipitation, because this space in the stand intercepts the largest amount of precipitation. The canopy gap and its interception losses are also significantly affected by the gross precipitation, but to a lesser extent. Although this space has no active surface above it to retain precipitation, it is mainly exposed to the wind. The higher the wind speed, the more the direction of rainfall deviates from the vertical direction, while the surrounding trees can act as a rain shadow. The vegetation may lead to 'precipitation shading' of the site in certain direction, but if the wind speed exceeds a certain limit, when it is able to carry the captured precipitation in the crowns, these may exceed the gross precipitation values (20 June, 4 July 2019 and 3 August 2020 (Fig. 3)). The gross precipitation total in the dripping zone at the crown periphery has the smallest effect on the interception loss, because in this area the variability of the interception loss is the highest and it is influenced by the effect of occult precipitation. In the dripping zone at the crown periphery, such a correlation was not statistically confirmed. Similar results at the same studied site during the growing seasons of 2007–2011 were reported by Oreňák et al. (2013), where the Pearson's correlation coefficient of interception loss was most significant in the central crown zone near the stem, followed by the canopy gap and least important in the dripping

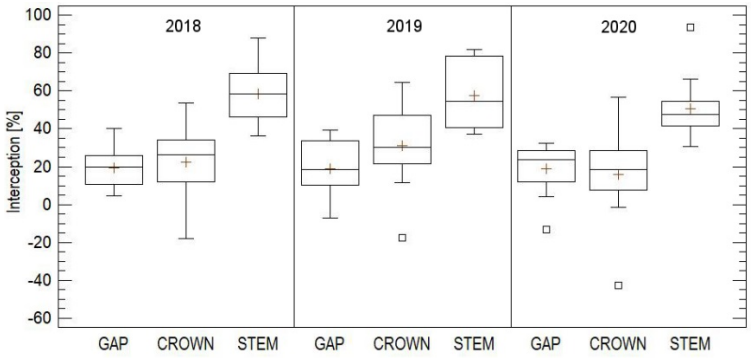

Fig. 4. Box-whisker plots (maximum-minimum; lower and upper quartiles; median; the crosses show the arithmetic mean, the squares show the outliers) of interception (%) for the growing seasons of 2018–2020.

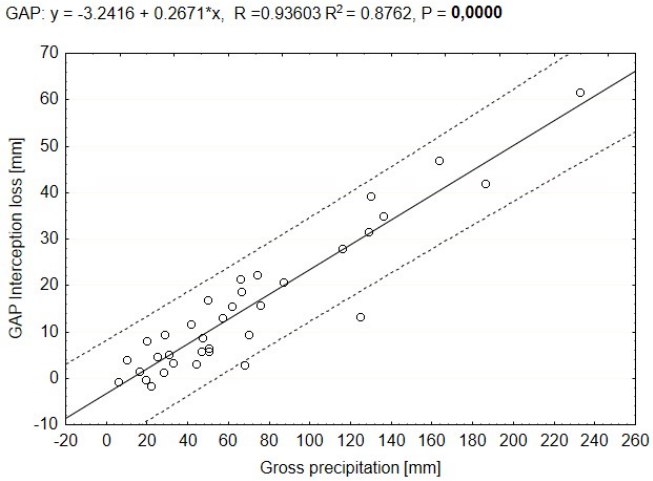

Fig. 5. Linear regression between canopy gap (GAP) interception loss (mm) and gross precipitation (2018–2020). The solid line represents the regression line; the dashed lines are the upper and lower 95% prediction intervals of the regression.

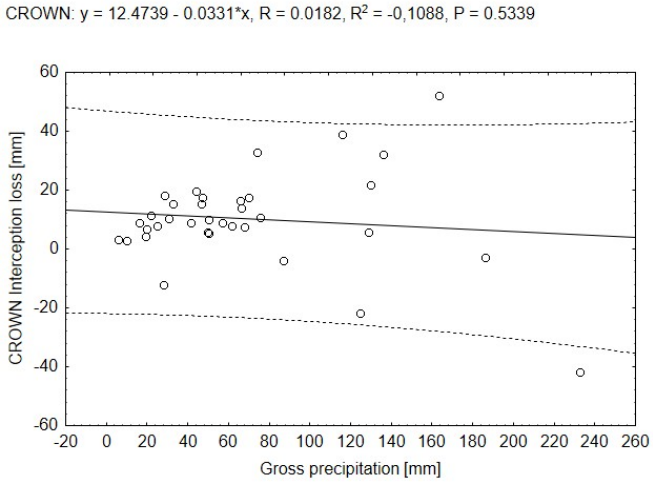

Fig. 6. Linear regression between the dripping zone at the crown periphery (CROWN) interception loss (mm) and gross precipitation (2018–2020). The solid line represents the regression line; the dashed lines are the upper and lower 95% prediction intervals of the regression.

zone at the crown periphery. Droughts, insects and fungi already contribute to the decline of spruce forests (Sierota et al., 2019). Given that interception is partially a function of forest structure and physiological characteristics of host trees (Bladon

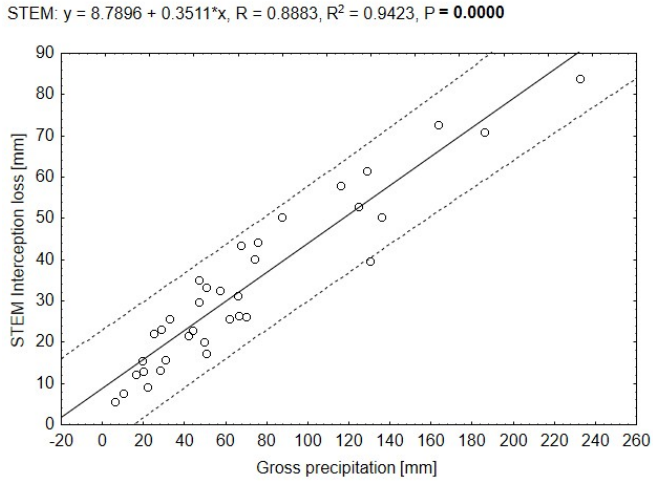

Fig. 7. Linear regression between central crown zone near the stem (STEM) interception loss (mm) and gross precipitation (2018–2020). The solid line represents the regression line; the dashed lines are the upper and lower 95% prediction intervals of the regression.

et al., 2019; Kaiser et al., 2013). Additionally, the topographic structure mediates the redistribution of water and the spatial patterns of forest vegetation, giving rise to temporal complexity in the ecological processes associated with vegetation.

CONCLUSION

Understanding how trees interact with interception processes is important for the development of effective strategies and tools for sustainable resource management in the future. Large parts of the Tatra Mts. have already been hit by significant ecosystem disturbances, including spruce bark beetle outbreaks. Our study aimed to evaluate the influence of mountain spruce forest on the distribution of throughfall in the growing seasons of 2018–2020 and provided a unique opportunity to analyze rainfall interception in an unaffected forest. And although the study design was constrained by rough terrain and challenges regarding periodical monitoring, the analysis of synoptic types points to the differences in meteorological conditions of occurrence of precipitation in the observed study plot. We recorded amounts of precipitation in the growing seasons in descending order as follows: 2020 > 2018 > 2019. Most of the precipitation totals in each period were recorded in cyclonic situations. Furthermore, based on the results of our measurements we can state that the distribution of precipitation differs within the stand structure in the sub-canopy space.

Our research can be used to develop a more mechanistic understanding of the feedbacks between hydrology and ecological processes. The lowest amount of throughfall in each evaluated period was recorded in the central crown zone near the stem, indicating that interception here was highest. The lowest values of interception were seen in the dripping zone at crown periphery, with the exception of during the growing season of 2019, when we recorded the lowest interception in the canopy gap. The mosaic of land-cover change that has affected the rest of the Tatra Mts. can alter ecosystem response and hydrology will be among the first affected ecosystem services. Interception of individual localities differed in each growing season in the cases of the canopy gap and the central crown near the stem, the dripping zone at the crown periphery and the central crown zone near the stem. Canopy gap and the central crown zone near the stem affected also the interception loss between the gross precipitation. This phenomenon owed to the presence of occult precipitation, which compensated for interception losses and enriched the stand with rainwater. The total interception of the stand reached 26.8% (2018), 30.3% (2019) and 28.3% (2020) of the gross precipitation total. In the future, we expect significant changes in the hydrological cycle in the Tatra Mts., mainly due to repeated wind storms, bark beetle outbreaks and subsequent sanitary measurements. Our study provides a basis for future comparison and changes in affected forests with baseline conditions described in the above-presented study.

Acknowledgements. This work was supported by the VEGA project nos. 1/0500/19 and 2/0065/19 awarded by the Ministry of Education, Science, Research and Sport of the Slovak Republic and the Slovak Academy of Sciences; and the projects of the Slovak Research and Development Agency nos. APVV-15-0425, APVV-16-0306, APVV-18-0347, APVV-19-0183 and APVV-19-0340. The authors thank the agencies for their support.

REFERENCES

Arnell, N., 2002. Hydrology and Global Environmental Change. Routledge, London, 364 p.

Ballon, L., Forgáč, P., Molnár, F., 1964. Weather over the territory of Slovakia in typical weather situations. Hydrometeorologický ústav, Praha, 30 p. (In Slovak.)

Bartík, M., Sitko, R., Oreňák, M., Slovík, J., Škvarenina, J., 2014. Snow accumulation and ablation in disturbed mountain spruce forest in West Tatra Mts. Biologia, 69, 1492–1501.

Bartík, M., Jančo, M., Střelcová, K., Škvareninová, J., Škvarenina, J., Mikloš, M., Vido, J., Waldhauserová, P.D., 2016. Rainfall interception in a disturbed montane spruce (*Picea abies*) stand in the West Tatra Mountains. Biologia, 2016, 71, 1002–1008.

Bartík, M., Holko, L., Jančo, M., Škvarenina, J., Danko, M., Kostka, Z., 2019. Influence of mountain spruce forest dieback on snow accumulation and melt. Journal of Hydrology and Hydromechanics, 67, 59–69.

Beranová, R., Huth, R., 2005. Long-term changes in the heat island of Prague under different synoptic conditions. Theoretical and Applied Climatology, 82, 113–118.

Bernsteinová, J., Bässler, C., Zimmermann, L., Langhammer, J., Beudert, B., 2015. Changes in runoff in two neighbouring catchments in the Bohemian Forest related to climate and land cover changes. Journal of Hydrology and Hydromechanics, 63, 342–352.

Bladon, K.D., Bywater-Reyes, S., LeBoldus, J. M., Keriö, S., Segura, C., Ritóková, G., Shaw, D.C., 2019. Increased streamflow in catchments affected by a forest disease epidemic. Science of the Total Environment, 691, 112–123.

Brádka, J., Dřevikovský, A., Gregor., Z., Kolesár, J., 1961. Weather over the territory of Bohemia and Moravia in typical weather situations. Hydrometeorologický ústav, Praha, 31 p. (In Czech.)

Bruijnzeel, L.A., 2004. Hydrological cycle. In: Burley, J., Evans, J., Youngquist, J. (Eds.): Encyclopedia of Forest Sciences. Elsevier Academic Press, Oxford, pp. 340–350.

Černohous, V., Švihla, V., Šach, F., 2018. Manifestation of drought in spruce pole-stage stand in summer 2015. Zprávy Lesnického Výzkumu, 63, 10–19. (In Czech.)

Chang, M., 2013. Forest Hydrology: An Introduction to Water and Forests (third edition). CRC Press, Boca Raton, 595 p.

Chroust, L., 1987. Ecology of forest education. Výzkumný ústav lesního hospodářství a myslivosti, Opočno. 277 p. (In Czech.)

Danáčová, M., Danko, M., Lajda, D., 2019. The influence of the degree-day factor determination on the snow water equivalent simulation. Meteorologický časopis, 22, 11–20. (In Slovak.)

Dohnal, M., Černý, T., Votrubová, J., Tesař, M., 2014. Rainfall interception and spatial variability of throughfall in spruce stand. Journal of Hydrology and Hydromechanics, 62, 277–284.

European Centre for Medium-Range Weather Forecasts, Copernicus Climate Change Service, 2020. Copernicus: 2019 was the second warmest year and the last five years were the warmest on record (https://climate.copernicus.eu/index.php/copernicus-2019-was-second-warmest-year-and-last-five-years-were-warmest-record).

Fazekašová, D., Boguská, Z., Fazekaš, J., Škvareninová, J., Chovancová, J., 2016. Contamination of vegetation growing on soils and substrates in the unhygienic region of Central Spiš (Slovakia) polluted by heavy metals. Journal of Environmental Biology, 37, 1335–1340.

Fišák, J., Řezáčová, D., Weignerová, V., Tesař, M, 2004. Synoptic Situations and Pollutant Concentrations in Fog Water Samples from the Milešovka Mt. Studia Geophysica et Geodaetica, 48, 469–481.

Fišák, J., Tesař, M., 2015. Evaluation of the contribution of deposited precipitation. Advances in Meteorology, 2015, Article ID 472963.

Fleischer, P., Pichler, V., Fleischer, P. Jr., Holko, L., Máliš, F., Gömöryová, E., Cudlín, P., Michalová, Z., Homolová, Z., Škvarenina, J., Střelcová, K., Hlaváč, P., 2017. Forest ecosystem services affected by natural disturbances, cliamte and land-use changes in the Tatra Mountains. Climate Research, 73, 57–71.

Fojt, V., Krečmer, V., 1975. Formation of horizontal precipitation from fog and its amount in spruce stands in the middle mountain region. Vodohospodářsky časopis, 23, 581–606. (In Czech.)

Gömöryová, E., Fleischer, P., Pichler, V., Homolák, M., Gere, R., Gömöry, D., 2017. Soil microorganisms at the windthrow plots: the effect of post-disturbance management and the time since disturbance. iForest-Biogeosciences and Forestry, 10, 515–521.

Gregersen, M.H., Ffolliott, F.P., Brooks, N.K., 2007. Integrated Watershed Management: People to their land and water. CABI, Cambridge, 288 p.

Grelle, A., Lundberg, A., Lindroth, A., Morén, A.S., Cienciala, E., 1997. Evaporation components of a boreal forest: variations during the growing season. Journal of Hydrology, 197, 70–87.

Grodzki, W., Jakuš, R., Lajzová, E., Sitková, Z., Maczka, T., Škvarenina, J., 2006. Effects of intensive versus no management strategies during an outbreak of the bark beetle *Ips typographus* (L.) (Col.: Curculionidae, Scolytinae) in the Tatra Mts. in Poland and Slovakia. Annals of Forest Science, 63, 55–61.

Grunicke, S., Queck, R., Bernhofer, C., 2020. Long-term investigation of forest canopy rainfall interception for a spruce stand. Agricultural and Forest Meteorology, 292, 108–125.

Halmová, D., Pekárová, P., Miklánek, P., 2006. Rainfall interception in hornbeam and spruce forest in Slovakia. Meteorologický časopis, 9, 123–129.

Hančinský L., 1972. Forest types of Slovakia. Príroda, Bratislava, 307 p. (In Slovak.)

Harr, R. D., Levno, A., Mersereau, R., 1982. Streamflow changes after logging 130-year-old Douglas fir in two small watersheds. Water Resources Research, 18, 637–644.

Hess, P., Brezowsky, H., 1977. Katalog der Großwetterlagen Europas 1881-1976. 3rd Ed. Berichte des Deutschen Wetterdienstes, 113, 1–140. (In German.)

Holko, L., Škvarenina, J., Kostka, Z., Frič, M., Staroň, J., 2009. Impact of spruce forest on rainfall interception and seasonal snow cover evolution in the Western Tatra Mountains, Slovakia. Biologia, 64, 594–599.

Holko, L., Sleziak, P., Danko, M., Bičárová, S., Pociask-Karteczka, J., 2020. Analysis of changes in hydrological cycle of a pristine mountain catchment: 1. Water balance components and snow cover. Journal of Hydrology and Hydromechanics, 68, 180–191.

Holko, L., Danko, M., Sleziak, P., 2021. Snowmelt characteristics in a pristine mountain catchment of the Jalovecký Creek, Slovakia, over the last three decades. Hydrological Processes, 35, e14128.

Homolák, M., Gömöryová, E., Pichler, V., 2020. Can soil electrical resistivity measurements aid the identification of forest areas prone to windthrow disturbance? Forests, 11, 234.

Hotový, O., Jeníček, M., 2020. The impact of changing subcanopy radiation on snowmelt in a disturbed coniferous forest. Hydrological Processes, 34, 5298–5314.

Hroššo, B., Mezei, P., Potterf, M., Majdák, A., Blaženec, M., Korolyova, N., Jakuš, R., 2020. Drivers of spruce bark beetle (*Ips typographus*) infestations on downed trees after severe windthrow. Forests, 11, 1290.

Iovino, M., Pekárová, P., Hallett, P.D., Pekár, J., Lichner, Ľ., Mataix-Solera, J., Alagna, V., Walsh, R., Raffan, A., Schacht, K., Rodný, M., 2018. Extent and persistence of soil water repellency induced by pines in different geographic regions. Journal of Hydrology and Hydromechanics, 66, 360–368.

Jančo, M., Bartík, M., Škvarenina, J., 2017. The impact of the decline of mountain spruces on the interception process in the Western Tatras. In: Hydrology of a small basin 2017. Institute of Hydrodynamics of the Czech Academy of Sciences, Prague, pp. 84–90. (In Slovak.)

Jeníček, M., Hotový, O., Matějka, O., 2017. Snow accumulation and ablation in different canopy structures at a plot scale: using degree-day approach and measured shortwave radiation. Acta Universitatis Carolinae Geographica, 52, 61–72.

Kaiser, K.E., McGlynn, B.L., Emanuel, R.E., 2013. Ecohydrology of an outbreak: mountain pine beetle impacts trees in drier landscape positions first. Ecohydrology, 6, 444–454.

Kantor, P., 1981. Interception of mountainous spruce and beech stands. Lesnictví, 27, 171–192. (In Czech.)

Klamerus-Iwan, A., Link, T.E., Keim, R.F., Van Stan II, J.T., 2020. Storage and routing of precipitation through canopies. In: Van Stan II, J.T., Gutmann, E., Friesen, J. (Eds.): Precipitation Partitioning by Vegetation: A Global Synthesis. Springer Nature, Cham, pp 17–34.

Kofroňová, J., Šípek, V., Hnilica, J., Vlček, L., Tesař, M., 2021. Canopy interception estimates in a Norway spruce forest and their importance for hydrological modelling. Hydrological Sciences Journal, 66, 1–15.

Konček, M., Orlicz, M., 1974. Synoptic climatology. In: Konček, M. (Ed.): Klíma Tatier. Veda, Bratislava, pp. 27–49. (In Slovak.)

Krečmer, V., 1968. Precipitation interception of spruce forest in middle mountain region. Opera Corcontica, 5, 83–96. (In Czech.)

Krečmer, V., 1973. Meteorological conditions for occurrence of fog precipitation, and its significance for the interception process in upland forests. Meteorologické zprávy, 27, 18–25. (In Czech.)

Krečmer, V., Fojt, V., Hynčica, V., 1981. Interception process in spruce stands. Vodohospodářsky časopis, 29, 6, 593–614. (In Czech.)

Landsberg, J., Waring, R., 2014. Forests in Our Changing World: New Principles for Conservation and Management. Island Press, Washington, 224 p.

Lapin, M., Faško, P., Melo, M., Šťastný, P., Tomlain, J., 2002. Climate zones. In: Landscape Atlas of the Slovak Republic. Ministry of Environment of the Slovak Republic, Bratislava. (In Slovak.)

Lichner, Ľ., Iovino, M., Šurda, P., Nagy, V., Zvala, A., Kollár, P., Pecho, J., Píš, V., Sepehrnia, N., Sándor, R., 2020. Impact of secondary succession in abandoned fields on some properties of acidic sandy soils. Journal of Hydrology and Hydromechanics, 68, 12–18.

Llorens, P., Gallart, F., 2000. A simplified method for forest water storage capacity measurement. Journal of Hydrology, 240, 131–144.

Lovett, G.M., Reiners, W.A., Olson, R.K. 1982. Cloud droplet deposition in subalpine balsam fir forests: hydrological and chemical inputs. Science, 218, 1303–1304.

Mezei, P., Jakuš, R., Pennerstorfer, J., Havašová, M., Škvarenina, J., Ferenčík, J., Slivinský, J., Bičárová, S., Bilčík, D., Blaženec, M., Netherer, S., 2017. Storms, temperature maxima and the Eurasian spruce bark beetle *Ips typographus* – An infernal trio in Norway spruce forests of the Central European High Tatra Mountains. Agricultural and Forest Meteorology, 242, 85–95.

Minďáš, J., 2003. Characteristics of snow conditions in forest stands of the central mountain area of Poľana. Lesnícky časopis, 49, 105–115. (In Slovak.)

Minďáš, J., Škvarenina, J., 1995. Chemical composition of fog cloud and rain snow water in Biosphere Reserve Poľana. Ekologia-Bratislava, 14, 125–137.

Minďáš, J., Bartík, M., Škvareninová, J., Repiský, R., 2018. Functional effects of forest ecosystems on water cycle – Slovakia case study. Journal of Forest Science, 64, 331–339.

Oreňák, M., Vido, J., Hríbik, M., Bartík, M., Jakuš, R., Škvarenina, J., 2013. Interception process of spruce forest in the phase of disintegration in the Western Tatras, Slovakia. Zprávy Lesnického Výzkumu, 58, 360–369. (In Slovak.)

Oulehle, F., Chuman, T., Majer, V., Hruška, J., 2013. Chemical recovery of acidified Bohemian lakes between 1984 and 2012: the role of acid deposition and bark beetle induced forest disturbance. Biogeochemistry, 116, 83–101.

Petrovič, Š., 1972. Weather and climate. In: Lukniš, M. (Ed.): Slovensko: Príroda. Obzor, Bratislava, pp. 203–282. (In Slovak.)

Pichler, V., Godinho-Ferreira, P., Zlatanov, T., Pichlerová, M., Gregor, J., 2010. Changes in forest cover and its diversity. In: Bredemeier, M., Cohen, S., Godbold, D.L., Lode, E., Pichler, V., Schleppi, P. (Eds.): Forest Management and the Water Cycle: An Ecosystem-Based Approach (Vol. 212). Springer Science & Business Media, Dordrecht, pp. 209–224.

Polčák, N., Mészáros, J., 2018. The effect of relief on the distribution of atmospheric precipitation in Slovakia in the southern cyclonic situations. Geografický časopis, 70, 259–272. (In Slovak.)

Pypker, T.G., Levia, D.F., Staelens, J., Van Stan, J.T., 2011. Canopy Structure in Relation to Hydrological and Biogeochemical Fluxes. In: Levia, F.D., Carlyle-Moses, D., Tanaka, T. (Eds.): Forest Hydrology and Biogeochemistry. Springer, Dordrecht, pp. 371–388.

Racko, S., 1996. A note on the change in the typing of synoptic situations. Meteorologické zprávy, 49, 89–89. (In Czech.)

Rehfuess, K.E., 1985. On the causes of decline of Norway spruce (*Picea abies* Karst.) in Central Europe. Soil Use and Management, 1, 30–31.

Robinson, M., Ward, R., 2017. Hydrology: Principles and Processes. IWA Publishing, London, 402 p.

Sadeghi, S.M.M., Gordon, D.A., Van Stan II, J.T., 2020. A global synthesis of throughfall and stemflow hydrometeorology. In: Van Stan II, J.T., Gutmann, E., Friesen, J. (Eds.): Precipitation Partitioning by Vegetation: A Global Synthesis. Springer Nature, Cham, pp. 49–70.

Seidl, R., Schelhaas, M.J., Lexer, M.J., 2011. Unraveling the drivers of intensifying forest disturbance regimes in Europe. Global Change Biology, 17, 2842–2852.

Seidl, R., Albrich, K., Erb, K., Formayer, H., Leidinger, D., Leitinger, G., Tappeiner, U., Tasser, E., Rammer, W., 2019. What drives the future supply of regulating ecosystem services in a mountain forest landscape? Forest Ecology and Management, 445, 37–47.

Shelton, M.L., 2009. Hydroclimatology: Perspectives and Applications. Cambridge University Press, Cambridge 2009. 426 p.

Sierota, Z., Grodzki, W., Szczepkowski, A., 2019. Abiotic and biotic disturbances affecting forest health in Poland over the past 30 years: Impacts of climate and forest management. Forests, 10, 75.

Slovak Hydrometeorological Institute, 2021. Types of weather situations (2018, 2019, 2021: http://www.shmu.sk/sk/?page=8). (In Slovak.)

Stanová, V., Valachovič, M. (Eds.) 2002. Catalog of Slovak Biotops. DAPHNE – Inštitút aplikovanej ekológie, Bratislava, 225 p. (In Slovak.)

Střelcová, K., Minďáš, J., Škvarenina, J., 2006. Influence of tree transpiration on mass water balance of mixed mountain forests of the West Carpathians. Biologia, 61, 305–310.

Šípek, V., Hnilica, J., Vlček, L., Hnilicová, S., Tesař, M., 2020. Influence of vegetation type and soil properties on soil water dynamics in the Šumava Mountains (Southern Bohemia). Journal of Hydrology, 582, 124285.

Šraj, M., Brilly, M., Mikoš, M., 2008. Rainfall interception by two deciduous Mediterranean forests of contrasting stature in Slovenia. Agricultural and Forest Meteorology, 148, 121–134.

Švihla, V., Šach, F., Černohous, V., 2016. Influence of clear-cuttings or impact of rapid broad disintegration of a forest on total run-off by growing seasons. Zprávy Lesnického Výzkumu, 61, 138–144. (In Czech.)

Tužinský, L., 2004. Water regime of forest soils. Technická univerzita vo Zvolene, Zvolen, 102 p. (In Slovak.)

Vacek, S., Hůnová, I., Vacek, Z., Hejcmanová, P., Podrázský, V., Král, J., Putalová, T., Moser, W.K., 2015. Effects of air pollution and climatic factors on Norway spruce forests in the Orlické hory Mts. (Czech Republic), 1979–2014. European Journal of Forest Research, 134, 1127–1142.

Valtýni, J., 1986. Water Management and Water Protection Significance of the Forest. Príroda, Bratislava, 68 p. (In Slovak.)

Viville, D., Biron, P., Granier, A., Dambrine, E., Probst, A., 1993. Interception in a mountainous declining spruce stand in the Strengbach catchment (Vosges, France). Journal of Hydrology, 144, 273–282.

Vorčák, J., Merganič, J., Škvarenina, J., Merganičová, K., 2009. Contribution to understanding precipitation regime in the mountain spruce forests of Babia hora–Oravské Beskydy using throughfall index. The Beskid Bulletin, 2, 85–94.

Ward, A.D., Trimble, S.W., 2003. Environmental Hydrology. CRC Press, Boca Raton, 504 p.

Zabret, K., Rakovec, J., Šraj, M., 2018. Influence of meteorological variables on rainfall partitioning for deciduous and coniferous tree species in urban area. Journal of Hydrology, 558, 29–41.

Received 14 July 2021
Accepted 23 August 2021

J. Hydrol. Hydromech., 69, 2021, 4, 378–386
DOI: 10.2478/johh-2021-0026
ISSN 1338-4333

sciendo Journal of Hydrology and Hydromechanics

Biocrust effects on soil infiltrability in the Mu Us Desert: Soil hydraulic properties analysis and modeling

Hongjie Guan[1,2,3*], Xinyu Liu[4]

[1] Yanchi Research Station, School of Soil and Water Conservation, Beijing Forestry University, Beijing 100083, China.
[2] Key Laboratory of State Forestry Administration on Soil and Water Conservation, Beijing Forestry University, Beijing 100083, China.
[3] Beijing Engineering Research Center of Soil and Water Conservation, Beijing Forestry University, Beijing 100083, China.
[4] State Key Laboratory of Earth Surface Processes and Resource Ecology, MOE Engineering Research Center of Desertification and Blown-sand Control, Faculty of Geographical Science, Beijing Normal University, Beijing 100875, China.
[*] Corresponding author. E-mail: guanhong311@163.com

Abstract: The presence of biocrusts changes water infiltration in the Mu Us Desert. Knowledge of the hydraulic properties of biocrusts and parameterization of soil hydraulic properties are important to improve simulation of infiltration and soil water dynamics in vegetation-soil-water models. In this study, four treatments, including bare land with sporadic cyanobacterial biocrusts (BL), lichen-dominated biocrusts (LB), early-successional moss biocrusts (EMB), and late-successional moss biocrusts (LMB), were established to evaluate the effects of biocrust development on soil water infiltration in the Mu Us Desert, northwest of China. Moreover, a combined Wooding inverse approach was used for the estimation of soil hydraulic parameters. The results showed that infiltration rate followed the pattern BL > LB > EMB > LMB. Moreover, the LB, EMB, and LMB treatments had significantly lower infiltration rates than the BL treatment. The saturated soil moisture (θ_s) and shape parameter (α_{VG}) for the EMB and LMB treatments were higher than that for the BL and LB treatments, although the difference among four treatments was insignificant. Water retention increased with biocrust development at high-pressure heads, whereas the opposite was observed at low-pressure heads. The development of biocrusts influences van Genuchten parameters, subsequently affects the water retention curve, and thereby alters available water in the biocrust layer. The findings regarding the parameterization of soil hydraulic properties have important implications for the simulation of eco-hydrological processes in dryland ecosystems.

Keywords: Cyanobacteria; Lichen; Moss; Infiltration; Inverse approach; Hydraulic parameter.

1 INTRODUCTION

Dryland landscape is usually characterized by woody plant patches, which is separated by open patches (Ludwig et al., 2005). The surface of these open patches is usually occupied by biocrusts (also named biological soil crusts), which result from a configuration between soil particles and cyanobacteria, algae, fungi, lichens, and mosses within the upper millimeters of the soil (Belnap, 2006; Eldridge et al., 2020; Weber et al., 2016). Biocrusts change physicochemical properties of topsoils and have a significant impact on water infiltration (Chamizo et al., 2016; Jiang et al., 2018).

A few studies have been performed to evaluate the effects of biocrusts on water infiltration. Nevertheless, contradicting results exist regarding the roles of biocrusts on soil water infiltration (Warren, 2003; Weber et al., 2016). Biocrusts modify soil infiltrability through different pathways. Biocrusts increase soil porosity, roughness and aggregate stability and improve physical structure, which in turn increase soil water infiltration (Felde et al., 2014; Jiang et al., 2018). On the other hand, biocrusts increase water repellency and cause pore clogging due to exopolysaccharide excretion, which impede soil water infiltration (Keck et al., 2016; Kidron et al., 2020; Xiao et al., 2019). These contradictory results were attributed to the difference in soil properties (soil structure and texture), biocrust characteristics (cover, morphology, and composition), and climate (mainly rainfall characteristics) (Weber et al., 2016). Therefore, further studies are necessary to test these contradicting results in other areas, such as the Mu Us Desert where the soil, climate, and biocrusts differ from other areas. In this area, a large number of shrubs died with the occurrence of late-successional biocrusts, possibly due to the reduced soil water infiltration caused by biocrusts (Guan and Liu, 2019; Xiao and Hu, 2017). However, no conclusive data are yet available and our understanding of the mechanisms of biocrusts in altering soil hydrology remains unknown.

In addition, the presence of biocrusts alters soil physical properties, and subsequently influences soil hydrological processes, and thus changes plant growth (Havrilla et al., 2019; Kidron, 2019; Xiao and Hu, 2017). Improved knowledge of the hydraulic properties of biocrusts and estimation of soil hydraulic parameters are crucial for improving simulation of infiltration, soil water dynamics, and soil water uptake in vegetation-soil-water models (Coppola et al., 2011; Wang et al., 2007; Yu et al., 2010), and have important implications for the simulation of eco-hydrological processes in dryland ecosystems (Chen et al., 2018). We hypothesized that biocrust development has a negative influence on water infiltration. Accordingly, the purposes of our study were: (1) to evaluate whether biocrust development influence soil water infiltration; (2) to estimate the hydraulic parameters in biocrust-covered soils.

2 MATERIALS AND METHODS

2.1 Experimental site

This study was undertaken at the Yanchi Research Station, Ningxia Province, northwestern China (106°30′−107°47′ E and 37°04′−38°10′ N, 1550 m above the sea level). The site is lo-

cated on the southwestern fringe of the Mu Us Desert and is characterized by a mid-temperate semi-arid climate with mean annual temperature of 8.1 °C. Mean annual precipitation in this area is 287 mm, most of which occurs from July to September. Soil texture is classified as sand. The average sand, silt, and clay content in the shallow soil profile (0- to 10-cm depth) are 79.1%, 18.5%, and 2.4%, respectively. The mean percentages of sand, silt and clay in lower soil (10- to 60-cm depth) are 93.0%, 4.3%, and 2.7%, respectively. The dominant shrubs are *Artemisia ordosica*, *Caragana korshinskii*, *Salix psammophila*, and *Hedysarum mongolicum*, which are distributed in patches covering 30–70% of the soil surface. The inter-canopy soil surface is commonly covered by biocrusts.

2.2 Experimental design

In this study, infiltration experiments were conducted in August 2017 to evaluate the influence of biocrust development on water infiltration. In this experiment, four treatments, including bare land with sporadic cyanobacterial biocrusts (BL) (Fig. 1A), lichen-dominated biocrusts (LB) (Fig. 1B), early-successional moss biocrusts (EMB) (Fig. 1C), and late-successional moss biocrusts (LMB) (Fig. 1D), were established to evaluate the effects of biocrust development on soil water infiltration. Five replicates with similar soil and topographic conditions were established for each treatment, thus totalling 20 experimental sites.

There are three main types of biocrusts in this area: cyanobacteria, lichens, and mosses. The cyanobacterial biocrusts are consisted of *Microcoleus vaginatus*. The lichen-dominated biocrusts are mainly composed of *Collema tenax* species with a low cover of cyanobacteria. The moss-dominated biocrusts, in addition to *Byumargenteum* p., include a certain amount of lichens and cyanobacteria. A vernier caliper and line intercept transects were used for measuring the thickness and cover of biocrusts, respectively. Biocrust samples, which were manually screened through a 2-mm screen and dried at 65 °C for 24 h, were used for measuring the biomass. The polysaccharide content of biocrust samples were also measured by the phenol-sulfuric acid method. Additionally, particle size distribution of the biocrust layer and the subsurface (at 5-cm depth under biocrust layer) was determined.

2.3. Infiltration experiments

The infiltration experiments were performed using a disc infiltrometer with a 15 cm-diameter disc. The height and diameter of the water reservoir tower was 100 and 3.5 cm, respectively. In order to estimate van Genuchten parameters, three pressure heads (h) of –3, –6, and –12 cm at each infiltration point were used. Prior to each measurement, a layer of fine sand with thickness of 2 mm was laid on soil surface at each infiltration point and then the disc infiltrometer was put on the fine sand. The water level in the reservoir tower was recorded until it reached steady state. The time interval for observation was 10 s during the first 3 min of the infiltration experiment. However, the time interval for observation was 30 s when the infiltration time reached 3 min.

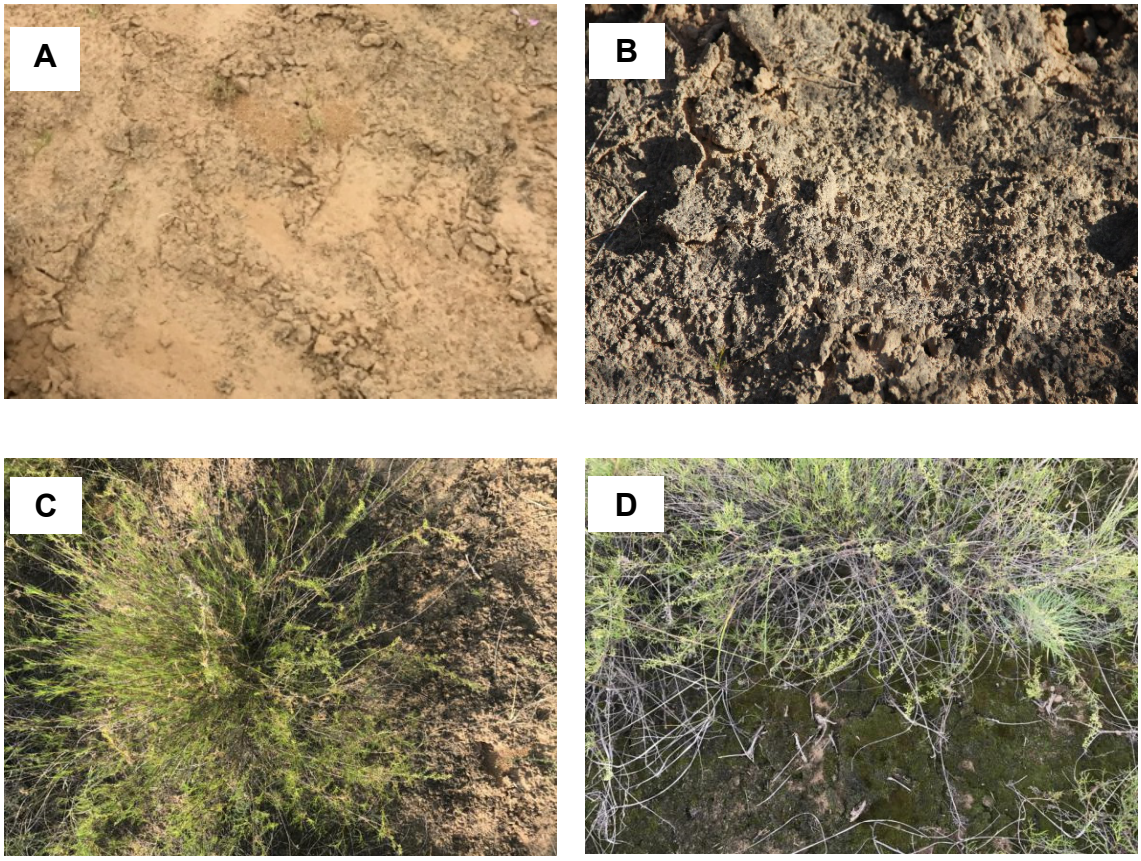

Fig. 1. Landscapes with the four treatments for study including (A) bare land with sporadic cyanobacterial biocrusts (BL), (B) lichen-dominated biocrusts (LB), (C) early-successional moss biocrusts (EMB), (D) late-successional moss biocrusts (LMB).

2.4 Calculation of soil hydraulic parameters

The following method was adopted to analyze the infiltration data. Over time, the infiltration from a circular source with a constant pressure head can be described by the Wooding's solution (Wooding, 1968):

$$Q = \pi r_0^2 K(h)[1+\frac{4\lambda_c}{\pi r_0}] \quad (1)$$

with λ_c is calculated according to White and Sully (1987):

$$\lambda_c = \frac{bS^2}{[K(h)(\theta_{fin}-\theta_{ini})]} \quad (2)$$

where r_0 is the radius of the disc (cm); h is the pressure head (cm), which was –3, – 6, and –12 cm; λ_c is the macroscopic capillary length; $K(h)$ is the unsaturated conductivity under a given pressure head (cm min^{-1}); Q is the steady-state infiltration rate (cm^3 min^{-1}); b is a shape parameter between 1/2 and π/4 (Smettem and Clothier, 1989); θ_{fin} is the final soil water content (cm^3 cm^{-3}); θ_{ini} is the initial surface soil water content (cm^3 cm^{-3}); and S is the sorptivity (cm min$^{-1/2}$).

The Q can be calculated as the following form by substituting Eq. (2) into (1):

$$\frac{Q}{\pi {r_0}^2} = K(h)+\frac{4bS^2}{[\pi r_0(\theta_{fin}-\theta_{ini})]} \quad (3)$$

with i_c is expressed as:

$$i_c = \frac{Q}{\pi {r_0}^2} \quad (4)$$

From Eqs. (3) and (4), the $K(h)$ can be calculated as the following form by replacing Q with constant infiltration rate (i_c, cm min^{-1}) (White and Sully, 1987):

$$K(h) = i_c - \frac{4bS^2}{[\pi r_0(\theta_{fin}-\theta_{ini})]} \quad (5)$$

In Eq. (5), S is estimated by the intercept of the regression line between $\Delta I/\Delta t^{1/2}$ and $t^{1/2}$ according to Vandervaere et al. (1997), where $\Delta t^{1/2}$ is the variable quantity of the square root of time (min) and ΔI is the variable quantity of cumulative infiltration (cm); and i_c is calculated by the slope of the linear fitted cumulative infiltration curves with the stable infiltration data.

According to the quasi-linear Gardner model (Gardner, 1958), the $K(h)$ (cm min^{-1}) could be expressed as:

$$K(h) = K_s e^{\alpha_{GRD} h} \quad (6)$$

where K_s is the saturated hydraulic conductivity (cm min^{-1}); and α_{GRD} is the exponential slope.

The K_s can be expressed using Eqs. (5) and (6).

$$K_s e^{\alpha_{GRD} h} = i_c - \frac{4bS^2}{[\pi r_0(\theta_{fin}-\theta_{ini})]} \quad (7)$$

The K_s and α_{GRD} in Eq. (7) are only the two unknown parameters, which could be calculated by two consecutive pressure heads. The approach assumes that parameter α_{GRD} is constant over the interval between two consecutive pressure heads (Coppola et al., 2011).

The microscopic pore radius (λ_m, mm) was calculated through Eq. (8) according to White and Sully (1987).

$$\lambda_m = \frac{\sigma \alpha_{GRD}}{\rho g} \quad (8)$$

where σ is the surface tension (N m^{-1}); ρ is the density of water (kg m^{-1}); and g is the acceleration due to gravity (N kg^{-1}).

2.5 Estimation of van Genuchten parameters using a combined Wooding inverse approach

Soil hydraulic properties are usually expressed by the soil hydraulic conductivity ($K(h)$) and water retention curve ($\theta(h)$). The most important work in determining the functional relationships between the soil hydraulic conductivity, water content, and matric potential is to obtain van Genuchten parameters, which are estimated using a coupled Wooding inverse approach that combined the results from Wooding's analytical solution with a parameter estimation method using a numerical solution of the Richards equation (Coppola et al., 2011; Lazarowitch et al., 2007).

The following form of the Richards equation is usually used to characterize the radially symmetric isothermal Darcian flow in a variably saturated isotropic rigid porous medium (Warrick, 1992):

$$\frac{\partial \theta}{\partial t} = \frac{1}{r}\frac{\partial}{\partial r}(rK(h)\frac{\partial h}{\partial r}) + \frac{\partial}{\partial z}(K(h)\frac{\partial h}{\partial z}-1) \quad (9)$$

where t is time; r is the radial coordinate; and z is the vertical coordinate positive downward. Initial and boundary conditions that are appropriate for a disc tension infiltrometer experiment are expressed by the following equations (Šimůnek and van Genuchten, 2000):

$$h(r,z,t) = h_{ini}(z) \quad t = 0 \quad (10)$$

$$h(r,z,t) = h_0(t) \quad 0 < r < r_0,\ z = 0 \quad (11)$$

$$\frac{\partial h(r,z,t)}{\partial z} = 1 \quad r > r_0,\ z = 0 \quad (12)$$

$$h(r,z,t) = h_{ini} \quad r^2 + z^2 \to \infty \quad (13)$$

where h_{ini} is the initial pressure head (cm); r_0 is the disc radius (cm); and h_0 is the time-variable supply pressure head (cm).

The van Genuchten model (van Genuchten, 1980) was chosen to express the soil water retention, $\theta(h)$, and hydraulic conductivity, $K(\theta)$:

$$S_e = \frac{\theta-\theta_r}{\theta_s-\theta_r} = [1+|\alpha_{VG} h|^n]^{-m} \quad (14)$$

$$m = \frac{n-1}{n} \quad (15)$$

$$K(S_e) = K_s S_e^{\,l}[1-(1-S_e^{1/m})m]^2 \quad (16)$$

where θ_s and θ_r are the saturated and residual soil moisture (cm^3 cm^{-3}), respectively; α_{VG} (cm^{-1}), m and n are the shape parameters; S_e is the effective fluid saturation; and l is the tortu-

osity parameter, which is usually fixed at 0.5 (Mualem, 1976).

The transient tension disc infiltration data, together with initial and final soil moisture, were used for the numerical inverse determination of van Genuchten parameters, by fixing K_s at the value obtained using Wooding's analytical solution. Given that all optimizations initially gave θ_r estimates very close to zero, we decided to fix θ_r to zero for all cases. The objective function, Φ, for the numerical inverse approach is:

$$\Phi(\beta) = \sum_{i=1}^{M} W_i [I_i^*(t_i) - I(\beta, t_i)]^2 \quad (17)$$

where M is the number of measurements in a particular set; β is the vector of optimized parameters; W_i is the weight of a particular measured point; I_i^* (cm) is the measured cumulative infiltration at time t_i; and I_i (cm) is the simulated cumulative infiltration at time t_i.

Water retention curves can be obtained through the estimated van Genuchten parameters. The plant available water, which was defined as the difference in soil moisture ($\Delta\theta$) within a pressure head ranged from –1 to –1000 cm, was estimated by water retention curves (Wang et al., 2007).

2.6 Data analyses

A two-way ANOVA was used for analyzing the effects of biocrust type and pressure head on the soil water infiltrability at the 5% probability level. The differences in soil hydraulic parameters among these treatments were analyzed using the least significant difference (LSD) tests at the 5% probability level. All statistical analyses were performed using the SPSS 19.0 software (SPSS, Chicago, IL, USA).

3 RESULTS

3.1 Characteristics of biocrusts

Generally, with the development of biocrusts, the cover, thickness, and biomass of the biocrusts significantly increased; however, the difference in biocrust cover between the EMB and LMB treatments was insignificant at the 0.05 level (Table 1). In comparison to the bare land, biocrusted soils had more silt and clay content. Moreover, higher fine content (i.e., silt and clay) was observed in the moss-covered biocrusts compared to lichen-covered biocrusts (Table 1).

3.2 Effects of biocrust development on water infiltration

As shown in Fig. 2, from initial to steady state, the BL treatment had significantly higher infiltration rates than the other treatments. Furthermore, infiltration rate was similar for the EMB and LMB treatments, but significantly lower than for the LB treatment. Specifically, the i_c under the pressure head of –3 cm followed the pattern BL > LB > EMB > LMB. Furthermore, for the BL treatment under the pressure head of –3 cm, the i_c was 92.3% higher than that for the LB treatment ($P < 0.05$) (Table 2). The i_c for the LB treatment under the pressure head of –3 cm was 25.8% and 38.7% higher than that for the EMB and LMB treatments, although there was no significant difference in the infiltration rate among the three treatments (Table 2).

In addition, the $K(h)$, S, K_s, and λ_c for the BL treatment were obviously higher than that for the other treatments. In detail, the $K(h)$ and K_s for the BL treatment under the pressure head of –3 cm were significantly higher than that for the LB treatment by 2.0- and 2.1-fold, respectively (Table 2). Similarly, the S averaged over three pressure heads followed the pattern BL > LB > EMB > LMB. On the contrary, the λ_m followed the pattern BL < LB < EMB < LMB, although the difference among them was insignificant. The two-way ANOVA results indicated that the influences of biocrust type or head on i_{ini}, i_c, S, $K(h)$, K_s, and λ_c were significant at the 0.01 or 0.05 level; however, the influence of biocrust type on λ_m was insignificant at the 0.05 level (Table 3). In addition, the influences of the interaction between the biocrust type and pressure head on i_{ini}, i_c, S, $K(h)$, and K_s were insignificant at the 0.05 level.

3.3 Determination of van Genuchten parameters

As can be seen in Table 4, the θ_s and α_{VG} increased with biocrust development. More specifically, the θ_s and α_{VG} for the EMB and LMB treatments were higher than that for the BL and LB treatments, although the difference among four treatments was insignificant. For instance, the θ_s for the LMB treatment was 28.0% higher than that for the LB treatment. Moreover, there was no significant difference in θ_s and α_{VG} between the BL and LB treatments. In addition, the relation between the parameter of the n and biocrust development was found to be non-unique. In detail, the BL and EMB treatments had slightly higher n than the LB and LMB treatments. Furthermore, there was no obvious difference in n between the BL and EMB treatments or between the LB and LMB treatments. The one-way ANOVA results indicated that the influences of biocrust development on θ_s, α_{VG} and n were insignificant at the 0.05 level (data not shown)

As shown in Fig. 3, biocrust development had a significant influence on water retention and hydraulic conductivity. Water retention increased with biocrust development at high-pressure heads, whereas the opposite was observed at low-pressure heads (Fig. 3A and B). In detail, water retention at high-pressure heads followed the pattern LMB > EMB > BL > LB.

Table 1. Characteristics of the biocrusts in the four treatments.

Treatments	Cover (%)	Thickness (mm)	Biomass (mg cm^{-2})	Polysaccharide content (μg mg^{-1})	Sand (%)	Silt (%)	Clay (%)
Bare land with sporadic cyanobacterial biocrusts (BL)	–	–	–	–	85.79±5.09 a	12.71±1.51 b	1.50±0.16 b
Lichen-dominated biocrusts (LB)	70±9.7 b†	4.8±0.9 c	0.81±0.08 c	2.26±0.03 b	84.59±4.43 a	13.53±2.21 b	1.88±0.13 b
Early-successional moss biocrusts (EMB)	76.8±3.5 a	8.9±0.7 b	1.84±0.36 b	3.76±0.05 a	77.50±5.26 b	20.60±2.56 a	1.90±0.21 b
Late-successional moss biocrusts (LMB)	95.8±1.8 a	15.2±0.8 a	2.94±0.57 a	3.94±0.02 a	75.34±4.82 b	21.33±2.29 a	3.33±0.18 a

† Different letters in the same column indicate significant differences at the probability level of 0.05.

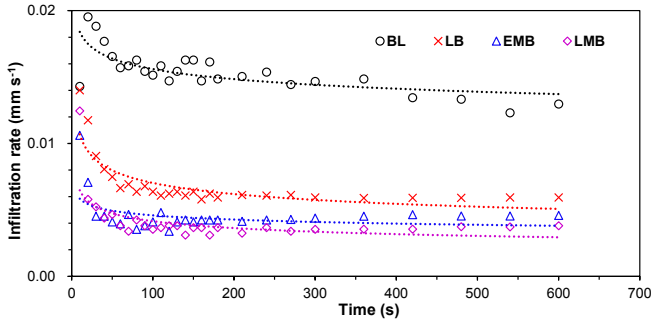

Fig. 2. Infiltration rate of the four treatments including bare land with sporadic cyanobacterial biocrusts (BL), lichen-dominated biocrusts (LB), early-successional moss biocrusts (EMB), and late-successional moss biocrusts (LMB).

On the contrary, Water retention at low-pressure heads followed the pattern LB > BL > LMB > EMB. Hydraulic conductivity for the BL treatment, as shown in Fig. 3C, was obviously higher than that of the other treatments. Furthermore, there was no obvious difference among the LB, EMB, and LMB treatments, and the difference was dependent on the pressure head.

In addition, the development of biocrusts influences the water retention curve, and thus alters the available water. In detail, $\Delta\theta$ for the moss-covered treatments were obviously higher than that for the cyanobacteria- or lichen-covered treatments. For example, the available water increased from $\Delta\theta$ = 0.251 m^3 m^{-3} and $\Delta\theta$ = 0.214 m^3 m^{-3} for the BL and LB treatments to $\Delta\theta$ = 0.281 m^3 m^{-3} for the EMB treatment. Moreover, for moss biocrusts, the available water increased from $\Delta\theta$ = 0.281 m^3 m^{-3} for the EMB treatment to $\Delta\theta$ = 0.290 m^3 m^{-3} for the LMB treatment. However, the available water decreased from $\Delta\theta$ = 0.251 m^3 m^{-3} for the BL treatment to $\Delta\theta$ = 0.214 m^3 m^{-3} for the LB treatment (Fig. 3A and B).

4 DISCUSSION

4.1 Influence of biocrust development on water infiltration

Our study shows that the presence and development of biocrusts had a negative effect on water infiltration when compared to the bare land (Table 2; Fig. 2). The negative biocrust effects on water infiltration are likely due to the higher amount of clay and silt in the biocrusted soils, which could reduce soil pores and result in a decrease in water infiltration (Table 1). Additionally, the biocrust effects could attributed to the higher biocrust thickness and the polysaccharide content (Table 1). We should note that the polysaccharides measured in this study is different from exopolysaccharides (EPS), and it can only serve as a measure for biocrust biomass (similar to chlorophyll content). Namely, the polysaccharides cannot be an indication of the capacity of the biocrusts to absorb water. Although not measured in this study, the involvement of the EPS cannot be neglected. Given that the ability of the EPS to absorb copious amounts of water (Chenu, 1993; Colica et al., 2014; Mazor et al., 1996), the cyanobacterial capacity to excrete copious amounts of EPS (Kidron et al., 2003), and the fact that cyanobacteria also inhabit the lichen- and moss-dominated biocrusts (Gentili et al., 2005; Paulsrud and Lindblad, 1998; Rossi et al., 2018), an efficient impediment of infiltration is expected. This issue deserves further research.

Our results correspond to the results of other authors (Coppola et al., 2011; Xiao et al., 2019; Yang et al., 2016), who concluded that the lichen- and moss-covered biocrusts led to a decrease in water infiltration (Table 5). However, some other studies have shown the opposite: biocrusts increased water infiltration (Jiang et al., 2018; Kakeh et al., 2021) (Table 5). The difference in soil surface roughness caused by biocrusts could partly explain these contradictive results (Warren, 2003). In detail, rugose or smooth biocrusts such as cyanobacteria are common in the areas without frost-heaving, thus resulting in a low surface roughness. Nevertheless, in the areas where soils freeze, frost-heaving of biocrusted surfaces results in a highly roughened surface. Higher roughness allows more residence time, and thus leads to an increased infiltration (Warren, 2003). In this study site with no obvious frost-heaving, low surface roughness resulted in a negative effect of biocrusts on water infiltration.

Additionally, our results concluded that moss-dominated biocrusts had much lower soil infiltrability compared to the lichen-dominated biocrusts (Table 2; Fig. 2). In comparison to lichen-covered biocrusts, higher cover, thickness, biomass, and

Table 2. Soil hydraulic parameters of biocrusts and bare soil under the different biocrust development.

Pressure head	Treatments	i_{ini} (mm min^{-1})	i_c (mm min^{-1})	$K(h)$ (mm min^{-1})	S (mm $min^{-1/2}$)	K_s (mm min^{-1})	λ_c (mm)	λ_m (mm)
–3 cm	BL	1.36±0.37 bc†	0.75±0.09 a	0.79±0.10 a	0.89±0.48 ab	1.44±0.18 b	4.87±3.27 bc	21.79±13.05 b
	LB	1.00±0.28 bc	0.39±0.06 b	0.39±0.06 b	0.18±0.06 b	0.70±0.11 c	0.54±0.24 c	453.81±390.96 b
	EMB	0.93±0.15 bc	0.31±0.04 bc	0.31±0.04 bc	0.11±0.02 b	0.57±0.08 c	0.14±0.05 c	168.72±109.64 b
	LMB	1.05±0.32 bc	0.27±0.07 bc	0.26±0.07 bc	0.09±0.06 b	0.48±0.13 c	0.31±0.26 c	3603.71±2192.01 a
–6 cm	BL	1.36±0.26 bc	0.72±0.19 a	0.69±0.16 a	0.61±0.34 b	2.30±0.52 a	3.89±3.01 bc	108.74±95.49 b
	LB	0.99±0.37 bc	0.33±0.07 b	0.32±0.07 b	0.25±0.04 b	1.07±0.23 bc	0.85±0.19 c	12.18±4.02 b
	EMB	0.49±0.16 c	0.23±0.06 bc	0.24±0.06 bc	0.07±0.02 b	0.79±0.19 c	0.13±0.08 c	1667.40±1192.36 ab
	LMB	0.49±0.13 c	0.18±0.05 bc	0.19±0.06 bc	0.12±0.04 b	0.64±0.20 c	0.35±0.14 c	187.57±162.26 b
–12 cm	BL	2.95±0.70 a	0.20±0.05 bc	0.12±0.02 c	1.20±0.29 a	1.32±0.19 bc	63.96±26.20 a	0.47±0.25 b
	LB	1.61±0.47 b	0.11±0.03 c	0.08±0.02 c	0.69±0.19 ab	0.91±0.18 bc	25.63±11.06 b	0.55±0.19 b
	EMB	0.79±0.26 bc	0.05±0.02 c	0.05±0.01 c	0.32±0.10 b	0.53±0.15 c	7.27±3.30 bc	1.78±0.51 b
	LMB	0.91±0.29 bc	0.06±0.02 c	0.05±0.01 c	0.37±0.12 b	0.57±0.16 c	12.40±5.96 bc	1.80±0.73 b

Note. † Different letters in the same column indicate significant differences at the probability level of 0.05. BL: bare land with sporadic cyanobacteria biocrusts; LB: lichen-dominated biocrusts; EMB: early-successional moss biocrusts; LMB: late-successional moss biocrusts.

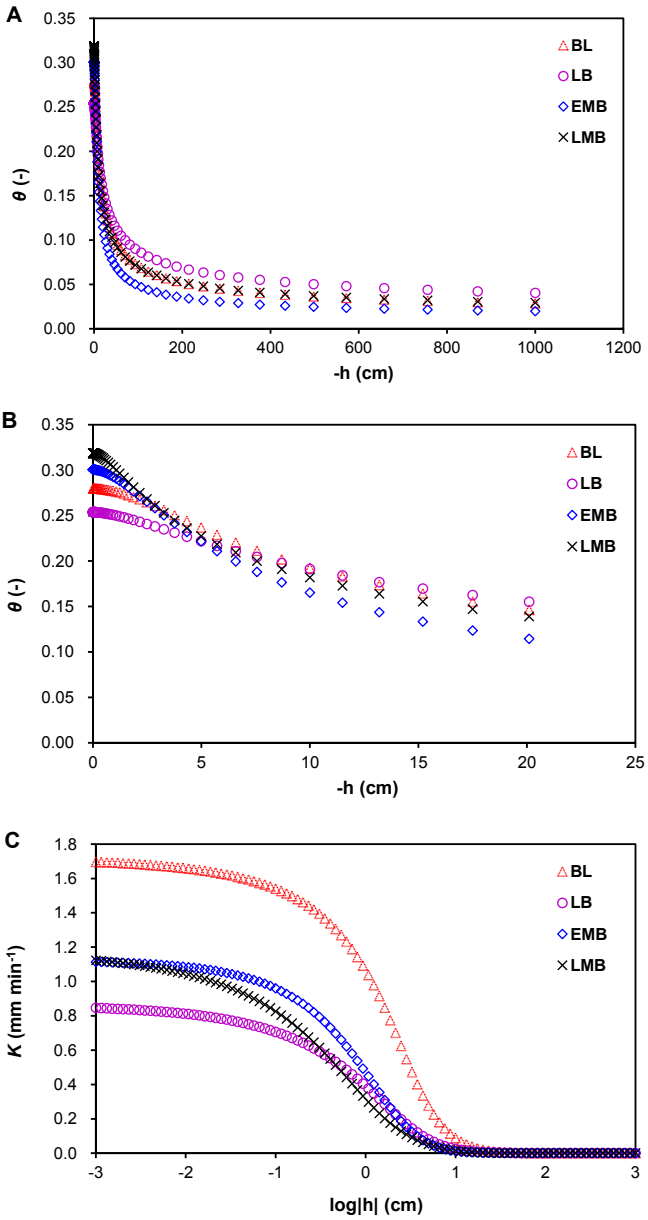

Fig. 3. Water retention (A and B) and hydraulic conductivity (C) of the four treatments including bare land with sporadic cyanobacterial biocrusts (BL), lichen-dominated biocrusts (LB), early-successional moss biocrusts (EMB), and late-successional moss biocrusts (LMB).

polysaccharide content for the moss-covered biocrusts could explain this phenomenon (Table 1; Kidron et al., 2003; Chamizo et al., 2012). Furthermore, higher fine content (i.e., silt and clay) in the moss-covered biocrusts may reduce soil infiltrability when compared to the lichen-covered biocrusts (Table 1; Xiao et al., 2019). Similarly, Wu et al. (2012) concluded that soil infiltrability was lower for the moss-covered biocrusts compared to the lichen-covered biocrusts. On the contrary, some other studies have found that infiltration increased when biocrusts shifted from cyanobacteria or algae to lichens or mosses, which is usually characterized by increased biomass (Barger et al., 2006; Chamizo et al., 2012). The different response of infiltration to biocrust type was dependent upon surface roughness. In these regions, greater roughness which may have been caused by frost-heaving for lichen- or moss-dominated biocrusts than those for the cyanobacteria or algae could explain the contradictory results (Belnap et al., 2013).

It should be noted that the use of a disc infiltrometer does not adequately reflect water flow under natural conditions. Firstly, it does not reflect surface roughness, because a layer of fine sand was laid on soil surface before infiltration experiments were performed. Therefore, the use of a disc infiltrometer could alleviate the influence of surface roughness caused by biocrusts on water infiltration. Secondly, unlike one-dimensional vertical flow under natural conditions, the unconfined three-dimensional infiltration (vertical and lateral flow) usually take place under tension condition when using a disc infiltrometer (Vandervaere et al., 1997). Although there are some above-mentioned limitations, the disc infiltrometer under tension condition can still reflect biocrust effect on soil infiltrability, as verified by a similar study of Xiao et al. (2019) that reported consistent results of the double-ring infiltrometer and the disc infiltrometer. Considering the above-mentioned issues, further research is needed to evaluate the difference between the double-ring infiltrometer and disc infiltrometer in our study site.

4.2 Determination of van Genuchten parameters

Parametrization of hydraulic properties on biocrusted soils and estimation of soil hydraulic parameters are crucial for improving simulation of infiltration and soil water dynamics in vegetation-soil-water models (Coppola et al., 2011; Yu et al., 2010), and thus the understanding of eco-hydrological processes in dryland ecosystems (Rodríguez-Caballero et al., 2015). Among them, the most important factor is to estimate the parameters of van Genuchten model. Our results indicated that moss-covered soils had lower K_s than lichen-covered soils; however, the θ_s for the moss-covered soils was higher than that for lichen-covered soils, although the differences were insignificant. This result could be attributed to the higher fine content and polysaccharide content of the moss-covered soils when compared to lichen-covered soils (Table 1). Furthermore, similar to our simulation study, the results of field experiments by Guan and Liu (2019) also found that well-developed moss-covered biocrusts had higher θ_s than lichen-covered biocrusts, suggesting a higher retention capacity for the moss-covered biocrusts.

Table 3. *P* values from the two-way ANOVA to test the influences of biocrust type and pressure head as well as their interaction effects on soil hydraulic parameters.

Effects	i_{ini} (mm min^{-1})	i_c (mm min^{-1})	S (mm min$^{-1/2}$)	$K(h)$ (mm min^{-1})	K_s (mm min^{-1})	λ_c (mm)	λ_m (mm)
Biocrusts	0.001**	<0.001**	<0.001**	<0.001**	<0.001**	0.013*	0.175
Pressure head	0.015*	<0.001**	<0.001**	0.024*	0.023*	<0.001**	0.133
Biocrusts × Pressure head	0.188	0.149	0.020*	0.431	0.949	0.031*	0.040*

Note. i_{ini}, initial infiltration rate; i_c, steady-state infiltration rate; S, sorptivity; $K(h)$, unsaturated hydraulic conductivity at h pressure head; K_s, saturated hydraulic conductivity; λ_c, macroscopic capillary length; λ_m, microscopic pore radius. * Effect is significant at .05 level of probability. ** Effect is significant at .01 level of probability.

Table 4. Water retention and hydraulic conductivity parameters for the biocrusted soils under the different biocrust development.

Treatments	θ_s	α_{VG} (cm^{-1})	n
Bare land with sporadic cyanobacterial biocrusts (BL)	0.28±0.02 a†	0.11±0.03 a	1.72±0.14 a
Lichen-dominated biocrusts (LB)	0.25±0.01 a	0.12±0.03 a	1.51±0.07 a
Early-successional moss biocrusts (EMB)	0.30±0.02 a	0.21±0.04 a	1.72±0.08 a
Late-successional moss biocrusts (LMB)	0.32±0.04 a	0.27±0.09 a	1.54±0.07 a

† Different letters in the same column indicate significant differences at the probability level of 0.05.

Table 5. Regional difference in the biocrust effects on soil water infiltrability (in increasing order of annual precipitation).

Locations	**Climate (annual precipitation in mm)**	**Soil texture**	**Biocrust type**	**Measured parameters**	**Biocrust effects on infiltration**	**References**
Heihe River Basin	Hyper arid (71)	Silty loam		Infiltration rate	Decreasing	Yang et al. (2016)
Central-Western Negev Desert	Hyper arid (90)	Sand	Cyanobacteria	Infiltration rate	Increasing under tension; no significant effect under ponding	Eldridge et al. (2000)
Western Negev Desert	Hyper arid (95)	Sand	Cyanobacteria	Runoff yield	Decreasing	Kidron (2016)
Mojave Desert	Arid (101)	Sand; loamy sand	Cyanobacteria	Infiltration rate	Decreasing	Herrick et al. (2010)
Tengger Desert	Arid (191)	Sand	Mosses	Infiltration rate	Increasing	Coppola et al. (2011)
Tabernas Desert	Semiarid (200–235)	Silty loam; sandy loam	Cyanobacteria; lichens; mosses	Infiltration rate	Decreasing with biocrust development	Chamizo et al. (2012)
Colorado Plateau	Semiarid (215)	Loamy sand	Cyanobacteria; cyanolichens	Runoff coefficient	Decreasing	Faist et al. (2017)
Southeastern Spain	Semiarid (220–235)	Silty loam; sandy loam	Cyanobacteria	Runoff coefficient	Decreasing with biocrust development	Cantón et al. (2020)
Western New South Wales	Semiarid (244)	Sand	Cyanobacteria; lichens; mosses	Infiltration rate	Increasing	Bowker et al. (2013)
Northern Chihuahuan Desert	Semiarid (250)	Sandy clay loam	Cyanobacteria	Infiltration depth	Increasing	Chung et al. (2019)
Quara Qir rangelands	Semiarid (273)	Loamy	Lichens; mosses	Infiltration rate	Increasing	Kakeh et al. (2021)
Qinghai-Tibet Plateau	Semiarid (389)	Silty loam	Mosses	Infiltration rate	Increasing	Jiang et al. (2018)
Loess Plateau	Semiarid (409)	Loamy sand	Cyanobacteria; mosses	Infiltration rate	Decreasing	Xiao et al. (2019)

Additionally, our results indicated that the shape parameter of α_{VG} followed the pattern LMB > EMB > LB > BL. This result suggests that the shape parameters of α_{VG} increased with biocrust development. A higher α_{VG} corresponds to a lower air entry value, and implies a lower water holding capacity near saturation (van Genuchten, 1980). Moreover, this result indicates that the higher α_{VG} was consistent with a higher content of clay and silt. On the contrary, Wang et al. (2007) reported that the shape parameter of α_{VG} declined as the time since stabilization increased, and the lower α_{VG} was related to a higher proportion of silt- and clay-sized particle. The difference in the inverse method and model uncertainty may lead to this discrepancy.

The development of biocrusts leads to different van Genuchten parameters, which alter the $\theta(h)$ and $K(h)$ curves. Our results indicate that $\theta(h)$ on the moss-covered soils was higher than on the lichen-covered soils at high-pressure heads; however, the opposite was observed at low-pressure heads (Fig. 3B). In addition, moss-covered soils had lower $K(h)$ than the lichen-covered soils. Decrease in $K(h)$ and increase in $\theta(h)$ are likely due to the characteristics of biocrusts when compared to bare land. In comparison to the bare land, greater water-holding capacity on the biocrust-covered soils could lead to an improved water conditions on the soil surface (Fig. 3B; Guan and Liu, 2019). Furthermore, the anchoring structures on lichen-covered soils allows for a longer residence time of the water, which could improve water retention at the soil surface. Moreover, higher content of clay and silt in the moss-covered biocrusts reduce the soil pores, and lead to a decrease in soil hydraulic conductivity. Accordingly, the presence of lichen or moss biocrusts on the soil surface enhances water retention, but inhibits soil hydraulic conductivity.

The occurrence and development of biocrusts change van Genuchten parameters and affect the water retention curve, and subsequently alters the available water in the biocrust layer. We found that available water in the biocrust layer increased with a shift in biocrusts from cyanobacteria to lichens or mosses (Fig. 3A and B). It is noted that available water mentioned above focused on the soil surface (i.e., biocrust layer). The increased water content on the soil surface implies a lower soil water content of the shrub root layer. This suggests that the presence and development of biocrusts could facilitate the growth of annual plants, but inhibit the growth of vascular plants. Moreover, higher soil surface water content has important implications for dryland productivity. Therefore, our results provide strong support for the explicit inclusion of biocrusts in hydrological and ecohydrological models.

Our study focused on the effects of biocrust development on soil infiltrability. The presence and development of biocrusts

change the water infiltration during rainfall events and alter soil evaporation during the drying periods, and consequently have the potential to influence plant water uptake, and eventually impact plant growth (Xiao and Hu, 2017; Zhang and Belnap, 2015; Zhuang et al., 2015). In addition, biocrusts are very fragile and are susceptible to disturbance, which could affect water infiltration during rainfall events (Barger et al., 2006; Chamizo et al., 2012). However, how the biocrust development and its disturbance influence soil water availability and shrub growth have not yet been well understood (Chamizo et al., 2016; Kidron and Aloni, 2018). Accordingly, further studies are necessary to evaluate the role of the biocrust development and its disturbance in soil water uptake and growth of vascular plants in drylands.

5 CONCLUSIONS

Infiltration rate decreases and saturated soil moisture increases with biocrust development, especially with the presence of moss biocrusts. Water retention increases with biocrust development at high-pressure head, whereas the opposite is found at low-pressure heads. The biocrust development influences van Genuchten parameters, subsequently affecting the water retention curve, and thereby altering the available water in the biocrust layer. The findings regarding the parameterization of soil hydraulic properties have important implications for the simulation of eco-hydrological processes in dryland ecosystems.

Acknowledgements. This study was funded by the Fundamental Research Funds for the Central Universities (BLX2013030).

Data availability statement. The data that support the findings of this study are available from the corresponding author upon reasonable request.

REFERENCES

Barger, N.N., Herrick, J.E., Van Zee, J., Belnap, J., 2006. Impacts of biological soil crust disturbance and composition on C and N loss from water erosion. Biogeochem., 77, 247–263.

Belnap, J., 2006. The potential roles of biological soil crusts in dryland hydrologic cycles. Hydrol. Process., 20, 3159–3178.

Belnap, J., Wilcox, B.P., Van Scoyoc, M.V., Phillips, S.L., 2013. Successional stage of biological soil crusts: an accurate indicator of ecohydrological condition. Ecohydrology, 6, 474–482.

Bowker, M.A., Eldridge, D.J, Val, J., Soliveres, S., 2013. Hydrology in a patterned landscape is co-engineered by soil-disturbing animals and biological crusts. Soil Biol. Biochem., 61, 14–22.

Cantón, Y., Chamizo, S., Rodriguez-Caballero, E., Lázaro, R., Roncero-Ramos, B., Román, J.R., Solé-Benet, A., 2020. Water regulation in cyanobacterial biocrusts from drylands: Negative impacts of anthropogenic disturbance. Water, 12, 3, 720.

Chamizo, S., Cantón, Y., Lázaro, R., Solé-Benet, A., Domingo, F., 2012. Crust composition and disturbance drive infiltration through biological soil crusts in semi-arid ecosystems. Ecosystems, 15, 148–161.

Chamizo, S., Cantón, Y., Rodríguez-Caballero, E., Domingo, F., 2016. Biocrusts positively affect the soil water balance in semiarid ecosystems. Ecohydrology, 9, 1208–1221.

Chen, N., Wang, X., Zhang, Y., Yu, K., Zhao, C., 2018. Eco-hydrological effects of biological soil crust on the vegetation dynamics of restoration in a dryland ecosystem. J. Hydrol., 563, 1068–1077.

Chenu, C., 1993. Clay- or sand-polysaccharide associations as models for the interface between micro-organisms and soil: water related properties and microstructure. Geoderma, 56, 143–156.

Chung, Y.A., Thornton, B., Dettweiler-Robinson, E., Rudgers, J.A., 2019. Soil surface disturbance alters cyanobacterial biocrusts and soil properties in dry grassland and shrubland ecosystems. Plant soil, 441, 147–159.

Colica, G., Li, H., Rossi, F., Li, D., Liu, Y., De Philippis, R., 2014. Microbial secreted exopolysaccharides affect the hydrological behavior of induced biological soil crusts in desert sandy soils. Soil Biol. Biochem., 68, 62–70.

Coppola, A., Basile, A., Wang, X., Comegna, V., Tedeschi, A., Mele, G., Comegna, A., 2011. Hydrological behaviour of microbiotic crusts on sand dunes: Example from NW China comparing infiltration in crusted and crust-removed soil. Soil Till. Res., 117, 34–43.

Eldridge, D.J., Zaady, E., Shachak, M., 2000. Infiltration through three contrasting biological soil crusts in patterned landscapes in the Negev, Israel. Catena, 40, 323–336.

Eldridge, D.J., Reed, S., Travers, S.K., et al. 2020. The pervasive and multifaceted influence of biocrusts on water in the world's drylands. Glob. Change Biol., 26, 10, 6003–6014.

Faist, A.M., Herrick, J.E., Belnap, J., Van Zee, J.W., Barger, N.N., 2017. Biological soil crust and disturbance controls on surface hydrology in a semi-arid ecosystem. Ecosphere, 8, e01691.

Felde, V.J.M.N.L., Peth, S., Uteau-Puschmann, D., Drahorad, S., Felix-Henningsen, P., 2014. Soil microstructure as an under-explored feature of biological soil crust hydrological properties: Case study from the NW Negev Desert. Biodivers. Conserv., 64, 133–140.

Gardner, W.R., 1958. Some steady-state solutions of the unsaturated moisture flow equation with application to evaporation from a water table. Soil Sci., 85, 4, 228–232.

Gentili, F., Nilsson, M.C., Zackrisson, O., DeLuca, T.H., Sellstedt, A., 2005. Physiological and molecular diversity of feather moss associative N_2-fixing cyanobacteria. J. Exp. Bot., 56, 422, 3121–3127.

Guan, H.J., Liu, X.Y., 2019. Does biocrust successional stage determine the degradation of vascular vegetation via alterations in its hydrological roles in semi-arid ecosystem? Ecohydrology, 12, e2075.

Havrilla, C.A., Chaudhary, V.B., Ferrenberg, S., Antoninka, A.J., Belnap, J., Bowker, M.A., … Barger, N.N., 2019. Towards a predictive framework for biocrust mediation of plant performance: A meta-analysis. J. Ecol., 107, 6, 2789–2807.

Herrick, J.E., Van Zee, J.W., Belnap, J., Johansen, J.R., Remmenga, M., 2010. Fine gravel controls hydrologic and erodibility responses to trampling disturbance for coarse-textured soils with weak cyanobacterial crusts. Catena, 83, 119–126.

Jiang, Z.Y., Li, X.Y., Wei, J.Q., Chen, H.Y., Li, Z.C., Liu, L., Hu, X., 2018. Contrasting surface soil hydrology regulated by biological and physical soil crusts for patchy grass in the high-altitude alpine steppe ecosystem. Geoderma, 326, 201–209.

Kakeh, J., Gorji, M., Mohammadi, M.H., Asadi, H., Khormali, F., Sohrabi, M., Eldridge, D.J., 2021. Biocrust islands enhance infiltration, and reduce runoff and sediment yield on a heavily salinized dryland soil. Geoderma, 404, 3, 115329.

Keck, H., Felde, V.J.M.N.L., Drahorad, S.L., Felix-Henningsen, P., 2016. Biological soil crusts cause subcritical water repellency in a sand dune ecosystem located along a rainfall gradient in the NW Negev desert, Israel. J. Hydrol. Hydromech., 64, 133–140.

Kidron, G.J., 2016. Goat trampling affects plant establishment,

runoff and sediment yields over crusted dunes. Hydrol. Process., 30, 2237–2246.
Kidron, G.J., 2019. The dual effect of sand-covered biocrusts on annual plants: Increasing cover but reducing individual plant biomass and fecundity. Catena, 182, 104120.
Kidron, G.J., Aloni, I., 2018. The contrasting effect of biocrusts on shallow-rooted perennial plants (hemicryptophytes): Increasing mortality (through evaporation) or survival (through runoff). Ecohydrology, 11, e1912.
Kidron, G.J., Yair, A., Vonshak, A., Abeliovich, A., 2003. Microbiotic crust control of runoff generation on sand dunes in the Negev Desert. Water Resour. Res., 39, 1108.
Kidron, G.J., Wang, Y., Herzberg, M., 2020. Exopolysaccharides may increase biocrust rigidity and induce runoff generation. J. Hydrol., 588, 125081.
Lazarowitch, N., Ben-Gal, A., Šimůnek, J., Shani, U., 2007. Uniqueness of soil hydraulic parameters determined by a combined Wooding inverse approach. Soil Sci. Soc. Am. J., 71, 860–865.
Ludwig, J., Wilcox, B., Breshears, D., Tongway, D., Imeson, A., 2005. Vegetation patches and runoff-erosion as interacting ecohydrological processes in semiarid landscapes, Ecology, 86, 2, 288–297.
Mazor, G., Kidron, G.J., Vonshak, A., Abeliovich, A., 1996. The role of cyanobacterial exopolysaccharides in structuring desert microbial crusts. FEMS Microbiol. Ecol., 21, 121–130.
Mualem, Y., 1976. A new model for predicting the hydraulic conductivity of unsaturated porous media. Water Resour. Res., 12, 513–522.
Paulsrud, P., Lindblad, P., 1998. Sequence variation of the $tRNA^{leu}$ intron as a marker for genetic diversity and specificity of symbiotic cyanobacteria in some lichens. Appl. Environ. Microb., 64, 310–315.
Rodriguez-Caballero, E., Cantón, Y., Jetten, V., 2015. Biological soil crust effects must be included to accurately model infiltration and erosion in drylands: An example from Tabernas Badlands. Geomorphology, 241, 331–342.
Rossi, F., Mugnai, G., De Philippis, R., 2018. Complex role of the polymeric matrix in biological soil crusts. Plant Soil, 429, 19–34.
Šimůnek, J., van Genuchten, M.Th., 2000. The DISC Computer Software for Analyzing Tension Disc Infiltrometer Data by Parameter Estimation, Version 1.0, Research Report No. 145. U.S. Salinity Laboratory, USDA, ARS, Riverside, California.
Smettem, K.R.J, Clothier, B.E., 1989. Measuring unsaturated sorptivity and hydraulic conductivity using multiple disc permeameters. J. Soil Sci., 40, 563–568.
van Genuchten, M.Th., 1980. A closed-form equation for predicting the hydraulic conductivity of unsaturated soils. Soil Sci. Soc. Am. J., 44, 892–898.
Vandervaere, J.P., Peugeot, C., Vauclin, M., Angulo Jaramillo, R., Lebel, T., 1997. Estimating hydraulic conductivity of crusted soils using disc infiltrometers and minitensiometers. J. Hydrol., 188–189, 203–223.
Wang, X.P., Young, M.H, Yu, Z., Li, X.R, Zhang, Z.S., 2007. Long-term effects of restoration on soil hydraulic properties in revegetation-stabilized desert ecosystems. Geophys. Res. Lett., 34, L24S22.
Warren, S.D., 2003. Synopsis: influence of biological soil crusts on arid land hydrology and soil stability. In: Belnap, J., Lange, O.L. (Eds.): Biological Soil Crusts: Structure, Function, and Management, vol 150, Ecological Studies. Springer, Berlin, pp. 349–360.
Warrick, A.W., 1992. Models for disc infiltrometer. Water Resour. Res., 28, 1319–1327.
Weber, B., Büdel, B., Belnap, J., 2016. The role of biocrusts in arid land hydrology. In: Chamizo, S., Belnap, J., Eldridge, D.J., Cantón, Y., Issa, O.M. (Eds.): Biological Soil Crusts: An Organizing Principle in Drylands. Ecological Studies. Springer, Berlin, pp. 321–326.
White, I., Sully, M.J., 1987. Macroscopic and microscopic capillary length and time scales from field infiltration. Water Resour. Res., 23, 1514–1522.
Wooding, RA., 1968. Steady infiltration from a shallow circular pond. Water Resour. Res., 4, 4, 1259–1273.
Wu, Y.S., Hasi, E., Wugetemole, Wu, X., 2012. Characteristics of surface runoff in a sandy area in southern Mu Us sandy land. Chinese Sci. Bull., 57, 2–3, 270–275.
Xiao, B, Hu, K.L., 2017. Moss-dominated biocrusts decrease soil moisture and result in the degradation of artificially planted shrubs under semiarid climate. Geoderma, 291, 47–54.
Xiao, B., Sun, F.H, Hu, K.L, Kidron, G.J., 2019. Biocrusts reduce surface soil infiltrability and impede soil water infiltration under tension and ponding conditions in dryland ecosystem. J. Hydrol., 568, 792–802.
Yang, J.L., Zhang, G.L., Yang, F., Yang, R.M., Yi, C., Li, D.C., Zhao, Y.G., Liu, F., 2016. Controlling effects of surface crusts on water infiltration in an arid desert area of Northwest China. J. Soils Sediment., 16, 2408–2418.
Yu, Z., Lü, H., Zhu, Y., Drake, S., Liang, C., 2010. Long-term effects of revegetation on soil hydrological processes in vegetation-stabilized desert ecosystems. Hydrol. Process., 24, 87–95.
Zhang, Y.M., Belnap, J., 2015. Growth responses of five desert plants as influenced by biological soil crusts from a temperate desert. Ecol. Res., 30, 1037–1045.
Zhuang, W.W., Serpe, M., Zhang, Y.M., 2015. The effect of lichen-dominated biological soil crusts on growth and physiological characteristics of three plant species in a temperate desert of northwest China. Plant Biol., 17, 1165–1175.

Received 28 June 2021
Accepted 18 August 2021

J. Hydrol. Hydromech., 69, 2021, 4, 447–455
DOI: 10.2478/johh-2021-0027
ISSN 1338-4333

sciendo Journal of Hydrology and Hydromechanics

Hydrophysical characteristics in water-repellent tropical Eucalyptus, Pine, and Casuarina plantation forest soils

D.A.L. Leelamanie[1*], H.I.G.S. Piyaruwan[1], P.K.S.C. Jayasinghe[2], P.A.N.R. Senevirathne[1]

[1] Department of Soil Science, Faculty of Agriculture, University of Ruhuna, Mapalana, Kamburupitiya 81100, Sri Lanka.
[2] Department of Information and Communication Technology, Faculty of Technology, University of Ruhuna, Karagoda-Uyangoda, Kamburupitiya 81100, Sri Lanka.
[*] Corresponding author. Tel.: +94-71-861-4380. Fax: +94-41-2292384. E-mails: leelamanie@soil.ruh.ac.lk; leelamaniee@yahoo.co.uk

Abstract: Soil water repellency (SWR) reduces the rates of wetting in dry soils and is known to interfere with water movement into as well as within the soils. The objective of this study was to investigate the hydrophysical characteristics of three water-repellent tropical exotic plantation forest soils in wet and dry seasons. The study sites were *Eucalyptus grandis* (EG), *Pinus caribaea* (PC), and *Casuarina equisetifolia* (CE) plantation forest soils located in the up-country intermediate zone (EG and PC), and low-country dry zone (CE). Field experiments were conducted to measure the infiltration rate, unsaturated hydraulic conductivity (k), water sorptivity (S_W). Laboratory experiments were conducted to measure the potential SWR and water entry value (h_{we}). All three soils showed higher SWR in the dry season, where CE soils showed the highest. The EG soils showed the highest SWR in the wet season. Although SWR in all soils decreased with increasing depth in the wet season, only CE soils showed a significant decrease in SWR with soil depth in the dry season. Compared with the wet season, the k(–1 cm) was lower and h_{we} was higher in the dry season. However, S_W did not show a significant difference between wet and dry seasons. Initial infiltration rate and k(–1 cm) showed a negative correlation with contact angle in all three soils. Soils showed positive linear correlations between k(–1 cm) and S_W, and negative linear correlations between S_W and h_{we} showing that surface water absorption is related to both subsurface unsaturated water flow and surface water entry pressure. It was clear that the water entry into soils and the subsurface water flow were hindered by the SWR. High water entry values in the dry season predict high potentials for intensified surface runoff and topsoil erosion. Future research will be required on the interactions between soil biology and soil properties such as pore structure that would influence water flow into and within soils.

Keywords: *Eucalyptus grandis*; *Pinus caribaea*; *Casuarina equisetifolia*; Hydrophysical characteristics; Water repellency.

INTRODUCTION

Soil water repellency (SWR) restricts the wetting of soils and may induce preferential flow paths resulting in irregular moisture or wetting patterns in soils (Šurda et al., 2020). SWR is caused by either the intermixed organic substances or organic coatings on the mineral soil particles of hydrophobic nature (DeBano, 1981; Hallett, 2007). The organic substances that are responsible for the development of SWR are usually considered to be plant roots, microbial exudates, surface waxes of leaves, and any other organic substances such as long-chain aliphatic acids, alcohols, wax esters (Bisdom et al., 1993).

The basic impact of SWR can be considered as the reduction of the rates of water infiltration into soils. Water repellency reduces the wetting rates in dry soils and lowers the plant available water, and is known to interfere with water movement into and within the soils affecting most of the hydrophysical properties and processes in soils (Lichner et al., 2012). SWR further leads to uneven patterns of water entry into soil generating unstable and irregular water flow within the soil matrix (Rodný et al., 2015). Hindered water entry into soils promotes surface runoff followed by intensified erosion, resulting in irregular moisture patterns in the soil. Localized high and less water-repellent zones lead to a selective water entry through the less water-repellent patches, stimulating preferential flow paths. Solute transport in soils through these specified flow channels can lead to accelerated transport of dissolved chemicals into groundwater (Lichner et al., 2013; Wessolek et al., 2008).

SWR has long been considered a widespread challenge to plant growth in many regions (Doerr et al., 2000). It is not limited to specific climates or soil types, and is reported in numerous types of land uses throughout the world. Water repellency is repeatedly observed in soils covered by tree species such as Japanese cypress (*Chamaecyparis obtusa*), Japanese cedar (*Cryptomeria japonica*), eucalyptus (*Eucalyptus grandis, Eucalyptus globulus*), pine (*Pinus sylvestris, Pinus pinaster, Pinus caribaea*), and casuarina (*Casuarina equisetifolia*), which are rich in various types of hydrophobic resins and waxes (Benito et al., 2019; Doerr et al., 1996; Iovino et al., 2018; Kobayashi and Shimizu, 2007; Keizer, et al., 2008; Leelamanie, 2016; Lichner, et al., 2013; Piyaruwan et al., 2020). Water-repellent phenomena observed in these specific forests are known to be natural circumstances rather than being induced by different external aspects such as forest fire conditions. This vegetation-induced SWR is usually associated with chemical compounds such as alkanoic acids, alkanes, and esters (Hansel et al., 2008).

Forests with SWR conditions are reported to have altered soil hydraulic properties (Kobayashi and Shimizu, 2007; Letey et al., 1962; Lichner et al., 2013; 2020; Wahl et al., 2003). Numerous impacts of SWR on soil water systems have been recognized by studies under different land-use types and climatic regions. SWR tends to be highly variable spatially as well as temporally, where it often disappears following prolonged wet periods. Intensified surface runoff and erosion in water-repellent soils are reported with heavy rainfall events usually

following long dry and hot periods (Onderka et al., 2012; Pavelková et al., 2012). Inherent water-repellent characteristics in soils under different types of tree species are known to influence soil hydrological processes more specifically following longer hot or dry spells (Lichner et al., 2012).

Forest plantations in Sri Lanka were mainly established using non-native species such as Eucalyptus, Pine, and Casuarina due to their faster growth rates over the indigenous species. The idea of this exercise was to have an alternative timber resource to protect the existing natural forest and to rehabilitate the environmentally damaged areas within a short period. However, these plantations created a dialogue over its unsuitability as demonstrated by the natural evidence, such as drying out of streams, reduction of groundwater level, the nonexistence of undergrowth, and lack of animal diversity, including the presence of SWR (Leelamanie 2016; Piyaruwan and Leelamanie, 2020; Piyaruwan et al., 2020). Although these plantations have proven to have some of the expected advantages, the water-repellent aspects and their hydrophysical consequences are yet to be explored comprehensively. The objective of this study was to investigate hydrophysical characteristics of three water-repellent tropical exotic plantation forest soils (Eucalyptus, Pine, and Casuarina), considering both rainy (wet) and dry seasons.

MATERIALS AND METHODS

Study area

The study was conducted at three water-repellent experimental sites, namely *Eucalyptus grandis* (EG), *Pinus caribaea* (PC), and *Casuarina equisetifolia* (CE) plantation forest soils. The EG forest (06°47'45" N 80°57'58" E) and the PC forest (06°46'13" N 080°55'52" E) were located in the up-country intermediate zone (EG: IU3c; PC: IU3a, IU3b agro-ecological regions), whereas the CE forest is located (6°06′52″ N 81°05′02″ E) in low-country dry zone (DL5 agro-ecological region) (National Atlas of Sri Lanka, 2007).

The first experimental site, EG forest (~100 ha) is in a slope land with considerably steep slopes ranging from ~10 to 35 °. The mean annual rainfall of the area is 1600–1700 mm. The highest rainfall is received in April and October to December (wet season), where February, June, July, and August are the dry months (dry season) receiving less than 10% of the average annual. The mean annual temperature is in a range of 20–22.5 °C. The soil is identified as Red Yellow Podzolic according to the local classification system (National Atlas of Sri Lanka, 2007) and Hapludults, according to the USDA classification system (Soil Survey Staff, 2014). A dense layer of litter (3–4 cm in thickness) was observed on the surface. The average field moisture content of soil in the wet and dry seasons were 12 and 8%, respectively.

The second experimental site, PC forest (~100 ha) was also located in a land with steep slopes ranging from ~10 to 40°. The mean annual rainfall of the area is 1700–1900 mm and the mean annual temperature is in a range of 20–22.5 °C. The highest rainfall in the area is received in March to May and October to December (wet season). February, June, July, and August are the dry months (dry season) receiving less than 10% of the average annual rainfall. Similar to the EG site, the soil of the area is classified as Red Yellow Podzolic under the local classification system and Hapludults under the USDA classification system. A 3–12 cm thick layer of litter consisting mostly of pine needles was observed on the surface. The average field moisture content of soil during the wet and dry seasons were 17 and 14%, respectively.

The third experimental site, the CE forest (~36 ha) is a sand dune in the Southern Dry zone, which is considered as one of the driest parts of Sri Lanka with an average annual rainfall of about 900 mm. About 70% of the annual total rainfall is received from mid-October to mid-January (wet season), and minor proportion during mid-March to mid-May. Mid-May to September is considered to be the dry period (dry season) receiving less than 20% of the annual rainfall. The average annual temperature varies from 25 to 31 °C, with the highest temperatures are recorded in the driest period of the year (May–September) (National Atlas of Sri Lanka, 2007). The soil type is identified locally as sandy Regosols, or according to USDA classification as Ustic Quartzipsamments. Sandy Regosols are soils that are in general found along or within proximity to the coastline, with no specific structural development, where both surface and subsurface soils are single-grained (National Atlas of Sri Lanka, 2007). Soil reaction is nearly neutral (pH: 7.4±0.2). The forest floor of the studied dune is covered with a thick mat of dry leaf litter layer or phylloclades (3–10 cm of thickness). The average field soil moisture content during the wet and dry seasons were 5–7% and 0.5–1.5%, respectively.

The litter layers at all three experimental sites vary in thickness interrelated with the climatic conditions, more specifically, the rainfall. The maximum litter thicknesses were observed in the driest periods, where the decomposition rate of the organic matter is very low. During these dry periods, extreme levels of water-repellent nature can be observed on the soil surfaces. During the rainy season, organic matter decomposition takes place at an accelerated rate and the thickness of the litter layer decreases. Simultaneously, the magnitude of water-repellent behavior also tends to drop. The thematic maps of normalized difference vegetation index (NDVI) for the three plantation forest sites that represent the greenness and the relative density of the vegetation covers are given in Figure 1. Most of the land area in all three study sites showed NDVI values above 0.5, indicating close to dense vegetation cover.

Soil sampling

Field experiments and laboratory experiments were conducted during the period from 2016 to 2020 dry (July, August) and wet (November, December) seasons in all three sites. After carefully removing the litter, both undisturbed core samples and bulk samples were collected from each site at the depths of 0–5, 5–10, and 10–15 cm for laboratory experiments. Nine sampling points were sleeted (about 2 m away from trees) per site to represent 3 blocks, in three replicates. The collected soil samples were tagged, sealed, and transported to the laboratory.

Laboratory experiments

In the laboratory, soils were air-dried at room temperature (27±3 °C) for 3 days and passed through a 2-mm sieve. The basic properties of the soils were measured in triplicates following standard laboratory procedures. The bulk density, the particle density, and the texture of soils were measured using the undisturbed soil core method (Blake and Hartge, 1986a), pycnometer method (Blake and Hartge, 1986b), and the hydrometer method (Bouyoucos, 1962), respectively. The organic matter content was measured using the loss on ignition (400 °C for 6 h) method (Rowell and Coetzee, 2003; Schumacher, 2002). The basic properties of the tested soils in the three experimental sites are given in Table 1.

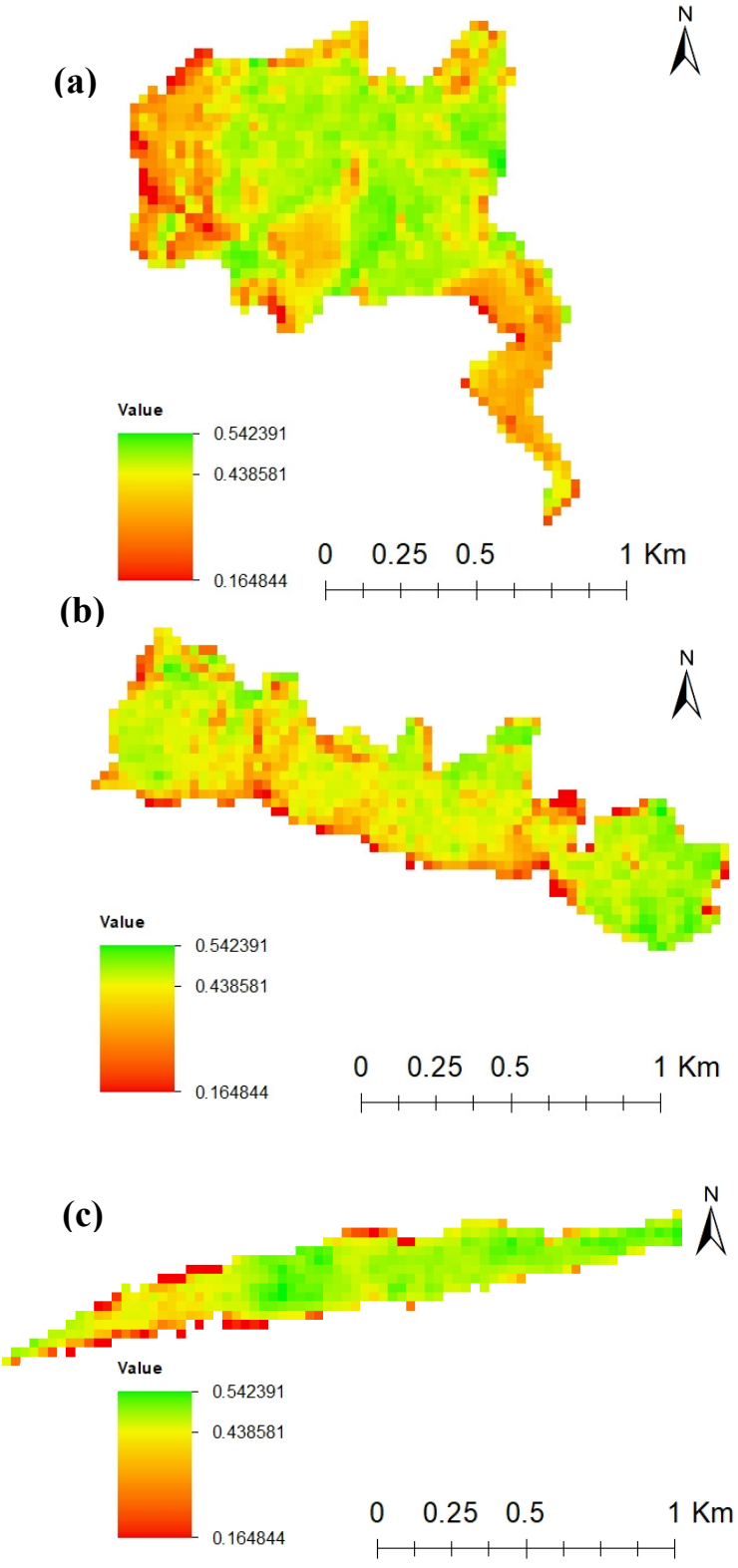

Fig. 1. Thematic maps of Normalized Difference Vegetation Index (NDVI) in 2020 for the (a) Eucalyptus, (b) Pine, and (c) Casuarina plantation forest sites.

Water repellency

The potential soil water repellency (SWR) was measured using the water drop penetration time (WDPT) and soil-water contact angle. Soil subsamples with a thickness of >5 mm were used for the WDPT test. Single drop (50±1 µL) of distilled water was placed on the surface of the soil from a height of about 10 mm using a burette. Containers were carefully covered with lids to minimize the effects of evaporation during the experiment. The time taken for water drops to completely penetrate the soil was measured using a stopwatch (Bisdom et al. 1993; Chenu et al., 2000; Leelamanie et al., 2008). Penetration

Table 1. The basic properties of the plantation forest soils (mean ± standard deviation).

Soil property		Eucalyptus			Pine			Casuarina		
		0–5 cm	5–10 cm	10–15 cm	0–5 cm	5–10 cm	10–15 cm	0–5 cm	5–10 cm	10–15 cm
Bulk density (g cm^{-3})		1.02±0.10	1.10 ±0.05	1.18 ±0.02	0.96±0.16	1.07±0.07	1.12±0.10	1.98 ±0.04	2.12 ±0.09	2.19 ±0.08
Particle density (g cm^{-3})		2.30±0.25	2.30 ±0.26	2.55 ±0.22	2.56±0.16	2.68±0.07	2.58±0.25	2.80 ±0.03	2.81 ±0.12	2.80 ±0.08
Porosity (%)		55.5 ±6.0	52.1±5.6	53.8±4.2	62.5±5.6	60.0±1.8	56.7±5.0	29.3±2.5	24.5±2.8	21.8±2.4
Sand %		80.4 ±1.8	74.8 ±2.1	79.5 ±0.1	73.7±3.9	72.6±2.3	72.6±3.2	96.7±2.1	96.9 ±4.1	97.0 ±2.9
Silt %		5.8±1.5	6.4±1.5	6.3±1.5	10.4±0.6	8.2±1.6	9.2±1.5	3.2±0.5	2.9±0.3	2.5±0.3
Clay %		13.8±4.2	17.8 ±4.4	14.2 ±2.4	15.9±3.7	19.3±3.4	18.2±1.9	0.1±0.05	0.2±0.3	0.5±0.2
Texture		Loamy sand	Sandy loam	Sandy loam	Sandy loam	Sandy loam	Sandy loam	Sand	Sand	Sand
Organic matter (%)	Wet	9.94±0.14	7.05 ±0.04	6.92 ±0.06	15.4±4.0	12.4±2.8	10.6±1.7	1.82 ±0.15	1.29 ±0.08	0.56 ±0.04
	Dry	13.2 ±1.1	9.83 ±0.72	7.95 ±0.74	19.1±1.6	15.5±1.1	12.4±0.4	2.04 ±0.06	1.64 ±0.03	1.17 ±0.03

times shorter than 0.5 s were considered as 0 s because the actual measurement could not be taken accurately corresponding to the instantaneous penetration. The measurement of penetration time was terminated after 6 h. The WDPT values were determined in three replicates for nine sampling points in each site.

The soil-water contact angle was measured using the modified sessile drop method (Bachmann et al., 2000) using a digital microscopic camera (FS-3100-PC, Fujikoden Co. Ltd., Japan). Monolayers of soil samples fixed on double-sided adhesive tapes (1.5 cm × 1.5 cm) using smooth glass slides were used for the measurements. A drop (10 µL) of distilled water was placed on the surface of soil monolayer using a micropipette (Nichipet EX II J15615241. Nichiriyo, Japan). A digital microphotograph of the water drop (horizontal view) was taken within 1–2 s. The contact angle was determined, in three replicates, using the digital micro-photographs of the horizontal view of the drop (Leelamanie, 2016).

Water-entry value

In water-repellent soils, low hydraulic pressures present on the soil surfaces are not sufficient to start the infiltration. Water starts to infiltrate into water repellent soils at a critical pressure showing an instantaneous breakdown of SWR (Wang et al., 2000). The critical pressure that is required for the breakdown of repellency and driving water into that soil can be determined using the water-entry value (h_{we}).

The h_{we} of the topsoil was tested in the laboratory, in triplicates, using the pressure head method (Wang et al., 2000), for the samples collected from the surface soils (0–5 cm). Air-dried soils, in 50-g soil subsamples, were placed in the Buchner funnel, where the porous plate was covered with a membrane filter and filter paper. The funnel was attached to a burette using a flexible tube. Increasing hydraulic pressure was applied to the soil sample using increasing water height by raising the burette level. The starting pressure head was kept negative to prevent initial wetting (Wang et al., 2000). The hydraulic pressure head was increased carefully by 5 min intervals up to the point where the water enters into the soil matrix. At this point of water entry, the height of the water column (burette water level compared to the reference level considering the soil) was recorded as the h_{we} of the samples (Liyanage and Leelamanie, 2016).

Field experiments

The actual SWR, infiltration rate, unsaturated hydraulic conductivity, k(–1 cm), and water sorptivity (S_W) of the soils in the forest soils were determined in the field. Sampling was conducted in triplicates, sectioning in the study area into three blocks (total of nine sample points), during wet and dry seasons.

The actual SWR was measured using the WDPT test by placing a drop (50±1 µL) of distilled water on the soil surface from a height of about 10 mm using a micropipette (Nichipet EX II, 1–100 µL Nichiriyo, Japan). The time taken for complete penetration of the drops were measured using a stop watch, where the average times of 5 drops was taken as the WDPT for one replicate. The SWR was categorized into classes (both field and laboratory measurements) as wettable (WDPT ≤ 5 s), slightly repellent (5–60 s), strongly repellent (60–600 s), severely repellent (600–3600 s), and extremely repellent (WDPT > 3600 s) (Bisdom et al., 1993). Penetration times shorter than 0.5 s were considered as 0 s and the measurement of penetration time was terminated after 1 h.

The mini-disk infiltrometer (Decagon devices, Inc.), with a suction head of 1 cm, was used for this purpose. A leveled area of the field at a minimum distance of 2 m to the tree trunks were selected as the sampling points and the litter layer was carefully removed without disturbing the soil before the measurements. Before placing the The method proposed by Zhang (1997) was used to determine the k(–1 cm) of the tested soils (Lichner et al., 2007), which requires the measuring of cumulative infiltration with time and fitting the obtained results with the function:

$$I = C_1 t + C_2 \sqrt{t} \quad (1)$$

where the C_1 (m s^{-1}) and C_2 (m s$^{-1/2}$) parameters are respectively related to the k(–1 cm) and the S_W of the soil. The k(–1 cm) for the respective soil is then to be computed from:

$$k = C_1/A \quad (2)$$

where C_1 is the slope of the cumulative infiltration, I (cm) versus the square root of time ($t^{1/2}$) curve, and A relates the van Genuchten parameters of soil to the suction rate and the infiltrometer disk radius. The slope of the cumulative infiltration versus the square root of the time curve, and the k(–1 cm) were calculated based on the infiltration data gathered with the support of the Microsoft Excel spreadsheet published by Decagon (www.decagon.com/macro). The linear approximation of the relationship between cumulative infiltration and the square root of time (Eq. 3) was used to estimate the water sorptivity (S_W).

$$I = S_W \sqrt{t} \quad (3)$$

Data analysis

The laboratory and field experiments were conducted in triplicates and the results were statistically analyzed using linear regression and the analysis of variance (ANOVA) at a 5% level of significance ($p < 0.05$) using Microsoft Excel (2016) and STATISTICA software. The mean values of the measurements were reported, where the error bars in the figures indicate ± standard deviation.

RESULTS AND DISCUSSION

Figure 2 shows the potential (a, b, c) and actual field (d, e, f) SWR values as measured by the WDPT of the three plantation forest soils in both wet and dry seasons. Among the three plantation forests, CE soils showed the highest SWR in the dry season, whereas the EG soils showed the highest SWR in the wet season. In the wet season, all three forest soils showed a decrease in water repellency with increasing soil depth. In contrast, in the dry season, only CE soils showed a significant decrease in SWR with soil depth. Both EG and PC soils maintained high levels of repellency with decreasing soil depth down 15 cm in the soil profile. Both actual and potential SWR in all three tested layers of EG soils, (0–5, 5–10, 10–15 cm) showed extreme water-repellent conditions (WDPT > 3600 s). The two upper layers (0–5, 5–10 cm) of PC soils showed extreme (WDPT > 3600 s) while the 10–15 cm showed severe (WDPT > 2000 s) water-repellent conditions.

Low SWR in the wet season seems to correspond with the thickness of the litter layer on the surface of all the forest soils. In the wet season, the thickness of the litter layer was low, which was very high in the dry season. The temperature of all the locations is sufficient enough to maintain higher decomposition rates when there is enough water available. Although CE soils showed very high water repellency in the topsoil in the dry season. Interestingly water repellency dropped significantly with the depth. It means that the highly repellent compounds added to the topsoil are not moving downward irrespective of the sandy nature of the soils. Furthermore, very low organic matter content (~1–2%) in these soils can be considered another reason for low SWR levels in the lower levels of the profile. Conversely, the other two soils showed considerable high values of water repellency throughout the top 15 cm of the soil showing that the water repellent compounds transferred to the lower levels of the profile.

Unsaturated hydraulic conductivity, k(–cm), water sorptivity (S_W), contact angle, and water entry value (h_{we}) of the tested forest soils in both wet and dry seasons are presented in Table 2. It should be noted that infiltration did not initiate in the CE soils in the dry season, even with a 0.5 cm suction level in the mini-disk infiltrometer, and therefore, it was not possible to get the measurements for k(–1 cm) and S_W in CE soils for the dry season. An interesting finding in the EG and PC soils in the dry season was the presence of very high initial infiltration rates in some locations. These can be considered as an indicator for the presence of preferential flow paths. The h_{we} of water-repellent soils are in general known to be positive due to the requirement of high hydraulic pressure for the cessation of the SWR and force water into the soils (Karunarathna et al., 2010). In all three soils, the dry season with higher repellency (Figure 2) showed higher h_{we} compared with the wet season (Table 2).

The S_W is a measure of the ability of a soil to capture water rapidly that is considered as a key parameter governing the early stages of entry of water into the soil through infiltration (Shaver et al., 2003). Wallis et al. (1991) pointed out that the entry of water into soils may be retarded by even minor levels of repellency, indicating its hydrological significance. However, irrespective of the higher levels of repellency in the dry season, EU and PC soils did not show any significant difference in S_W for wet and dry seasons. Other than the wetting status of soils governed by the repellency, another potential reason for high rates of water absorption into soils in dry conditions is the differences in water potential of soils between dry and moist conditions. As the wetting of soil with water would theoretically be accelerated when the soil is in a drier condition, it might also be factored in, together with restriction for water movements caused by water-repellent effects, to the actual S_W of the soils. These contradictory influences can be considered as the reasons for soils to show no differences in S_W between dry and wet seasons.

Soils having water-repellent features are reported to resist or retard surface water infiltration (Doerr et al., 2000; Wahl et al., 2003). Our results are in line with some of the previous studies which report that water infiltration into hydrophobic soil is slower than into more hydrophilic soil (Letey et al., 1962). Relation of potential SWR, as measured by soil water contact angle, to the initial infiltration rate during the period of first 30 s is given in Figure 3. Initial infiltration rate showed moderate to strong negative linear correlation with soil-water contact angle in all three soils ($R^2 = 0.55$, 0.55, and 0.91, respectively in

Table 2. Unsaturated hydraulic conductivity (k), water sorptivity (S_W), contact angle, and water entry value (h_{we}) of the tested forest soils in wet and dry seasons.

	k(–1 cm) (cm h^{-1})		S_W (cm s$^{-1/2}$)		Contact angle (°)		h_{we} (cm)	
	Wet	Dry	Wet	Dry	Wet	Dry	Wet	Dry
Eucalyptus								
Minimum	1.23	0.01	0.028	0.062	119	124	3.8	6.3
Maximum	6.97	4.45	0.130	0.133	78	110	3.3	4.0
Mean	2.46	1.83	0.082	0.080	103	115	3.6	4.9
S.D.	1.63	1.35	0.025	0.018	13	4	0.3	0.9
Pine								
Minimum	0.47	0.02	0.021	0.019	97	107	3.4	4.4
Maximum	2.89	5.86	0.168	0.164	67	69	1.3	1.4
Mean	2.33	2.11	0.148	0.143	83	83	2.4	2.8
S.D.	0.76	1.98	0.019	0.050	10	14	1.4	1.2
Casuarina								
Minimum	1.66	–	0.035	–	106	119	5.3	8.2
Maximum	44.83	–	0.259	–	85	104	3.8	5.4
Mean	23.39	–	0.127	–	100	111	4.8	6.8
S.D.	17.60	–	0.095	–	7	6	0.4	0.9

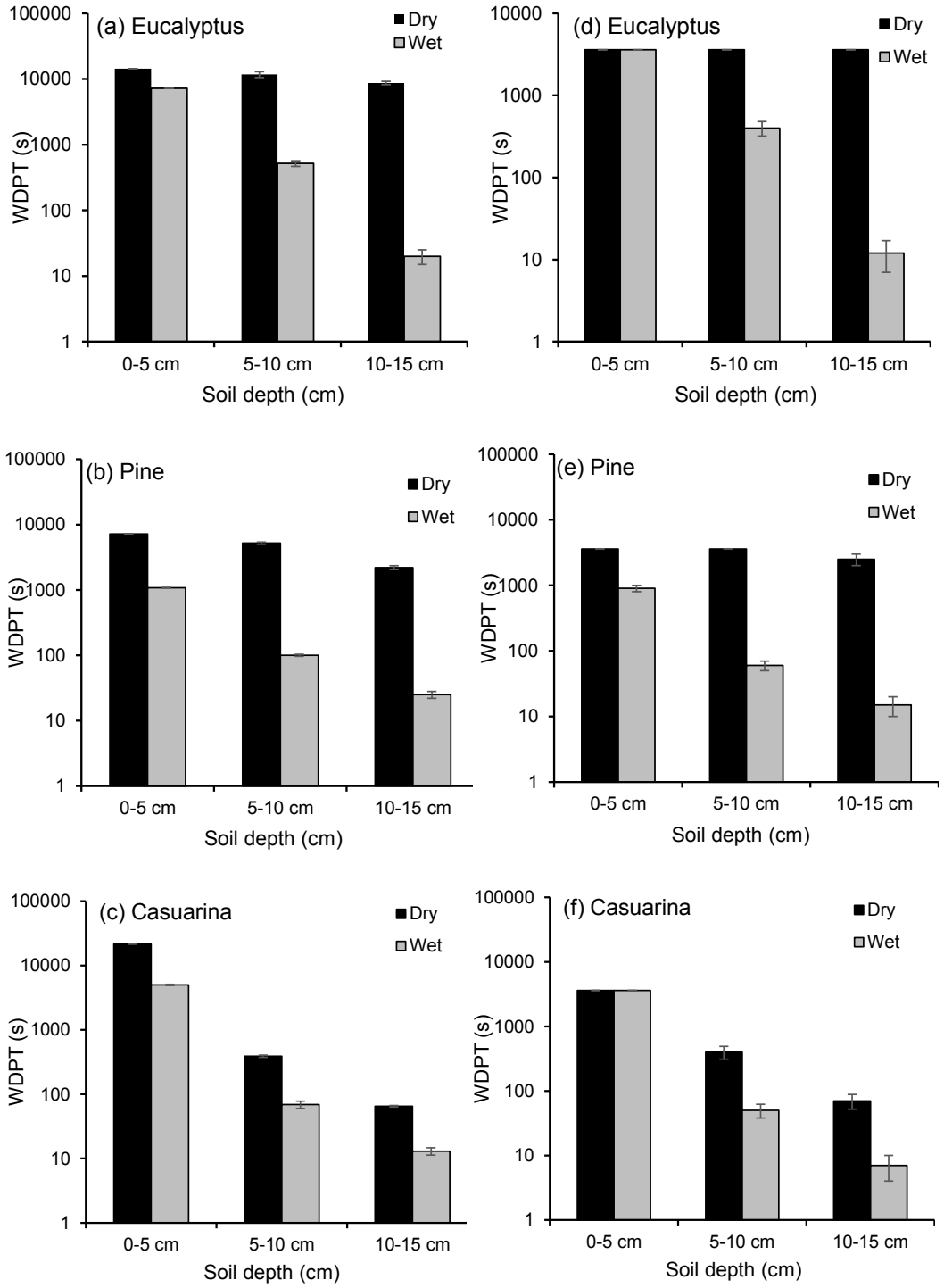

Fig. 2. Potential (a, b, c) and actual (d, e, f) soil water repellency as measured by water drop penetration time (WDPT) of Eucalyptus, Pine, and Casuarina plantation forest soils in both wet and dry seasons.

EU, PC, and CE soils). It was clear that the level of SWR decelerates water infiltration into all three soils at the initial level. The influence of SWR is reported to be more pronounced during the early stages of the infiltration process. (Letey et al., 1962; Lozano-Baez et al., 2020). This diminished water flow rate into soils can be considered as a result of increased flow resistance with increasing contact angle (Diamantopoulos and Durner, 2013).

Figure 4 shows the relation between the potential SWR as measured by soil-water contact angle and the $k(-1$ cm). Similar to the initial infiltration rate, $k(-1$ cm) in all the three forest soils decreased with increasing contact angle showing a negative exponential correlation ($R^2 = 0.34$, 0.37, and 0.44, respectively in EU, PC, and CE soils). The results on $k(-1$ cm) are comparable with Moody et al. (2009), who reported that hydraulic conductivity near saturation is inversely proportional to the SWR in fire-affected soils.

The relationship between $k(-1$ cm) and S_W, as obtained from the linear approximation of cumulative infiltration and the square root of the time, is presented in Figure 5. All three soils showed moderate to strong positive linear correlations between $k(-1$ cm) and S_W ($R^2 = 0.82$, 0.66, and 0.61, respectively in EU,

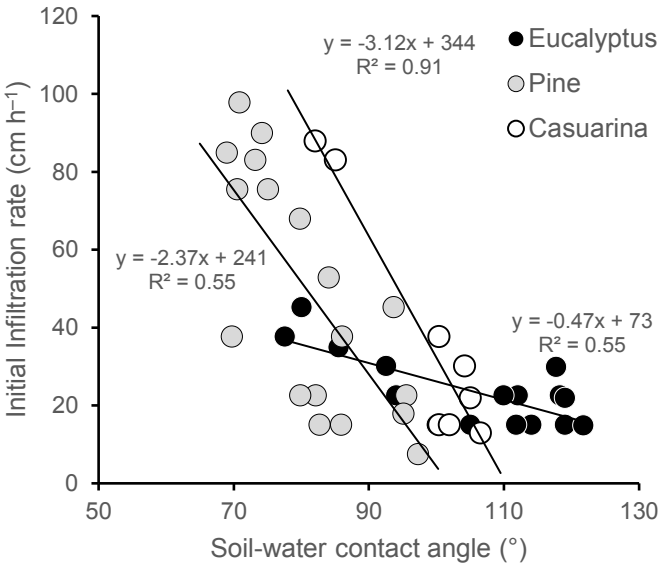

Fig. 3. Relation of Soil water repellency, as measured by soil water contact angle, to the initial infiltration rate during the period of first 30 s of infiltration in Eucalyptus, Pine, and Casuarina plantation forest soils.

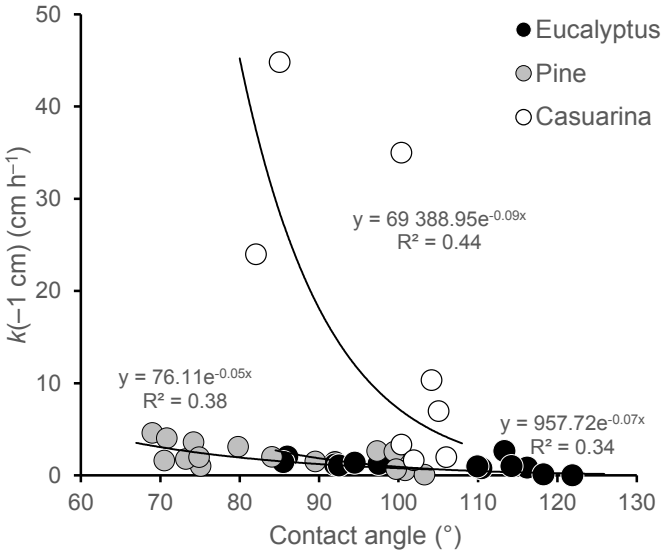

Fig. 4. Relationship between soil-water contact angle and the unsaturated hydraulic conductivity, k(–1 cm), in Eucalyptus, Pine, and Casuarina plantation forest soils.

PC, and CE soils), which were statistically significant at 0.05 probability level. It appeared that surface sorptivity is related to the subsurface unsaturated water flow in all three water-repellent soils.

The S_W is the ability of soil for the rapid capture of, or to uptake, water without any influence of gravitational effects (Philip, 1969). The h_{we} explains the critical pressure at the point of accomplishing instantaneous entry of water into soils. As both these parameters explain the entering of water into the soil at different conditions, S_W was plotted against h_{we} to observe the interrelation. The S_W showed a negative linear correlation (Figure 6) between h_{we} and S_W (R^2 = 0.70, 0.42, and 0.65, respectively in EU, PC, and CE soils), where the correlation between the two parameters for all three soils was statistically significant at 0.05 probability level. The result shows that the surface water absorption related to the critical surface water entry pressure that force water into the soil.

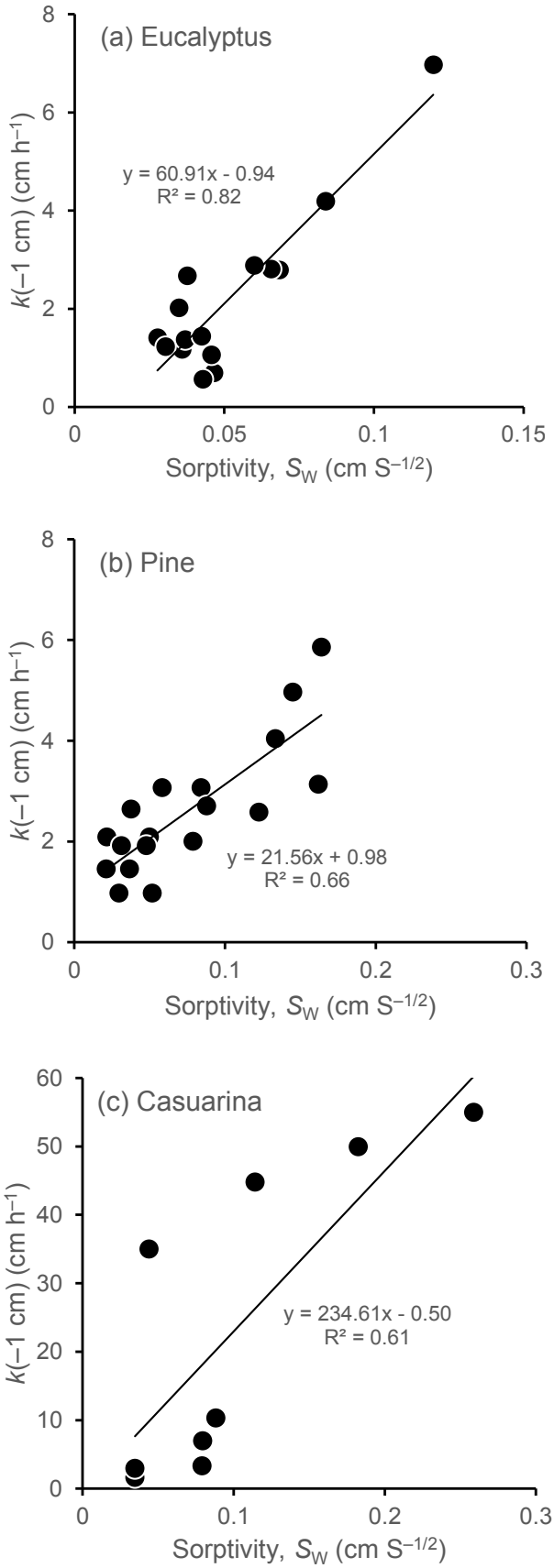

Fig. 5. Relationship between unsaturated hydraulic conductivity, k(–1 cm), and water sorptivity, S_W , in (a) Eucalyptus, (b) Pine, and (c) Casuarina plantation forest soils.

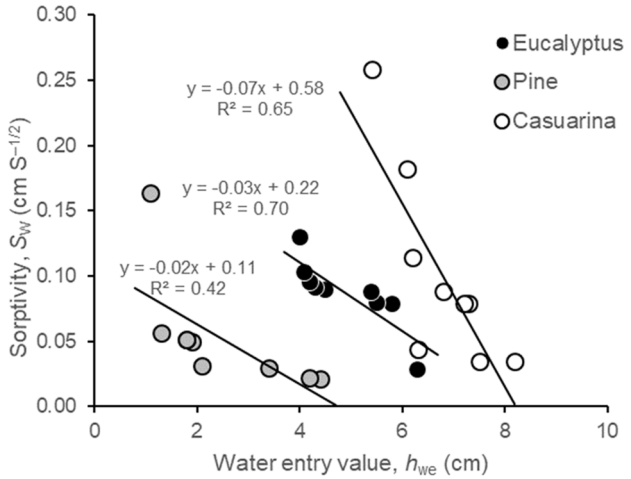

Fig. 6. Relationship between water entry value (h_{we}) and water sorptivity (S_W) in Eucalyptus, Pine, and Casuarina plantation forest soils.

CONCLUSIONS

All three plantation forest soils showed clear differences in repellency between wet and dry seasons. The dry season showed higher repellency that seems to correspond to the thickness of the litter layer on the surface. Positive linear correlations between k(–1 cm) and S_W, and negative linear correlations between S_W and h_{we}, confirmed that the surface water absorption is related to both subsurface unsaturated water flow and surface water entry pressure.

Water entry into soils as well as the subsurface water flow was hindered by the SWR. For the initiation of water to infiltrate into the soil under natural conditions, the ponding depth of water on the soil surface should be equal to or exceed the water entry value. High water entry values in the dry season predict high potentials for intensified surface runoff and topsoil erosion in the dry season. Considering the localized points with very high infiltration rates, presence of preferential flow paths can be suggested as the possible mode of water entry into soils in rainfall events after strong dry spells. Future research will be required on the interactions between soil biology and soil properties such as pore structure that would influence water flow into and within soils, and the potential runoff levels.

Acknowledgements. This work was financially supported by the University Grants Commission (UGC) Block grant for strengthening research [RU/PG-R/16/01].

Conflicts of interest. As the authors of the manuscript, herewith we confirm that the study has not received any funds from interested parties, except for the UGC Block grant [RU/PG-R/16/01] and that there are no conflicts of interest in any manner.

REFERENCES

Bachmann, J., Ellies, A., Hartge, K.H., 2000. Development and application of a new sessile drop contact angle method to assess soil water repellency. Journal of Hydrology, 231–232, 66–75. https://doi.org/10.1016/S0022-1694(00)00184-0

Benito, E., Varela, E., Rodríguez-Alleres, M., 2019. Persistence of water repellency in coarse-textured soils under various types of forests in NW Spain**.** Journal of Hydrology and Hydromechanics, 67, 2, 129–134**.** https://doi.org/10.2478/johh-2018-0038

Bisdom, E.B.A., Dekker, L.W., Schoute, J.F.T., 1993. Water repellency of sieve fractions from sandy soils and relationships with organic material and soil structure. Geoderma, 56, 105–118.https://doi.org/10.1016/B978-0-444-81490-6.50013-3

Blake, G.R., Hartge, K.H., 1986a. Bulk density. In: Klute, A. (Ed.): Methods of Soil Analysis. Part 1: Physical and Mineralogical Methods. 2nd Ed. Soil Science Society of America: Madison, WI., pp. 363–375. https://doi.org/10.2136/sssabookser5.1.2ed.c13

Blake, G.R., Hartge, K.H., 1986b. Particle density. In: Klute, A. (Ed.): Methods of Soil Analysis. Part 1: Physical and Mineralogical Methods. 2nd Ed. Soil Science Society of America: Madison, WI., pp. 377–382. https://doi.org/10.2136/sssabookser5.1.2ed.c14

Bouyoucos, G.J., 1962. Hydrometer method improved for making particle size analyses of soils. Agronomy Journal, 54, 5, 464–465. https://doi.org/10.2134/agronj1962.00021962005400050028x

Chenu, C., Le Bissonnais, Y., Arrouays, D., 2000. Organic matter influence on clay wettability and soil aggregate stability. Soil Science Society of America Journal, 64, 4, 1479–1486. https://doi.org/10.2136/sssaj2000.6441479x

Debano, L.F., 1981. Water repellent soils: a state-of-the art. General Technical Report PSW-46, Berkeley, CA: USDA Forest Service, Pacific Southwest Forest and Range Experiment Station, pp. 2–4.

Diamantopoulos, E., Durner, W., 2013. Physically-based model of soil hydraulic properties accounting for variable contact angle and its effect on hysteresis. Advances in Water Resources, 59, 169–180. https://doi.org/10.1016/j.advwatres.2013.06.005

Doerr, S.H., Shakesby, R.A., Walsh, R.P.D., 1996. Soil hydrophobicity variations with depth and particle size fraction in burned and unburned *Eucalyptus globulus* and *Pinus pinaster* forest terrain in the Águeda Basin, Portugal. Catena, 27, 25–47. https://doi.org/10.1016/0341-8162(96)00007-0

Doerr, S.H., Shakesby, R.A., Walsh, R.P.D., 2000. Soil water repellency: Its causes, characteristics and hydro-geo morphological significance. Earth Sci. Rev., 51, 33–65. https://doi.org/10.1016/S0012-8252(00)00011-8

Hallett, P.D., 2007. An introduction to soil water repellency. In: Gaskin, R.E. (Ed.): Proc. 8th Int. Symp. on Adjuvants for Agrochem. Hand Multimedia, Christchurch, NZ. 13 p. ISBN 978-0-473-12388-8.

Hansel, F.A., Aoki, C.T., Maia, C.M., Cunha Jr, A. and Dedecek, R.A., 2008. Comparison of two alkaline treatments in the extraction of organic compounds associated with water repellency in soil under *Pinus taeda*. Geoderma, 148, 2, 167–172. https://doi.org/10.2134/agronj1962.00021962005400050028x

Iovino, M., Pekárová, P., Hallett, P.D., Pekár, J., Lichner, Ľ., Mataix-Solera, J., Alagna, V., Walsh, R., Raffan, A., Schacht, K., Rodný, M., 2018. Extent and persistence of soil water repellency induced by pines in different geographic regions. Journal of Hydrology and Hydromechanics, 66, 4, 360–368. https://doi.org/10.2478/johh-2018-0024

Karunarathna, A.K., Chhoden, T., Kawamoto, K., Komatsu, T., Moldrup, P., de Jonge, L.W., 2010. Estimating hysteretic soil-water retention curves in hydrophobic soil by a minitensiometer-TDR coil probe. In: Proc. 19th World Congress of Soil Science, Soil Solutions for a Changing World, Brisbane, Australia, pp. 58–61. Published on DVD.

Keizer, J.J., Doerr, S.H., Malvar, M.C., Prats, S.A., Ferreira, R.S.V., Oñate, M.G., Coelho, C.O.A., Ferreira, A.J.D., 2008. Temporal variation in topsoil water repellency in two recently burnt eucalypt stands in north-central Portugal. Catena, 74, 192–204. https://doi.org/10.1016/j.catena.2008.01.004

Kobayashi, M., Shimizu, T., 2007. Soil water repellency in a Japanese cypress plantation restricts increases in soil water

storage during rainfall events. Hydrological Processes, 21, 2356–2364. https://doi.org/10.1002/hyp.6754

Leelamanie, D.A.L., 2016. Occurrence and distribution of water repellency in size fractionated coastal dune sand in Sri Lanka under Casuarina shelterbelt. Catena, 142, 206–212. https://doi.org/10.1016/j.catena.2016.03.026

Leelamanie, D.A.L., Karube, J., Yoshida, A., 2008. Characterizing water repellency indices: Contact angle and water drop penetration time of hydrophobized sand. Soil Science & Plant Nutrition, 54, 2, 179–187. https://doi.org/10.1111/j.1747-0765.2007.00232.x

Letey, J., Osborn, J., Pelishek, R.E., 1962. The influence of the water-solid contact angle on water movement in soil. Hydrological Sciences Journal, 7, 3, 75–81. https://doi.org/10.1080/02626666209493272

Lichner, Ľ., Capuliak, J., Zhukova, N., Holko, L., Czachor, H., Kollár, J., 2013. Pines influence hydrophysical parameters and water flow in a sandy soil. Biologia, 68, 6, 1104–1108. https://doi.org/10.2478/s11756-013-0254-7

Lichner, L., Hallett, P.D., Feeney, D.S., Ďurová, O., Šír, M., Tesař, M., 2007. Field measurement of soil water repellency and its impact on water flow under different vegetation. Biologia, 62, 5, 537–541. https://doi.org/10.2478/s11756-007-0106-4

Lichner, L., Holko, L., Zhukova, N., Schacht, K., Rajkai, K., Fodor, N., Sandor, R., 2012. Plants and biological soil crust influence the hydrophysical parameters and water flow in an aeolian sandy soil. Journal of Hydrology and Hydromechanics, 60, 4, 309–318. DOI: 10.2478/v10098-012-0027-y

Lichner, Ľ., Iovino, M., Šurda, P., Nagy, V., Zvala, A., Kollár, J., Pecho, J., Píš, V., Sepehrnia, N., Sándor, R., 2020. Impact of secondary succession in abandoned fields on some properties of acidic sandy soils. Journal of Hydrology and Hydromechanics, 68, 1, 12–18. https://doi.org/10.2478/johh-2019-0028

Liyanage, T.D.P., Leelamanie, D.A.L., 2016. Influence of organic manure amendments on water repellency, water entry value, and water retention of soil samples from a tropical Ultisol. Journal of Hydrology and Hydromechanics, 64, 2, 160–166. https://doi: 10.1515/johh-2016-0025

Lozano-Baez, S.E., Cooper, M., de Barros Ferraz, S.F., Ribeiro Rodrigues, R., Lassabatere, L., Castellini, M., Di Prima, S., 2020. Assessing water infiltration and soil water repellency in Brazilian Atlantic forest soils. Applied Sciences, 10, 6, 1950. https://doi.org/10.3390/app10061950

Moody, J.A., Kinner, D.A., Úbeda, X., 2009. Linking hydraulic properties of fire-affected soils to infiltration and water repellency. Journal of Hydrology, 379, 3–4, 291–303. https://doi.org/10.1016/j.jhydrol.2009.10.015

National Atlas of Sri Lanka, 2007. 2nd Ed. Survey Department of Sri Lanka. Colombo, Sri Lanka.

Onderka, M., Wrede, S., Rodný, M., Pfister, L., Hoffmann, L., Krein, A., 2012. Hydrogeologic and landscape controls of dissolved inorganic nitrogen (DIN) and dissolved silica (DSi) fluxes in heterogeneous catchments. Journal of Hydrology, 450, 36–47. https://doi.org/10.1016/j.jhydrol.2012.05.035

Ouyang, L., Wang, F., Tang, J., Yu, L., Zhang, R., 2013. Effects of biochar amendment on soil aggregates and hydraulic properties. J. Soil Sci. Plant Nutr., 13, 4, 991–1002. http://dx.doi.org/10.4067/S0718-95162013005000078

Pavelková, H., Dohnal, M., Vogel, T., 2012. Hillslope runoff generation-comparing different modeling approaches. Journal of Hydrology and Hydromechanics, 60, 73–86. DOI: 10.2478/v10098-012-0007-2

Philip, J., 1969. Theory of infiltration. Advances in Hydroscience, 5, 215–296.

Piyaruwan, H.I.G.S., Leelamanie, D.A.L., 2020. Existence of water repellency and its relation to structural stability of soils in a tropical Eucalyptus plantation forest. Geoderma, 380, 114679. https://doi.org/10.1016/j.geoderma.2020.114679

Piyaruwan, H.I.G.S., Jayasinghe, P.K.S.C., Leelamanie, D.A.L., 2020. Water repellency in eucalyptus and pine plantation forest soils and its relation to groundwater levels estimated with multi-temporal modeling. Journal of Hydrology and Hydromechanics, 68, 4, 382–391. https://doi.org/10.2478/johh-2020-0030

Rodný, M., Lichner, L., Schacht, K., Holko, L., 2015. Depth-dependent heterogeneity of water flow in sandy soil under grass. Biologia, 70, 11, 1462–1467. http://dx.doi.org/10.1515/biolog-2015-0167

Rowell, M.J., Coetzee, M.E., 2003. The measurement of low organic matter contents in soils. South African Journal of Plant Soil, 20, 2, 49-53. https://doi.org/10.1080/02571862.2003.10634907

Schumacher, B.A., 2002. Methods for the determination of total organic carbon (TOC) in soils and sediments. Ecological Risk Assessment Support Center Office of Research and Development, US Environmental Protection Agency, 25 p.

Shaver, T.M., Peterson, G.A., Sherrod, L.A., 2003. Cropping intensification in dryland systems improves soil physical properties: regression relations. Geoderma, 116, 149–164. https://doi.org/10.1016/S0016-7061(03)00099-5

Soil Survey Staff, 2014. Keys to Soil Taxonomy. 12th Ed., United States Department of Agriculture, Natural Resources Conservation Service, pp. 290–303.

Šurda, P., Lichner, Ľ., Kollár, J., Nagy, V., 2020. Differences in moisture pattern, hydrophysical and water repellency parameters of sandy soil under native and synanthropic vegetation. Biologia, 75, 6, 819–825. https://doi.org/10.2478/s11756-020-00415-z

Wahl, N.A., Bens, O., Schäfer, B., Hüttl, R.F., 2003. Impact of changes in land-use management on soil hydraulic properties: hydraulic conductivity, water repellency and water retention. Physics and Chemistry of the Earth, 28, 1377–1387. https://doi.org/10.1016/j.pce.2003.09.012

Wallis, M.G., Scotter, D.R., Horne, D.J., 1991. An evaluation of the intrinsic sorptivity water repellency index on a range of New Zealand soils. Soil Research, 29, 3, 353–362. https://doi.org/10.1071/SR9910353

Wang, Z., Wu, L., Wu, Q.J., 2000. Water-entry value as an alternative indicator of soil water-repellency and wettability. Journal of Hydrology, 231–232, 76–83. https://doi.org/10.1016/S0022-1694(00)00185-2

Wessolek, G., Schwärzel, K., Greiffenhagen, A., Stoffregen, H., 2008. Percolation characteristics of a water-repellent sandy forest soil. European Journal of Soil Science, 59, 14–23. https://doi.org/10.1111/j.1365-2389.2007.00980.x

Zhang, R., 1997. Determination of soil sorptivity and hydraulic conductivity from the disk infiltrometer. Soil Science Society of America Journal, https://doi.org/10.2136/sssaj1997.03615995006100040005x

Received 31 May 2021
Accepted 25 August 2021

J. Hydrol. Hydromech., 69, 2021, 4, 360–368
DOI: 10.2478/johh-2021-0028
ISSN 1338-4333

sciendo Journal of Hydrology and Hydromechanics

The role of biocrust-induced exopolymeric matrix in runoff generation in arid and semiarid zones – a mini review

Giora J. Kidron

Institute of Earth Sciences, The Hebrew University of Jerusalem, Givat Ram Campus, Jerusalem 91904, Israel.
Tel: +972-54-4967-271. Fax: 972-2-566-2581. E-mail: kidron@mail.huji.ac.il

Abstract: Although playing an important role in shaping the environment, the mechanisms responsible for runoff initiation and yield in arid and semiarid regions are not yet fully explored. With infiltration-excess overland flow, known also as Hortonian overland flow (HOF) taking place in these areas, the uppermost surface 'skin' plays a cardinal role in runoff initiation and yield. Over large areas, this skin is composed of biocrusts, a variety of autotrophs (principally cyanobacteria, green algae, lichens, mosses) accompanied by heterotrophs (such as fungi, bacteria, archaea), which may largely dictate the infiltration capability of the surface. With most biocrust organisms being capable of excreting extracellular polymeric substances (EPS or exopolymers), and growing evidence pointing to the capability of certain EPS to partially seal the surface, EPS may play a cardinal role in hindering infiltration and triggering HOF. Yet, despite this logic thread, great controversy still exists regarding the main mechanisms responsible for runoff generation (runoff initiation and yield). Elucidation of the possible role played by EPS in runoff generation is the focus of the current review.

Keywords: Biological soil crusts; Extracellular polymeric substances; Pore clogging; Hydrophobicity; Infiltration-excess overland flow; Water repellency.

1 INTRODUCTION

Mainly attributed to the low vegetal cover, high-magnitude runoff events and occasional hazardous floods commonly take place in arid and semiarid regions. In contrast to humid areas where runoff takes place once a large volume of soil reaches saturation, known therefore as saturation excess overland flow (SOF) (Beven and Kirkby, 1979; Dunne, 1990; Dunne and Black, 1970), runoff in arid and semiarid regions takes place even when almost the entire soil profile is dry. Runoff takes place due to infiltration-excess overland flow, known also as Hortonian overland flow (HOF), during which only the uppermost soil skin reaches saturation, thus hindering water infiltration into the subsurface, which may therefore remain dry or relatively dry (Blackburn, 1975; Cammeraat, 2004; Horton, 1933).

The crust thickness required to impede infiltration is assumed to be extremely thin, within millimeters. Following the widely-held belief that physical crusts trigger runoff, a possible link between the thickness of physical crusts and runoff was made. According to some scholars it is <1 mm-thick (Epstein and Grant, 1993; Heil et al., 1997; McIntyre, 1958; Onofiok and Singer, 1984; Pagliai et al., 1983), while according to others it may be 2–4 mm thick (Chen et al., 1980; de Jong et al., 2011; Tarchitzky et al., 1984), i.e., within the range of thickness of most biocrusts.

With biocrusts (biological soil crusts) constituting the upper skin of extensive areas in arid and semiarid regions (Rodriguz-Caballero et al., 2018) and with many of the biocrust microorganisms being known to excrete exopolymers (extracellular polymeric substances, EPS), which may affect surface hydrology (Brotherson and Rushforth, 1983; Chamizo et al., 2016; Kidron et al., 2003; Li et al., 2021; Sun et al., 2021; Xiao et al., 2019a), research on the interrelations between biocrusts and biocrust-induced EPS and runoff was called for. Papers aiming to study the possible relationships between these variables were subsequently published (Fischer et al., 2010; Kidron and Yair, 1997; Lichner et al., 2012). The research also focused on the EPS properties.

Research aiming to elucidate the different constituents of biocrust-induced EPS and the possible roles played by the EPS is indeed not uncommon. Excreted by microorganisms and microflora (cyanobacteria, archaea, bacteria, fungi, diatoms, green algae, lichens, but not by mosses) of the biocrusts, EPS is believed to protect and to assist the cell against possible stress and danger, and to accomplish some physiological needs. EPS facilitate cell adhesion and cohesion (Galle and Arendt, 2014; Rossi et al., 2018), filament gliding and therefore motility (Campbell, 1979; Pringault and Garcia-Pichel, 2004), protecting the cell from UV radiation (Rossi et al., 2018), and the nitrogenase from excess oxygen (Otero and Vincenzini, 2003). It plays a role in scavenging essential nutrients (Rossi et al., 2018), and is believed to scavenge free radicals which otherwise may harm the cell (Chen et al., 2009). Among other roles attributed to EPS is its role to protect the cell from lysis (Ehling-Schultz and Schere, 1999) and from shifts in the environmental conditions such as desiccation, salinity, extreme temperatures, pH or exposure to toxic materials (Demig and Young, 2017; Ehling-Schultz and Schere, 1999). The EPS is also believed to protect the cell from freezing damage (Nagar et al., 2021) and from viral/bacterial infection and predation (Brüll et al., 2000). While the above-mentioned roles are widely accepted by the scientific community, this is not the case with the possible hydrological role played by the EPS, as reflected in recent reviews (Mager and Thomas. 2011; Rossi and De Philippis, 2015), and the absence of this category in a list of major roles played by the EPS most recently published (Rossi et al., 2018).

It is customary to divide the EPS to tightly bound EPS (TB-EPS), whether constituting sheaths (around filamentous cells) or capsules (around single cells) and loose bound (released, scattered) EPS (LB-EPS), i.e., slime which has an amorphous

shape, not necessarily related to the shape of the cell (More et al., 2014; Otero and Vincenzini, 2003; Pereira et al., 2009). While the slime is mostly comprised of low molecular weight (MW) polysaccharides, the sheaths are complex, mainly characterized by high-MW molecules, and as such are much less degradable. This may explain the fact that unlike LB-EPS which can be extracted by water, the use of Na_2EDTA is required for the extraction of TB-EPS. It was suggested that TB-EPS is responsible for the crust structure (De Philippis, 2015).

The high capability of EPS to absorb high amounts of water (Chenu, 1993; Or et al., 2007) may have important hydrological consequences. For instance, EPS may hinder evaporation and facilitate longer cell activity (Chenu, 1993). This may be the case for some cyanolichens such as *Collema* sp. which takes advantage of the short rain events in deserts to accumulate substantial amounts of water, which will facilitate long hours of photosynthesis, especially during the cool weather that characterize the cool season rains (Lange et al., 1998). On the other hand, with some EPS having dark sunscreen pigments (Ehling-Schulze and Shere, 1999), the resultant reduction in the albedo may lead to temperature rise which may increase evaporation (Harper and Marble, 1988; Kidron and Tal, 2012; Xu and Singh, 2001), and as such may not necessarily act to prolong cell activity.

An additional suggested hydrological role of EPS is the facilitation of vapor absorbance and subsequent dew formation, suggested to serve as an additional and important water source for biocrusts (Colica et al., 2014; Fischer et al., 2012; Hagemann et al., 2015; Jia et al., 2014; Lange et al., 1992; Mager and Thomas, 2011; Veste et al., 2001). While reported to trigger vapor absorption by Colica et al. (2014) following cyanobacteria inoculation in the Hobq Desert in China, extensive field measurements, which were carried out in the dewy Negev, failed to show vapor condensation on the ground (Kidron and Kronenfeld, 2020a,b). Only once, very limited dew formation was noted (Kidron et al., 2002). Yet, based on a detailed analysis, it was too short to allow for net photosynthesis by the cyanobacterial biocrusts (Kidron and Starinsky, 2019), therefore casting doubt on the possible role played by EPS in providing dew water which will serve as an additional water source for the cyanobacterial biocrusts. No net photosynthesis was also recorded from a mixed cyanobacteria and crustose lichens in the Negev following dew (Wilske et al., 2008). Contrary to detached cobbles or stones which readily condense dew and subsequently serve as an important water source for the stone-dwelling lichens (Lange et al., 1970), minimum temperatures at the soil surface rarely reach the dew point temperature (Td) – a prerequisite for dew formation (Beysens, 2018).

Not less controversial is the possible effect of EPS on infiltration and runoff. In light of the cardinal role played by runoff in shaping many aspects of the environment (hydrological, geomorphological, pedological, ecological), elucidation of the possible role played by EPS in runoff generation is of major importance. Toward this end, the current state-of-the art knowledge will be briefly presented, ungrounded conclusions published in the literature will be discussed, and a wide array of direct and indirect evidence which point to the possible role of EPS in runoff generation will be analyzed.

2 THE POSSIBLE INVOLVEMET OF EPS IN RUNOFF GENERATION

2.1 Enhanced soil aggregation

With EPS assisting in cell adhesion and cohesion, EPS may increase soil aggregation, contributing to a better soil structure which will facilitate aeration and water infiltration (Cantón et al., 2020; Or et al., 2007; Redmile-Gordon et al., 2020). Thus for instance EPS shrinkage during desiccation might promote infiltration through the soil crevices. While these functions were convincingly shown and are not a matter of dispute, some scholars maintain that higher rates of infiltration are induced by subsurface EPS, especially in developed crusts, which will hinder in turn runoff generation (Belnap, 2006; Brotherson and Rushforth, 1983; Chamizo et al., 2013; Rossi et al., 2012). This conclusion is however very problematic. EPS as well as clay tend to absorb water within minutes, resulting in the closure of the crevices (Fox et al., 2004). This is especially the case once higher amounts of EPS, which are associated with biocrusts and therefore concentrate at the surface, will readily swell upon wetting, blocking easy entry of rainwater to depth. Furthermore, the view that soil aggregation hinders runoff does not coincide with the prevailing runoff mechanism which takes place in arid and semiarid regions. Due to limited rain, SOF does not take place in these areas, and runoff generation takes place only following HOF (Horton, 1933; Kidron, 2021), which implies infiltration impediment only following surface saturation regardless of subsurface water content and regardless whether the subsurface is aggregated or not.

This was clearly reflected on sand-covered biocrusts at the Nizzana research site (NRS) in the Hallamish dune field, Negev Desert, Israel. Even when covering semi pure sand (~98% sand with only ~2% of silt and clay), extremely thin immature cyanobacterial crusts, only 0.5 mm thick, were able to generate runoff (Kidron, 2015). Similarly, 1 mm-thick biocrusts which covered the xeric aspects of the dunes commonly generate runoff (Kidron, 1999; Kidron et al., 2003). With typical soils, some of which are well aggregated, having infiltration rates of 10–150 mm/h (Dunkerley, 2000; Kato et al., 2009; Wood and Blackburn, 1981), i.e., substantially lower than sand (having >300 mm/h of infiltration; Lichner et al., 2010; Xiao et al., 2019b), one may safely conclude that runoff over the 0.5 mm-thick biocrusts was not impacted by the underlying sand, but rather by the biocrust. With HOF being the prevailing mechanism that determines runoff generation in arid and semiarid regions, the aggregation capability of the subsurface is of minor relevance.

2.2 Hydrophobicity

Hydrophobicity (water repellency) is a temporal phenomenon (Francis et al., 2007) during which a switch in the molecule position of hydrophyllic and hydrophobic ends takes place (Hallett, 2008). Accordingly, with moisture decrease, the hydrophilic ends tend to strongly bond with each other leaving the hydrophobic ends exposed, resulting in hydrophobicity. While the duration during which the soil turns hydrophobic may be long, the process during which hydrophobicity ceases is however rapid, sometimes within minutes (Oostindie et al., 2013). Some of the biocrust population, such as cyanobacteria, algae, bacteria, and fungi were found to posses temporal hydrophobic properties, assumed to be caused by EPS (Mugnai et al., 2020a).

Hydrophobicity was extensively reported from humid regions (Dekker and Ritsema, 1994, 2000; Doerr et al., 2006; Drahorad et al., 2013; Fischer et al., 2010, 2013; Jungerius and van der Muellen, 1988; Lichner et al., 2013; Rutin, 1983). However, runoff was convincingly shown to result from hydrophobicity mainly in northern and central Europe (Fischer et al., 2010; Lichner et al., 2010, 2012, 2018). The first example that I am aware of and which linked between hydrophobicity and

runoff generation on biocrusts was reported from the Dutch coast during the end of the summer (Jungerius and de Jong, 1989; Rutin, 1983). While hydrophobicity was also reported from semiarid regions (Chamizo et al., 2012; Mayor et al., 2009; Rodriguez-Caballero et al., 2013), the link between hydrophobicity and runoff was not yet substantiated.

At the subhumid Dutch coast hydrophobicity was reported following unusual weather conditions during which a long dry period followed a wet period, i.e., during the end of the summer. Runoff generation took place regardless of rain intensities (Rutin, 1983). It was temporal and vanished once the surface was sufficiently wetted. According to Oostindie et al. (2013), hydrophobicity ceased once the moisture content of sand reaches ~3%. One may therefore conclude that (a) hydrophobicity may only take place once a very dry spell follows a wet period, such as at the end of the summer or during long breaks between rain events, (b) runoff induced by hydrophobicity will cease once the soil gets sufficiently wet, (c) runoff induced by hydrophobicity will take place regardless of rain intensity, as was indeed recorded at the Dutch coast (Rutin, 1983).

Runoff due to hydrophobicity was thought to take place in the Negev (Felde et al., 2014; Keck et al., 2013), the Tabernas (Chamizo et al., 2012; Rodriguez-Caballero et al., 2013), and the Sahel (Malam-Issa et al., 2009; Talbot and Williams, 1978), but nevertheless no convincing data for meter-scale runoff which stems from hydrophpbocity were yet published. On the contrary, in all places a close link between rain intensity and runoff took place, and runoff generation was higher on the wet soils, all pointing to runoff due to pore clogging rather than hydrophobicity. Thus for instance, an attempt to attribute runoff generation to hydrophobicity was also made for NRS (Felde et al., 2014; Keck et al., 2013). However, further measurements in NRS by the same group of scholars did not show hydrophobicity (Mugnai et al., 2018), and the "hydrophobicity hypothesis" was not further advanced (Keck et al., 2016).

I may add that although theoretically runoff due to hydrophobicity may be followed by HOF (triggered by the intermittent character and high intensity fluctuation of the rain; Lázaro et al., 2001; Kidron, 2011), no distinction between both mechanisms was yet reported, and more importantly, no meter-scale runoff yield that stems from hydrophobicity, was yet reported. One may thus assume that even if taking place, the hydrophobic effect on runoff in these sites is marginal.

Additionally, even when specific hydrophobic constituents within the EPS were identified by various scholars in different biocrusts, hydrophobicity was not necessarily detected. Thus for instance, although fucose and rhamnose are considered hydrophobic (Mugnai et al., 2018), no hydrophobicity was detected in *Scytonema* sp. albeit the fact that both of these sugars were present in relatively high amounts in the EPS of this species (Chamizo et al., 2019). Similarly, although containing rhamnose, no hydrophobicity was found in *Schizothrix* sp. (Mugnai et al., 2018).

2.3 Partial surface pore clogging

A close link between partial surface pore clogging (PSPC) and EPS and between PSPC and runoff was long ago reported (Kidron and Yair, 1997; Mazor et al., 1996; Verrecchia et al., 1995). Not only that a close link was found between rain intensity and runoff, but the lack of runoff on dry crusts during the beginning of rain events even when subjected to high-intensity rains was attributed to the necessary delay that stems from the time duration required to allow for water imbibitions by the crust, which will result in turn in PSPC (Kidron and Yair, 1997). Additional supportive evidence was obtained when the ratio of total carbohydrates to the chlorophyll content was sought. Thus, assuming a similar amount of carbohydrates within a single cell, and given the fact that most EPSs are carbohydrates (Mazor et al., 1996), excess of carbohydrates relative to the chlorophyll content (i.e., high ratio of carbohydrates to chlorophyll) may attest to carbohydrates which are located outside the cell walls, i.e., extracellular carbohydrates, which constitute the majority of the EPS (De Brower and Stal, 2001; Kidron et al., 1999). Indeed, when the runoff yield of variable plots having 5 different crust types was compared against the ratio of carbohydrates to chlorophyll, a linear relation was obtained, pointing to a possible link between EPS and runoff generation (Kidron et al., 2003).

This measure for assessing the amount of EPS is obviously crude and may be applicable for a similar population of microorganisms characterizing habitats with similar climate and soil properties. For a more comprehensive comparison of different climates and different soils, a study of the properties of the constituents of the EPS is required. This was done once a comparison between the cyanobacterial biocrusts of NRS (which receive an annual precipitation of 95 mm) and the cyanobacteria-algae biocrust that cover the Israeli Mediterranean coast, the Nizzanim dune field (NIM) (which receives an annual precipitation of 500 mm) was carried out. The comparison was triggered by the different populations of the crusts (cyanobacterial in NRS and cyanobacteria-algae in NIM) and by the fact that while runoff was commonly produced in NRS already during medium rain intensities as low as 9 mm/h (Kidron and Yair, 1997), no runoff was generated by the NIM crust during three years of field measurements albeit the fact that the NIM crusts had substantially higher chlorophyll content and was subjected to substantially higher rain intensities (Kidron and Büdel, 2014).

Figure 1 shows a comparison between two interdunal types of crusts from Nizzana and one interdunal crust from Nizzanim. No runoff was generated from the NIM crust following sprinkling (with 22.5 mm/h for 15 min). The Nizzana crusts (NIZa, NIZb) yielded however runoff (Fig. 1a). While exhibiting substantially higher thickness and chlorophyll content (Fig. 1b, c), the NIM crust showed however lower water-holding capacity (WHC) (Fig. 1d), lower compressive strength (Fig. 1e), lower rigidity (Fig. 1f) and a lower ratio between total carbohydrates and chlorophyll (Fig. 1g). Notwithstanding is the ratio of carbohydrates to chlorophyll, which showed a close link with runoff coefficient and pointed to the apparent important role played by the EPS in runoff generation. This was further verified by the properties of the EPS, such as the higher rigidity that characterized the NRS biocrusts, which may exert high integrity to the crust. Clear differences were also noted in SEM pictographs. Thus for instance, while mainly TB-EPS characterized the NIM biocrusts (Fig. 2a), abundant LB-EPS characterize the NRS biocrusts, (Fig. 2b). One may conclude that while the ratio of carbohydrates to chlorophyll may serve as a basic indication for the total amount of EPS, which may serve in turn as a useful crude estimation for the possible dominance of the EPS, a full exploration of the EPS role in runoff generation also requires the study of the properties of the EPS.

3 SYNTHESIS

Attempts to link between the different constituents that make up the biocrust EPS and the hydrological role of the biocrusts had only limited success. On the one hand, scholars tried to identify constituents with hydrophobic characteristics such as

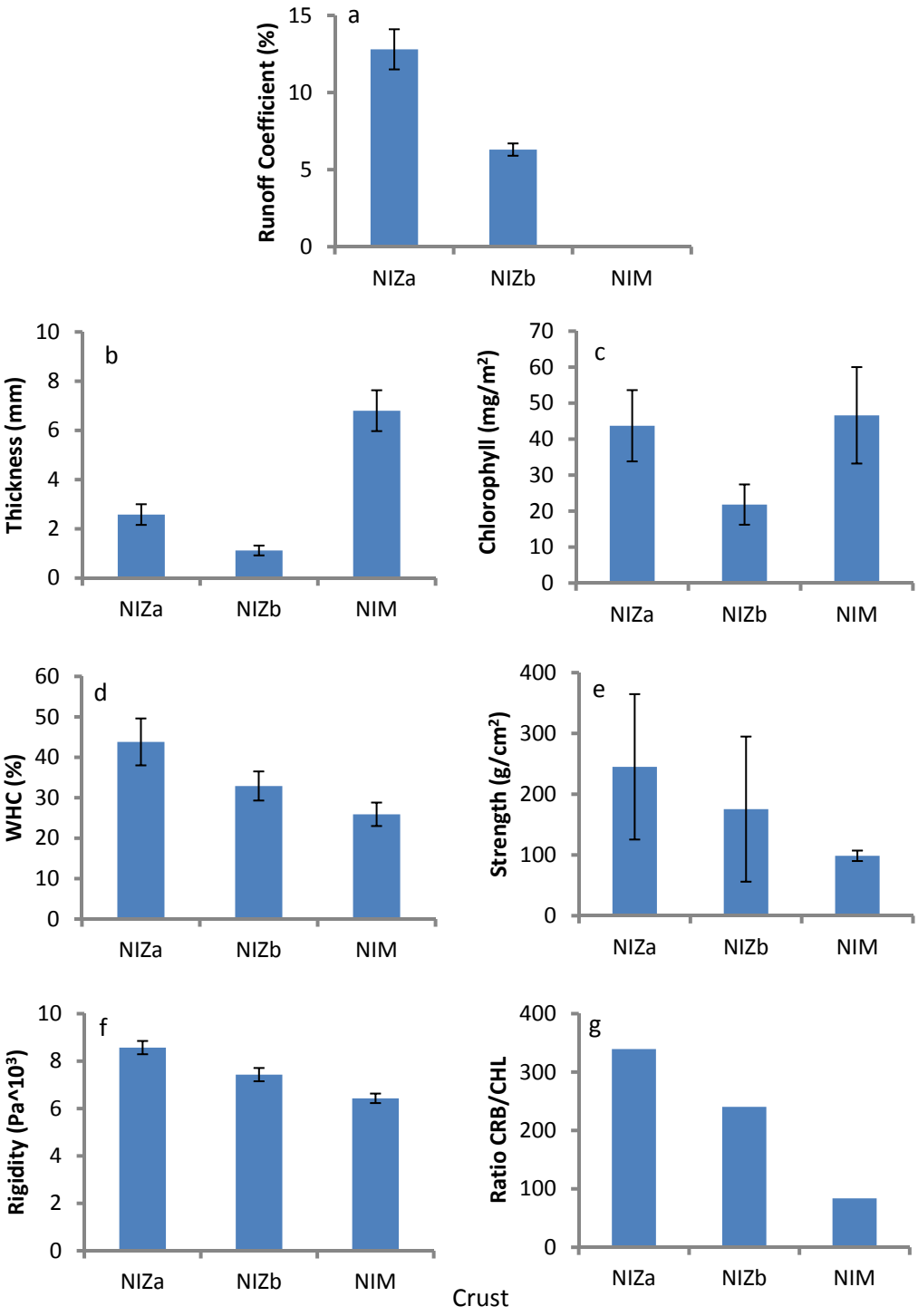

Fig. 1. A comparison between two interdunal crust types taken from Nizzana (NIZ) and were shown to readily generate runoff under field conditions and one from the Nizzanim dune field (NIM) that failed to produce runoff under field conditions. The figure shows runoff coefficient following sprinkling experiments (a), the thickness (b), chlorophyll content (c), water holding capacity (d), compressive strength (e), rigidity (f) and the ratio of total carbohydrates (CRB) to chlorophyll (CHL) (g). Modified from Kidron et al. (2020).

fucose and rhamnose and yet, even when they occupy a fairly high proportion of the total EPS, hydrophobicity was not always detected. Moreover, given the fact that hydrophobicity may vanish within minutes given that sufficient amount of water is supplied to the soil, the hypothesis regarding the transient nature of hydrophobicity during which polar and non-polar ends of the EPS molecules switch their position is supported, making the link between hydrophobicity and certain types of sugars less likely. Furthermore, the rapidity during which hydrophobicity is vanished also brings into question the attempts to link between hydrophobic constituents and biocrust hydrophobicity. Thus for instance, while sulfated groups and uronic acids are hydrophilic (Rossi and De Philippis, 2016), their presence cannot fully explain water absorption by the crust. For example, while young cyanobacterial crusts were found to only posses low amounts of uronic acids (Mugnai et al., 2020b), young cyanobacterial crusts were still observed to readily absorb water during a sprinkling experiment, and

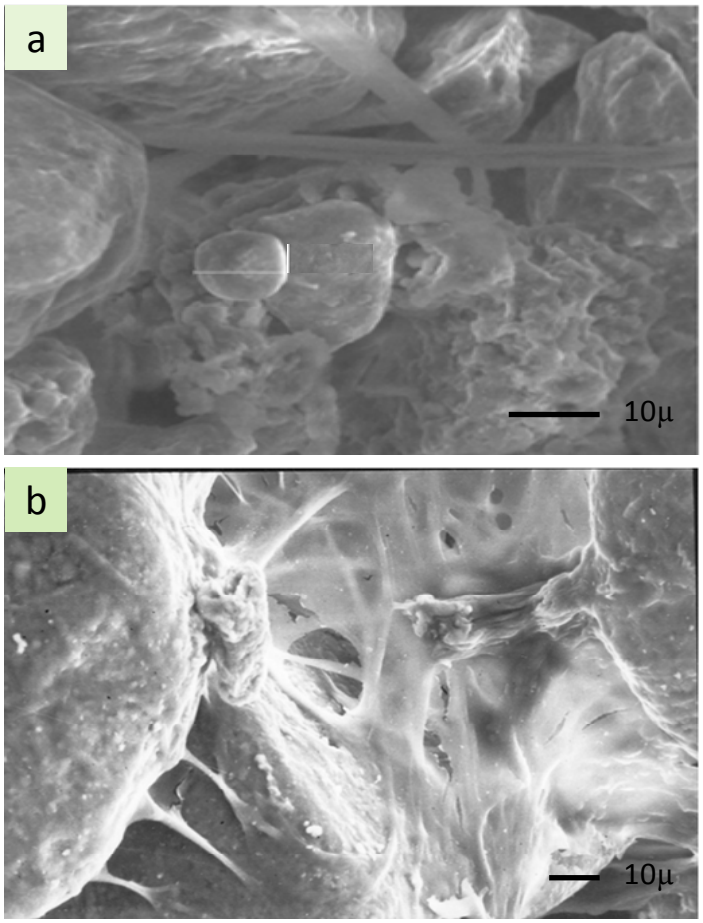

Fig. 2. SEM pictographs showing the Nizzanim (NIM) (a) and the Nizzana (NIZ) (b) crusts. Whereas LB-EPS is hardly noted in NIM it abounds in NIZ.

subsequently to generate runoff (Kidron, 2015). Nevertheless, it is believed that water absorbance may vary in accordance with the EPS properties (Chenu, 1993).

When the water-holding capacity (WHC) of the cyanobacterial crusts from NRS was compared to cyanobacteria-algae crusts from NIM, substantially higher WHC characterize the NRS crusts. Interestingly, the NRS crusts were also characterized by abundant LB-EPS (Fig. 2b). I would like to suggest that LB-EPS may play a cardinal role in water absorption and hence in PSPC. Contrary to TB-EPS which is limited by physiological constraints, and therefore has distinct thickness (Rossi and De Philippis, 2015), LB-EPS commonly occupies large pore volume (Nicolaus et al., 1999), and as such may absorb exceptionally large amounts of water.

In this regard, it is suggested that rather than TB-EPS, which was considered to play major role in crust hydrology (De Philippis, 2015), LB-EPS may play the central role in runoff generation. Occupying a much larger pore volume, LB-EPS may principally determine the WHC of the crust, as clearly shown in the SEM pictographs of the NRS crusts. High WHC implies high degree of swelling (Chenu, 1993; Or et al., 2007) and subsequently efficient pore clogging and infiltration impediment. For instance, according to Chenu (1993), addition of EPS to kaolinite and montmorillonite decreased the pore diameter in high water potentials from 0.5–4 μ to an average of 0.2 μ. According to Verrecchia et al (1995), within <30 min of wetting, 8–12-fold decrease in the volume of the biocrust micropores took place. Both groups of scholars report on one-order decrease in the micropores volume. Subsequently, I would like to suggest that the relative amount of WHC may therefore serve as a possible indicator for the crust potentiality to generate runoff. The higher the amount of WHC, the higher is the amount of water occupying the pores, and the higher the probability that the water-filled pores are efficiently clogged. This may be also facilitated by the high rigidity of the crust that will resist the rain drop impact and possible infiltration through the crust openings. With the impediment of infiltration, rain, which will exceed a certain rate of input, will run off the surface.

With water addition, the biocrust readily reaches saturation leading in turn to infiltration-excess (Hortonian) overland flow (HOF). Unlike the case of hydrophobicity during which water repellency takes place and runoff results from the incapability of the water to infiltrate the soil, runoff following pore clogging depends upon the capability of the water to readily saturate the upper soil surface skin. Runoff will not begin instantly as in the case of hydrophobicity, but only following several minutes or more during which water absorption by the biocrust-induced EPS will suffice to partially clog the pores (Verrecchia et al., 1995).

During the current review, an attempt was made to link between the crust properties and above all, the biocrust-induced EPS and the hydrological mechanisms responsible for runoff generation in arid and semiarid regions. While under similar environmental conditions the amount of EPS may serve as a crude indicator for the crust capability to partially clog the

surface pores (Kidron et al., 2003), for a more complete and reliable outcome, evaluating the EPS properties is of major importance (Chenu, 1993; Fick et al., 2019; Kidron et al., 2020). It follows that among the important functions carried out by the EPS, EPS may play an important role in runoff generation, as in the case of NRS, which may therefore substantially impact the hydrology, geomorphology, pedology and ecology of arid and semiarid ecosystems.

Currently, although occasional hydrophobicity was reported from arid and especially semiarid zones, there are no convincing data that link between EPS-induced hydrophobicity to meter-scale runoff generation in arid and semiarid regions. The occurrence of both mechanisms is theoretically feasible, as reported during lab measurements with biocrusts that were induced to develop hydrophobicity, during which two separated runoff peaks (with a ~5 min interval) were recorded during continuous sprinkling: following hydrophobicity and following pore clogging (Kidron et al., 1999). This was not yet shown under field conditions, and unlike PSPC, hydrophobicity was not yet shown to play an important role in runoff generation in arid and semiarid zones. In this regard it is useful to refer to William of Occam: "Entia non sunt multiplicanda praeter necessitate", i.e., "Entities should not be multiplied more than necessary".

REFERENCES

Belnap, J., 2006. The potential roles of biological soil crusts in dryland hydrologic cycles. Hydrol. Process., 20, 3159–3178.

Beven, K.J., Kirkby, M.J., 1979. A physically based, variable contributing area model of basin hydrology. Hydrol. Sci. Bull., 24, 43–69. DOI: 10.1080/02626667909491834

Beysens, D., 2018. Dew Water. River Publishers, Gistrup, Denmark.

Blackburn, W.H., 1975. Factors influencing infiltration and sediment production of semiarid rangelands in Nevada. Water Resour. Res., 6, 929–937. DOI: 10.1029/WR011i006p00929

Brotherson, J.D., Rushforth, S.R., 1983. Influence of cryptogamic crusts on moisture relationships of soils in Navajo National Monument, Arizona. Great Basin Natur., 43, 73–78.

Brüll, L.P., Huang, Z., Thomas-Oates, J.E., Paulsen, B.S., Cohen, E.H., Michaelsen, T.E., 2000. Studies of polysaccharides from three edible species of *Nostoc* (cyanobacteria) with different colony morphologies: Structural characterization and effect on the complement system of polysaccharides from *Nostoc commune*. J. Phycol., 36, 871–881.

Cammeraat, E.L.H., 2004. Scale dependent thresholds in hydrological and erosion response of a semi-arid catchment in southeast Spain. Agric. Ecosys. Environ., 104, 317–332. DOI: 10.1016/j.agee.2004.01.032

Campbell, S.E., 1979. Soil stabilization by prokaryotic desert crusts: Implications for Precambrian land biota. Orig. Life, 9, 335–348.

Cantón, Y., Chamizo, S., Rodríguez-Caballero, E., Lazáro, R., Roncero-Ramos, B., Roman, J.R., Solé-Benet, A., 2020. Water regulation in cyanobacterial biocrusts from drylands: Negative impacts of anthropogenic disturbance. Water, 12, 720. https://doi.org/10.3390/w12030720

Chamizo, S., Cantón, Y., Lázaro, R., Domingo, F., 2013. The role of biological soil crusts in soil moisture dynamics in two semiarid ecosystems with contrasting soil textures. J. Hydrol., 489, 74–84.

Chamizo, S., Cantón, Y., Rodríguez-Caballero, E., Domingo, F., Escudero, A., 2012. Runoff of contrasting scales in a semiarid ecosystem: A complex balance between biological soil crust features and rainfall characteristics. J. Hydrol., 452–453, 130–138.

Chamizo, S., Belnap, J., Eldridge, D.J., Cantón, Y., Malam-Issa, O., 2016. The role of biocrusts in arid land hydrology. In: Weber, B., Büdel. B., Belnap. J. (Eds.): Biological Soil Crusts: An Organizing Principle in Dryland. Ecological Studies 226. Springer, Switzerland, pp. 321–346.

Chamizo, S., Adessi, A., Mugnai, G., Simiani, A., De Philippis, R., 2019. Soil type and cyanobacteria species influence the macromolecular and chemical characteristics of the polysaccharide matrix in induced biocrusts. Microbial Ecol., 78, 482–493. DOI: 10.1007/s00248-018-1305-y

Chen, L.Z., Wang, G.H., Hong, S., Liu, A., Li, C., Liu, Y.D., 2009. UV-B-induced oxidative damage and protective role of exopolysaccharides in desert cyanobacterium *Microcoleus vaginatus*. J. Integrat. Plant Biol., 51, 2, 194–200. DOI: 10.1111/j.1744-7909.2008.00784.x

Chen, Y., Tarchitzky, J., Brouwer, J. Morin, J., Banin, A., 1980. Scanning electron microscope observations in soil crusts and their formation. Soil Sci., 130, 49–55.

Chenu, C., 1993. Clay-or sand- polysaccharide associations as models for the interface between micro-organisms and soil: water related properties and microstructure. Geoderma, 56, 143–156.

Colica, G., Li, H., Rossi, F., Li, D., Liu, Y., De Philippis, R., 2014. Microbial secreted exopolysaccharides affect the hydrological behavior of induced biological soil crusts in desert sandy soils. Soil Biol. Biochem., 68, 62–70.

De Brouwer, J.F.C., Stal, L.J., 2001. Short-term dynamics in microphytobenthos distribution and associated extracellular carbohydrates in surface sediments of the intertidal mudflat. Marine Ecol. Progress Series, 218, 33–44.

de Jong, S.M., Addink, E.A., Van Beek, L.P.H., Duijsings, D., 2011. Physical characterization, spectral response and remotely sensed mapping of Mediterranean soil surface crusts. Catena, 86, 24–35.

Dekker, L.W., Ritsema, C.J., 1994. How water moves in a water repellent sandy soil. 1. Potential and actual water repellency. Water Resour. Res., 30, 2507–2517.

Dekker, L.W., Ritsema, C.J., 2000. Wetting patterns and moisture variability in water repellent Dutch soils. J. Hydrol., 231–232, 148–164.

De Philippis, R., 2015. The stability and the hydrological behavior of biological soil crusts is significantly affected by the complex nature of their polysaccharide matrix. EGU General Assembly, 12–17 April, 2015, Vienna, Austria. ID: 3513.

Demig, J.W., Young, J.N., 2017. The role of exopolysaccharides in microbial adaptation to cold habitats. In: Margesin, R. (Ed.): Psychrophiles: From Biodiversity to Biotechnology. Springer Inter Pub. AG. DOI: 10.1007/978-3=319-57057-0-0122.

Doerr, S.H., Shakesby, R.A., Dekker, L.W., Ritsema, C.J., 2006. Occurrence, prediction and hydrological effects of water repellency amongst major soil and land-use types in a humid temperate climate. Eur. J. Soil Sci., 57, 741–754.

Drahorad, S., Steckenmesser, D., Felix-Henningsen, P., Lichner, L., Rodny, M., 2013. Ongoing succession of biological soil crusts increases water repellency – a case study on Arenosols in Sekule, Slovakia. Biologia, 68, 1089–1093.

Dunkerley, D., 2000. Hydrological effects of dryland shrubs: defining the spatial extent of modified soil water uptake rates at an Australian desert site. J. Arid Environ., 45, 159–172. DOI: 10.1006/jare.2000.0636

Dunne, T., 1990. Hydrology, mechanics, and geomorphic implications of erosion by subsurface flow. In: Higgins, C.G., Coates, D.R. (Eds.): Groundwater Geomorphology: The Role of Subsurface Water in Earth-Surface Processes and Landforms. Geological Society of America, Special Paper 252, pp. 1–28.

Dunne, T., Black, R.D., 1970. An experimental investigation of runoff production in permeable soils. Water Resour. Res., 6, 478–490. DOI: 10.1029/WR006i002p00478

Ehling-Schulz, M., Schere, S., 1999. UV protection in cyanobacteria. Eur. J. Phycol., 34, 329–338.

Epstein, E., Grant, W.J., 1993. Soil crust formation as affected by raindrop impact. In: Hadas, A., Swartzendruber, D., Ritjema, P.E., Fuchs, M., Yaron, B. (Eds.): Physical Aspects of Soil Water and Salts in Ecosystems. Springer, Berlin and Heidelberg, pp. 195–201.

Felde, V.J.M.N.L., Peth, S., Uteau-Puschmann, D., Drahorad, S., Felix-Henningsen, P., 2014. Soil microstructure as an under-explored feature of biological soil crust hydrological properties: case study from the NW Negev Desert. Biodivers. Conserv., 23, 1687–1708.

Fick, S.E., Barger, N.N., Duniway, M.C., 2019. Hydrological function of rapidly induced biocrusts. Ecohydrology, 12, e2089. DOI: 10.1002/eco.2089

Fischer, T., Veste, M., Wiehe, W., Lange, P., 2010. Water repellency and pore clogging at early successional stages of microbiotic crusts on inland dunes, Brandenburg, NE Germany. Catena, 80, 47–52. DOI: 10.1016/j.catena.2009.08.009

Fischer, T., Veste, M., Bens, O., Hüttl, R.F., 2012. Dew formation on the surface of biological soil crusts in central European sand ecosystems. Biogeosciences, 9, 4621–4628.

Fischer, T., Yair, A., Veste, M., Geppet, H., 2013. Hydraulic properties of biological soil crusts on sand dunes studied by ^{13}C-CP/MAS-NMR: A comparison between an arid and temperate site. Catena, 110, 155–160.

Fox, D.M., Bryan, R.B., Price, A.G., 2004. The role of soil surface crusting in desertification and strategies to reduce crusting. Environ. Monitor. Assess., 99, 149–159.

Francis, M.L., Fey, M.V., Prinsloo, H.P., Ellis, F., Mills, A.J., Medinski, T.V., 2007. Soils of Namaqualand: Compensations for aridity. J. Arid Environ., 70, 588–603.

Galle, S., Arendt, E.K., 2014. Exopolysaccharides from sourdough lactic acid bacteria. Critical Rev. Food Sci. Nutr., 54, 891–901. DOI: 10.1080/10408398.2011.617474

Hagemann, M., Henneberg, M., Felde, V.J.M.N.L., Drahorad, S.L., Berkowicz, S.M., Felix-Henningsen, P. Kaplan, A., 2015. Cyanobacterial diversity in biological soil crusts along a precipitation gradient, Northwest Negev Desert, Israel. Microbiol. Ecol., 70, 219–230.

Hallett, P.D., 2008. A brief overview of the causes, impacts and melioration of soil water repellency – a review. Soil Water Res., 3, S21–S29.

Harper, K.T., Marble, J.R., 1988. A role for nonvascular plants in management of arid and semiarid rangelands. In: Tuller, P.T. (Ed.): Applications of Plant Sciences to Rangeland Management and Inventory. Kluwer, Amsterdam, pp. 135–169.

Heil, J.W., Juo, A.S.R., McInnes, K.J., 1997. Soil properties influencing surface sealing of some sandy soils in the Sahel. Soil Sci., 162, 459–469.

Horton, R.E., 1933. The role of infiltration in the hydrological cycle. EOS Transactions AGU, 14, 446–460. DOI: 10.1029/TR014;001p00446

Jia, R.L., Li, X.R., Liu, L.C., Pan, Y.X., Gao, Y.H., Wei, Y.P., 2014. Effects of sand burial on dew deposition on moss soil crust in a revegetated area of the Tengger Desert, Northern China. J. Hydrol., 519, 2341–2349.

Jungerius, D., van der Meulen, F., 1988. Erosion processes in a dune landscape along the Dutch coast. Catena, 15, 217–228.

Jungerius, P.D., de Jong, J.H., 1989. Variability of water repellence in the dunes along the Dutch coast. Catena, 16, 491–497.

Kato, H., Onda, Y., Tanaka, Y., Asano, M., 2009. Field measurement of infiltration rate using an oscillating nozzle rainfall simulator in the cold, semiarid grassland of Mongolia. Catena, 76, 173–181. DOI: 10.1016/j.catena.2008.11.003

Keck, H., Felde, V.J.M.N.L., Drahorad, S.L., Felix-Henningsen, P., 2013. Effects of biological soil crusts on water repellency in a sand dune ecosystem of the NW Negev, Israel. Second Intgernational Workshop on Biological Soil Crusts, Madrid, 10th–13th June, 2013.

Keck, H., Felde, V.J.M.N.L., Drahorad, S.L., Felix-Hennigsen, P., 2016. Biological soil crusts cause subcritical water repellency in a sand dune ecosystem located along a rainfall gradient in the NW Negev Desert, Israel. J. Hydrol. Hydromech., 64, 133–140.

Kidron, G.J., 1999. Differential water distribution over dune slopes as affected by slope position and microbiotic crust, Negev Desert, Israel. Hydrol. Process., 13, 1665–1682. DOI: 10.1002/(SICI)1099-1085(19990815)

Kidron G.J., 2011. Runoff generation and sediment yield on homogeneous dune slopes: scale effect and implications for analysis. Earth Surf. Process. Landf., 36, 1809–1824. DOI: 10.1002/esp.2203

Kidron, G.J., 2015. The role of crust thickness in runoff generation from microbiotic crusts. Hydrol. Process., 29, 1783–1792. DOI: 10.1002/hyp.10243

Kidron, G.J., 2021. Comparing overland flow processes between semiarid and humid regions: Does saturation overland flow take place in semiarid regions? J. Hydrol., 593, 125624. DOI: 10.1016/j.jhydrol.2020.125624

Kidron, G.J., Büdel, B., 2014. Contrasting hydrological response of coastal and desert biocrusts. Hydrol. Process., 28, 361–371. DOI: 10.1002/hyp.9587

Kidron, G.J., Kronenfeld, R., 2020a. Assessing the likelihood of the soil surface to condense vapor: The Negev experience. Ecohydrology, 13, e2200. DOI: 10.1002/eco.2200

Kidron, G.J., Kronenfeld, R., 2020b. Atmospheric humidity is unlikely to serve as an important water source for crustose soil lichens in the Tabernas Desert. J. Hydrol. Hydromech., 68, 359–367. DOI: 10.2478/johh-2020-0034

Kidron, G.J., Starinsky, A., 2019. Measurements and ecological implications of non-rainfall water in desert ecosystems – A review. Ecohydrology, 12, e2121. DOI: 10.1002/eco.2121

Kidron, G.J., Tal, S.Y., 2012. The effect of biocrusts on evaporation from sand dunes in the Negev Desert. Geoderma, 179-180, 104–112. DOI: 10.1016/j.geoderma.2012.02.021

Kidron, G.J., Yair, A., 1997. Rainfall-runoff relationships over encrusted dune surfaces, Nizzana, Western Negev, Israel. Earth Surf. Process. Landf., 22, 1169–1184. DOI: 10.1002/esp.1532

Kidron, G.J., Yaalon, D.H., Vonshak, A., 1999. Two causes for runoff initiation on microbiotic crusts: hydrophobicity and pore clogging. Soil Sci. 164, 18–27.

Kidron, G.J., Herrnstadt, I., Barzilay, E., 2002. The role of dew as a moisture source for sand microbiotic crusts in the Negev Desert, Israel. J. Arid Environ., 52, 517–533. DOI: 10.1016/jare.2002.1014

Kidron, G.J., Wang, Y., Herzberg, M., 2020. Exopolysaccharides may increase biocrust rigidity and

induce runoff generation. J. Hydrol., 588, 125081. DOI: 10.1016/J.JHYDROL.2020.125081

Kidron, G.J., Yair, A., Vonshak, A., Abeliovich A., 2003. Microbiotic crust control of runoff generation on sand dunes in the Negev Desert. Water Resour. Res., 39, 1108. DOI: 10.1029/2002WR001561.2003

Lange, O.L., Schulze, E.D., Koch, W., 1970. Ecophysiological investigations on lichens of the Negev Desert, III: CO_2 gas exchange and water metabolism of crustose and foliose lichens in their natural habitat during the summer dry period. Flora, 159, 525–538.

Lange, O.L., Belnap, J., Reichenberger, H., 1998. Photosynthesis of the cyanobacterial soil-crust lichen *Collema tenax* from arid lands in southern Utah, USA: role of water content on light and temperature response of CO_2 exchange. Func. Ecol., 12, 195–202.

Lange, O.L., Kidron, G.J., Büdel, B., Meyer, A., Kilian, E., Abeliovitch, A., 1992. Taxonomic composition and photosynthetic characteristics of the biological soil crusts covering sand dunes in the Western Negev Desert. Func. Ecol., 6, 519–527.

Lázaro, R., Rodrigo, F.S., Gutiérrez, L., Domingo, F., Puigdegabregas, J., 2001. Analysis of 30-year rainfall record (1967-1997) in semi-arid SE Spain for implications on vegetation. J. Arid Environ., 48, 373–395.

Li, S., Xiao, B., Sun F., Kidron, G.J., 2021. Moss-dominated biocrusts greatly enhance water vapor sorption capacity and increase non-rainfall water deposition in drylands. Geoderma, 388, 114930. DOI: 10.1016/j.geoderma.2021.114930

Lichner, L., Hallett, P.D., Orfánus, T., Czachor, H., Rajkai, K., Šir, M., Tesař, M., 2010. Vegetation impact on the hydrology of an aeolian sandy soil in a continental climate. Ecohydrology, 3, 413–420.

Lichner, L., Holko, L., Zhukova, N., Shacht, K., Rajkai, K., Fodor, N., Sándor, R., 2012. Plants and biological soil crust influence the hydrophysical parameters and water flow in an aeolian sandy soil. J. Hydrol. Hydromech., 60, 309–318.

Lichner, L., Hallett, P.D., Drongova, Z., Czachor, H., Kovacik, L., Mataix-Solera, J., Homolák, M., 2013. Algae influence the hydrophysical parameters of a sand soil. Catena, 108, 58–68.

Lichner, L., Felde, V.J.M.N.L., Büdel, B., Leue, M., Gerke, H.H., Ellerbrock, R.H., Kollár, J., Rodny, M., Šurda, P., Fodor, N., Sándor, R., 2018. Effect of vegetation and its succession on water repellency in sandy soils. Ecohydrology, 11, e1991. DOI: 10.1002/eco.1991

Mager, D.M., Thomas, A.D., 2011. Extracellular polysaccharides from cyanobacterial soil crusts: A review of their role in dryland soil processes. J. Arid Environ., 75, 91–97.

Malam-Issa, O., Défarge, C., Trichet, J., Valentin, C., Rajot, J.L., 2009. Microbiotic soil crusts in the Sahel of western Niger and their influence on soil porosity and water dynamics. Catena, 77, 48–55.

Mayor, A.G., Bautista, S., Bellot, J., 2009. Factors and interactions controlling infiltration, runoff, and soil loss at the microscale in a patchy Mediterranean semiarid landscape. Earth Surf. Process. Landf., 34, 1702–1711. DOI: 10.1002/esp.1875

Mazor, G., Kidron, G.J., Vonshak, A., Abeliovich, A., 1996. The role of cyanobacterial exopolysaccharides in structuring desert microbial crusts. FEMS Microbiol. Ecol., 21, 121–130. DOI: 10.1111/j.1574-6941.1996.tb00339.x

McIntyre, D.S., 1958. Soil splash and the formation of surface crusts by raindrop impact. Soil Sci., 85, 261–266.

More, T.T., Yadav, J.S.S., Yan, S., Tyagi, R.D., Surampalli, R.Y., 2014. Extracellular polymeric substances of bacteria and their potential environmental applications. J. Environ. Manage., 144, 1–25. DOI: 10.1016/j.jenvman.2014.05.010.

Mugnai, G., Rossi, F., Chamizo, S., Adessi, A., De Philippis, R., 2020a. The role of grain size and inoculums amount of biocrust formation by *Leptolyngbya ohadii*. Catena, 184, 104248. DOI: 10.1016/j.catena.2019.104248

Mugnai, G., Rossi, F., Mascalchi, C., Ventura, S., De Philippis, R., 2020b. High arctic biocrusts: characterization of the exopolysaccharidic matrix. Polar Biol., 43, 1805–1815. DOI: 10.1007/s00300-020-02746-8

Mugnai, G., Rossi, F., Felde, V.J.M.N.L., Colesie, C., Büdel, B., Peth, S., Kaplan, A., De Philippis, R., 2018. Development of the polysaccharide matrix in biocrusts induced by a cyanobacterium inoculated in sand microcosms. Biol. Fert. Soils, 54, 27–40.

Nagar, S., Antony, R., Thamban, M., 2021. Extracellular polymeric substances in Antarctic environments: A review of their ecological roles and impact on glacier biogeochemical cycles. Polar Sci. DOI: 10.1016/j.polar.2021.100686

Nicolaus, B., Panico, A., Lama, L., Romano, I., Manca, M.C., De Giulio, A., Gambacorta, A., 1999. Chemical composition and production of exopolysaccharides from representative members of heterocystous and non-heterocystous cyanobacteria. Phytochemistry, 52, 639–647.

Onofiok, O., Singer, M.J., 1984. Scanning electron microscope studies of surface crusts formed by simulated rainfall. Soil Sci. Soc. Am. J., 48, 1137–1143.

Oostindie, K., Dekker, L.W., Wesseling, J.G., Ritsema, C.J., Geissen, V., 2013. Development of actual water repellency in a grass-covered dune sand during dehydration experiment. Geoderma, 204–205, 23–30.

Or, D., Smets, B.F., Wraith, J.M., Dechesne, A., Friedman, S.P., 2007. Physical constraints affecting bacterial habitats and activity in unsaturated porous media – a review. Adv. Water Resour., 30, 1505–1527.

Otero, A., Vincenzini, M., 2003. Extracellular polysaccharide synthesis by *Nostoc* strains as affected by N source and light intensity. J. Biotechnol., 102, 143–152.

Pagliai, M., Bisdom, E.B.A., Ledin, S., 1983. Changes in surface structure (crusting) after application of sewage sludge and pig slurry to cultivated agricultural soils in northern Italy. Geoderma, 30, 35–53.

Pereira, S., Zille, A., Micheletti, E., Moradas-Ferreira, P., De Philippis, R., Tamagnini, P., 2009. Complexity of cyanobacterial exopolysaccharides: composition, structures, inducing factors and putative genes involved in their biosynthesis and assembly. FEMS Microbiol. Rev., 33, 917–941.

Pringault, O., Garcia-Pichel, F., 2004. Hydrotaxis of cyanobacteria in desert crusts. Microb. Ecol., 47, 366–373.

Redmile-Gordon, M., Gregory, A.S., White, R.P., Watts, C.W., 2020. Soil organic carbon, extracellular polymeric substances (EPS), and soil structural stability as affected by previous and current land-use. Geoderma, 363. 114143. DOI: 10.1016/j.geoderma.2019.114143

Rodriguez-Caballero, E., Cantón, Y., Chamizo, S., Lázaro, R., Escudero, A., 2013. Soil loss and runoff in semiarid ecosystems: A complex interaction between biological soil crusts, micro-topography, and hydrological drivers. Ecosystems, 16, 529–546.

Rodriguez-Caballero, E., Belnap, J., Büdel, B., Crutzen, P.J., Andreae, M.O., Pöschl, U., Weber, B., 2018. Dryland photoautotrophic soil surface communities endangered by global change. Nat. Geosci., 11, 185–189. DOI: 10.1038/s41561-018-0072-1

Rossi, F., De Philippis, R., 2015. Role of cyanobacterial exopolysccharides in phototrophic biofilms and in complex microbial mats. Life, 5, 1218–1238. DOI: 10.3390/life5021218

Rossi, F., De Philippis, R., 2016. Excocellular polysaccharides in microalgae and cyanobacteria: Chemical features, role and enzymes and genes involved in their biosynthesis. In: Borowitzka, M.A., Beardall, J., Raven, J.A. (Eds.): The Physiology of Microalgae. Developments in Applied Phycology, Springer, Switzerland. pp. 565–590. DOI: 10.1007/978-3-319-24945-2_21

Rossi, F., Mugnai, G., De Philippis, R., 2018. Complex role of the polymeric matrix in biological soil crusts. Plant Soil, 429, 19–34. DOI: 10.1007/s11104-017-3441-4

Rossi, F., Potrafka, R.M., Garcia-Pichel, F., De Philippis, R., 2012. The role of exopolysaccharides in enhancing hydraulic conductivity of biological soil crusts. Soil Biol. Biochem., 46, 33–40.

Rutin, J., 1983. Erosional processes on a coastal sand dune, De Blink, Noordwijkerhout. Publication 35 of the Physical Geography and Soils Laboratory, University of Amsterdam, Amsterdam.

Sun, F., Xiao, B., Li S., Kidron, G.J., 2021. Towards moss biocrust effects on surface soil water holding capacity: Soil water retention curve analysis and modeling. Geoderma, 399, 115120. DOI: 10.1016/j.geoderma.2021.115120

Talbot, M.R., Williams, M.A.J., 1978. Erosion of fixed dunes in the Sahel, central Niger. Earth Surf. Process. Landf., 3, 107–113.

Tarchitzky, J., Banin, A., Morin, J., Chen, Y., 1984. Nature, formation and effects of soil crusts formed by water drop impact. Geoderma, 33, 135–155.

Verrecchia, E., Yair, A., Kidron, G.J., Verrecchia, K., 1995. Physical properties of the psammophile cryptogamic crust and their consequences to the water regime of sandy soils, Northwestern Negev Desert, Israel. J. Arid Environ., 29, 427–437. DOI: 10.1016/S0140-1963(95)80015-8

Veste, M., Littmann, T., Friedrich, H., Breckle, S.-W., 2001. Microclimatic boundary conditions for activity of soil lichen crusts in sand dunes of the north-western Negev desert, Israel. Flora, 196, 465–474.

Wilske, B., Burgheimer, J., Karnieli, A., Zaady, E., Andreae, M.O., Yakir, D., Kesselmeir, J., 2008. The CO_2 exchange of biological soil crusts in a semiarid grass-shrubland at the northern transition zone of the Negev Desert, Israel. Biogeosci. Discuss., 5, 1969–2001.

Wood, M.K., Blackburn, W.H., 1981. Grazing systems: Their influence on infiltration rates in the rolling plains of Texas. J. Range Manage., 34, 331–335.

Xiao, B., Sun, F., Hu, K., Kidron, G.J., 2019a. Biocrusts reduce surface soil infiltrability and impede soil water infiltration under tension and ponding conditions in dryland ecosystem. J. Hydrol., 568, 792–802. DOI: 10.1016/j.jhydrol.2018.11.51

Xiao, B, Sun, F., Yao, X., Hu, K., Kidron, G.J., 2019b. Seasonal variations in infiltrability of moss-dominated biocrusts on aeolian sand and loess soil in the Chinese Loess Plateau. Hydrol. Process., 33, 2449–2463. DOI: 10.1002/hyp.13484

Xu, C.-Y., Singh, V.P., 2001. Evaluation and generalization of temperature-based methods for calculating evaporation. Hydrol. Process., 15, 205–319. DOI: 10.1002/hyp.119

Received 24 June 2021
Accepted 27 August 2021

J. Hydrol. Hydromech., 69, 2021, 4, 387–399
DOI: 10.2478/johh-2021-0029
ISSN 1338-4333

sciendo Journal of Hydrology and Hydromechanics

Defining minimum runoff length allows for discriminating biocrusts and rainfall events

Roberto Lázaro[1*], Adolfo Calvo-Cases[2], Eva Arnau-Rosalén[3], Consuelo Rubio[1], David Fuentes[4,5], Clément López-Canfín[1,6]

[1] Estación Experimental de Zonas Áridas (CSIC), Carretera Sacramento s/n, 04120 La Cañada, Almería, Spain.
[2] Inter-University Institute for Local Development (IIDL), Department of Geography, University of Valencia, Edifici d'Instituts, 4ª Planta C/ Serpis 29, 46022, València, Spain.
[3] Department of Natural Sciences, Manchester Metropolitan University, John Dalton Building E410a, Chester Street, Manchester M1 5GD, UK.
[4] Department of Ecology, University of Alicante, C/ de San Vicente del Raspeig, s/n, 03690 San Vicente del Raspeig, Alicante, Spain.
[5] Ecodrone Works, C/ Señores Maripino Rosello, 4, 03550, Sant Joan d'Alacant, Spain.
[6] Departamento de Física Aplicada, Universidad de Granada, Avenida Fuente Nueva s/n, 18071 Granada, Spain.
[*] Corresponding author. E-mail: lazaro@eeza.csic.es

Abstract: The runoff coefficient (RC) is widely used despite requiring to know the effective contributing area, which cannot be known *a priori*. In a previous work, we defined runoff length (RL), which is difficult to measure. This work aimed to define the minimum RL (mRL), a quantitative and easy proxy of RL, for use in a pilot study on biocrusts in the Tabernas Desert, Spain. We show that RC decreases according to a hyperbola when the contributing area increases, the independent variable being the length of the effective contributing area and its coefficient involving the effects of rainfall and surface features and antecedent conditions. We defined the mRL as the length of the effective contributing area making RC = 1, which is calculated regardless of the area. We studied mRL from three biocrust types and 1411 events clustered in seven categories. The mRL increased with rain volume and intensity, catchment area and slope, whereas plant cover and biocrust succession (with one exception) had a negative effect. Depending on the plot, mRL reached up 3.3–4.0 m on cyanobacterial biocrust, 2.2–7.5 m on the most widespread lichens, and 1.0–1.5 m on late-successional lichens. We discuss the relationships of mRL with other runoff-related parameters.

Keywords: Semiarid; Biological soil crust; Runoff connectivity; Length slope factor; Infiltration; Tabernas Desert.

INTRODUCTION

Abundant evidence shows that runoff is highly dependent on rainfall features (volume and intensity), surface hydrological properties (vegetation, biocrust, litter, stones, and other soil surface components), soil characteristics (texture, porosity, and organic matter), previous soil conditions (antecedent soil moisture), and topography (slope angle and contributing area). To study and compare the effects of these multiple factors controlling runoff, the runoff coefficient (RC) is a widely used parameter.

Nevertheless, using the RC, requires knowing the contributing area. Closed runoff plots (surrounded by a wall delimiting the monitored drainage area) have been widely used under the assumption that the complete delimited area is the effective drainage area. Because this assumption is unfounded (Kidron and Yair, 1997; Kidron, 2011), delimiting an area does not make sense and, open runoff plots are preferable because they do not alter the natural fluxes and prevent the relative exhaustion of sediments (Boix-Fayos et al., 2006). However, using open runoff plots, we continue without knowing the effective contributing area, even if we topographically delimit an area *in situ*, which would be the maximum possible contributing area. Thus, we should assume that we never know *a priori* the real drainage area corresponding to a runoff measurement nor, consequently, the real RC. Therefore, we need an alternative parameter enabling characterisation of the hydrological behaviour.

Non-concentrated runoff seems to form a continuous water sheet on the soil surface during rainfall, whereas infiltration occurs simultaneously in a spatially irregular manner dependent on the distribution of soil features. However, although the water sheet completely occupies a surface, runoff does not travel an undefined length because there is evidence that RC considerably decreases while the considered area increases (Kidron, 2011; Mayor et al., 2011; Xu et al., 2009). The farther a water input occurs from a runoff collector, the lower the amount of that input is collected. According to Lázaro et al. (2015), runoff length (RL) is the length of the hillslope travelled by runoff; that is, for any point, RL is the maximum distance, in a straight line following the maximum slope line, from which the runoff comes. (RL is different from the length of the path travelled by water, which depends on the surface microtopography). RL is important because it (i) contains some information on the hydrological connectivity, because at least the drainage area delimited by RL is necessarily fully connected; (ii) enables efficient comparisons of the hydrological properties of different surface types, rainfall types, and minimum inter-event times (MITs), etc., at least because it allows for determining the drainage area by its length; (iii) provides information on the sediment transport capacity; and (iv) seems to have potential to enable predictions about runoff flow at a point as a function of rainfall.

However, because RL cannot be directly observed, the RL concept is elusive. Little is known about the RL values in given circumstances, although Agassi and Ben-Hur (1991) studied the

effect of slope length on infiltration and runoff. Puigdefábregas et al. (1999) and Arnau-Rosalén et al. (2008) suggested that the slope length travelled by runoff is often only a part of the catchment length. This idea also underlies the work of Puigdefábregas (2005), who stated that temporal variability of rainfall controls runoff re-infiltration and its decay with slope length. Lázaro et al. (2015) experimentally determined RL on biocrusts, although at only 1 m of spatial resolution. However, such experiments were logistically complex and time consuming. Here, we propose a high-resolution, quantitative subrogate of RL that is simple and easy to measure, using data from the same study area.

Biocrusts are complex communities constituted by microorganisms, lichens, bryophytes, fungi, and algae inhabiting the soil surface and within the upper soil centimetres. They are widespread on a planetary scale (Büdel, 2003) at the sites where vascular plants are limited by climatic factors, and they play an important ecological role because they affect almost every ecological process (Belnap and Lange, 2003; Maestre et al., 2011; Webber et al., 2016). Chamizo et al. (2016) published a review on the biocrusts' hydrological role. Biocrusts constitute a good system model (Bowker et al., 2010; Maestre et al., 2016) as well as adequate surface cover to study runoff due to the existence of previous experimental studies in the same area (e.g., Chamizo et al., 2012a; Lázaro and Mora, 2014; Solé-Benet et al., 1997). On the other hand, biocrusts develop in plant interspaces where vegetation cannot form a continuous layer (mostly in drylands), and they are considered runoff sources, providing water to the plant patches (Rodríguez-Caballero et al., 2014; 2018). Thus, knowing their RL would provide insights to advance the current source–sink theory.

The initial hypotheses were as follows:

a) RL is often much shorter than the topographical drainage area, which represents the historical maximum of RL. Kidron and Yair (1997), Puigdefábregas et al. (1999), and Puigdefábregas (2005) and Arnau-Rosalén et al. (2008) already made suggestions in this line.

b) RL widely varies across numerous factors, such as the rainfall features (intensity, volume and timing), the surface characteristics (including vegetation, soil, topography, biocrusts, and stoniness), and the antecedent soil moisture. Because runoff strongly depends on these factors (Castillo et al., 2003; Le Bissonnais et al., 1995), we assume that RL will also depend on them.

c) In the study area, RL will be centimetres long rather than metres long for most natural rainfall (Lázaro et al., 2015), which very often has low intensity or small volume (Lázaro et al., 2001).

d) Biocrust will generally have high RC, but it will vary according to its species composition (Lázaro et al., 2015).

The objectives of this work were (i) to define the minimum RL (mRL) and propose it as a concrete, quantitative, and easy proxy of RL, and (ii) to use mRL for a pilot study to show the effect of biocrust type and rainfall class on RL from open runoff plots.

METHODS

The study area and the runoff plots

The Tabernas Desert is a place in southeast Spain, in the Sorbas–Tabernas basin, surrounded by the Gador, Nevada, Filabres, and Alhamilla Betic ranges. The first three of these ranges intercept most rainfall fronts, which come mainly from the west, explaining the annual precipitation of around 230 mm (Lázaro et al., 2001). Because the annual potential evapotranspiration is around 1600 mm, water deficit occurs every month, in particular during summer (June–September). Insolation is over 3000 hours per year, and the average annual temperature is 18 °C (Lázaro et al., 2004). The study area was the El Cautivo field site, within the Tabernas Desert. Although calcareous sandstones are locally abundant, Miocene soft marine marls dominate the lithology and produce an extensive badlands landscape and a complex geomorphology developed during the Quaternary (Alexander et al., 1994; Alexander et al., 2008). The parent material is mainly composed of silt-size (>60%), gypsum-calcareous and siliceous particles; fine sand ranges from 20% to 35%, and clay ranges from 5% to 10%. (Cantón et al., 2003). El Cautivo includes a series of parallel catchments, with residual hanging pediments between some of them. A clear surface-type pattern exists. A third of the territory is bare and eroded; biocrust is the main cover in another third; and also occupies the plant interspaces in the rest (Cantón et al., 2004; Lázaro et al., 2000; Lázaro et al., 2008).

The biocrust types described by Lázaro et al. (2008) in this study area were simplified to three for this research: (i) dominated by Cyanobacteria (Cyano); (ii) dominated by the lichens *Squamarina lentigera* and/or *Diploschistes diacapsis* (Squam); and (iii) characterized by the lichen *Lepraria isidiata* (Lepra). The site of Cyano where the runoff plots were constructed has a mature, relatively rough cyanobacterial biocrust, including small pioneer lichens, such as *Endocarpon pusillum*, *Fulgensia desertorum,* and *Fulgensia poelti*. This biocrust is the colonizing one (beginning with a purely cyanobacterial biocrust) and is widespread in any orientation, constituting a matrix-like layer on which the other biocrust types successively develop when possible. In the sunniest non-eroded sites, Cyano is dominant and almost permanent. Squam is the most widespread lichen-dominated biocrust. It usually develops after Cyano, preferring the unaltered north-to-east hillslopes with low plant cover, and including numerous lichen species, such as *Buellia zoharyi*, *Fulgensia fulgida*, *Diploschistes ocellatus,* and *Psora decipiens*. Lepra biocrust is late successional and exclusive to the shadiest north-faced hillslopes, where it occupies the plant interspaces. Lichen species such as *Squamarina carthilaginea*, *Xantoparmelia pokornyi,* and *Teloschistes lacunosus* are characteristic of Lepra, as well as some mosses such as *Grimmia pulvinata, Didymodon luridus,* and *Tortula revolvens*.

Runoff monitoring

Two open runoff plots and a rain gauge were installed in each biocrust. The plots at Cyano were labelled C1 and C2, those of Squam S1 and S2, and those at Lepra L1 and L2. Their appearance is shown in Fig. 1. The available data cover approximately 10 years (2005–2015). Each plot consists of a PVC channel, normal to the line of maximum slope, collecting runoff and driving the water to a tank at the bottom of the hillslope. The channels, covered with a lid to avoid direct rain, are embedded into the soil, and the contact of its upslope edge with the soil was *in situ* plasticised by means of fiberglass and epoxy resin, warranting the transit of the runoff to the trough. Inside the tank is a non-purpose tipping-bucket mechanism (0.5 L in resolution) connected to an on–off Hobo Event data logger, like that of the rain-gauge (0.25 mm in resolution).

Definition and calculation of mRL

Because the effective contributing area is not known *a priori*, examining the way RC varies in relation to it becomes essential. To conduct this theoretical examination, we used

three minimum inter-event times (MITs): 24, 12, and 1 hour, constructing three datasets with 436, 593, and 1411 rainfall – runoff events, respectively. For every event and each plot, we calculated four RC values by successively assuming different lengths (1, 2, 3, and 4 m) for the effective contributing area. These hillslope lengths, multiplied by the width of the plot (length of the collector, 2.18 m except for L2, at 2.16 m) gave rise to four nested, rectangular, and progressively larger supposed drainage areas per event, generating four RC figures. This procedure implies assuming that they were ideal smooth and homogeneous hillslopes. Our real plots only approximate these conditions, but this preliminary assumption is useful to explain the concept and calculation of mRL. Next, we applied this approach to real data, examining the way RC varies when successively larger portions of the real catchment are considered effective contributing areas.

As the width of the plot is assumed to remain constant for any channel length, the assumption of a series of hillslope lengths (for the supposed effective drainage area) increasing according to the series of natural numbers produces a series of nested areas, increasing in arithmetic progression. Because runoff must be divided by the area, while the plot length increases linearly, the corresponding RC potentially decreases because the value of a series of fractions with arithmetically increasing denominators decreases according to a potential curve of exponent –1, forming a hyperbola. Thus, for any pair of runoff and precipitation values (i.e., for any rainfall or surface type and any slope angle), the RCs generated by assuming successively longer contributing areas always decrease according to the following curve:

$$RC = a \times x^{-1} \quad (1)$$

where x is the length of the part of the hillslope that is assumed to be the effective contributing area and a is a coefficient that varies widely, because it involves the effects on runoff of the rainfall and surface characteristics, and can be experimentally calculated.

Thus, although we cannot calculate RC, we can determine its distribution. Furthermore, for a rectangular plot, RC is as follows:

$$RC = R_{(L)} / (P_{(mm)} \times cw_{(m)} \times x_{(m)}) \quad (2)$$

where $R_{(L)}$ is the runoff measured in litres, $P_{(mm)}$ is the measured precipitation in millimetres, $cw_{(m)}$ is the width of the collector in metres, and $x_{(m)}$ is the hillslope length of the supposed effectively contributing area in metres. Therefore, it is

$$a = R_{(L)} / P_{(mm)} \times cw_{(m)} \quad (3)$$

These curves relating RC with the length of the contributing area for any event of any surface type are determined by only one parameter (a). Any value for length leads to a value for RC that exactly matches a point in the hyperbola. Because the hyperbola has an indefinite length, a length of contributing area corresponding to RC = 1 always exists, independently from the surface and rain characteristics. As some infiltration always occurs, the actual RL will be larger than the hillslope length corresponding to RC = 1 is. Therefore, the hillslope length of the supposed effectively contributing area corresponding to RC = 1 can be considered the minimum RL (mRL) for the given set of circumstances (rainfall event, surface and antecedent conditions) and enables an easy definition for mRL. This means that the minimum hillslope length travelled by runoff for a certain site and event is larger than the mRL. RC hyperbola values that are larger than 1 simply mean that runoff comes from upslope of the length attributed to the drainage area. The larger than 1 the RC value is, the larger the mRL is in relation to the supposed length. As can be verified from Equation (1), when RC = 1, $x = a$. Therefore, we can define the following:

$$mRL_{(m)} = a = R_{(L)} / P_{(mm)} \times cw_{(m)} \quad (4)$$

Note that in Equation (4), only three known parameters intervene, and the contributing area does not.

To show these hyperbolic relationships, we used Equation (1) to plot the hyperbolas of the average (thus blurring the effect of the antecedent soil moisture) RC *vs* lengths successively assumed for the contributing area, for one plot of each biocrust type and two different rainfall classes. Later, to explore the effect of rainfall type on runoff, we classified the rainfall events into seven categories: >0–1, >1–3, >3–5, >5–10, >10–20, >20–30, and >30 mm. Because most of the rainfall events were small, we divided the group of events ≤5 mm into three classes to avoid an extremely large lower class and to gain resolution to establish the rainfall threshold generating runoff.

Analysis of mRL at El Cautivo field site throughout biocrust types and rainfall events

On natural hillslopes whose topography generates somewhat irregular drainage areas, in such a way that a regular increment in the length of the supposed effective catchment does not imply a regular increment in its area, the theoretical relationship in Equation (1) is only fulfilled in an approximate way and a potential curve must be fitted.

To examine the variation of RC with the length of the supposed contributing area using real data from El Cautivo runoff plots, we first determined the perimeter of the catchment of each plot. Then we calculated the successively larger real areas delimited by successive 10-cm buffers in parallel to the trough.

To establish the catchment areas and soil surface components, a series of manual photogrammetric flights were carried out by means of a DJI Phantom 4 Pro drone carrying a high-resolution, 1-inch sensor (20 Mp). Images were taken at 3.5–5 m above ground level, combining nadir and oblique images with an estimated overlap of 80 and 70% (forward and side, respectively) to obtain an average of 596 images per experimental plot. Images were processed in Agisoft Metashape Pro (Agisoft LLC, Russia). Resolution ranged from 0.95 to 1.13 mm pixel^{-1} and 1.9 and 2.7 mm pixel^{-1} for orthomosaics and the digital elevation model, respectively.

After removing most of the plants, using the Agisoft Metashape image classification software and then manually, the digital terrain model was processed to identify the catchment areas draining to the collectors (Hydrology Tools, ArcMap 10.8). Then, each catchment area was divided into parallel 10-cm bands, parallel to the runoff collector (Multi-ring Buffer, QGIS 3.14). From the digital terrain model, the average slope of each catchment was also obtained (Zonal Statistics, ArcGis 10.8).

Thus, every regular increase in slope length corresponds to a different, but real, increase of contributing area. Then we calculated the RCs for every area (10 cm longer than the previous), plotted those RCs *vs* the hillslope length, and fitted a potential curve. In a first step, we did this not for any concrete event but for the average and for the maximum RCs of every rain type and every biocrust type to verify the quality of the fittings and obtain a graphical reference of the mRL values.

We determined the cover of vascular plants, biocrusts, and bare soil in each plot by adding the segments occupied by every

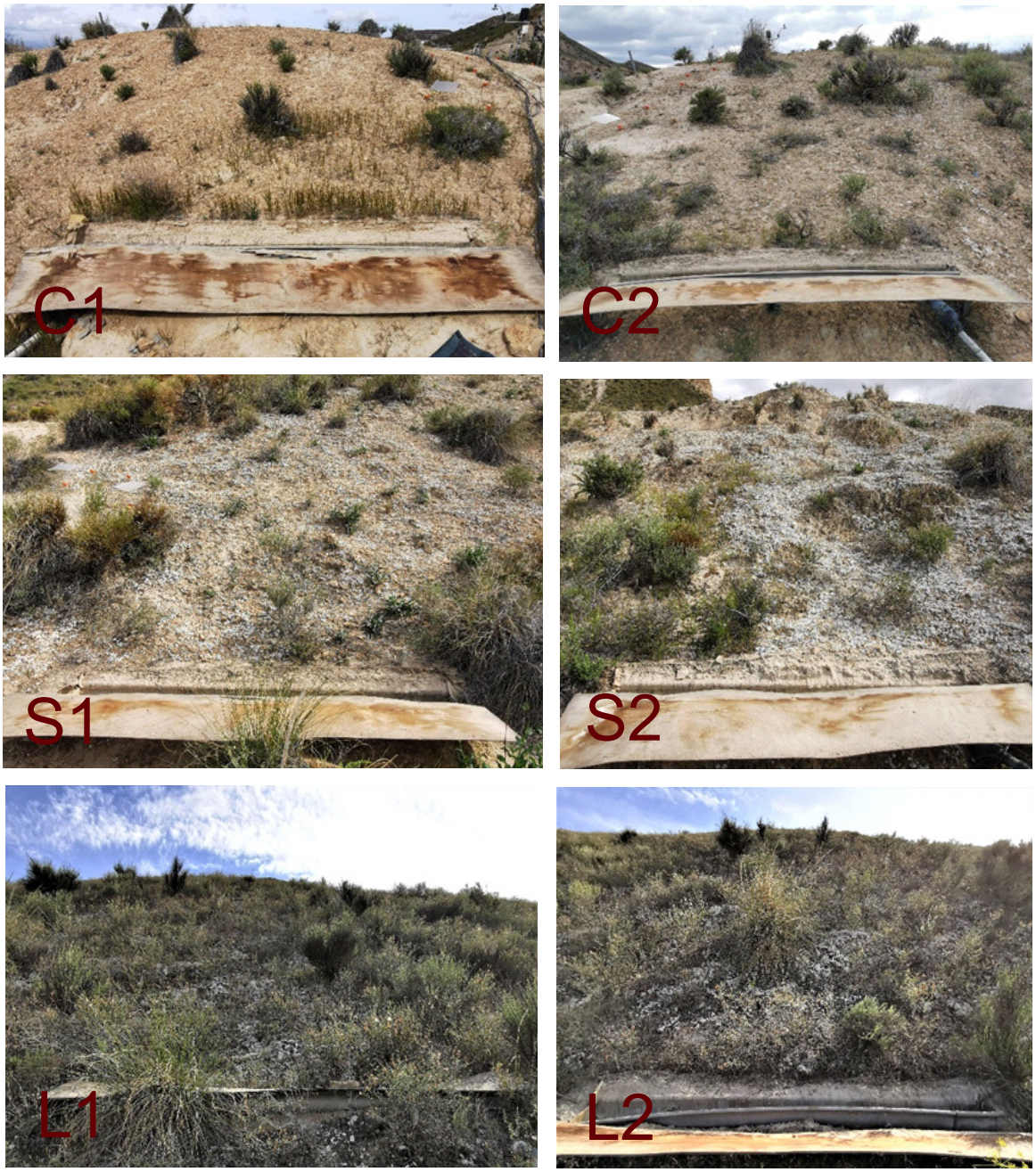

Fig. 1. El Cautivo hillslope scale open runoff plots.

surface type at 1 mm resolution in transects along the catchment area drawn on the plot orthophotomap (to avoid trampling the plots). The length occupied by each type of coverage in relation to the total length of the transect was directly considered its cover percentage.

We used Equation (4) to calculate mRL directly for every rain and runoff event of each MIT (24, 12 and 1 hour). We carried out generalized linear modelling analyses to test for differences in mRL according to two factors and their interaction: rain classes (seven categories) and biocrust types (three). We explored the instantaneous rain intensity and the rain duration as covariates; the volume of precipitation was not included due to its redundancy with the rain class factor. To account for the differences among individual plots, catchment areas, slope angles, the covers of vascular plants, biocrusts, and bare soil, and the covers of vascular plants in the catchment areas delimited by 1 m, 2 m, and 8 m upstream of the channel were also initially considered as covariates. Instantaneous rain intensity was calculated for every rainfall record (rainfall volume input divided by the difference between the time of that record and the time of the previous), and the data used here were the average and the maximum intensities for each event. Then, we reduced the number of covariates, taking into account their interrelationships, the available statistical power, and the significance levels that the covariates reached in preliminary, tentative analyses (see in Results). To perform these analyses, we selected a gamma data distribution and log as link function, including the records having mRL larger than zero, and used Statistica 7.1 software (StatSoft, Hamburg, Germany).

RESULTS

Features of runoff plots and rainfall events

The characteristics of the runoff plots determined by analysing the drone images are shown in Table 1.

The duration, volume, intensity, and number of events for every rain type and every MIT are summarized in Table 2.

The regression coefficient between runoff and rainfall was quite similar for the events from the three MITs in every plot and slightly higher for the 1-hour MIT (0.630 on average *vs* 0.572 and 0.575 for the 24- and 12-hour MITs, respectively). Thus, we show the analyses with the 1-hour MIT, which, moreover, produces the largest number of events. The larger maximum rain intensity belonged to event class 5 (although the average intensities were not very different among MITs). The very large maximum intensity recorded in event class 1 when we used MIT 1 lasted 5 seconds and did not generate runoff.

Every pair of plots on the same kind of surface have a similar hydrological behaviour (Fig. 2), except for Squam biocrust. The shape of the point clouds in Fig. 2, resembling a partially open "fan" and curved upwards, shows the increasing effect of rain intensity and antecedent soil moisture as the precipitation volume increases. The amplitude of these "fans" shows the variance due to the rainfall type and timing. Additionally, we can obtain an idea about the effect of biocrust type on runoff by comparing the scaling in the *y*-axes.

Rainfall volume to start runoff progressively increases through biocrust types; it is short at Cyano, medium at Squam, and larger at Lepra. Considering all the plots and events of the 1-hour MIT, we found 2336 cases (sum of events including all the plots) with an mRL equal to zero and 21 with an mRL larger than zero within the rainfall class 1. The same values were, respectively, 1029 and 70 for class 2; 305 and 121 for class 3; 181 and 245 for class 4; 85 and 215 for class 5; 9 and 81 for class 6; and 3 and 33 for class 7.

Table 1. Features of the runoff plots used at the El Cautivo field site. Biocrust types are described in the main text. Area is the contributing area according topography (m^2). Length is the slope length of the area (m). Slope is the average slope angle (degrees). Aspect is the general orientation (degrees in eastward direction). Covers are given as %. Plant cover 1 m is the plant cover in the first meter upstream from the collector.

Plot	Biocrust	Area	Length	Slope	Aspect eastward	Plant cover	Biocrust cover	Bare cover	Plant cover 1m
C1	Cyano	8.59	7.04	24.46	265	22.13	73.65	4.22	8.45
C2	Cyano	10.79	6.19	16.79	84	8.58	81.63	9.79	5.87
S1	Squam	19.15	13.64	33.18	7	27.04	70.20	2.76	14.24
S2	Squam	22.38	9.72	43.59	4	11.58	69.00	19.42	27.30
L1	Lepra	21.91	12.56	40.92	20	30.95	57.94	11.12	5.59
L2	Lepra	31.08	11.44	41.96	22	34.57	54.05	11.37	49.10

Table 2. Features of the rainfall events; averages from the three rain-gauges. Average and maximum duration are in days; average volume is rainfall in mm; average and maximum intensity are in mm/hour. *Remember that maximum intensity lasted only 5 seconds.

	Rain class	1 >0–1 mm	2 >1–3 mm	3 >3–5 mm	4 >5–10 mm	5 >10–20 mm	6 >20–30 mm	7 >30 mm
MIT 24 h	number of events	199	72	31	42	52	21	19
	average duration, days	0.33	0.65	0.80	1.18	1.33	1.73	2.68
	maximum duration, days	3.26	4.16	3.25	8.93	4.60	4.66	6.86
	average volume, mm	0.32	1.72	3.63	6.58	13.13	23.31	39.07
	average intensity, mm/h	5.75	0.64	0.40	0.85	0.96	1.22	1.21
	maximum intensity, mm/h	542.99*	12.08	1.15	13.17	8.48	7.06	7.13
MIT 12 h	number of events	323	94	36	48	54	22	16
	average duration, days	0.14	0.29	0.50	0.56	0.80	1.17	1.26
	maximum duration, days	0.86	0.90	1.94	2.02	2.96	3.62	2.61
	average volume, mm	0.27	1.66	3.74	6.53	12.93	24.69	34.83
	average intensity, mm/h	1.37	1.06	0.48	1.03	1.23	1.56	1.74
	maximum intensity, mm/h	20.27	12.08	1.26	13.17	8.48	7.06	7.13
MIT 1 h	number of events	1014	184	71	71	50	15	6
	average duration, days	0.02	0.06	0.10	0.16	0.25	0.30	0.39
	maximum duration, days	0.12	0.27	0.34	0.41	0.76	0.74	0.68
	average volume, mm	0.22	1.64	3.62	6.76	13.38	23.55	36.16
	average intensity, mm/h	1.57	2.33	2.73	3.07	3.67	5.51	4.61
	maximum intensity, mm/h	20.27	18.41	19.44	18.61	40.88	20.12	9.16

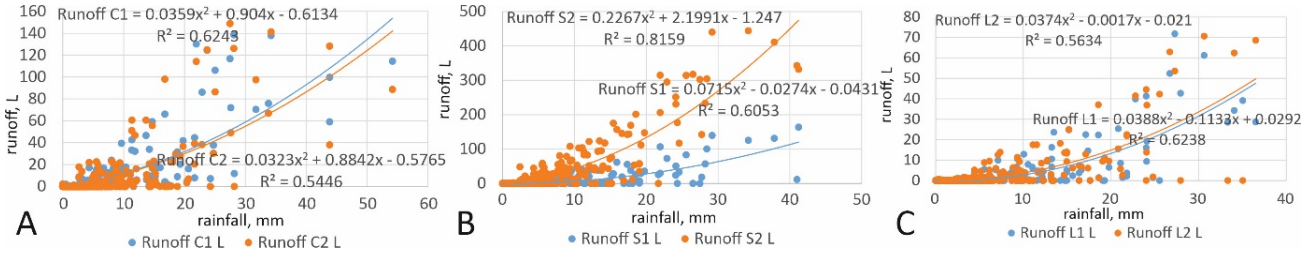

Fig. 2. Runoff (*y*-axis in litres) *vs* rainfall (*x*-axis, mm). Data are the total of each event, using the 1411 events distinguished by the 1-hour MIT. Every graph shows the two plots of the same biocrust type. Graphs A, B, and C correspond to Cyano, Squam, and Lepra, respectively, and are presented in ascending successional order. Note that the scales of the *y*-axes are different.

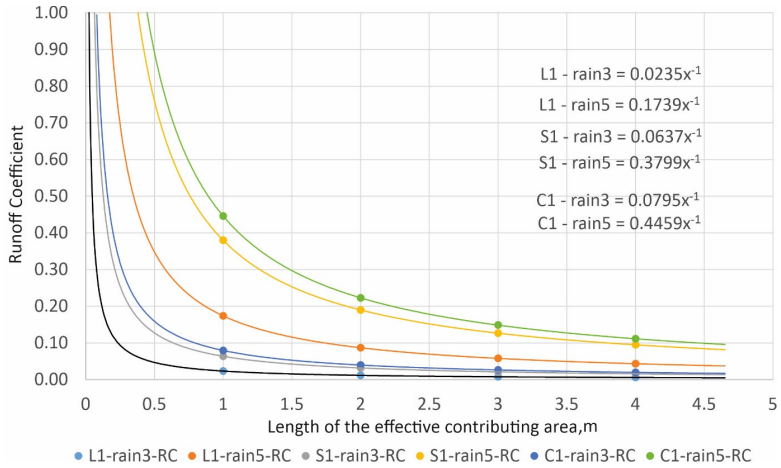

Fig. 3. Examples of hyperbolas relating to the RC with the length of the supposed effective contributing area. For each plot, we use the mean runoff and precipitation of all events of the rainfall classes 3 (>3–5 mm) and 5 (>10–20 mm), generated with the 1-hour MIT. For every pair of rain and runoff data points, we successively assumed four rectangular, nested, effective contributing areas having the length of the channel as width and 1, 2, 3, and 4 m as length. All hyperbolas are asymptotic with respect to the Y axis, thus, a length for the effective contributing area that makes RC = 1 always exists. A RC value > 1 or >> 1 indicates that the assumed length for the contributing area is less or much less than the real one.

Theoretical curves of decrease of RC according to regular increase of contributing area

The RC hyperbolas differed in the distance of the vertex from the origin of coordinates, which vary according to surface types, topography, antecedent soil moisture, rainfall types, etc. Fig. 3 shows some examples for theoretical regularly increasing areas. Even for a surface with high infiltration (with the hyperbola vertex close to the coordinates' origin), a positive slope length for which RC = 1 (an mRL value) always exists.

In these theoretical curves, the greater the MIT, the greater the RCs and the further the hyperbola vertex were from the origin of the coordinates, because of the greater proportion of large events (Table 2).

Goodness of fit of the real drainage areas to the theoretical hyperbolas

When we used successive bands of the real catchment areas of every plot to exam the relationship between RC and increasing contributing areas, the fit of the hyperbolas (Fig. 4) was very good, because the plots' catchments are vaguely smooth and rectangular, at least along the hillslope meters closer to the channel.

The abscissa corresponding to the point where the hyperbola crosses the value 1 of ordinates is the mRL. These curves show that for any surface and rainfall, maximum RCs are much larger than average. Therefore, for a case in which a curve refers to a set of events, it is crucial to specify whether the used mRL is based in the maximum runoff peaks, the average runoff, or any other runoff parameter. The maximum mRL (Fig. 4) was between 3.3 and 4 m at Cyano, about 2.2 m at S1 (although it was about 7.5 m at S2), and between 1.0 and 1.5 m at Lepra.

Using the 12-hour MIT and 24-hour MIT, the number of events changes, as well as the proportion of events belonging to every rainfall class. However, the goodness of fit and the general features of the results are practically the same as those shown in Fig. 4.

Fig. 5 shows that runoff peaks were different in every biocrust, as well as for every rain class. Note that the largest RCs are produced by rain class 5.

These graphs offer an understanding of the relationship between RC and contributing area, verify the goodness of the fit, and provide a graphical value of mRL. Once a good fit was established, we analysed mRL data calculated event by event by using Equation (4).

Analysis of mRL with regard to rainfall, surface and topography features

The analyses showed significant differences in mRL according to all of the factors and included covariates. Rain duration and the cover of bare soil were removed because they were not significant when analysed along with the other variables. The biocrust cover was also removed because it shows a clear negative relationship ($R^2 = 0.86$) with plant cover. The plant cover within 1, 2 and 8 m upstream from the runoff collector, although often independent from the general plant cover, were

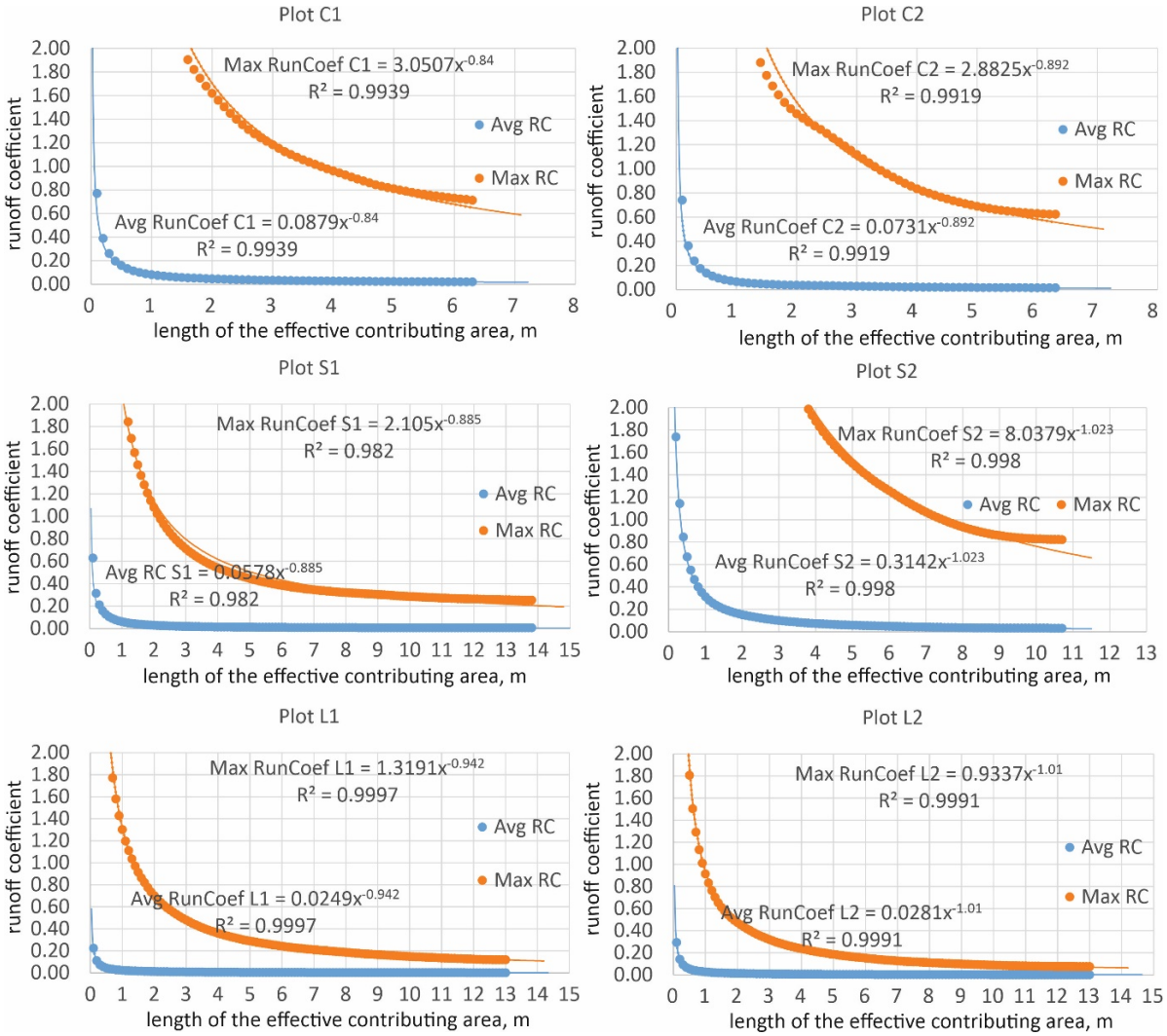

Fig. 4. Difference between the average and maximum runoff. Hyperbolas fitting the variation of RC when successively larger portions of the real topographic catchment of every plot, delimited by parallel lines spaced 10 cm from each other, are assumed to be the effective contributing areas. Data using the 1-hour MIT. All hyperbolas are asymptotic with respect to the Y axis, thus, a length for the effective contributing area that makes RC = 1 always exists. A RC value > 1 or >> 1 indicates that the assumed length for the contributing area is less or much less than the real one.

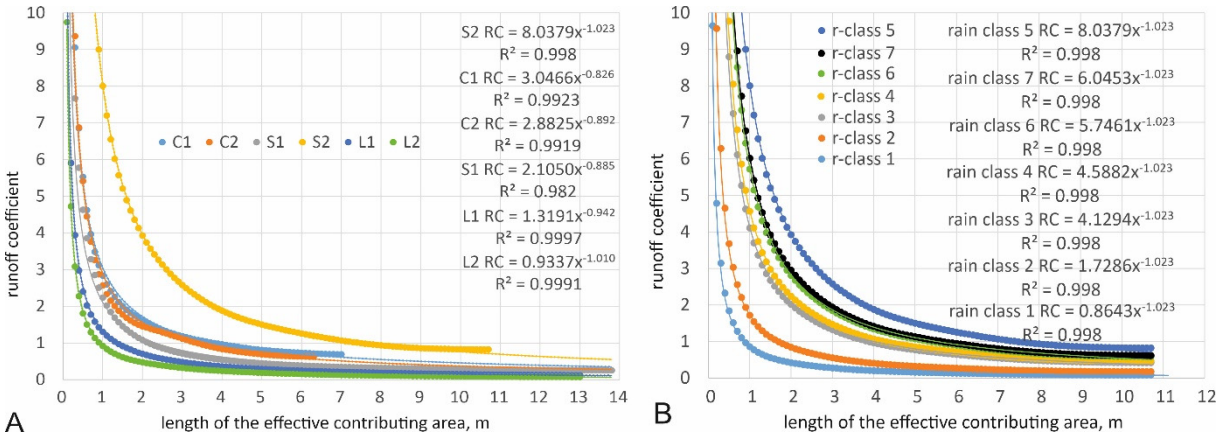

Fig. 5. Graph A: Hyperbolas of RC *vs* contributing area for each plot using the maximum RC of the entire event series and the bands of the real topographical catchments. Graph B: Hyperbolas using the maximum RC of the event classes in the most responsive runoff plot (S2), and the bands of the real topographical catchments (R^2 are the same for all the rain classes because all the curves refer to the same plot and to the same increments of contributing area). Both graphs used data from the 1-hour MIT. All hyperbolas are asymptotic with respect to the Y axis, thus, a length for the effective contributing area that makes RC = 1 always exists. A RC value > 1 or >> 1 indicates that the assumed length for the contributing area is less or much less than the real one.

also removed to gain statistical power and used in alternative analyses instead of the general plant cover. Thus, the final analysis included both factors (biocrust type and rain class) and their interaction, three covariates to account for the features of every particular plot (catchment area, slope, and plant cover), and the rain intensity as an additional covariate, because it is poorly related to the rainfall volume. Table 3 summarizes the results of the final analysis.

The mRL consistently increases when rainfall increases, and the differences between rain classes are often significant. An mRL threshold in at about 3 mm of rainfall has been found (Fig. 6): At less than 3 mm of rainfall, the peaks of mRL never reached 10 cm (runoff was rare in rain classes 1 and 2, but sometimes it occurred; see above).

The biocrust type significantly affected the mRL (Fig. 7A), and when we removed the data from plot S2, the mRL decreased along biocrust succession (Fig. 7B). However, the features of S2, with much larger runoff due to other factors (such as larger bare soil area and slope angle), deform the relationship between mRL and the successional sequence if S2 is included.

Table 3. Significance of the effects of the different factors, interactions, and covariates on mRL, according to hypothesis testing using generalized linear modelling.

Effect	Degrees of freedom	Log-likelihood	Chi-square	p
Event class	6	–205.644	221.2202	0.000000
Biocrust type	2	–164.662	81.9652	0.000000
Event class × Biocrust type	12	–146.243	36.8361	0.000237
Rain intensity	1	–476.893	56.0725	0.000000
Catchment area	1	–464.168	25.4504	0.000000
Slope angle	1	–456.728	14.8815	0.000114
Plant cover	1	–316.254	280.9465	0.000000

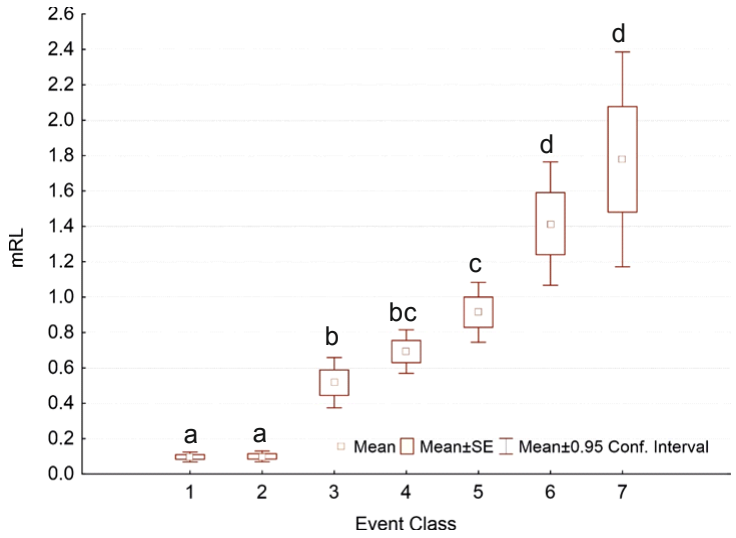

Fig. 6. Average mRL for the sets of events in every rain class produced using an MIT of 1 hour, including the data from all the plots. Different letters on the boxes indicate significant differences.

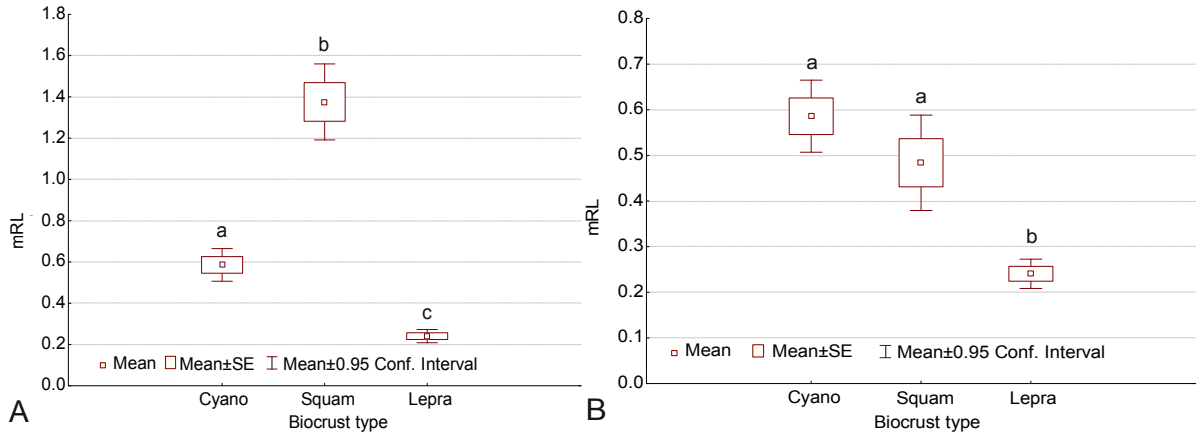

Fig. 7. Differences in mRL according to biocrust type. Graph A includes all the plots, and the differences are highly influenced by the larger runoff in plot S2. Graph B does not include the data from plot S2 and shows that infiltration increases along the ecological succession. Different letters on the boxes indicate significant differences.

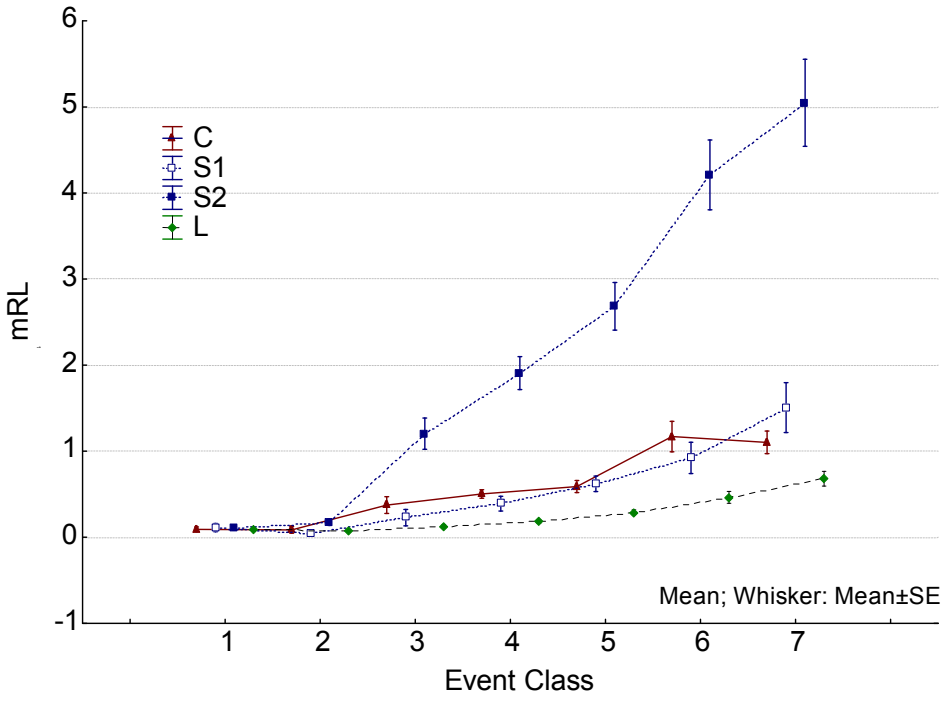

Fig. 8. Interaction between biocrust type and rain event class. Every line corresponds to a biocrust type, but for Squam the plots are shown separately because they behave quite differently. Except for plot S2, mRL decreases along biocrust succession. The threshold of mRL at 3 mm rainfall is distinguishable in this figure as well.

The interaction between biocrust type and rain class is shown in Fig. 8. The larger the rainfall, the larger the difference in mRL is among biocrusts. Biocrust type modulates the way in which the different rainfall classes affect runoff. However, the difference is also due to the slope and other causes such as plant and bare soil covers; the influence of plot S2 expanded the range of mRL along the event classes in the Squam biocrust.

Average rain intensity, contributing area and slope angle had a positive significant effect on mRL, whereas plant cover had a negative significant effect (Table 3). When we carried out the alternative analyses replacing plant cover successively by the plant cover at 1, 2, or 8 m upstream of the channels, each cover showed a significant effect on mRL.

The number of events decreases when the MIT increases and, whereas the duration of the events tends to increase exponentially when MIT increases, the rain intensity tends to decrease potentially when MIT increases. However, the generalized-linear-model results show the same pattern with all the MITs, with all the considered factors, interactions, and covariates of the final model being significant.

DISCUSSION

RL and mRL

RL and mRL are different from hydrological connectivity. A stream or river can connect large distances; however, a certain concrete water volume usually does not cover all the connected distance because it stops at some point on the shore, infiltrates, evaporates, or is absorbed by plants. Similarly, when diffuse surface runoff (not concentrated in rills) occurs, the entire hillslope length can be hydrologically connected, but that does not necessarily mean that RL is the entire hillslope length. (However, it is certain that all the space covered by RL is connected.) If we progressively increase the length of the plot undergoing simulated rainfall, runoff volume increases until a certain plot length (Lázaro et al., 2015) because, beyond that length, all the water felt in the upper end of the plot infiltrates before reaching the collector. This threshold plot length is RL, a concept providing a measurement of the decay of RC as the drainage area increases. Connectivity is usually larger, sometimes drastically larger, than RL.

To explore and discuss the relationship of RL or mRL with the length slope factor (LSF) or potential sediment transport index (Moore and Burch, 1986), a parameter derived from the digital elevation model, could be interesting. The LSF is a surrogate that indicates the erosive potential of runoff, and its formula is $LSF = (Xh / 72.6)^m$, where *Xh* is the horizontal length in meters of the slope and *m* is the exponent of the slope variable, defined as $m = \varepsilon / (1 + \varepsilon)$. The term ε relates to erosion in the furrows and between furrows and is defined as $\varepsilon = \sin\theta / 0.0896 \times (3 \times (\sin\theta)^{0.8} + 0.56)$, where θ is the angle of the slope (McCool et al., 1997; Zhang et al., 2017). RL and mRL should relate closely to LSF because the (potential) transport capacity of sediments depends on runoff. Interestingly, LSF is a factor deduced from topography, but mRL is calculated from runoff and precipitation from specific events. In reality, both concepts are independent and complementary approximations. As a first tentative hypothesis, if we replace the slope length with the mRL in the LSF formula, the resulting potential sediment transport capacity would become actual capacity, that is, actual sediment transport if sediments are available. This could be verified empirically, and if so, mRL could be highly useful for a predictive erosion model where sediment availability is not a limiting factor.

As Lázaro et al (2015) discussed, the "flow length index" of Mayor et al. (2008) is conceptually comparable to RL. However, it does not include the incoming rainfall.

The slightly higher regression coefficient between runoff and rainfall for the 1-hour MIT we found agrees with the results of Molina-Sanchís et al. (2016).

We believe that mRL is a proxy of RL with general validity. By changing the rainfall or surface features, the parameter '*a*'of Equation (1) changes, but it does not change the concepts or interpretations of the processes. The hyperbolic relationship we

found between RC and real drainage area length (Fig. 4) is consistent with the potential decrease of RC experimentally determined by Lázaro et al (2015). In the experiments, the curves fit worse because different plots (although close, homogeneous, and under the same simulated rainfall) represented the different lengths. The goodness of the fits in Fig. 4, along with a certain irregularity of the shapes and micro-reliefs of our real drainage areas, show that our proposal is applicable in an extensive range of plots, because when we installed our plots in 2005, we did not look for 'ideal-like' hillslopes.

Runoff on biocrusts at the El Cautivo field site

As expected, the larger the rainfall, the larger the mRL. We found occasional runoff even in rain classes 1 and 2, which Rodríguez-Caballero et al. (2014) also found in the same study area. Despite an mRL value existing as long as the runoff is measurable, a clear threshold can be observed in the relationship between mRL and rainfall (Fig. 6). The way in which the rain class affected the mRL depended often on the biocrust type (Fig. 8). Lázaro et al. (2015) also observed that interaction: A threshold of runoff *vs* rainfall is associated with a different rain class depending on the biocrust type.

The larger the rain intensity, the larger the mRL. This caused that the rain class 5 gave rise to the largest runoff coefficients (Fig. 5B), despite classes 6 and 7 involving larger rainfall volumes, as the intensity of class 5 was clearly larger when using MIT 1 (Table 2). This is consistent with what was previously stated in the same study area, under natural rainfall (Rodríguez-Caballero et al., 2014) and rain simulations (Lázaro et al., 2015). The same was found in other locations (Guan and Cao, 2019).

As expected, there were significant differences in mRL among biocrust types. Except for the Squam biocrust, the differences among plots belonging to the same biocrust type were much smaller than the differences among types (Fig. 2). The larger slope of plot C1 with regard to C2 was compensated by a lower contributing area. The lower plant cover of plot L1, particularly in the first meter upstream of the collector (Table 1), compensated for its smaller drainage area. However, the two plots at the Squam biocrust behaved differently. Much larger runoff was consistently recorded for plot S2 during the sampled period. It has larger slope, less plant cover, and much higher cover of bare soil, with its upper part eroded (Table 1). The slope angle in S2 is 45º in the first 8 m upstream of the collector, which is relevant because the maximum recorded mRL was shorter than 8 m. We did not find in the literature a slope threshold beyond which runoff disproportionately increases. However, where soil is silty, runoff is larger on bare than on biocrusted soil (Wei et al., 2015; Xiao et al., 2019). Soil texture seems determinant: In Tabernas' silty soils, biocrusts often generate less runoff than bare soil, but in the sandy soils of the Negev, biocrust shows threefold higher runoff than bare soil (Kidron, 1999). Chamizo et al. (2012a) and Lázaro et al. (2015) also found significant differences in runoff between biocrust types. Although cyanobacterial biocrusts tend to produce larger mRL, Rodríguez-Caballero et al. (2013) and Chamizo et al. (2012b) noted that the difference in runoff between cyanobacterial and lichenic biocrusts decreases to nothing as rainfall volume increases. Our result is consistent with Kidron et al. (2003), who found in Negev a substantial reduction in the RC from cyanobacterial to moss-dominated biocrust, explained by the lower amounts of extracellular polymeric substances and the higher roughness of moss-dominated biocrust. Small differences in the micro-relief already affect the runoff (Kidron, 2007). Our result partly agreed with Belnap (2006), who found two hydrological behaviours: Green algae and microfungi behave similarly to cyanobacteria, whereas bryophytes are similar to lichens.

Because the development of some biocrust types takes longer than that of others, and eventually one type is replaced by another (Lázaro et al., 2008), it is widely agreed that different biocrust types can be understood as successional steps (Belnap et al., 2006; Li et al., 2013; Rodríguez-Caballero et al., 2015), although some scholars do not regard different crust types as being necessarily successional stages (Kidron, 2019). In our area, the succession begins from Cyano and progresses to Squam and finally to Lepra (Lázaro et al., 2008). However, succession shows different speeds at different habitats and can stop at any point. It strongly depends on the microclimate, mainly on sun radiation and water availability. Where there are not conditions for development of lichens or mosses, Cyano can be almost permanent on a human life timescale.

Except for plot S2, our results show that infiltration tends to increase along biocrust succession. This is consistent with our previous experiments and with Gypser et al. (2016). Although biocrusts are often considered runoff sources (Cantón et al., 2002; Rodríguez-Caballero et al., 2018), their RC is generally lower than that of bare soil with physical crust (Eldridge et al., 2020) because biocrust succession progressively increases water retention (Gypser et al., 2016) and soil moisture (Chamizo et al., 2013). This increase of infiltration along succession is due to multiple factors, including (i) the effect of pore clogging increasing runoff in the early successional stages, favoured by cyanobacterial exopolysaccharides (Kidron et al., 1999); (ii) the increase of surface roughness increasing infiltration as the succession progresses (Chamizo et al., 2010; Kidron, 2007; Rodríguez-Caballero et al., 2012); and (iii) the larger proportion of mosses and vascular plants in the latest-successional biocrust (Lázaro et al., 2008), because mosses show larger infiltration capacity than do lichens (Fischer et al., 2014). In addition, plants, which develop progressively, are the main runoff sinks (Minea et al., 2018; Solé-Benet et al., 1997). Hydrological changes associated with successional stages have also been found in more mesic and larger vegetation including biocrusts (Lichner et al., 2012).

Comparable data on RL from other areas are scarce. Kidron (2011) reported an average RL of 5.0 m, while Kidron and Yair (1997) estimated a length of 7 to 10 m for the effective contributing area in the case of the peak runoff produced at the end of the heaviest storm, when the biocrust was already saturated, in their most responsive plot, which had only 10% of plant cover and a relatively smooth biocrust. This length is close ourmaximum mRLvalue, which reached 7.5 m in our most responsive plot.

To our knowledge, this is the first study on the hydrological behaviour of the Lepra biocrust. Chamizo et al. (2012a; 2012b) and Lázaro et al. (2015) did not include Lepra to avoid severe alterations, as its typical large slope angle generates significant challenges in the experiments. This is interesting because Lepra is the permanent biocrust community that occupies the plant interspaces in non-eroded mature grassland or scrubland sites. Furthermore, because the sites chosen for the Lepra plots have relatively low grass cover, the runoff will be still lower in mature grasslands.

The mRL is consistently lower in Lepra over time, despite the slope, because of the greater plant cover (Minea et al., 2018) and number of small plant patches and annual plants. First, there is a larger number of plant roots acting as preferential infiltration routes; second, fine-grained plant patches are

more efficient in reducing runoff than the coarse-grained ones (Bautista et al., 2007). In addition, soil porosity is larger under plants (Mora and Lázaro, 2014), and plants further increase infiltration by intercepting rainfall and producing stemflow (Jian et al., 2018). Furthermore, under alpha grass, biocrust rarely develops (Eldridge et al., 2010), but under plants such as *Euzomodendron bourgaeanum*, *Helianthemum almeriense* or *Salsola genistoides*, which are in the Lepra plots, biocrust (which favours runoff) is much more frequent than the 20% of cases that Kidron (2015) found under the canopy at Nizana (Israel). This occurs because the canopies of these species are less dense or more separated from the ground.

We found a positive relationship of mRL with slope, consistent in time and space in Cyano and Squam. This agrees with Chamizo et al. (2012b), who found, in the same study area, that the effect of slope might be irrelevant at the microplot scale, but is important at the small hillslope scale. However, the effect of slope was mainly due to the S2 plot. This slope effect is logical but its significance is relatively unexpected here due to (i) the opposite effect of the vegetation in the Lepra plots; and, (ii) the relatively higher RC of the Cyano biocrust (Alexander and Calvo, 1990; Chamizo et al., 2012a) having plots of lower steepness. Cerdá and García-Fayos (1997) found a positive relationship between slope and runoff initiation and sediment yield, but not between slope and runoff volume.

The effect of the catchment area was significant, despite the effective contributing area in most plots usually being much smaller than the topographic one. This was relatively unexpected because it only accounted for about 1% of the mRL variance. The effective contributing area would be the one delimited by RL. It is expected that an area longer than the RL would have little effect on runoff. However, it does have some effect: The rain falling above the RL but into a distance of up 2RL, although it does not reach the collector, increases soil moisture in the part of the plot delimited by RL, therefore increasing the RC. Additionally, the factor area was significant because the mean area of the Lepra plots was the largest, although the lowest runoff was recorded. In any case, the effect of the drainage area is fuzzy in this design. For example, the area of L2 is 50% larger than that of L1, and both slopes are similar. However, the plant cover of L2 is also larger (mainly in the first meter upstream of the channel), and the runoff is similar.

CONCLUSIONS

The mRL, a new parameter to characterize the runoff, is defined here as the hillslope length of the supposed effective contributing area that makes the RC = 1. It is quantitative, easy to calculate from runoff plots, and does not require the contributing area: It is a function of the runoff, precipitation, and the width of the runoff plot. Furthermore, mRL coincides with the coefficient of the hyperbola relating to the decrease of the RC as the contributing area increases. Because the hyperbola equation has only one coefficient, the concept of mRL enables knowing the whole hyperbole for any couple of runoff and rainfall values (if the shape or the relief of the plot catchment is not very irregular). We propose mRL as a proxy of RL and discuss its relationships with hydrological conductivity and the length slope factor.

We completed an mRL-based hydrological study with 10 years of runoff data from six open plots at a (small) hillslope scale including three biocrust types, in a badlands area of the Tabernas Desert (semiarid southeast Spain). The results show that the main features of rainfall affecting runoff (volume and intensity), as well as those of the surface (biocrust type and plant cover) and those of topography (contributing area and slope angle), determined mRL. Different biocrusts had different mRLs and whereas rainfall, area, and slope had a positive relationship with mRL, plant cover had a negative relationship.

Acknowledgements. Funding: This study was started in the context of the research projects PECOS (REN2003-04570/GLO) and PREVEA (CGL2007-63258/BOS), both funded by the Spanish National Plan for RD&I and by the European ERDF Funds (European Regional Development Fund), and continued during the project SCIN (Soil Crust InterNational, PRI-PIMBDV-2011-0874, European project of ERA-NET BIODIVERSA, the Spanish team being funded by the Spanish Ministry of Economy and Competitiveness). The work was finally supported and culminated by the DINCOS project (CGL2016-78075-P, Spanish State Programme for Scientific Research) and by the European ERDF Funds (European Regional Development Fund). Consuelo Rubio's participation was possible thanks to the contract as a doctoral student FPU18 / 00035. Dr. Javier Barbero advised us on mathematical issues.

Special thanks: This research was kindly facilitated by the Viciana brothers, landowners of the El Cautivo field site.

REFERENCES

Agassi, M., Ben-Hur, M., 1991. Effect of slope length, aspect and phosphogypsum on runoff and erosion from steep slopes. Aust. J. Soil Res., 29, 2, 197–207.

Alexander, R.W., Calvo, A., 1990. The influence of lichens on slope processes in some Spanish badlands. In: Thornes, J.B. (Ed.): Vegetation and Erosion: Processes and Environments. Wiley, New York, pp. 385–398.

Alexander, R.W., Harvey, A.M., Calvo-Cases, A., James, P.A., Cerda, A., 1994. Natural stabilisation mechanisms on badlands slopes: Tabernas, Almería, Spain. In: Millington, A.C., Pye, K. (Eds.): Environmental Change in Drylands: Biogeographical and Geomorphological Perspectives. Wiley, Chichester, pp. 85–111.

Alexander, R.W., Calvo-Cases, A., Arnau-Rosalén, E., Mather, A.E., Lázaro, R., 2008. Erosion and stabilization sequences in relation to base level changes in the El Cautivo badlands, SE Spain. Geomorphology, 100, 1–2, 83–90.

Arnau-Rosalén, E., Calvo-Cases, A., Boix-Fayos, C., Lavee, H., Sarah, P., 2008. Analysis of soil surface components patterns affecting runoff generation. An example of methods applied to Mediterranean hillslopes in Alicante (Spain). Geomorpholgy, 101, 4, 595–606.

Bautista, S., Mayor, Á. G., Bourakhouadar, J., Bellot, J., 2007. Plant spatial pattern predicts hillslope runoff and erosion in a semiarid Mediterranean landscape. Ecosystems, 10, 6, 987–998.

Belnap, J., Lange, O. (Eds.), 2003. Biological Soil Crusts: Structure, Function and Management. Springer, Berlin, 506 p.

Belnap, J., 2006. The potential roles of biological soil crusts in dryland hydrologic cycles. Hydrol. Process., 20, 3159–3178.

Belnap, J., Phillips, S., Troxler, T., 2006. Soil lichen and moss cover and species richness can be highly dynamic: The effects of invasion by the annual exotic grass *Bromus tectorum*, precipitation, and temperature on biological soil crusts in SE Utah. App. Soil Ecol., 32, 1, 63–76.

Boix-Fayos, C., Martínez-Mena, M., Arnau-Rosalén, E., Calvo-Cases, A., Castillo, V., Albaladejo, J., 2006. Measuring soil erosion by field plots: Understanding the sources of varia-

tion. Earth-Science Reviews, 78, 3–4, 267–285.
Bowker, M.A., Maestre, F.T., Escolar, C., 2010. Biological crusts as a model system for examining the biodiversity-ecosystem function relationship in soils. Soil Biology and Biochemistry, 42, 3, 405–517.
Büdel, B., 2003. Synopsis: comparative biogeography of soil–crust biota. In: Belnap, J., Lange, O. (Eds.): Biological Soil Crusts: Structure, Function and Management. Springer, Berlin, pp. 141–152.
Cantón, Y., Domingo, F., Solé-Benet, A., Puigdefábregas, J., 2002. Influence of soil surface types on the overall runoff of the Tabernas badlands (south-east Spain): field data and model approaches. Hydrol. Process., 16, 2621–2643.
Cantón, Y., Solé–Benet, A., Lázaro, R., 2003. Soil–geomorphology relations in gypsiferous materials of the Tabernas desert (Almería, SE Spain). Geoderma, 115, 193–222.
Cantón, Y., Del Barrio, G., Solé-Benet, A., Lázaro, R., 2004. Topographic controls on the spatial distribution of ground cover in a semiarid badlands area. Catena, 55, 341–365.
Castillo, V.M., Gómez-Plaza, A., Martínez-Mena, M., 2003. The role of antecedent soil water content in the runoff response of semiarid catchments: a simulation approach. J. Hydrol., 284, 114–130.
Cerdá, A., García-Fayos, P., 1997. The influence of slope angle on sediment, water and seed losses on badland landscapes. Geomorphology, 18, 77–90.
Chamizo, W., Rodríguez-Caballero, E., Miralles-Mellado, I., Afana, A., Lázaro, R., Domingo, F., Calvo-Cases, A., Solé-Benet, A., Cantón, Y., 2010. Características de las costras físicas y biológicas del suelo con mayor influencia sobre la infiltración y la erosión en ecosistemas semiáridos. Pirineos, 165, 69–96.
Chamizo, S., Cantón, Y., Lázaro, R., Solé-Benet, A., Domingo, F., 2012a. Crust composition and disturbance drive infiltration through biological soil crusts in semiarid ecosystems. Ecosystems, 15, 1, 148–161.
Chamizo, S., Cantón, Y., Rodríguez-Caballero, E., Domingo, F., Escudero, A., 2012b. Runoff at contrasting scales in a semiarid ecosystem: A complex balance between biological soil crust features and rainfall characteristics. J. Hydrol., 452–453, 130–138.
Chamizo, S., Cantón, Y., Lázaro, R., Domingo, F., 2013. The role of biological soil crusts in soil moisture dynamics in two semiarid ecosystems with contrasting soil textures. J. Hydrol., 489, 74–84.
Chamizo, S., Belnap, J., Eldridge, D.J., Canton, Y., Malam Issa, O., 2016. The role of biocrusts in arid land hydrology. In: Weber, B., Büdel, B., Belnap, J. (Eds.): Biological Soil Crusts: An Organizing Principle in Drylands. Springer, pp. 321–346.
Eldridge, D.J., Bowker, M.A., Maestre, F.T., Alonso, P., Mau, R.L., Papadopoulos, J., Escudero, A., 2010. Interactive effects of three ecosystem engineers on infiltration in a semiarid Mediterranean grassland. Ecosystems, 13, 499–510.
Eldridge, D.J., Reed, S., Travers, S.K., Bowker, M.A., Maestre, F.T., Ding, J., Havrilla, C., Rodríguez-Caballero, E., Barger, N., Weber, B., Antoninka, A., Belnap, J., 2020. The pervasive and multifaceted influence of biocrusts on water in the world's drylands. Glob. Change Biol., 26, 10,6003–6014.
Fischer, T., Gypser, S., Subbotina, M., Veste, M., 2014. Synergic hydraulic and nutritional feedback mechanisms control surface patchiness of biological soil crusts on tertiary sands at a post-mining site. J. Hydrol. Hydromech., 62, 4, 293–302.
Guan, H., Cao, R., 2019. Effects of biocrusts and rainfall characteristics on runoff generation in the Mu Us Desert, northwest China. Hydrology Research, 50, 5, 1410–1423.
Gypser, S., Veste, M., Fischer, T., Lange, P., 2016. Infiltration and water retention of biological soil crusts on reclaimed soils of former open-cast lignite mining sites in Brandenburg, north-east Germany. J. Hydrol. Hydromech., 64, 1, 1–11.
Jian, S.Q., Zhang, X.L., Wu, Z.N., Hu, C.H. 2018. The effects of stemflow on redistributing precipitation and infiltration around shrubs. J. Hydrol. Hydromech., 66, 1, 79–86.
Kidron, G.J., Yair, A., 1997. Rainfall-runoff relationships over encrusted dune surface, Nizzana, western Negev Israel. Earth Surf. Process. Landf., 22, 1169–1184.
Kidron, G.J., 1999. Differential water distribution over dune slopes as affected by slope position and microbiotic crust, Negev Desert, Israel. Hydrological Processes, 13, 1665–1682.
Kidron, G.J., 2007. Milimeter-scale microrelief affecting runoff yield over microbiotic crust in the Negev Desert. Catena, 70, 266–273.
Kidron, G.J., 2011. Runoff generation and sediment yield on homogeneous dune slopes: scale effect and implications for analysis. Earth Surf. Process. Landf., 36, 1809–1824.
Kidron, G.J., 2015. Runoff and sediment yields from under-canopy shrubs in a biocrusted dunefield. Hydrological Processes, 30, 11, 1665–1675.
Kidron, G.J., 2019. Biocrust research: A critical view on eight common hydrological-related paradigms and dubious theses. Ecohydrology, 12, 2, e2061.
Kidron, G.J., Yaalon, D.H. Vonshak, A., 1999. Two causes for runoff initiation on microbiotic crusts: hydrophobicity and pore clogging. Soil Science, 164, 18–27.
Kidron, G.J., Yair, A., Vonshak, A., Abellovich, A., 2003. Microbiotic crust control of runoff generation on sand dunes in the Negev Desert. Water Resources Research, 39, SWC51-SWC55.
Lázaro, R., Alexander, R.W., Puigdefábregas, J., 2000. Cover distribution patterns of lichens, annuals and shrubs in the Tabernas Desert, Almería, Spain. In: Alexander, R.W., Millington, A.C. (Eds.): Vegetation Mapping: from Patch to Planet. Wiley, Chichester, pp.19–40.
Lázaro, R., Rodrigo, F.S., Gutiérrez, L., Domingo, F., Puigdefábregas, J., 2001. Analysis of a 30-year rainfall record (1967–1997) in semi-arid SE Spain for implications on vegetation. J. Arid Environ., 48, 373–395.
Lázaro, R., Rodríguez-Tamayo, M.L., Ordiales, R., Puigdefábregas, J., 2004. El Clima. In: Mota, J., Cabello, J., Cerrillo, M.I., Rodríguez-Tamayo, M.L. (Eds.): Subdesiertos de Almería: naturaleza de cine. Consejería de Medio Ambiente, Junta de Andalucía, Almería, pp. 63–79.
Lázaro, R., Cantón, Y., Solé-Benet, A., Bevan, J., Alexander, R., Sancho, L.G., Puigdefábregas, J., 2008. The influence of competition between lichen colonization and erosion on the evolution of soil surfaces in the Tabernas badlands (SE Spain) and its landscape effects. Geomorphology, 102, 252–266.
Lázaro, R., Mora, J.L., 2014. Sediment content and chemical properties of water runoff on biocrusts in drylands. Biologia, 69, 11, 1539–1554.
Lázaro, R., Calvo-Cases, A., Lázaro, A., Molina, I., 2015. Effective run-off flow length over biological soil crusts on silty loam soils in drylands. Hydrological Processes, 29, 2534–2544.
Le Bissonnais, Y., Renaux, B., Delouche, H., 1995. Interactions between soil properties and moisture content in crust for-

mation, runoff and interrill erosion from tilled loess soils. Catena, 25, 1–4, 33–46.

Li, X.R., Zhang, Z.S., Huang, L., Wang, X.P., 2013. Review of the ecohydrological processes and feedback mechanisms controlling sand-binding vegetation systems in sandy desert regions of China. Chin. Sci. Bull., 58, 1483–1496. DOI: 10.1007/s11434-012-5662-5

Lichner, L., Holko, L., Zhukova, N., Schacht, K., Rajkai, K., Fodor, N., Sándor, R., 2012. Plants and biological soil crust influence the hydrophysical parameters and water flow in an aeolian sandy soil. J. Hydrol. Hydromech., 60, 309–318.

Maestre, F.T., Bowker, M.A., Cantón, Y., Castillo-Monroy, A.P., Cortina, J., Escolar, C., Escudero, A., Lázaro, R., Martínez, I., 2011. Ecology and functional roles of biological soil crusts in semi-arid ecosystems of Spain. J. Arid Environ., 75, 1282–1291.

Maestre, F.T., Eldridge, D.J., Soliveres, S., Kéfi, S., Delgado-Baquerizo, M., Bowker, M.A., García-Palacios, P., Gaitán, J., Gallardo, A., Lázaro, R., and Berdugo, M., 2016. Structure and functioning of dryland ecosystems in a changing world. Annual Review of Ecology, Evolution, and Systematics, 47, 215–237.

Mayor, A.G., Bautista, S., Small, E.E., Dixon, M., Bellot, J., 2008. Measurement of the connectivity of runoff source areas as determined by vegetation pattern and topography: a tool for assessing potential water and soil losses in drylands. Water Resour. Res., 44, 10, W10423.

Mayor, A., Bautista, S., Bellot, J., 2011. Scale-dependent variation in runoff and sediment yield in a semiarid Mediterranean catchment. Journal of Hydrology, 397, 128–135.

McCool, D., Foster, G., Weesies, G., 1997. Slope Length and Steepness Factors (LS). In: Renard, K., Foster, G., Weesies, G., McCool, D., Yoder, D. (Coord.): Predicting Soil Erosion by Water: A Guide to Conservation Planning with the Revised Universal Soil Loss Equation (RUSLE). Agriculture Handbook, No. 703, USDA, Washington, D.C., pp. 101–142.

Minea, G., Ioana-Toroimac, G., Moroşanu, G., 2018. The dominant runoff processes on grassland hillslopes within different land uses of Romania – an experimental study. J. Hydrol. Hydromech., 67, 4, 297–304.

Molina-Sanchís, I., Lázaro, R., Arnau-Rosalén, E., Calvo-Cases A., 2016. Rainfall timing and runoff: The influence of the criterion for rain event separation. J. Hydrol. Hydromech., 64, 3, 226–236.

Moore, I.D., Burch, G.J., 1986. Physical basis of the length-slope factor in the universal soil loss equation. Soil Sci. Soc. Am. J., 50, 5, 1294–1298.

Mora, J.L., Lázaro, R., 2014. Seasonal changes in bulk density under semiarid patchy vegetation: the soil beats. Geoderma, 235–236, 30–38.

Puigdefábregas, J., Solé, A., Gutierrez, L., del Barrio, G., Boer, M., 1999. Scales and processes of water and sediment redistribution in drylands: results from the Rambla Honda field site in southeast Spain. Earth-Science Reviews, 48, 39–70.

Puigdefábregas, J., 2005. The role of vegetation patterns in structuring runoff and sediment fluxes in drylands. Earth Surf. Process. Landf., 30, 133–147.

Rodríguez-Caballero, E., Cantón, Y., Chamizo, S., Afana, A., Solé-Benet, A., 2012. Effects of biological soil crusts on surface roughness and implications for runoff and erosion. Geomorphology, 145–146, 81–89.

Rodríguez-Caballero, E., Cantón, Y., Chamizo, S., Lázaro, R., Escudero, A., 2013. Soil loss and runoff in semiarid ecosystems: A complex interaction between biological soil crusts, micro-topography and hydrological drivers. Ecosystems, 16, 529–546.

Rodríguez-Caballero, E., Cantón, Y., Solé-Benet, A., Lazaro, R., 2014. Cross-scale interactions between surface components and rainfall properties. Non-linearities in the hydrological and erosive behaviour of semiarid catchments. Journal of Hydrology, 517, 815–825.

Rodríguez-Caballero, E., Aguilar, M.A., Cantón, Y., Chamizo, S., Aguilar, F.J., 2015. Swelling of biocrusts upon wetting induces changes in surface micro-topography. Soil Biology and Biochemistry, 82, 107–111.

Rodríguez-Caballero, E., Chamizo, S., Roncero-Ramos, B., Román, R., Cantón, Y., 2018. Runoff from biocrust: A vital resource for vegetation performance on Mediterranean steppes. Ecohydrology, 11, e1977.

Solé-Benet, A., Calvo-Cases, A., Cerdá, A., Lázaro, R., Pini, R., Barbero, J., 1997. Influences of micro-relief patterns and plant cover on runoff related processes in badlands from Tabernas (SE Spain). Catena, 31, 23–38.

Weber, B., Büdel, B., Belnap, J. (Eds.), 2016. Biological Soil Crusts: An Organizing Principle in Drylands. Springer, 549 p.

Wei, W., Yu, Y., Chen, L., 2015. Response of surface soil hydrology to the micro-pattern of biocrust in a dry-land loess environment, China. PLoS ONE, 10, 7, e0133565. DOI: 10.1371/journal. pone.0133565

Xiao, B., Sun, F., Hu, K., Kidron, G.J., 2019. Biocrusts reduce surface soil infiltrability and impede soil water infiltration under tension and ponding conditions in dryland ecosystem. Journal of Hydrology, 568, 792–802.

Xu, X.L., Liu, W., Kong, Y.P., Zhang, K.L., Yue, B., Chen, J.D., 2009. Runoff and water erosion on road side-slopes: Effects of rainfall characteristics and slope length. Transportation Research Part D, 14, 497–501.

Zhang, H., Wei J., Yang, Q., Baartman, J.E.M., Gai, L., Yang, X., Li, S.Q., Yu, J., Ritsema, C.J., Geissen, V., 2017. An improved method for calculating slope length (λ) and the LS parameters of the Revised Universal Soil Loss Equation for large watersheds. Geoderma, 308, 36–45.

Received 16 June 2021
Accepted 13 September 2021

J. Hydrol. Hydromech., 69, 2021, 4, 400–420
DOI: 10.2478/johh-2021-0030
ISSN 1338-4333

sciendo Journal of Hydrology and Hydromechanics

Mapping past, present and future dew and rain water resources for biocrust evolution in southern Africa

Marc Muselli[1, 2], Daniel Beysens[2, 3*]

[1] Università di Corsica Pasquale Paoli, Avenue du 9 septembre, BP 52, 20250 Corte, France.
[2] OPUR, 2 rue Verderet, 75016 Paris, France.
[3] Physique et Mécanique des Milieux Hétérogènes, CNRS, ESPCI Paris - PSL University, Sorbonne Université, Sorbonne Paris Cité, 10 rue Vauquelin, 75005 Paris, France.
[*] Corresponding author. Tel.: +33(0)689864717. E-mail: daniel.beysens@espci.fr

Abstract: Biocrust sustainability relies on dew and rain availability. A study of dew and rain resources in amplitude and frequency and their evolution is presented from year 2001 to 2020 in southern Africa (Namibia, Botswana, South Africa) where many biocrust sites have been identified. The evaluation of dew is made from a classical energy balance model using meteorological data collected in 18 stations, where are also collected rain data. One observes a strong correlation between the frequency of dew and rain and the corresponding amplitudes. There is a general tendency to see a decrease in dew yield and dew frequency with increasing distance from the oceans, located west, east and south, due to decreasing RH, with a relative minimum in the desert of Kalahari (Namibia). Rain amplitude and frequency decreases when going to west and north. Short-term dew/rain correlation shows that largest dew yields clearly occur during about three days after rainfall, particularly in the sites where humidity is less.

The evolution in the period corresponds to a decrease of rain precipitations and frequency, chiefly after 2010, an effect which has been cyclic since now. The effect is more noticeable towards north. An increase of dew yield and frequency is observed, mainly in north and south-east. It results in an increase of the dew contribution with respect to rain, especially after 2010. As no drastic changes in the distribution of biomass of biocrusts have been reported in this period, it is likely that dew should compensate for the decrease in rain precipitation. Since the growth of biocrust is related to dew and rain amplitude and frequency, future evolution should be characterized by either the rain cycle or, due to global change, an acceleration of the present tendency, with more dew and less rainfalls.

Keywords: Biocrust; Dew and rain evolution; Dew/rain ratio; Dew/rain correlation; Southern Africa; Climate change.

1 INTRODUCTION

Biocrust are typically found in drylands with arid or semi-arid ecosystems. In great interaction with the soil, biocrust concern cyanobacteria, lichens, algae and mosses. These organisms contribute strongly in the ecosystem's functioning and plant organization and are present all around the world.

Numerous works detail their physical, chemical and biological characteristics in semi-arid or arid climates. Negev (Jacobs et al., 2002; Kidron and Tal, 2012), Europe (Raggio et al., 2021), Spain (Cano-Díaz et al., 2018), China (Yao et al., 2019), USA (Aguirre-Gutiérrez et al., 2019) are a few examples. According to Chen et al. (2020), biocrust correspond to 30% of global drylands. It is in China, Australia, North America and Spain in Europe that are found the more studied biocrust sites. In the present study, a representative area for biocrust studies was chosen in a less investigated area, the southern part of Africa. Namibia, South Africa and Bostwana are the main countries involved in this study, representing 18 sites of measurement (7 in Namibia, 7 in South Africa and 4 in Bostwana, respectively). One should note that these locations are based on previous works of a few scholars within certain research sites and cannot obviously replace an objective map. A map of soil can help to locate biocrust, it is given in Fig. 1 together with the above studied sites.

Moisture from atmosphere (rainfall, fog, dew, vapor absorption) plays an important role in sustaining life in arid or semi-arid climates. Pan et al. (2010) concluded on the mutual enhanced effect between dew and artificially revegetation ecosystems in the arid desert ecosystem in Shapotou (China). Li et al. (2021a, b), in recent papers, determine that biocrust benefits from non-rainfall water deposition and modify their distribution in drylands soils. Dewfall can be presented as a critical source of water in deserts environments allowing to determine the sustainability of sand to stabilize planted vegetation (Zhuang and Zhao, 2017). Dew, fog and rain can play an important role for the development of biocrust in semi-arid regions. Kidron (2019) suspects dew to be a necessary water source for cyanobacteria. Biocrust alter non-rainfall distribution by depth, concentrating it in the surface (Li et al., 2021a, b). Biocrust can boost the use of non-rainfall water according to Ouyang et al. (2017). Büdel et al. (2009) conclude their study by noting that the time frequency of rain precipitations is more important than their amount.

The amount and frequency of rain and dew are then the main factors which influence the growth of biocrust. This paper aims to evaluate the evolution of these contributions to over a long period of time (20 years, from 2001 to 2020) in order to put in evidence the long term trend and extrapolate to the near future. Because certain data are lacking before 2011, a few analyses are restricted to 10 years (2011–2020).

The paper is organized as follows. After having reported on measurements and methods in Section 2, mainly concerning the physical model used to determine the dew yields, Section 3 is devoted to the main results with maps i) for dew and rain atmospheric deposition, ii) cumulative rainfall and dew yields

comparisons and iii) short time and longtime evolution of dew and rainfalls yield and frequency. A Section 4 is devoted to discussions and relation of the rain and dew studies with biocrust.

2 METEOROLOGICAL DATA AND METHODS

2.1 Dew yield estimation from meteorological data

In order to estimate the dew potential, Beysens (2016) developed an energy balance model which, thanks to some approximation, uses only a few classical meteorological data without adjustable parameters: cloud cover (N, oktas), wind speed (V, m s^{-1}), air temperature (T_a, °C), air relative humidity (RH, %) and dew point temperature (T_d, °C). Near the ground level where dew forms, in the atmospheric boundary layer, the contribution from water vapor (about 0.2–2% by volume) and, to a lower extent, carbon dioxide (about 0.03% in volume) is of great importance for the radiative balance, with radiation from water vapor being by far the more important of the two. The results are concerned with dew yields h [mm $(\Delta t)^{-1}$] where Δt corresponds to the period (in hours) of the analyzed data. It is assumed that the substrate emissivity is unity (which is close to the emissivity ≈ 0.98 of a wet substrate, see Trosseille et al., 2021) and is thermally insulated from below. The data can be obtained from the airport meteo stations by using the following formulation:

$$h = \left(\frac{\Delta t}{12}\right)(HL + RE) \tag{1}$$

The factor Δt is the measurement period of the data (here 6, 3 or 1 h. depending on the stations). The data for $h > 0$ correspond to condensation and $h < 0$ to evaporation, which have to be discarded. The quantity HL represents the convective heat losses between air and condenser, with a cut-off for windspeed $V > V_0 = 4.4$ m s^{-1} where condensation vanishes:

$$h = \begin{cases} \left(\frac{\Delta t}{12}\right)\left[0.06(T_d - T_a) + RE\right] & if\ V < V_0 \\ 0 & if\ V > V_0 \end{cases} \tag{2}$$

The quantity RE is the available radiative energy, which depends on air water content (measured by the dew point temperature T_d, in °C), site elevation H (in km) and cloud cover N (in oktas):

$$RE = 0.37 \times \left(\begin{array}{l} 1 + 0.204323H - 0.0238893H^2 - \\ \left(18.0132 - 1.04963H + 0.21891H^2\right) \times 10^{-3} T_d \end{array}\right) \times \left(\frac{T_d + 273.15}{285}\right)^4 \left(1 - \frac{N}{8}\right) \tag{3}$$

By filtering the rain and fog events and integrating the time series on a daily time-step corresponding to $h > 0$, calculated daily yields and their cumulated values are obtained. We give an example of calculation in Appendix 1.

2.2 Studied area

The study area (Fig. 1) is characterized by a spatial extent of about 3 000 000 km^2 between 15° to 35° south latitude and 13° to 30° for east longitude. In the following are detailed the different climate characteristics of the countries.

Namibia (824 292 km² surface area). The country shows three different climates, the most prevalent being semi-arid (Köppen-Geiger classification BSh) and hot desert (BWh). The less frequent is cold desert climates (BWk). The climate is characterized by great differences in day and nighttime temperatures, low rainfall and overall low humidity. Along the coast, the average annual precipitation does not exceed 15 mm. Inside the country, the continental plateau has a more contrasted situation with abundant precipitations (> 500 mm). The dry season, between May to October, correspond to little or no rainfall during July and August. Wildlife uses mainly waterholes and rivers when the water sources dry up. In desert areas, the average minimum temperature is cold and can fall below freezing at night. The wet season, between November to April, present daytime temperatures of about 30 °C with the first rains observed in November (mean rainfall 26 mm to a maximum in January with 91 mm). Sometimes, torrential downpours are observed in the afternoon up to March and April, where rainfall decrease and stops before the dry season.

Botswana (581 730 km² surface area). The climate is characterized as hot semi-arid, the dominant climate (Köppen-Geiger classification BSh), and hot desert (BWh). During summer months (November–March), a rainy season is observed with high temperatures. The mean annual rainfall varies from over 650 mm in the extreme northeast area (Chobe District) to a minimum of 250 mm in the extreme southwest part (Kgalagadi District). The winter season during May to August corresponds to the dry season with less than 10% of the annual rainfall. The variability of rainfall increases while the quantity decreases toward the south and west.

South Africa (1.22 million km² surface area). The country corresponds to a subtropical area, influenced by the vicinity of the oceans along the coastlines and the altitude of interior plateau (1 500 m in the dolerite-capped Roggeveld scarp in the south-west, to a height of 3 482 m in the KwaZulu-Natal Drakensberg). The country has several climatic zones depending on its geography: in the northwest, near the Atlantic coast stretching to the center of the country, the climate is mainly characterized by arid lime (BWh) or cold (BWk) deserts. In the south-east, the country offers a temperate climate with dry and hot (Csa) or warm (Csb) summers. Finally, along the southern coast of the country, one finds a hot (BSh) or cold (BSk) arid climate with steppes but also a temperate zone, along the ocean between the towns of George and Port Elisabeth with dry winters and hot summers (Cwa). The eastern part of the country, which is more mountainous, is characterized by a predominantly temperate climate, without a dry season, with hot to temperate (Cfb) or cold (Cfc) summers. Mean rainfall is about 460 mm with a large dispersion according to the location. Usually, the western Cape presents major rainfalls in winter whereas the rest of the country exhibits summer rainfalls.

The spatial distribution of rainfall between Namibia, Bostwana and South Africa presents some differences in space and time (New et al., 2000). In Namibia, for the locations of Dante Cave at the north of the country, summer rainfall is observed from October to April, with mean annual rainfall between 500 and 600 mm yr^{-1}, a value much less than the potential evapotranspiration estimated to 2900 mm yr^{-1} (Railsback et al., 2019). A similar behavior is observed at the frontier between Bostwana and South Africa (27°S, 21°E), with summer rainfall. The situation is more complex in South Africa. According to the location, one observes winter rainfall as in Cape Town with precipitations mainly during April to September, weak precipitations but year-round in George and summer rainfall with a dry winter in Pretoria (Railsback et al., 2019).

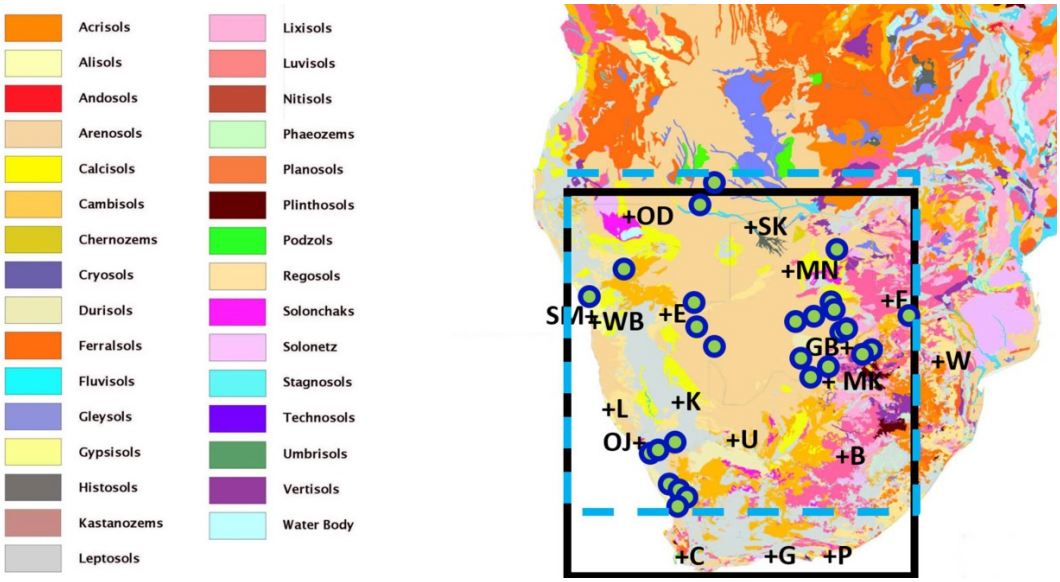

Fig. 1. Map of soils in the studied area (from Jones et al., 2013). Black rectangle and black letters are airport stations. The interrupted blue rectangle corresponds to the biocrust sites (green circles, see Chen et al., 2020).

Table 1. Sites where atmospheric data are collected (7 stations in Namibia, 4 stations in Bostwana and 7 stations in South Africa). They are sorted according to their longitude (west to east). The sky condition data availability (% of the total sky conditions data) is reported for each station.

Country Name	Site	Abbreviations	Latitude	Longitude	Altitude (m asl)	Distance to the sea (km)	data period	Sky conditions data (%)
Namibia	Swakopmund	SM	22° 40' 0'' S	14° 34' 0'' E	61	8	2010-2020	52.4
Namibia	Walvis Bay	WB	22° 58′ 47″ S	14° 38′ 43″ E	86	14	2010-2020	52.4
Namibia	Luderitz	L	26° 41′ 15″ S	15° 14′ 34″ E	131	1	2006-2020	0.0
Namibia	Ondangwa	OD	17° 52′ 41″ S	15° 57′ 09″ E	1099	385	2011-2020	47.7
Namibia	Oranjemund	OJ	28° 35′ 05″ S	16° 26′ 48″ E	5	6	2005-2020	0.0
Namibia	Eros	E	22° 36′ 44″ S	17° 04′ 50″ E	1699	266	2011-2020	45.2
Namibia	Keetmanshoop	K	26° 32' 13'' S	18° 06′ 40″ E	1069	285	2011-2020	40.0
South Africa	Cape Town	C	33° 58′ 10″ S	18° 35′ 50″ E	46	3	2001-2020	100.0
South Africa	Upington	U	28° 24′ 04″ S	21° 15′ 35″ E	844	432	2001-2020	77.3
Botswana	Shakawe	SK	18° 22′ 25″ S	21°50′ 00″ E	1008	895	2005-2020	100.0
South Africa	George	G	34° 0' 20'' S	22° 22' 42'' E	197	7	2001-2020	89.9
Botswana	Maun	MN	19° 59' 0'' S	23° 26' 0'' E	945	1106	2001-2020	100.0
South Africa	Mahikeng	MK	25° 48' 27"S	25° 32' 40" E	1274	680	2001-2020	65.6
South Africa	Port Elizabeth	P	33° 59' 5'' S	25° 37' 2'' E	68	3	2001-2020	100.0
Botswana	Gaborone	GB	24° 33′ 19″ S	25° 55′ 06″ E	1006	695	2001-2020	99.9
South Africa	Bram Fischer	B	29° 05′ 38″ S	26° 18′ 14″ E	1349	418	2001-2020	76.1
Botswana	Francistown	F	21° 10' 0'' S	27° 29' 0'' E	1002	726	2002-2020	100.0
South Africa	Wonderboom	W	25° 39′ 13″ S	28° 13′ 27″ E	1240	460	2005-2020	88.6

2.3 Extraction data

All ground stations are installed on international or national airports where standard meteorological parameters are measured. The meteorological stations meet the data measurement standards of the World Meteorological Organization. Air T_a (°C) and dew T_d (°C) temperatures, relative humidity (RH, %), atmospheric pressure (P, Pa) are measured in a meteorological shelter, 1.5 m from the ground. The windspeed (V, km h^{-1}) and direction (sectors or degrees) are measured at 10 m from the ground. Note that wind speed can be extrapolated at any height z above the ground by the classical logarithmic variation (see e.g. Pal Arya, 1988) $V(z) = V_{10} \ln\left(\frac{z}{z_c}\right) / \ln\left(\frac{10}{z_c}\right)$ where V_{10} is windspeed at 10 m and z_c is the roughness length (generally ≈ 0.1 m in flat areas) where $V = 0$. Available data were extracted from the online data base "Weather Underground" (Weather Underground database, 2021) during a period of maximum 20 years (2001–2020) with a minimum of 10 years (2011–2020) depending on data availability (Table 1).

Dew yields have been computed from Eq. (2) using the above standard meteorological databases extracting air and dew point temperatures (T_a and T_d, °C), relative humidity (RH, %), wind speed (km h^{-1} to be transformed in m s^{-1}), wind direction (sectors), absolute pressure (hPa) and sky cover. An hourly time-step for measured data is accessible except for Oranjemund and Luderitz (Namibia) where two time-steps are available (Oranjemund: 6 h on 2005–2014 and 3 h on 2014–2020); Luderitz (6 h on 2006–2012 and 3 h on 2012–2020).

Wind direction values in degrees have been computed from wind direction sectors (N, NNE, NE, E, ESE, SE, S, etc.) using

a standard law of proportionality: 0° for north, 180° for south and calculation of all intermediate values with respect to these references.

The sky cover was considered variable if it varies by one or more of the reported values (CLR, FEW, SCT, BKN, or OVC) during the period of observation (NOAA's national weather service glossary, 2021). Cloud cover in oktas was computed from the nightly observation of sky cover using the correspondence listed in Table SM2 in Supplementary Materials, which was used in a previous work (Muselli et al., 2020). However, cloud cover is sometimes not available at night on some sites (the missing percentage of total values is noted for each site in Table 1). When the sky conditions data are unavailable, we imposed to these sites three possible values, corresponding to the most probable: $N = 0$, 1 and 3.

Measured rainfall data, available on a daily time step, are extracted from the meteorological data base (Infoclimat database, 2021). All data are obtained for the same stations as used for dew calculation except for Swakopmund where the rainfall data of Walvis Bay are used (both sites are only 25 km apart).

2.4 Kriging maps

Kriging methodologies are mainly used for mapping spatial distribution of a given variable. The classical algorithm is presented in Appendix 2. Belkiri et al. (2020) use Kriging to study ground water composition. Tomaszkiewicz et al. (2016) propose ordinary Kriging to develop dew maps integrating projected climate changes in the Mediterranean basin. Martinez et al. (2017) present median polish Kriging (MPK) for space-time analysis of monthly precipitation in Colombia. Pue et al. (2021) introduce a Kriging-based Gaussian process for the evaluation for the prediction of soil water retention in tropical and temperate climates. Other studies combine Kriging models for the estimation of rainfall with Lagrangian (Amani and Lebel, 1997) or Bayesian (Lima et al., 2021) approaches.

3 RESULTS

3.1 Evolution

For each site, dew (subscript $i = d$) and rain (subscript $i = r$) monthly yields h_i (mean, min, max in mm) are computed. Annual dew yield (mm) is deduced by adding the monthly h_i:

$$H_i = \sum_{t=1}^{12} h_i(t) \tag{4}$$

In order to estimate the evolution, monthly dew yields can be fitted by a linear regression on the measured period:

$$h_i(t) = \alpha_i t + h_{i,0} \tag{5}$$

With t in month, the coefficient $\alpha_i = dh_i / dt$ represents the monthly evolution rate.

3.2 Dew yields

3.2.1 Data description

Mean, minimum and maximum dew yields are calculated on monthly and yearly time bases and reported in Table SM3 in Supplementary Materials. The calculated annual dew yields show significant variations depending on the sites studied even within the same country (Fig. 2 and Table SM3).

In Namibia, the sites on the west coast (Walvis Bay, Luderitz, Swakopmund and Oranjemund) benefit from high dew yields (> 10 mm yr^{-1}) mainly explained by the high humidity due to the vicinity of the Atlantic Ocean. For example, mean dew yields in the range 12.6 to 38.2 mm yr^{-1} (for $N_{\text{missing}} = 0$, 1, 3) have been obtained in Swakopmund and Walvis Bay, located near the Namib national Park, corresponding to mean monthly dew yields between 2.8 and 6.9 mm. For both stations, dewy days represent between 79.1 (Swakopmund, $N = 3$) and 85.8% (Walvis Bay, $N = 0$) of the year. On the other hand, the stations established in the interior of the country suffer from very low annual dew yield (< 5 mm yr^{-1}). For example, Eros, Keetmanshoop and Ondangwa, respectively located at about 250 and 350 km from the ocean, exhibit annual dew yields less than 4.9 mm. In Keetmanshoop, monthly dew yields are very weak with a mean of 0.1–0.3 mm and a monthly maximum of up to 1.8 mm. For Eros and Keetmanshoop, only 10–20% of the days are dewy (min = 8.7% and max = 18.4%), while for Ondangwa it is 25% or even 15% ($N = 0$ for missing data) or even one day a week in the most unfavorable case ($N = 3$ for missing data).

The situation is more homogeneous in Botswana. The mean annual dew yields are between 6.9 and 16.2 mm depending on the sites (annual dew yield min = 1.8–6.6 mm and max = 16.5–26 mm), with monthly yields averaging between 0.6 and 1.4 mm (min = 0 mm and max = 4.2–5.9 mm).

Except in Upington (mean < 5.5 mm), located in the northern Cape Province of South Africa on the banks of the Orange River, and Mahikeng, near to the Bostwana frontier (mean < 9.8 mm), all the South Africa country exhibits mean annual dew yields more than 15 mm. For example, Cape Town, Port Elizabeth and George cities, on the south coast, or Wonderboom and Bram Fischer (near respectively Pretoria and Johannesburg), present averaged annual dew yields of more than 18.3 mm, and up to 27 mm. Whereas the maximum monthly dew yields do not exceed 4.7 mm in Upington and Mahikeng, the other cities present monthly dew yields larger than 4.5 mm, and up to 7.7 mm.

The spatial distribution of dew yields was determined by Kriging (Fig. 2, for $N = 0$, 1, 3 for missing data). Maps of mean annual dew yields are presented in (Figs. 2a, b, c). As expected and described in the literature (Henschel et al., 2007; Soderberg, 2010), dew exhibits the highest yields along the west coast of Namibia corresponding to the Namib Desert. This desert represents about 81 000 km² and stretches over 1,500 km along an 80 to 160 km wide north-south coastal strip along the Atlantic Ocean. One also clearly observes the decrease in yields inland, especially from the central plateau towards the desert of Kalahari representing a surface of 900 000 km² with 600 000 km² in Namibia. However, one notes that in these critical areas, monthly dew yields can reach mean and maximal values up to 2–3 mm and 6–8 mm, respectively. Note that the biocrust sites are located in regions of moderate dew yield.

More generally, there is a tendency to see a decrease in dew yield with increasing distance from the oceans, located W, E and S. A clear decrease in nocturnal RH from west to east is obvious (Fig. 2d), with the largest dew yields (Fig. 2a, b, c) corresponding to the regions of highest RH.

3.2.2 Evolution map 2001–2020

In Fig. SM1 (Supplementary Materials) are plotted the evolution of the summed value of dew yield, $\text{sum}(h_d) = \int_{t_0}^{t} h_d dt$ on a monthly basis, with t_0 the starting year (see Table 1). The dew rate is either nearly constant during the period

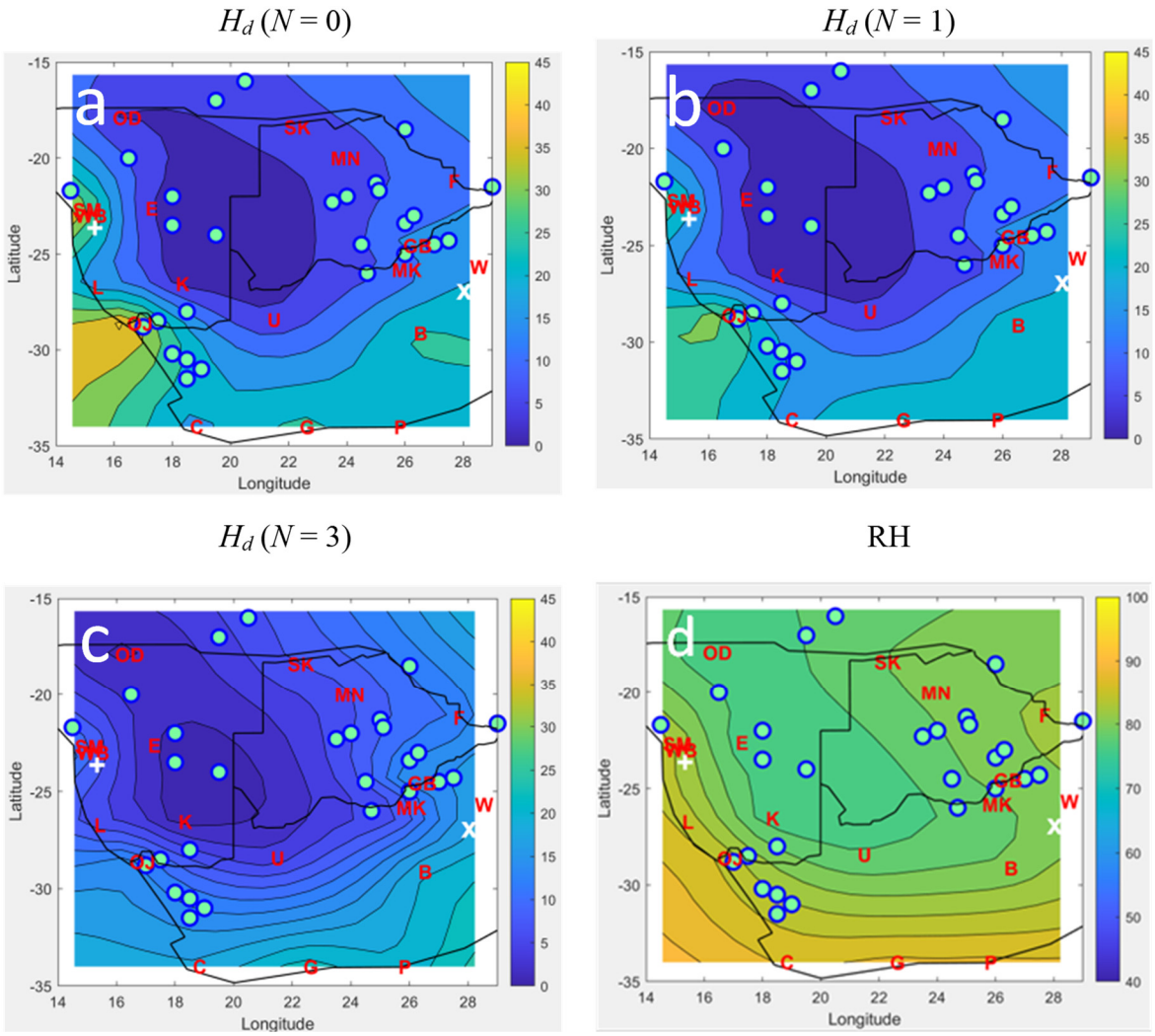

Fig. 2. (a, b, c): Map of annual dew yield H_d (in mm) in the period 2001–2020 corresponding to three scenarios for missing N data (see text and Table 1). (d): Mean nocturnal RH (%) during dew events. Red letters: Meteo sites (see Table 1); circles: Biocrust sites according to Chen et al. (2020); right cross: Gobabeb site studied by Henschel et al. (2007) and Soderberg (2010); inclined cross: Potchefstroom site studied by Baier (1966).

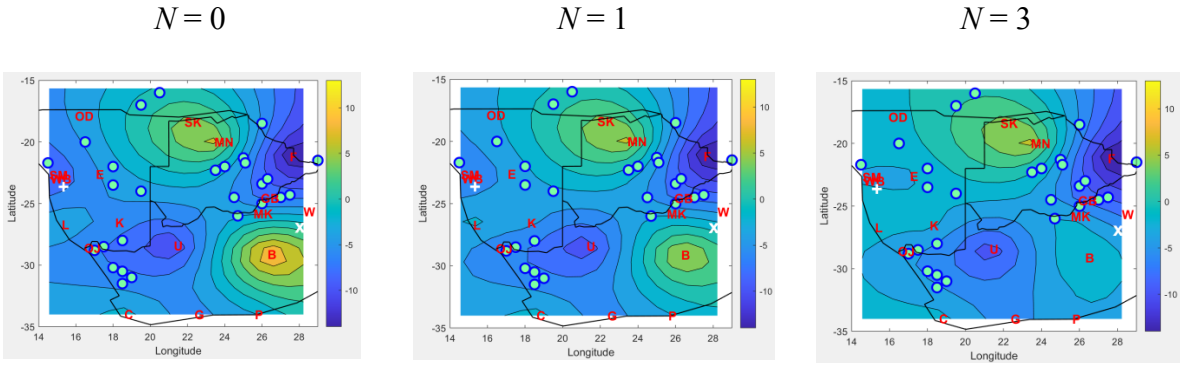

Fig. 3. Difference between 2020 and 2011 annual dew yields (mm) for three scenarios corresponding to the missing N data (see text and Table 1). Red letters: Measurement sites (see Table 1); circles: biocrust sites according to Chen et al. (2020); right cross: Gobabeb site studied by Henschel et al. (2007) and Soderberg (2010); inclined cross: Potchefstroom site studied by Baier (1966).

(Swakopmund, Walvis Bay, Eros, Keetmanshoop, Cape Town, Port Elizabeth, Gaborone, Bram Fischer) or increases (Luderitz, Oranjemund, Upington, Shakawe, George, Maun, Mahikeng, Wonderboom) after year 2010. One will see in Section 3.3 that the year 2010 is also the year where rainfalls significantly decrease.

By considering the period where meteorological data are available on all sites (2011–2020), one can determine the evolution of the average yield at any point in the study area by subtracting annual dew yields between years 2020 and 2011. Figure 3 shows the difference $\Delta h_d = h_d(2020) - h_d(2011)$. One sees that the evolution is different according to the locations.

Although dew decreases in two places where it was the most abundant (SW and NE to a lesser extent), it increases in the NW (Ondangwa, Eros) where dew was the lowest. A noticeable increase is seen in *N* (Maun, Shakawe) and SE regions (Bram Fischer). One notes that the biocrust sites are mostly located in regions of null or moderate dew decrease.

3.3 Rainfall

3.3.1 Data description

Table 2 and Fig. 4 present annual and monthly mean, min and max rainfall extracted from Infoclimat database (2021) for the studied period (sites: See Table 1). From a general point of view, rain decreases towards W and N. As described below, cities located at the Namib Desert exhibit lower rain precipitations: 13.4 mm in Swakopmund and Walvis Bay (i.e. 1% of rainfall events by year) and in a lesser extent, Oranjemund with a mean annual rainfall of about 42 mm (i.e. 5% of rainfall events by year). In these areas, precipitations are very erratic, with no rain for several months and few intense precipitations events. In the inland, rainfall is slightly more abundant with annual averages of 115, 189 and 306 mm for Keetmanshoop, Ondangwa and Eros, respectively. Although these areas can exhibit months without any rain, the monthly averages are greater than 10 mm. However, one notes that less than 11% of the days of the year are rainy days (10.9%, 5.3% and 3.7% in Eros, Ondangwa and Keetmanshoop, respectively).

For Botswana, the situation is more homogenous, with a mean rainfall of 463.2 mm observed in the four cities of Gaborone, Maun, Francistown and Shakawe. With one or two months during the year without rain, this region present mean regular monthly rainfall of about 39 mm, with 13.4% of the days being rainy.

South Africa exhibits a contrasted behavior. The regions located along the ocean in the south and south east of the country have heavy rainfall with annual amounts greater than 500 mm (Mahikeng, Cape Town, George, Port Elizabeth, Bram Fischer, Wonderboom), with up to 715 mm in George (18–31% of the year are rainy days). Monthly averages are important with a mean of about 49.6 mm (23.5% rainy days in the year). Upington is an exception, located further west of the country, but with lower rainfall (285 mm year^{-1} with a mean of 23.8 mm month^{-1}).

One notes a marked decrease in precipitation during the 20 years period, all sites show $\alpha(h_r) < -0.2$, particularly in Eros and Ondangwa in Namibia, the 4 cities of Bostwana, and George and Bram Fisher in South Africa. Coastal sites in Namibia (Oranjemund, Luderitz, Swakopmund and Walvis Bay) show a smaller decrease ($\alpha(h_r) \approx 0$). When looking at Fig. SM1 in Supplementary Materials (summed values of h_r), one realizes that the main change in rainfalls occurred in 2010. It is from this year that a gradual change in rain can be observed.

The rainfall repartition presented in Table 2 is confirmed by the Kriging map obtained for the annual mean rainfall (Fig. 4a). Rainfall increases markedly from west to east (0–200 mm at the Atlantic coast to 600 to 700 measured at the south-east of South Africa). The same trend is observed with the monthly mean and maximum rainfall volumes (Figs. 4b, c). The monthly average varies from 0 to 20 mm (W) to 50 to 60 mm (SE).

3.3.2 Evolution map

By subtracting the precipitation values between years 2020 and 2011 one can map (Fig. 5) the difference $\Delta h_r = h_r(2020) - h_r(2011)$. Although the mean precipitation decreases, the evolution is different depending on the locations. Rain mainly decreases in the north regions (Maun, Shakawe, Eros), where dew was seen to increase during the same time period (Fig. 3). A small zone in south west (Cape Town, Oranjemund) exhibits a precipitation increase. It is worthy to note that the biocrust zones are mostly in the regions that experienced a decrease in rain.

3.4 Correlation between dew and rain yields

The occurrence of dew is related to the presence of atmospheric high humidity. Some correlations therefore exist between the frequency and amplitude of rain and the amplitude of dew yields. Two kinds of correlation can occur, a temporal correlation, where dew forms after rain events, which have increased the atmosphere RH, and an amplitude correlation. Both correlations are studied in the following.

Table 2. Mean, minimum and maximum yearly (H_r) and monthly (h_r) rainfall calculated from meteorological from 2001 to 2020 are fitted to Eq. (5) with free parameters $\alpha_r = dh_r/dt$ and $h_{r,0}$.

Site	H_r (mm yr^{-1})			h_r (mm)			α_r (mm month^{-1})	$h_{r,0}$ (mm)	year frequency (%)
	Mean	Min	Max	Mean	Min	Max			
Swakopmund	**13.4**	0.0	56.0	**1.1**	0.0	41.2	–0.005	1.5	0.9
Walvis Bay	**13.4**	0.0	56.0	**1.1**	0.0	41.2	–0.005	1.5	0.9
Luderitz	**18.6**	1.0	83.5	**12.4**	0.0	64.1	–0.024	3.2	1.8
Ondangwa	**189.4**	6.6	453.0	**15.8**	0.0	155.0	–0.283	32.9	5.3
Oranjemund	**42.2**	7.0	225.8	**3.5**	0.0	115.6	–0.030	6.4	5.0
Keetmanshoop	**115.7**	20.8	278.4	**9.6**	0.0	145.1	–0.044	11.0	3.7
Cape Town	**542.1**	249.0	888.8	**45.2**	0.0	238.0	–0.148	57.0	24.8
Upington	**285.1**	53.0	518.4	**23.8**	0.0	261.4	–0.167	38.3	10.4
Shakawe	**423.5**	8.4	1072.3	**35.3**	0.0	447.1	–0.493	82.8	13.0
George	**715.4**	333.0	1223.7	**59.6**	0.0	290.5	–0.260	79.7	30.7
Maun	**482.8**	20.0	1115.9	**40.2**	0.0	375.3	–0.468	79.8	14.9
Mahikeng	**582.8**	182.0	1158.1	**48.6**	0.0	320.3	–0.135	55.5	19.7
Port Elizabeth	**641.8**	308.0	1103.8	**53.5**	0.0	235.5	–0.171	64.2	26.8
Gaborone	**464.3**	80.2	1023.3	**38.7**	0.0	372.5	–0.374	68.0	11.9
Bram Fischer	**590.0**	160.0	1190.0	**49.2**	0.0	274.7	–0.253	68.8	20.2
Francistown	**482.3**	46.2	1199.9	**40.2**	0.0	423.3	–0.342	66.2	13.6
Wonderboom	**497.5**	123.0	769.9	**41.5**	0.0	183.6	–0.095	49.9	18.5

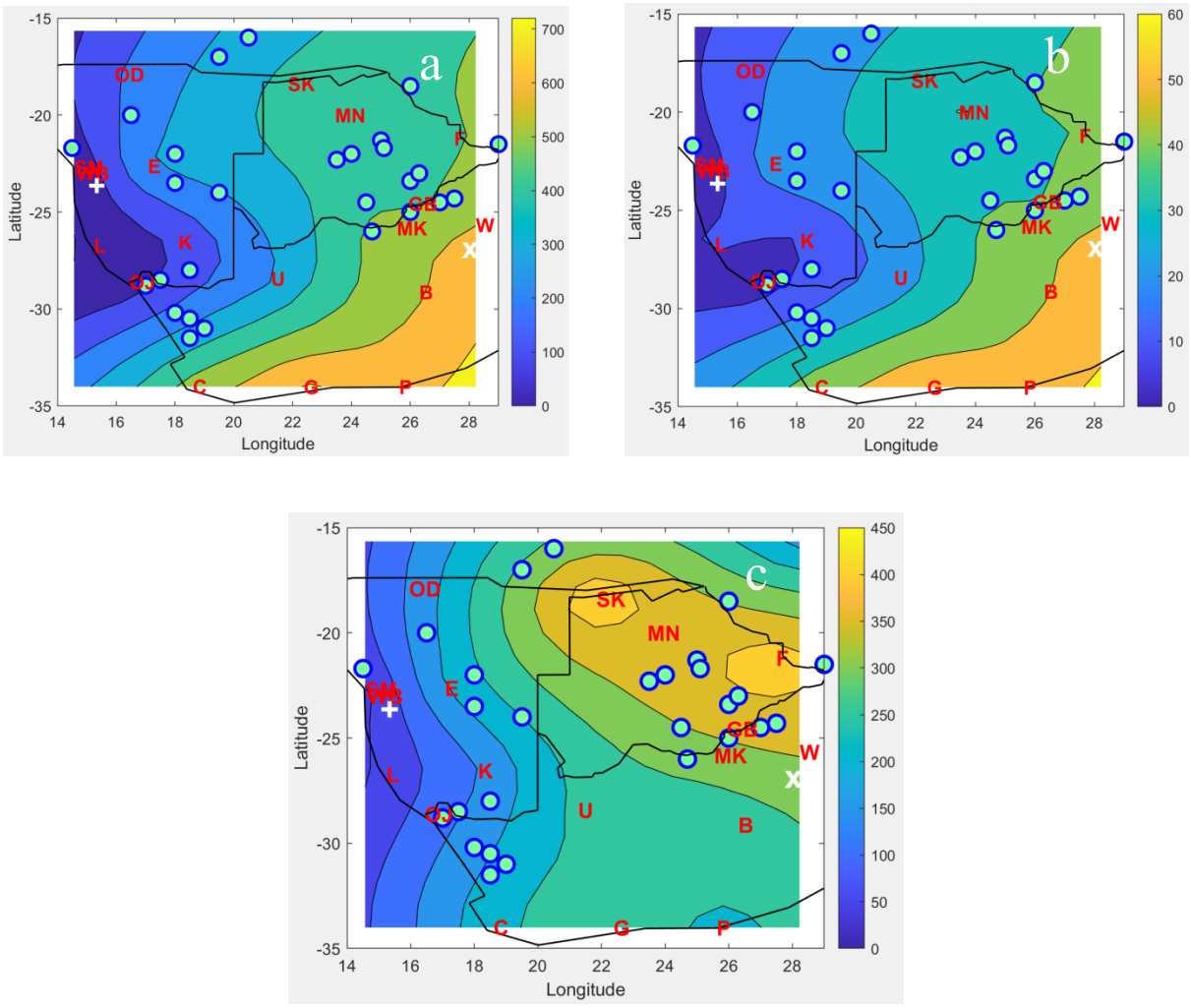

Fig. 4. Mean rainfalls (mm) during the period 2001–2020. (a) Mean annual rainfall. (b) Mean monthly rainfall. (c) Maximum monthly rainfall. Red letters: Measurement sites (see Table 1); circles: biocrust sites according to Chen et al. (2020); right cross: Gobabeb site studied by Henschel et al. (2007) and Soderberg (2010); inclined cross: Potchefstroom site studied by Baier (1966).

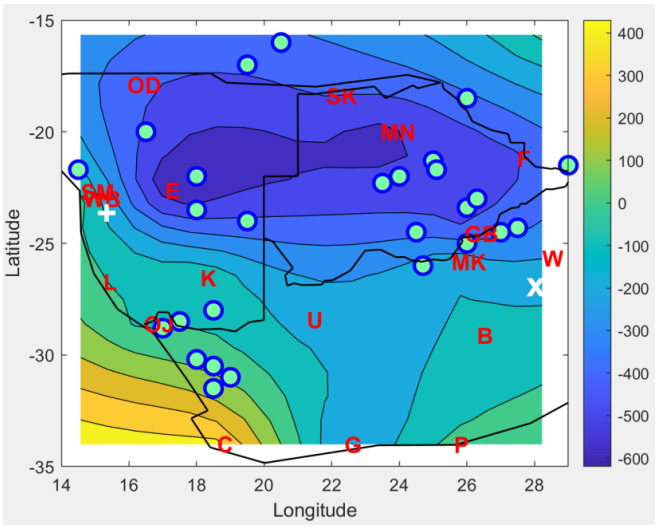

Fig. 5. Difference between 2020 and 2011 of the annual rainfalls (mm). Red letters: Measurement sites (see Table 1); circles: biocrust sites from Chen et al. (2020); right cross: Gobabeb site studied by Henschel et al. (2007) and Soderberg (2010); inclined cross: Potchefstroom site studied by Baier (1966).

3.4.1 Temporal correlation

The temporal correlation between rainfall and dew yield is evaluated by a correlation coefficient r between the daily rainfall, $h_r(t)$, and the time-shifted daily dew yield, $h_d(t+\tau)$, estimated at the same location. The delay time τ corresponds to the previous and next days of time t and is counted in days in the interval [–31, +31]. The covariance between $h_d(t+\tau)$ and $h_r(t)$ is calculated as:

$$C\left[h_r(t), h_d(t+\tau)\right] = \frac{1}{n}\sum_{j=1}^{n}\left(h_{r,j}(t)-\overline{h_r}\right)\left(h_{d,j}(t+\tau)-\overline{h_d}\right) \quad (6)$$

With $\sigma_{h_r}, \sigma_{h_d}$ the rain and dew standard deviation, respectively, one infers the correlation coefficient:

$$r\left[h_r(t), h_d(t+\tau)\right] = \frac{C\left[h_r(t), h_d(t+\tau)\right]}{\sigma_{h_r}\sigma_{h_d}} \quad (7)$$

Considering that $-1 < r < 1$, a negative correlation leads to an opposite evolution of h_r and h_d, a positive correlation corresponds to the two variables moving in the same trend and $r \to 0$ means that both variables are not correlated.

The r correlation plots for each meteorological site according to the three N scenarii are reported in Fig. 6. One observes the following:

(i) For $\tau < 0$, no correlations between dew and rain amplitudes are observed (mostly $r < 0.05$). It means that a rain event at a given day does not explain dew events a few days earlier.

(ii) For $\tau = 0$, all curves present negative values for r, with amplitude in the range between –0.3 and 0.1. This is due to the fact that, in the calculation of the dew yields in Section 2.1, one had to discard the days with rain.

(iii) For $\tau > 0$, some correlation can be observed for $\tau \leq 3$ days. For the Eros and Keetmanshop sites, $r = 0.29$ ($N = 3$) and $r = 0.18$ ($N = 1$). For Mahikeng and Upington, $r = 0.12$ ($N = 1$) and $r = 0.13$ ($N = 0$). To a lesser extent, for Bram Fischer $r = 0.097$ for $N = 1$. These values thus indicate a weak but real positive correlation between rain and dew events. It means that, due to the increase of atmosphere humidity after rain events, dew events are more likely to be observed between one to three days after rainfalls.

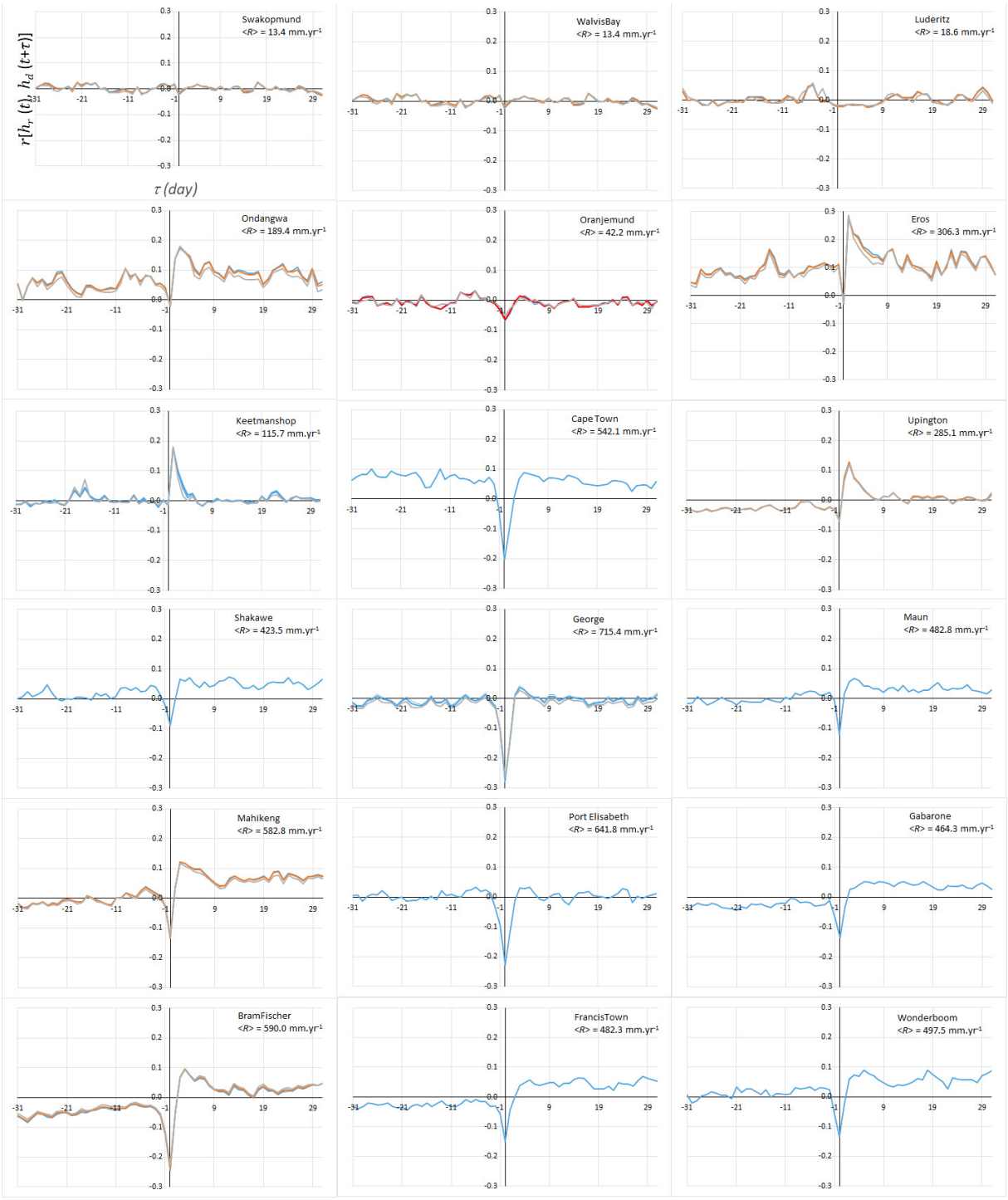

Fig. 6. Daily correlation coefficients $r\left[h_r(t), h_d(t+\tau)\right]$ for time $\tau \epsilon [-31 - +31]$ days. For stations with incomplete cloud cover data, the curves are presented assuming $N = 0$ (blue), $N = 1$ (red) and $N = 3$ (grey).

The correlation dew-rain is most noticeable (Ondangwa, Eros, Keetmanshop; Upington, Mahikeng, Bram Fisher) when the distance from the ocean increases, the atmosphere RH then decreases (see Fig. 2d). In contrast, for stations close to the coast in arid climate (distance < 15 km) and with low annual rainfall (H_r < 50 mm) but large RH, such as Luderitz, Oranjemund, Swakopmund and Walvis Bay, the correlation is very low regardless of the τ value. For the cities of Cape Town, Port Elizabeth and George, presenting a more temperate climate, the correlation shows at most a weak increase for τ < 4 to 5 days (with r < 0.1). All these sites have an altitude below 200 m.

Whatever is the N scenario, for altitudes between 800 m and 1700 m asl and > 200 km away from the ocean, the correlation is clearer with values of r showing a steady increase at Eros (1700 m asl, 266 km from the ocean), Keetmanshoop (1069 m asl, 285 km from the ocean). Ondangwa (1099 m asl, 385 km from the ocean) and Bram Fischer (1349 m asl, 418 km from the ocean) show a correlation with r > 0.1, respectively for τ = 2 and 3. For the other mountainous stations, the correlation coefficients exhibit values that does not exceed 0.1, with τ = 5 for Gaborone (r = 0.0532) or τ = 3 for Maun (r = 0.0665).

3.4.2 Summed dew and rain yields

One now investigates the correlation between the cumulative dew and rain monthly yields, $\mathrm{sum}(h_d) = \int_{t_0}^{t} h_d dt$ and $\mathrm{sum}(h_r) = \int_{t_0}^{t} h_r dt$, respectively, with t_0 the starting time (see Table 1). Each data point will thus correspond to a monthly mean value. For each month, a ratio $a(t)$ is calculated:

$$a(t) = \frac{[\mathrm{sum}(h_d)]_t}{[\mathrm{sum}(h_r)]_t} \quad (8)$$

In Fig. 7a the $\mathrm{sum}(h_d)$, the $\mathrm{sum}(h_r)$ and their ratio $a(t)$ for two sites (Upington and Cape Town sites) are reported (at small times the dispersion is large because the smoothing effect of the summation is still weak). In Cape Town, both rain and dew amounts are nearly linear during the research period, with a decrease in rainfall rate after 2010 while the dew rate remains constant. In Upington, one observes a decrease in the rain amount and an increase in the dew amount after 2010. For sake of comparison in the whole time period, the data (Fig. 7b) can be fitted to a mean constant value

$$a(t) = a_0 \quad (9)$$

The values of a_0 according to the three N scenarios are summarized in Table 3. Taking into account all stations, the parameter a_0 shows a large variability: $\overline{a_0}$ = 0.4 ± 0.8 (N = 0), $\overline{a_0}$ = 0.3 ± 0.6 (N = 1) and $\overline{a_0}$ = 0.15 ± 0.27 (N = 3). This variability is due to the small number and erratic character of the precipitations in arid areas. When the very small quantities of rain at these sites (Namib Desert: Oranjemund, Luderitz, Swakopmund and Walvis Bay) are removed, the variability of values becomes much smaller ($\overline{a_0}$ = 0.022 ± 0.008 (N = 0), $\overline{a_0}$ = 0.020 ± 0.009 (N = 1) and $\overline{a_0}$ = 0.017 ± 0.011 (N = 3)).

The parameter $\overline{a_0}$ is mapped by the Kriging method in Fig. 8. One can clearly observe the increasing importance of dew in

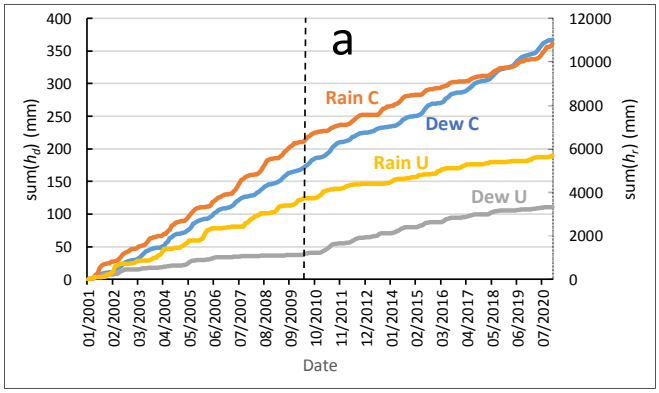

Fig. 7. Two typical evolutions (Upington U and Cape Town C sites) of dew and rain summed yields in the studied period (2001–2020). The vertical dotted line corresponds to year 2010 where rainfalls begin to significantly decrease. (a) sum(h_d) and sum(h_r) with N = 0 missing data scenario (see text and Table 1). (b) Ratio $a(t)$ = [sum(h_d)]$_t$ / [sum(h_r)]$_t$. The horizontal straight lines are fits to $a(t)$ = a_0 = constant.

Table 3. Ratio dew/rain summed amplitudes a_0 (Eq. 9) according to different N assumptions for the missing data (see text and Table 1).

Site	a_0 (N = 0)	a_0 (N = 1)	a_0 (N = 3)
Swakopmund	2.384	1.793	0.792
Walvis Bay	2.444	1.841	0.832
Luderitz	1.154	0.940	0.569
Ondangwa	0.023	0.016	0.006
Oranjemund	0.858	0.651	0.282
Eros	0.014	0.011	0.006
Keetmanshoop	0.020	0.014	0.006
Cape Town	0.028	0.028	0.028
Upington	0.017	0.015	0.012
Shakawe	0.011	0.011	0.011
George	0.031	0.027	0.024
Maun	0.007	0.007	0.007
Mahikeng	0.013	0.011	0.007
Port Elizabeth	0.026	0.026	0.026
Gaborone	0.028	0.028	0.028
Bram Fischer	0.034	0.032	0.029
Francistown	0.018	0.018	0.018
Wonderboom	0.034	0.034	0.034

the total precipitations along the Namibian coast and more generally the dependence of a on longitude. It corroborates the fact that the distance from the ocean, which controls the atmosphere RH (see Fig. 2), is the important parameter for the formation of dew. Toward the west, dew increases (Fig. 2) and rain decreases (Fig. 4), leading to an increase in a.

The variation of the ratio a between 2020 and 2011 is reported in Fig. 9. One verifies the general increase of the contribution of dew with respect to rain, especially towards west.

3.5 Time period of events

Because the frequency or time period between rain events is also an important parameter, which in itself can control the biocrust growth, we investigate below this parameter for rain only, dew only and dew plus rain. For that purpose, one considers the histogram of rain, dew and rain plus dew events (Fig. 10) where two important parameters can be extracted, the mean time period between events, θ_0 (in days) and the maximum time period, θ_M (in days).

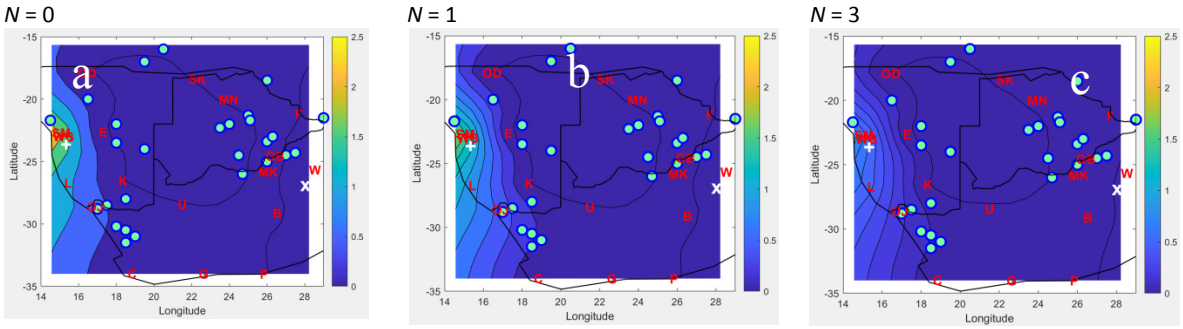

Fig. 8. Map of ratio a_0 corresponding to the average of a = sum(dew)/sum(rain) (Eqs. 8, 9) for the period 2001–2020 and three scenarios for missing N data (see text and Table 1). Letters: meteo sites; circles: biocrust sites according to Chen et al. (2020); right cross: Gobabeb site studied by Henschel et al. (2007) and Soderberg (2010); inclined cross: Potchefstroom site studied by Baier (1966).

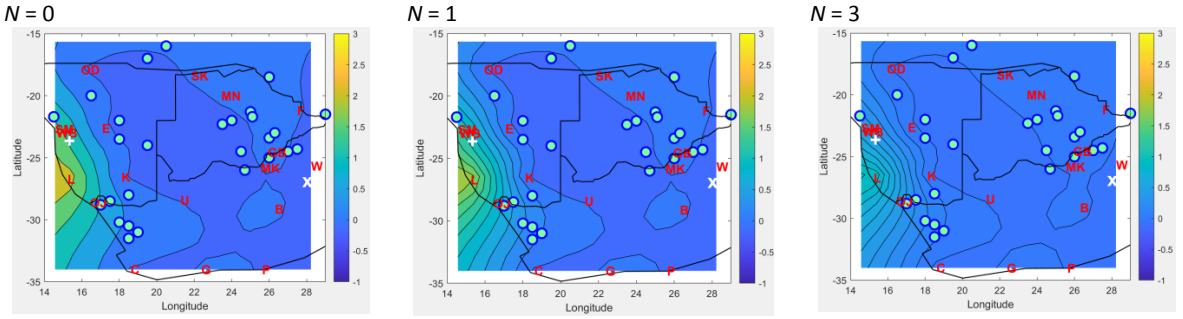

Fig. 9. Variation between 2020 and 2011 of the ratio a_0 = sum(dew)/sum(rain), corresponding to 3 scenarios for missing N data (see text and Table 1). Letters: meteo sites; circles: biocrust sites according to Chen et al. (2020); right cross: Gobabeb site studied by Henschel et al. (2007) and Soderberg (2010); inclined cross: Potchefstroom site studied by Baier (1966).

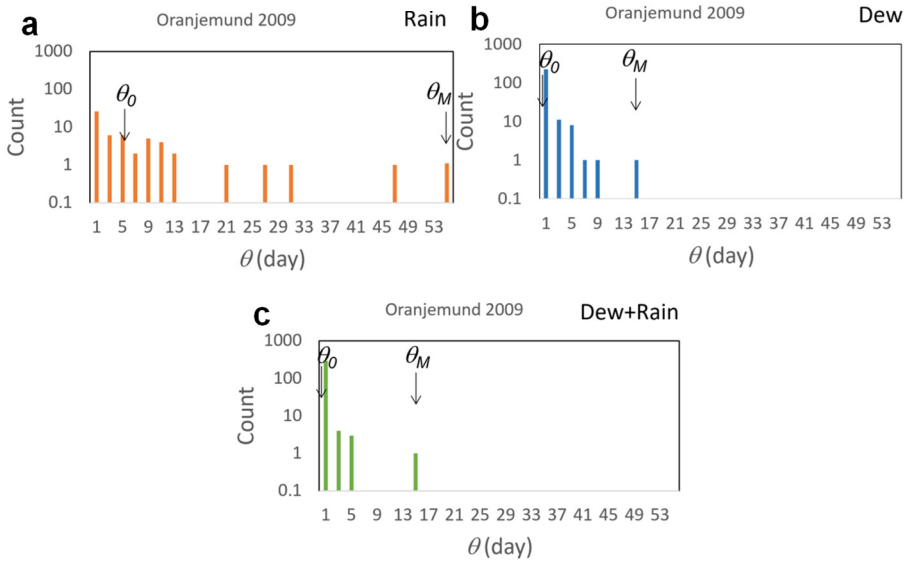

Fig. 10. Typical histograms of time period θ (day) beetween (a) rain events, (b) dew events (c) rain and dew events. θ_0 is the mean time and θ_M is the maximum time. Note that some dew or rain events can disappear in the histogram dew + rain because dew or rain events occur during the dew or rain time periods.

The evolution of θ_0 and θ_M can be then considered (Fig. SM2) and maps of mean values can be drawn for the considered period (Fig. 11), with the difference between 2011 and 2020 values (Fig. 12). Some curves are interrupted due to the lack of data.

One first notes from Figs. 10 and SM2 (in Supplementary Materials) that the number of events is larger for dew than for rain. In addition, the timescale for mean and maximum time period between events is much larger for rain than for dew, a difference which can reach two orders of magnitudes. It results from the above observations that the dew events will determine the behavior of the dew + rain time period (see Fig. SM2, Figs. 11–12).

When comparing the maps of dew and rain mean annual times (Fig. 11) and dew and rain amplitudes (Figs. 2 and 4), one observes a strong correlation between the zones of large times and low yield, and short times and high yield. This simply means that large water yields correspond to frequent dew or rain events.

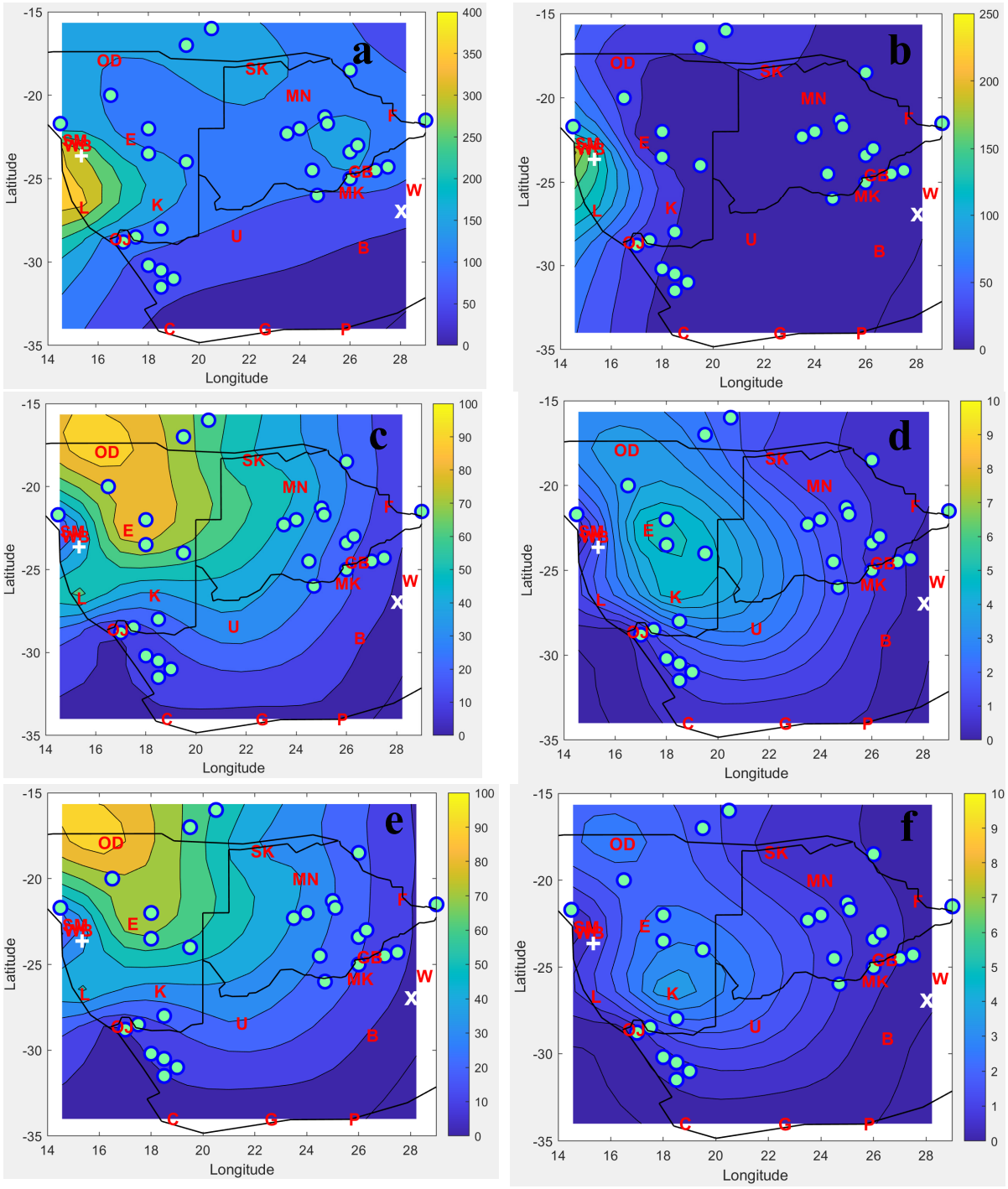

Fig. 11. Annual mean in the period 2001–2020 of the maximum time θ_M (day) (left column) and mean time θ_0 (day) (right column). (a), (b): Rain; (c), (d): Dew; (e), (f): Rain+dew. Red letters: Measurement sites (see Table 1); circles: biocrust sites according to Chen et al. (2020); right cross: Gobabeb site studied by Henschel et al. (2007) and Soderberg (2010); inclined cross: Potchefstroom site studied by Baier (1966).

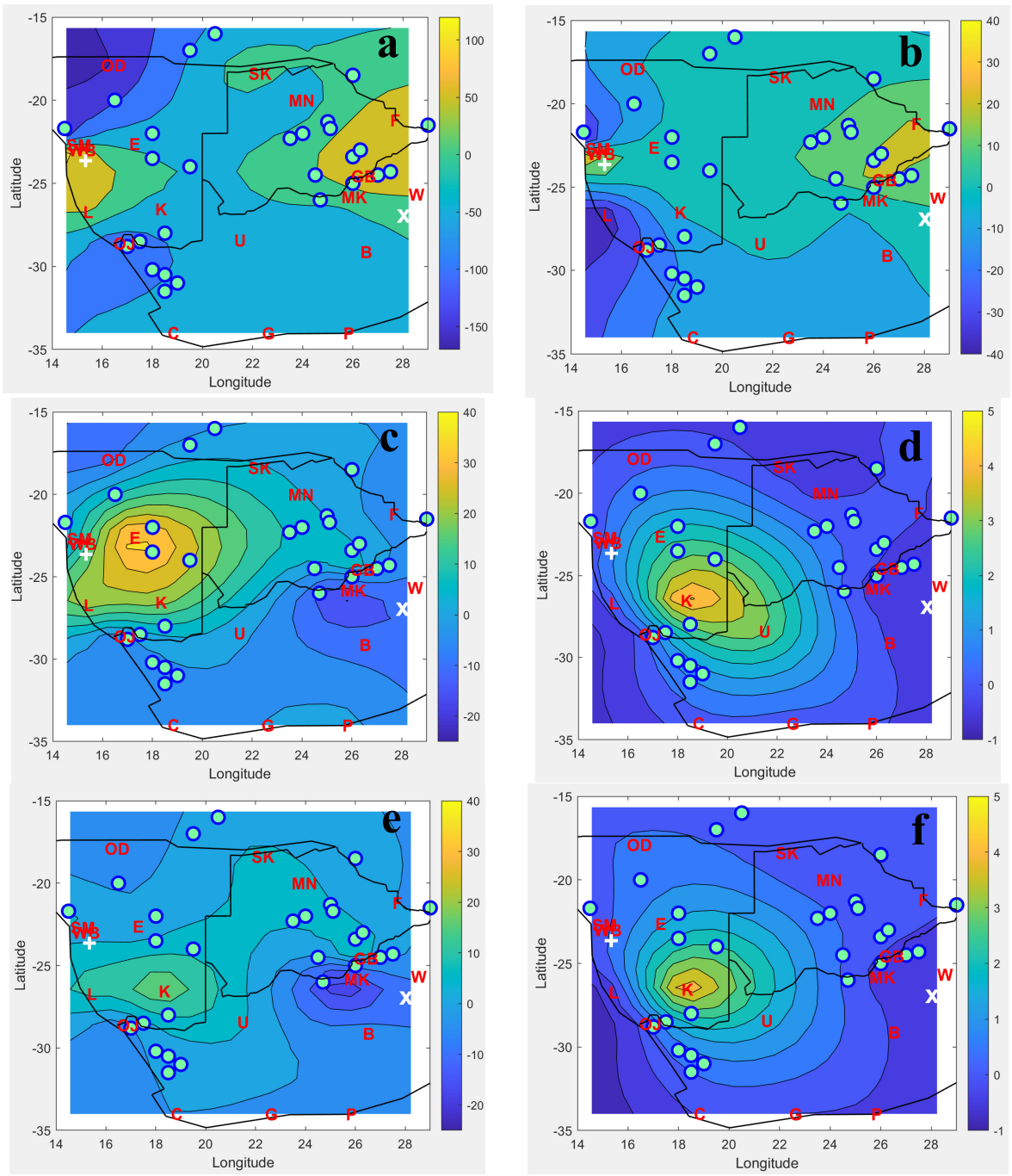

Fig. 12. Difference between 2020 and 2011 of the maximum time θ_M (left column, day) and mean time θ_0 (right column, day). (a), (b): Rain; (c), (d): Dew; (e), (f): Rain+dew. Red letters: Measurement sites (see Table 1); circles: biocrust sites from Chen et al. (2020); right cross: Gobabeb site studied by Henschel et al. (2007) and Soderberg (2010); inclined cross: Potchefstroom site studied by Baier (1966).

The evolution of the mean and maximum time period between 2001 and 2020 (Fig. SM2) show that mean and maximum time periods evolve about the same way. The times keep nearly constant over the whole period for dew, noting some decrease after 2010. Dew frequency is well correlated with the dew yield amplitude, which remains constant or weakly increases in the same period (Fig. SM1 in Supplementary Materials). In contrast, for rain, while the times keep constant between 2001 and 2010, the times increase after 2010. This evolution corresponds well with the decrease of rain amplitude (Fig. SM1).

The maps of evolution for the period 2011–2020 concerning the differences in rain, dew and rain + dew times are reported in Fig. 12. The evolution of mean and maximum times are qualitatively similar to the evolution of the rain and dew amplitudes (Figs. 3 and 5). The inverse evolution of rain + dew times rather follows the dew evolution, as expected from the fact noted above that the dew events mostly determine the behavior of the dew + rain times.

4 DISCUSSION AND RELATION WITH BIOCRUST

4.1 Dew height dependence

Biocrust forms at the ground level while the calculation of Section 2.1 deals with a 30° tilted condenser at 1 m off the ground. Dew condensation can vary for three reasons. (i) RH can be height dependent. This is the case if wind speed is near

zero and soil is wet, for instance after a rain event. (ii) Air flow depends on height, and then, the heat and mass exchange with the surrounding air. The variation of air flow velocity is known to follow a log dependence above a roughness length z_c (see Section 2.3) where air flow velocity is zero. In addition to the forced air flow induced by wind, there exists a natural convection induced by the substrate temperature colder than ambient air, with typical velocity 0.6 m s^{-1} (Beysens et al., 2005; Clus et al., 2009). The log dependence of the windspeed and the presence of natural convection make the heat exchange coefficient and then the mass diffusion coefficient, which determines the condensation yield, depend weakly of windspeed for values below ~ 1 m s^{-1} (measured at the standard height of 10 m). It results a weak dependence of condensation with height for such windspeeds, making the calculation of Section 2.1 valid at the ground level.

For larger windspeeds, the heat exchange coefficients will be larger, decreasing the dew yield. The latter will be then larger at the ground level and the calculation of Section 2.1 will be a conservative value.

4.2 Comparison with direct dew yield measurements

The calculated dew yields can be compared with previous works available in the literature. Baier (1966) reported dew and rainfall measurements from a weather station set at Potchefstroom (inclined cross in Fig. 2), located in the vast interior plateau of South Africa (26°44' S, 27°05' E, 1352 m asl), about 160 km from the Wonderboom site. During the period 1957–1958, the annual percentage of dew days was 45.7% (Wonderboom: 65.5%) with a mean annual dew amount of 12.6 mm (Wonderboom: 19.9 mm). The values in Wonderboom are slightly larger, but the measurement time was earlier and we will see in the next Section that the general tendency is a positive dew yield evolution.

Dew collection were also carried out in 2006 by Henschel et al. (2007) at Gobabeb (Namib Desert, 23°33.704 S, 15°02.466 E, right cross in Fig. 2) in Namibia's Central Namib Desert, situated about 84 km from Walvis Bay and 110 km from Shakopmund. The site elevation is 406 m. Only a few data were collected on a specially-designed 1 m^2 passive dew collector. In July 2006, 3.3 mm of dew water was collected (12 dew days), 1.2 mm in August (10 dew days), and 1.5 mm in September (10 dew days). Meteo data at Walvis Bay and Shakopmund are, however, available only between 2010 and 2020. In these cities, the calculated annual mean in July, August and September are nearly the same: 2.6 mm (July), 2.2 mm (August) and 2.2 mm (September) (N = 0), 1.2 mm, 1.8 mm and 1.7 mm (N = 1) and 0.7 mm, 0.9 mm and 0.9 mm (N = 3). Although not determined at the same dates, these values compare relatively well with the above measured values of 3.3 mm (July), 1.2 (August) and 1.5 mm (September).

Between July 2008 and June 2009, Soderberg (2010) measured a greater amount of dew at Gobabeb, with 143 yearly dew events. The corresponding volume was 12.3 mm, which compares relatively well with the Walvis Bay and Shakopmund data for the same year: 21 mm (N = 0), 15.8 mm (N = 1), 7 mm (N = 3).

4.3 Variation in rain precipitation

As mentioned in Section 3.3, we observed a decrease of precipitation from west to east. All sites present a negative variation in rain precipitation during 2001 to 2020. In particular, the decrease in precipitation is quite noticeable from 2010. In Namibia Lu et al. (2016) also observed a tendency to a diminution of rainfall precipitations. On the Ghaap plateau in west center of South Africa, oscillations of rain precipitations have been already noted by Tfwala et al. (2018) by analyzing interannual rainfall variability on the Ghaap plateau. The cycles last about 18–22 years in Postmarburg and between 12 and 16 years in Douglas. Another analysis of rainfall in South Africa by Zvarevashe at al. (2018) also concluded to quasi-decadal oscillations. The question whether the decrease we observed since 2010 is related to these oscillations or to the global climate change remains thus open.

4.4 Water availability and biocrust distribution

As outlined in the Introduction, the amount of rain and dew are considered as the main factors which influence the growth of biocrust (see e.g. Kidron and Kronenfeld, 2020; Li et al., 2021a, b; Ouyang et al.; 2017; Pan et al., 2010; Zhuang and Zhao, 2017). However, the frequency of rain events (longest period of drought) is the main factor according to Büdel et al. (2009). Although there are no studies concerning the effect of frequency of dew events, one can reasonably assume that this parameter also matters.

Frequency of events and their amplitude are strongly correlated (see Section 3.5), the regions of large dew or rain amplitudes corresponding to the regions of small dew or rain time periods. Both criteria (amplitude, frequency) should thus correspond in the studied regions to the same characteristics favoring biocrust growth.

The evolution between 2001 and 2020 is seen to exhibit two regimes, one from 2001 to 2010, where all parameters (dew and rain amplitude, dew and rain frequency) keep nearly constant. The second regime, from 2010 to 2020, corresponds to a neat decrease of rain amplitude and frequency of events, while dew amplitude and frequency either keeps constant or slightly increase. As far as rain is concerned, it should result in a decrease of biocrust growth. However, dew yield is nearly constant or increases after 2010. We are not aware of drastic changes in the distribution of biomass of biocrusts during the 2001–2020 period. This may be attributed to the increase of dew amplitude and frequency, which should act to compensate for the decrease in rain precipitation.

5 CONCLUSION AND TRENDS FOR THE FUTURE

The determination of dew yield using a physical model and rainfall data from 18 meteorological stations in Namibia, Botswana and South Africa in the period 2001–2020 allow clear tendencies to be evaluated. Dew decreases from the East, South, West coasts following the decrease in RH decrease, and rainfalls diminish toward the West and North. A noticeable decrease in rain precipitations after 2010 and a corresponding rise in dew yield are noted. It results in a steady increase of dew contribution with respect to rain after 2010. In addition, a clear increase in dew for three days in average after rainfall is observed in the arid regions where the humidity is low. These results are corroborated with the frequency of dew and rain events, which are closely correlated with dew and rain yields.

The effect on biocrust is to show zones with less rain but with increasing dew water. As far as rain is concerned, one therefore should expect a decrease of biocrust growth. However, dew yield is nearly constant or even increases after 2010, which could possibly compensate the rain decrease as we are not aware of drastic changes in the distribution of biomass of biocrusts during the 2001–2020 period.

The observed evolution, studied from 2001, exhibits a change after 2010. The question whether this decrease is related to oscillations or to a general tendency due to the global climate change remains open. A more precise scenario will need the use of climate change models as was done by Tomaszkiewicz et al. (2016). We plan such a study in a near future.

Acknowledgements. We gratefully G. Kidron for his valuable remarks and G.A. Faggianelli for his work in data extraction from the Weather Undergound database.

REFERENCES

Aguirre-Gutiérrez, C.A., Holwerda, F., Goldsmithc, G.R., Delgado, J., Yepez, E., Carbajal, N., Escoto-Rodríguez, M., Arredondo, J.T., 2019. The importance of dew in the water balance of a continental semiarid grassland. J. Arid Environ., 168, 26–35.

Amani, A., Lebel, T., 1997. Lagrangian Kriging for the estimation of Sahelian rainfall at small time steps. J. Hydrol., 192, 125–157.

Baier, W., 1966. Studies on dew formation under semi-arid conditions. Agric. Meteorol., 3, 103–112.

Bargaoui, Z., Chebbi, A., 2009. Comparison of two Kriging interpolation methods applied to spatiotemporal rainfall. J. Hydrol., 365, 56–73.

Belkiri, L., Tiri, A., Mouni, L., 2020. Spatial distribution of the groundwater quality using Kriging and Co-Kriging interpolations. Groundw. Sustainable Dev., 11, 100473.

Beysens, D., 2016. Estimating dew yield worldwide from a few meteo data. Atmos. Res., 167, 146–155.

Beysens, D., Muselli, M., Nikolayev, V., Narhe, R., Milimouk, I., 2005. Measurement and modelling of dew in island, coastal and alpine areas. Atmos. Res., 73, 1–22.

Büdel, B., Darienko, T., Deutschewitz, K., Dojani, S., Friedl, S., Mohr, K.I., Salisch, M., Reisser, W., Weber, B., 2009. Southern African biological soil crusts are ubiquitous and highly diverse in drylands, being restricted by rainfall frequency. Microb. Ecol., 57, 229–247.

Cano-Díaz, C., Mateoa, P., Muñoz-Martína, M.A., Maestre, F.T., 2018. Diversity of biocrust-forming cyanobacteria in a semiarid gypsiferous site from Central Spain. J. Arid Environ., 151, 83–89.

Chen, N., Yu, K., Jia, R., Teng, J., Zhao, C., 2020. Biocrust as one of multiple stable states in global drylands. Sci. Adv., 6, eaay3763.

Clus, O., Ouazzani, J., Muselli, M., Nikolayev, V.S., Sharan, G. Beysens, D., 2009. Comparison of various radiation-cooled dew condensers using computational fluid dynamics. Desalination, 249, 707–712.

Goovaerts, P., 1997. Geostatistics for Natural Resources Evaluation. Oxford University Press, New York, 500 p.

Henschel, J., Siteketa, V., Berkowicz, S.M., Beysens, D., Milimouk-Melnytchouk, I., Muselli, M., Heusinkveld, B.G., Jacobs, A.F.G., 2007. Dew occurrence and collection in Gobabeb, Central Namib Desert. In: Proc. 4th Conf. on Fog, Fog Collect. and Dew (La Serena, Chile, 23-27 July 2007), p. 251.

Infoclimat database, 2021. https://www.infoclimat.fr

Jacobs, A.F.G., Heusinkveld, B.G., Berkowicz, S.M., 2002. A simple model for potential dewfall in an arid region. Atmos. Res., 64, 285–295.

Jones, A., Breuning-Madsen, H., Brossard, M., Dampha, A., Deckers, J., Dewitte, O., Gallali, T., Hallett, S., Jones, R., Kilasara, M., Le Roux, P., Micheli, E., Montanarella, L., Spaargaren, O., Thiombiano, L., Van Ranst, E., Yemefack, M., Zougmoré R., (eds.), 2013. Soil Atlas of Africa. European Commission, Publications Office of the European Union, Luxembourg, 176 p.

Kidron, G.J., 2019. The enigmatic absence of cyanobacterial biocrust from the Namib fog belt: Do dew and fog hold the key? Flora, 257, 151416.

Kidron, G.J., Tal, S.Y., 2012. The effect of biocrust on evaporation from sand dunes in the Negev Desert. Geoderma, 179–180, 104–112.

Kidron, G.J., Kronenfeld, R., 2020. Assessing the likelihood of the soil surface to condense vapour: The Negev experience. Ecohydrol., 13, e2200.

Lepioufle, J.M., Leblois, E., Creutin, J.D., 2012. Variography of rainfall accumulation in presence of advection. J. Hydrol., 464–465, 494–504.

Li, S., Bowker, M.A., Xiao, B., 2021a. Biocrust enhance non-rainfall water deposition and alter its distribution in dryland soils. J. Hydrol., 595, 126050.

Li, S., Xiao, B., Kidron, G.J., 2021b. Moss-dominated biocrust enhance water vapor sorption capacity of surface soil and increase non-rainfall water deposition in drylands. Geoderma 388, 114930.

Lima, C.H.R., Kwon, H.H., Kim, Y.T., 2021. A Bayesian Kriging model applied for spatial downscaling of daily rainfall from GCMs. J. Hydrol., 597, 126095.

Lu, X., Wang, L., Pan, M., Kaseke, K.F., Li, B., 2016. A multiscale analysis of Namibian rainfall over the recent decade – comparing TMPA satellite estimates and ground observations. J. Hydrol. Reg. Stud., 8, 59–68.

Martinez, W.A., Melo, C.E., Melo, O.O., 2017. Median Polish Kriging for space–time analysis of precipitation. Spat. Stat., 19, 1–20.

Muselli, M., Clus, O., Ortega, P., Milimouk, I., Beysens, D., 2020. Physical, chemical and biological characteristics of dew and rain water during the dry oceans on of tropical islands. Atmos., 12, 69.

New, M., Hulme, M., Jones, P., 2000. Representing twentieth-century space–time climate variability. Part II: Development of 1901–96 monthly grids of terrestrial surface climate. J. Climatol., 12, 829–856.

NOAA's national weather service glossary, 2021. Available online: https://www.forecast.weather.gov (accessed on 13 February 2021).

Ouyang, H., Lan, S., Yang, H., Hu, C., 2017. Mechanism of biocrust boosting and utilizing non-rainfall water in Hobq Desert of China. Appl. Soil Ecol., 120, 70–80.

Pal Arya, S., 1988. Introduction to Micrometeorology. Acad. Press, San Diego, 307 p.

Pan, Y., Wan, X., Zhang, Y., 2010. Dew formation characteristics in a revegetation-stabilized desert ecosystem in Shapotou area, northern China. J. Hydrol., 387, 265–272.

Pue, J.D., Botula, Y.D., Nguyen, P.M., Meirvenne, M.V., Cornelis, W.M., 2021. Introducing a Kriging-based Gaussian Process approach in pedotransfer functions: Evaluation for the prediction of soil water retention with temperate and tropical datasets. J. Hydrol., 597, 125770.

Raggio, J., Green, A., Pintado, A., Sancho, L.G., Büdel, B., 2021. Functional performance of biocrust across Europe and its implications for drylands. J. Arid Environ., 186, 104402.

Rahmawati, N., 2020. Space-time variogram for daily rainfall estimates using rain gauges and satellite data in mountainous tropical Island of Bali, Indonesia (Preliminary Study). J. Hydrol., 590, 125177.

Railsback, L.B., Kraft, S., Liang, F., Brook, G.A., Marais, E., Cheng, H., Edwards, R.L., 2019. Control of insolation on

stalagmite growth, rainfall, and migration of the tropical rain belt in northern Namibia over the last 100 kyr, as suggested by a rare MIS 5b-5c stalagmite from Dante Cave. Palaeogeogr., Palaeoclimatol., Palaeoecol., 535, 109348.

Soderberg, K.S., 2010. The role of fog in the ecohydrology and biogeochemistry of the Namib Desert. MSc. Thesis, University of Cape Town, Department of Environmental Sciences, University of Virginia.

Tomaszkiewicz, M., Najm, A., Beysens, D., Alameddine, I., Zeid, E.B., El-Fadel, M., 2016. Projected climate change impacts upon dew yield in the Mediterranean basin. Sci. Total. Environ., 566–567, 1339–1348.

Trosseille, J., Mongruel, A., Royon, L., Beysens, D., 2022. Effective surface emissivity during dew water condensation. International Journal of Heat and Mass Transfer, 183, 122078.

Tfwala, C.M., Van Rensburga, L.D., Schallb, R., Dlamini, P., 2018. Drought dynamics and interannual rainfall variability on the Ghaap plateau, South Africa, 1918–2014. Phys. Chem. Earth, 107, 1–7.

Van de Beek, C.Z., Leijnse, H., Torfs, P.J.J.F., Uijlenhoet, R., 2012. Seasonal semi-variance of Dutch rainfall at hourly to daily scales. Adv. Water Resour., 45, 76–85.

Weather Underground database, 2021. https://www.wunderground.com

Yao, X., Xia, B., Kidron, G.J., Hu, K., 2019. Respiration rate of moss-dominated biocrust and their relationships with temperature and moisture in a semiarid ecosystem. Catena, 183, 104195.

Zhuang, Y., Zhao, W., 2017. Dew formation and its variation in Haloxylon ammodendron plantations at the edge of a desert oasis, northwestern China. Agric. For. Meteorol., 247, 541–550.

Zvarevashe, W., Krishnannair, S., Sivakumar, V., 2018. Analysis of Austral Summer and Winter Rainfall Variability in South Africa Using Ensemble Empirical Mode Decomposition. IFAC paperOnline, 51–5, 132–137.

Received 20 June 2021
Accepted 1 October 2021

Appendix 1 – Dew yield calculation

We give below in Table SM1 an example of determination of dew yield from Section 2.1. The model (Eq. 2) is applied to one night (March 21–22, 2010) in Cape Town (South Africa). Considering the sky cloud cover (N, oktas), the air (T_a, °C) and dew (T_d, °C) temperatures, the relative humidity (RH, %) and the wind-speed (V, m s^{-1}) at 10 meters of the ground, recorded every Δt = 1h., we compute an hourly yield h_i (mm) corresponding to evaporation ($h_i < 0$) or condensation ($h_i > 0$) events. By discarding evaporation ($h_i < 0$) and rain events, the cumulative dew yield h for each night is computed. For the studied night, h = 0.185 mm.

Table SM1. Exemple of calculation of dew yields from meteorological data.

Date (dd/mm/aaaa)	Hour (hh:mm)	N (oktas)	V (m/s)	T_a (°C)	RH (%)	T_d (°C)	T_d–T_a (°C)	h_i (mm)	$h_i > 0$ (mm)	sum(h_i) (mm)
21/03/2010	12:00	5	6.1	22	69	16	–6	–0.030	0.000	**0.000**
21/03/2010	13:00	5	7.2	23	65	16	–7	–0.035	0.000	**0.000**
21/03/2010	14:00	3	7.8	22	69	16	–6	–0.030	0.000	**0.000**
21/03/2010	15:00	1	7.8	22	69	16	–6	–0.030	0.000	**0.000**
21/03/2010	16:00	1	6.1	22	69	16	–6	–0.030	0.000	**0.000**
21/03/2010	17:00	1	5.6	21	68	15	–6	–0.030	0.000	**0.000**
21/03/2010	18:00	1	4.7	19	83	16	–3	–0.015	0.000	**0.000**
21/03/2010	19:00	0	3.1	18	88	16	–2	0.014	0.014	**0.014**
21/03/2010	20:00	0	0.6	18	88	16	–2	0.014	0.014	**0.027**
21/03/2010	21:00	0	1.9	15	94	14	–1	0.019	0.019	**0.046**
21/03/2010	22:00	0	3.1	14	100	14	0	0.024	0.024	**0.070**
21/03/2010	23:00	0	3.1	17	88	15	–2	0.014	0.014	**0.084**
22/03/2010	00:00	0	3.1	17	88	15	–2	0.014	0.014	**0.098**
22/03/2010	01:00	0	3.1	17	94	16	–1	0.019	0.019	**0.117**
22/03/2010	02:00	0	4.2	17	94	16	–1	0.012	0.012	**0.128**
22/03/2010	03:00	0	5.3	17	100	17	0	0.000	0.000	**0.128**
22/03/2010	04:00	0	3.6	18	94	17	–1	0.018	0.018	**0.146**
22/03/2010	05:00	0	3.1	17	100	17	0	0.023	0.023	**0.170**
22/03/2010	06:00	1	3.6	17	94	16	–1	0.015	0.015	**0.185**
22/03/2010	07:00	1	4.7	18	88	16	–2	–0.010	0.000	**0.185**
22/03/2010	08:00	1	6.7	21	83	18	–3	–0.015	0.000	**0.185**
22/03/2010	09:00	1	7.8	24	69	18	–6	–0.030	0.000	**0.185**
22/03/2010	10:00	1	9.2	25	61	17	–8	–0.040	0.000	**0.185**
22/03/2010	11:00	1	9.2	26	57	17	–9	–0.045	0.000	**0.185**
22/03/2010	12:00	1	10.8	25	65	18	–7	–0.035	0.000	**0.185**

Appendix 2 – Kriging method

Kriging is a stochastic spatial interpolation method that predicts the value of a natural phenomenon at non-sampled sites by an unbiased, minimal variance linear combination of observations of the phenomenon at nearby sites. The Kriging tool assumes that the distance or direction between the sample points reflects a spatial correlation that can explain the surface variations. The Kriging tool applies a mathematical function to all points, or certain determined points, located within a specific radius. It determines the output value of each location.

The Kriging tool is particularly suitable for cases where it is known that there is a spatial correlation of distance or a directional deviation in the data. Kriging deduces, by weighting existing readings, the probable values of unmeasured locations. To calculate the interpolated data $\hat{Z}(s_0)$ at a specific location s_0, the general formula of ordinary Kriging (OK) method consists of a weighted sum of the data (Goovaerts, 1997):

$$\hat{Z}(s_0) = \sum_{i=1}^{P} \lambda_i Z(s_i)$$

Here $Z(s_i)$ corresponds to the measured value at the i^{th} location, λ_i the ponderation coefficient to determine and relate to the i^{th} location, s_0 the predicted location and p the number of measured data.

With the Kriging method, the λ_i weighted coefficients are not only based on the distance between the surveyed points and the forecast location, but also on the general spatial organization of the surveyed points. To use the spatial arrangement in the weighing, the spatial autocorrelation is quantified. Thus, in ordinary Kriging, the weighting λ_i depends on the distance from the forecast location and the spatial relationships between the values recorded around it.

The experimental semi-variogram can be estimated from point pairs:

$$\hat{\gamma}(h) = \frac{1}{2n(h)} \sum_{i=1}^{n(h)} \left[Z(s_i) - Z(s_i + h) \right]^2$$

where $n(h) = Card\left\{ (s_i, s_j) / |s_i - s_j| \approx h \right\}$

with "card" represents the number of elements for the given condition.

Classically, estimated semi-variogram are fitted by a spherical variogram model as proposed in previous studies on rainfall spatial estimation (Bargaoui and Chebbi, 2009; Lepioufle et al., 2012; Rahmawati, 2020; Van de Beek et al., 2012).

Supplementary Materials

We present below supplementary materials for additional calculated data.

Figure SM1 reports the evolution of the dew summed values sum(h_d) (dew, mm, full blue line) and the rain summed values sum(h_r) (rain, mm, interrupted red line) for the studied sites.

Figure SM2 is concerned with the evolution of the mean time θ_0 (day) and the maximum time θ_M (day) between (a) rain (orange line), dew (blue short interrupted line) and rain plus dew events (green long interrupted line).

Table SM2 gives the correlation between the sky conditions and the cloud cover in oktas according to NOAA.

Table SM3 reports the yearly (H_d) and monthly (h_d) mean, minimum and maximum dew yields calculated from meteorological data.

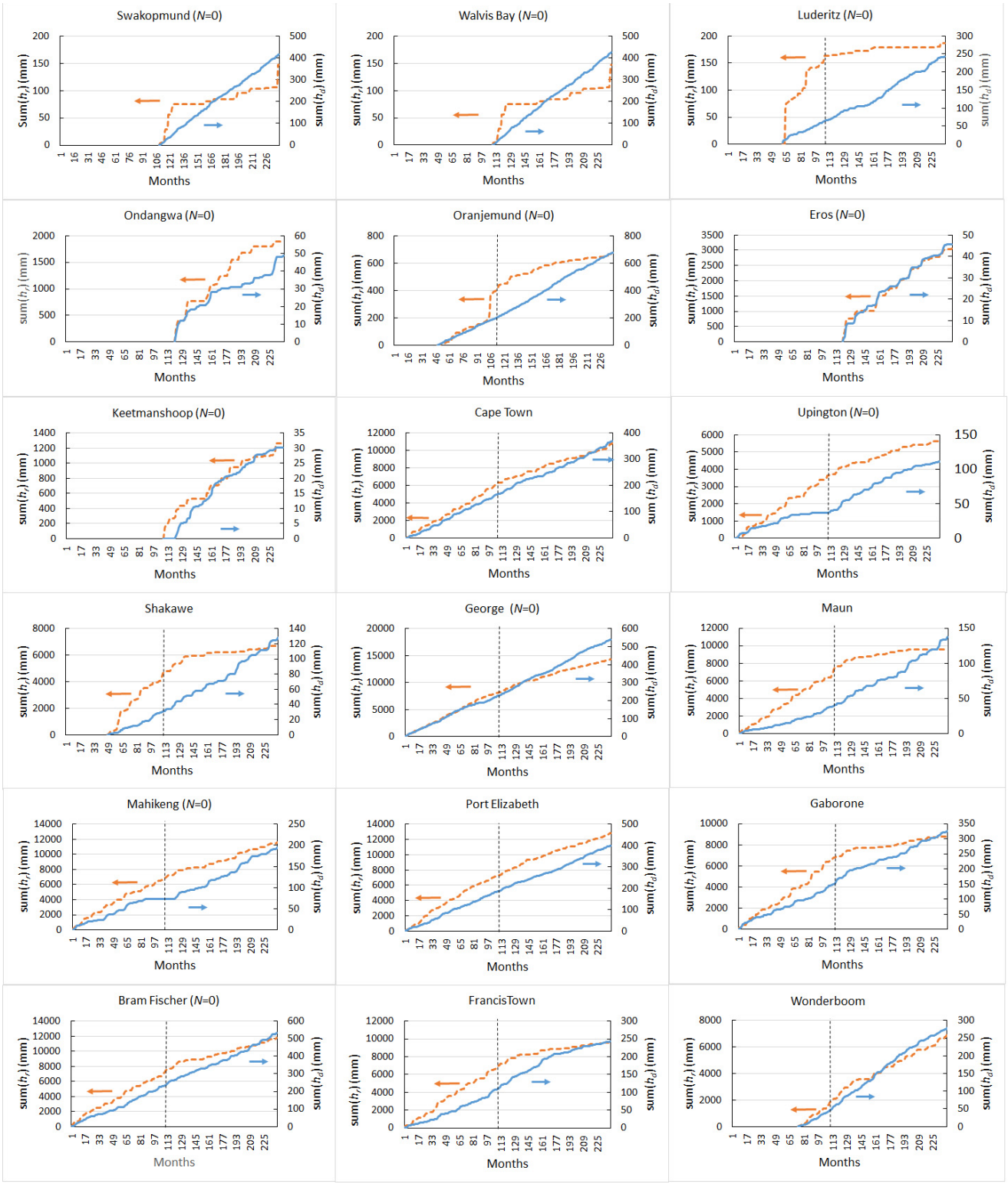

Fig. SM1. Evolution of the summed values sum(h_d) (dew, mm, full blue line) and sum(h_r) (rain, mm, interrupted red line) for the studied sites. The vertical interrupted line corresponds to a significant decrease of rainfall after 2010 with dew yield remaining constant or weakly increasing.

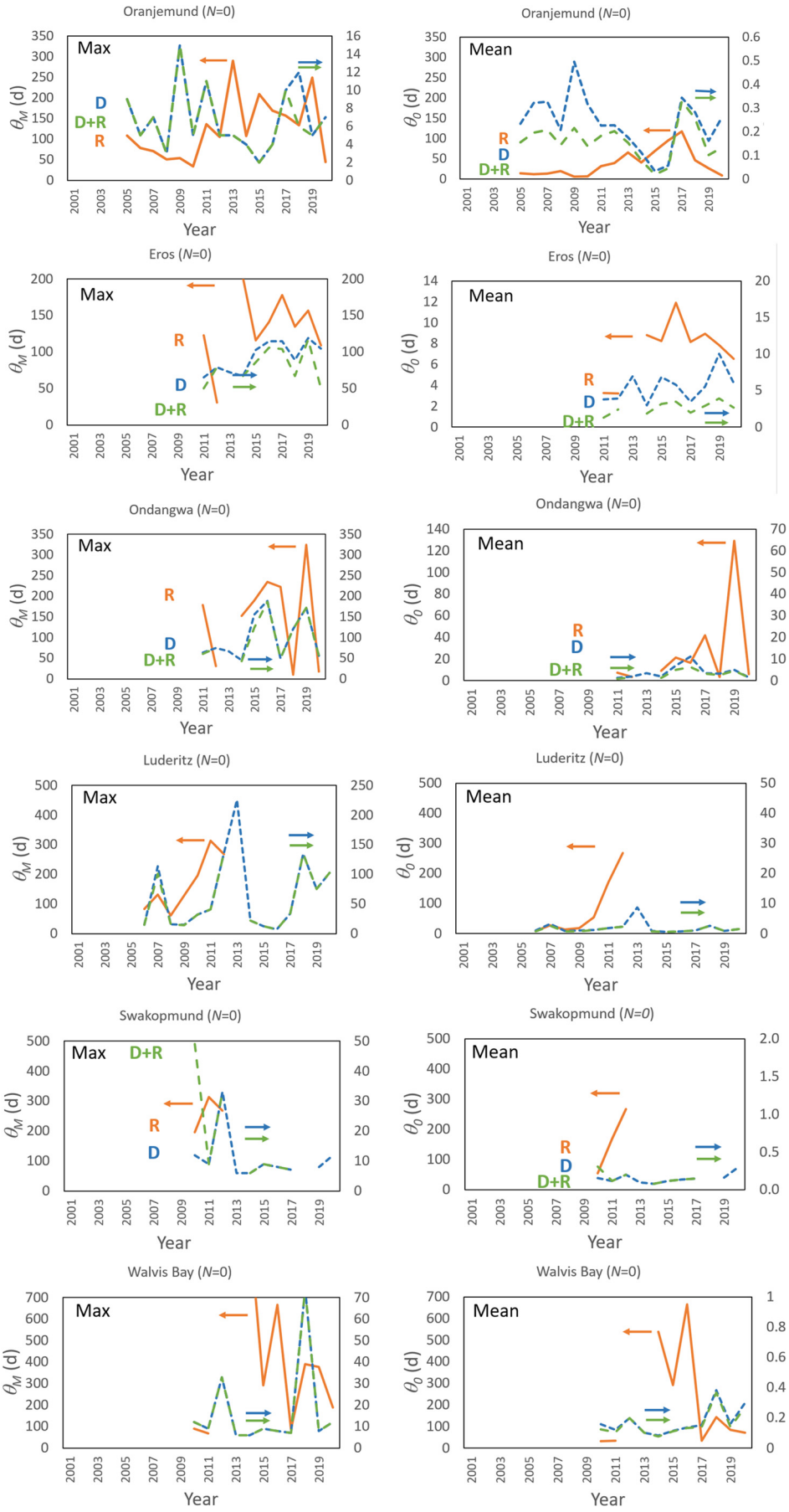
Oranjemund (N=0)
Max
D
D+R
R
θM (d)
Year
Oranjemund (N=0)
Mean
R
D
D+R
θ0 (d)
Year
Eros (N=0)
Max
R
D
D+R
θM (d)
Year
Eros (N=0)
Mean
R
D
D+R
θ0 (d)
Year
Ondangwa (N=0)
Max
R
D
D+R
θM (d)
Year
Ondangwa (N=0)
Mean
R
D
D+R
θ0 (d)
Year
Luderitz (N=0)
Max
θM (d)
Year
Luderitz (N=0)
Mean
θ0 (d)
Year
Swakopmund (N=0)
Max
D+R
R
D
θM (d)
Year
Swakopmund (N=0)
Mean
R
D
D+R
θ0 (d)
Year
Walvis Bay (N=0)
Max
θM (d)
Year
Walvis Bay (N=0)
Mean
θ0 (d)
Year

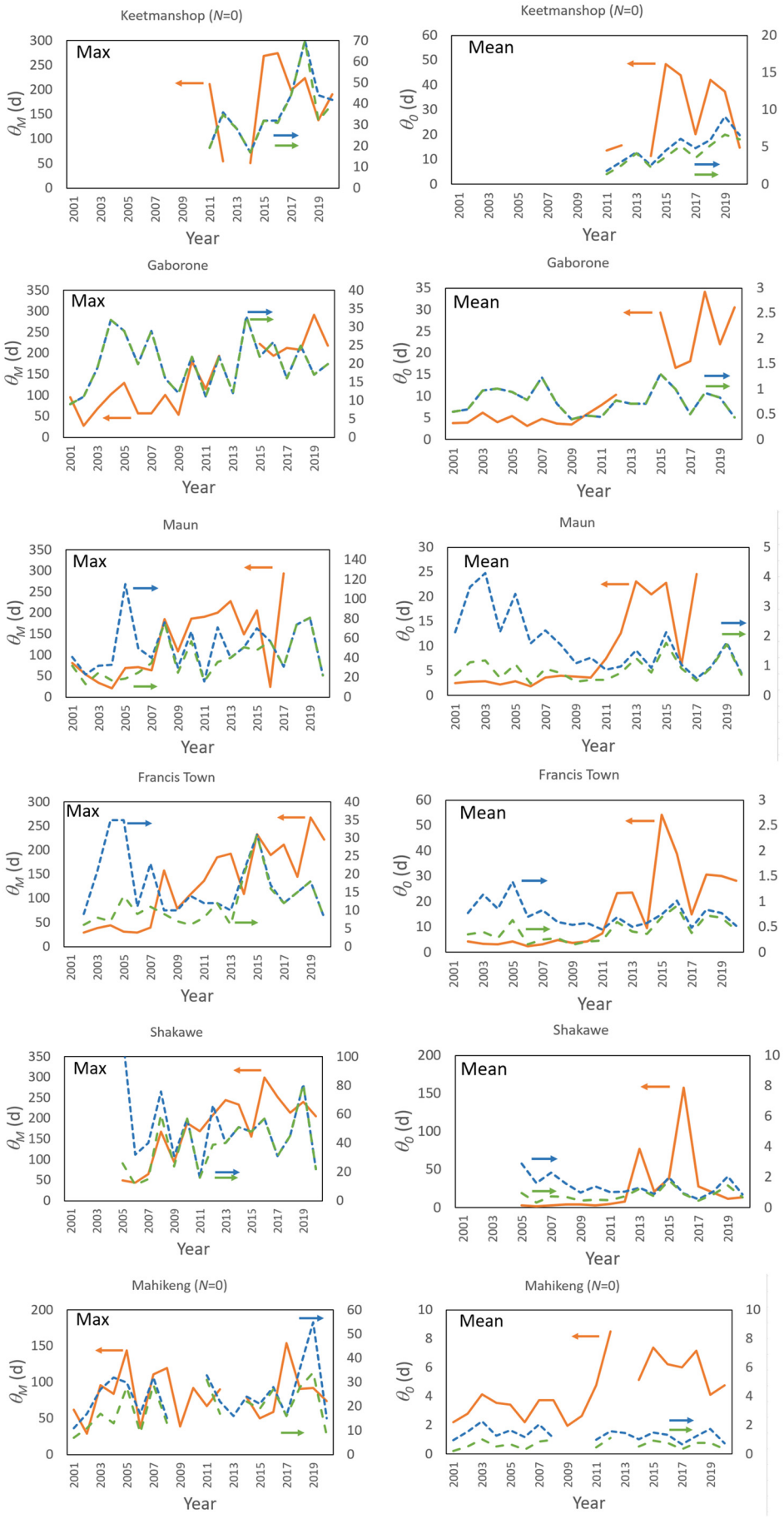
Keetmanshop (N=0)
Max
Mean
Gaborone
Maun
Francis Town
Shakawe
Mahikeng (N=0)
θM (d)
θ0 (d)
Year

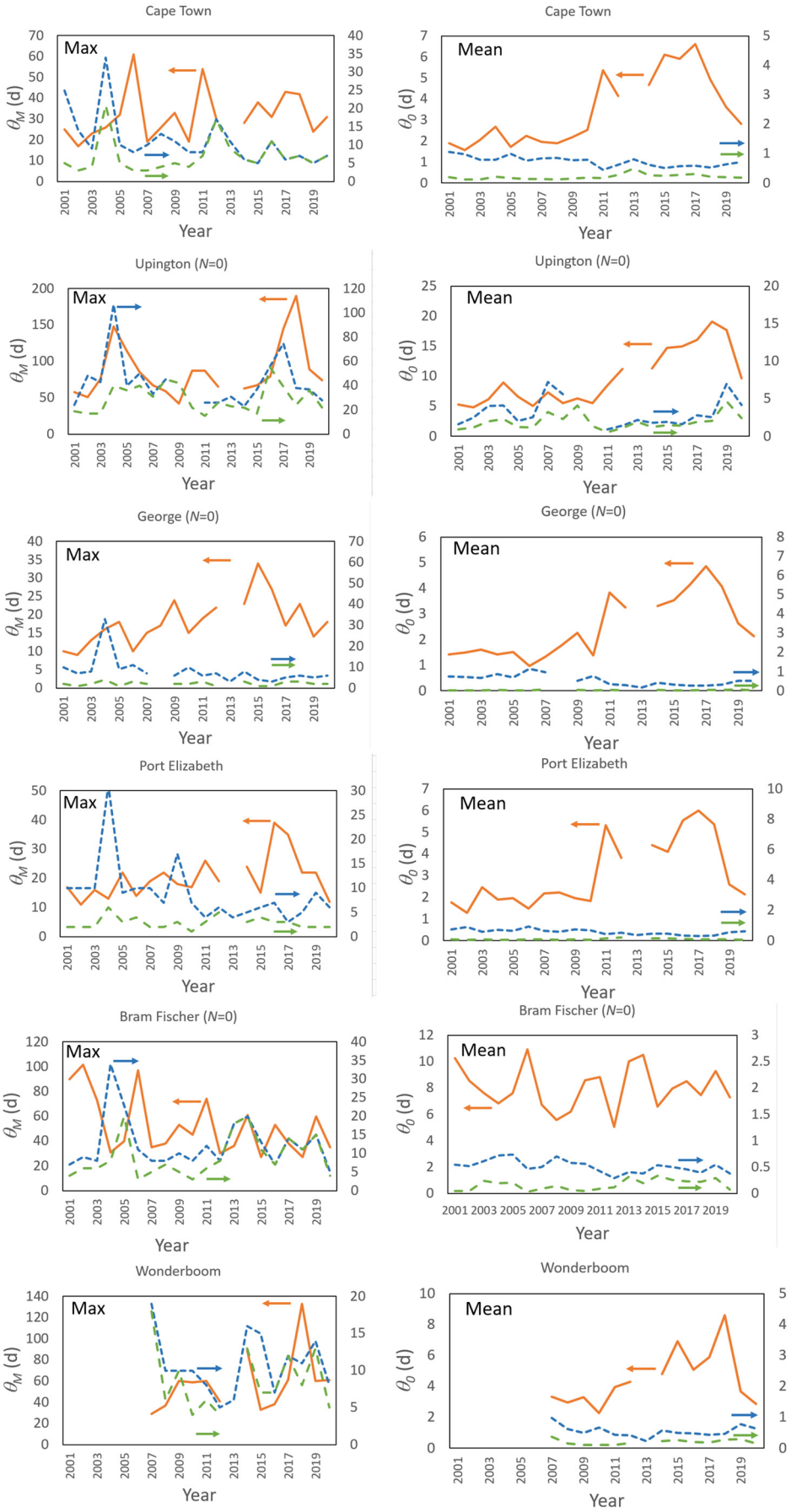

Fig. SM2. Evolution of mean time θ_0 (day) and maximum time θ_M (day) between (a) rain (orange line), dew (blue short interrupted line) and rain plus dew events (green long interrupted line). Some curves are interrupted because data are missing.

Table SM2. Correlation between sky conditions and cloud cover according to NOAA's national weather service glossary, 2021. The abbreviations for sky conditions are the following: CLR = Clear; FEW = few; SCT = Scattered; BKN = Broken; OVC = Overcast.

Observation	*N* (oktas)
CLR	0
FEW	1
SCT	3
BKN	5
OVC	8

Table SM3. Yearly (H_d) and monthly (h_d) mean, minimum and maximum dew yields calculated from meteorological data. The mean evolution data during from 2001 to 2020 are fitted to Eq. (5) with free parameters $\alpha_d = dh_d / dt$ and $h_{d,0}$. Red values correspond to a decrease of dew yield evolution, blue values to an increase. Cloud coverage *N* is assumed to be 0, 1 or 3 oktas when cloud cover data are missing (see text and Table 1).

Site	*N* (oktas)	H_d (mm)			h_d (mm)			α_d (mm month^{-1})	$h_{d,0}$ (mm)	year frequency (%)
		Mean	Min	Max	Mean	Min	Max			
Swakopmund	0	**37.7**	31.2	45.5	**3.1**	0.0	6.8	–0.002	3.2	85.6
	1	**28.4**	22.9	34.6	**2.4**	0.0	5.4	–0.001	2.4	84.9
	3	**12.6**	9.4	15.9	**1.0**	0.0	2.8	–0.001	1.1	79.1
Walvis Bay	0	**38.2**	31.7	46.1	**3.2**	0.0	6.9	–0.002	3.2	85.8
	1	**28.8**	23.3	35.1	**2.4**	0.0	5.4	–0.001	2.4	85.0
	3	**12.8**	9.6	16.1	**1.0**	0.0	2.9	–0.001	1.1	79.3
Luderitz	0	**16.2**	3.6	26.3	**1.3**	0.0	4.9	0.001	1.3	42.3
	1	**12.6**	2.8	21.4	**1.0**	0.0	4.3	0.001	0.1	40.3
	3	**6.6**	1.3	13.3	**0.6**	0.0	3.0	0.000	0.5	34.8
Ondangwa	0	**4.9**	0.4	13.5	**0.4**	0.0	3.7	–0.004	0.6	25.3
	1	**3.5**	0.3	9.8	**0.3**	0.0	2.8	–0.003	0.5	22.0
	3	**1.4**	0.1	3.8	**0.1**	0.0	1.2	–0.001	0.2	13.5
Oranjemund	0	**42.5**	32.4	56.8	**3.5**	0.9	8.2	0.003	3.2	81.5
	1	**32.8**	23.9	45.2	**2.7**	0.5	6.8	0.003	2.4	80.4
	3	**15.4**	9.6	24.3	**1.3**	0.2	4.1	0.003	1.0	70.6
Eros	0	**4.6**	1.4	8.9	**0.4**	0.0	2.6	–0.004	0.6	16.7
	1	**3.5**	0.9	7.0	**0.3**	0.0	2.1	–0.003	0.5	14.6
	3	**1.9**	0.3	3.8	**0.2**	0.0	1.1	–0.002	0.3	13.3
Keetmanshoop	0	**3.0**	0.8	5.7	**0.3**	0.0	1.8	–0.003	0.5	18.4
	1	**2.2**	0.5	4.2	**0.2**	0.0	1.4	–0.002	0.3	15.3
	3	**0.9**	0.2	2.0	**0.1**	0.0	0.8	–0.001	0.1	8.7
Cape Town	–	**18.3**	8.9	24.1	**1.5**	0.0	5.1	0.000	1.6	58.2
Upington	0	**5.5**	0.4	13.8	**0.5**	0.0	2.9	0.000	0.5	27.0
	1	**5.1**	0.4	13.2	**0.4**	0.0	2.8	0.000	0.4	26.6
	3	**4.5**	0.4	12.4	**0.4**	0.0	2.6	0.001	0.3	25.7
Shakawe	–	**8.0**	3.5	16.5	**0.7**	0.0	4.5	0.003	0.4	43.9
George	0	**27.0**	12.8	38.5	**2.2**	0.0	4.7	0.004	2.1	64.5
	1	**25.7**	12.8	37.4	**2.1**	0.0	4.7	0.003	1.9	64.3
	3	**23.3**	12.8	35.3	**1.9**	0.0	4.7	0.002	1.6	64.0
Maun	–	**6.9**	1.8	18.0	**0.6**	0.0	4.9	0.003	0.3	40.3
Mahikeng	0	**9.8**	0.1	21.7	**0.8**	0.0	4.7	0.003	0.6	37.6
	1	**8.1**	0.1	18.1	**0.7**	0.0	4.1	0.002	0.5	35.8
	3	**5.5**	0.1	12.2	**0.5**	0.0	2.9	0.001	0.3	33.2
Port Elizabeth	–	**20.0**	14.3	26.8	**1.7**	0.0	4.5	0.000	1.6	64.1
Gaborone	–	**16.2**	6.6	26.0	**1.4**	0.0	5.9	–0.001	1.4	57.8
Bram Fischer	0	**26.5**	14.4	38.8	**2.2**	0.0	7.7	0.001	2.2	66.4
	1	**24.0**	11.9	38.7	**2.0**	0.0	6.8	0.000	2.2	65.6
	3	**20.1**	8.7	38.4	**1.7**	0.0	5.6	0.000	2.2	64.8
Francistown	–	**12.1**	4.9	23.8	**1.0**	0.0	4.2	–0.004	1.4	58.3
Wonderboom	–	**19.9**	8.0	27.4	**1.7**	0.0	5.0	0.000	1.7	65.5

J. Hydrol. Hydromech., 69, 2021, 4, 357–359
DOI: 10.2478/johh-2021-0031
ISSN 1338-4333

sciendo Journal of Hydrology and Hydromechanics

Biological factors impacting hydrological processes: Pecularities of plants and biological soil crusts

Giora J. Kidron[1], Maik Veste[2], Ľubomír Lichner[3]

[1] Institute of Earth Sciences, The Hebrew University of Jerusalem, Givat Ram Campus, 91904 Jerusalem, Israel. E-mail: kidron@mail.huji.ac.il
[2] Institute of Environmental Sciences, Soil Protection and Recultivation, Brandenburg University of Technology Cottbus-Senftenberg, Konrad-Wachsmann-Allee 6, 03046 Cottbus, Germany. E-mail: maik.veste@b-tu.de
[3] Institute of Hydrology, Slovak Academy of Sciences, Dúbravská cesta 9, 84104 Bratislava, Slovakia. E-mail: lichner@uh.savba.sk

The effects of biological factors on the water cycle and subsequently on hydrological processes have wide and profound consequences on ecosystem structure, function and management. A profound understanding of their effects is of prime importance especially in light of climate change projection.

Whether regarding water infiltration or release (via evapotranspiration), the water cycle is central for the assessment of ecosystem services provided by soil (Vereecken et al., 2016). With soil being a home to about 25% of all living species on Earth (Turbé et al., 2010), the interrelationship soil-biota has large consequences, beyond the obvious effects on the hydrology, pedology or ecology. Geologists for instance believe that the biota is involved in the formation of 2/3 of about 4300 known minerals (Hazen et al., 2008). The biota, especially plants and microorganisms, plays a central role in geomorphological processes, a field currently termed biogeomorphology (Corenblit et al., 2011). Among the microorganisms and small organisms that may fundamentally affect the water dynamics are biological soil crusts, also known as biocrusts, which are composed of variable proportions of autotrophs (cyanobacteria, green algae, lichens, mosses, liverworts) accompanied by heterotrophs such as fungi, bacteria and archaea (Belnap and Lange, 2003).

As far as plants are concerned, water consumption facilitates photosynthesis and growth, as well as evapotranspiration, along with numerous biochemical reactions. Water provides the necessary turgor and facilitates the mechanism whereby leaf cooling takes place (Ehlers and Goss, 2003). Plants may have also indirect effects. Thus, by water (whether rain or dew and fog) interception (Miralles et al., 2010; Simonin et al., 2009), or their impact on infiltration, whether by increasing infiltration (Lange et al., 2009) or partially hindering it through water repellency (WR) (Doerr et al., 2000; Lichner et al., 2010). Plants may affect runoff, thus hindering runoff generation and flow (Cerdà, 1997). They may also affect the water cycle by impacting the microclimate (e.g. Gillner et al., 2015; Kidron, 2009).

As far as the microorganisms are concerned, they may increase surface temperatures (Harper and Marble, 1988), the water-holding capacity (Chenu, 1993), aggregation and subsequently infiltration (Or et al., 2007), but also hinder infiltration due to WR (Lichner et al., 2013) or pore clogging (Kidron et al., 1999). As for plants, while most processes are in consensus and the research nowadays mainly focuses on the study of species-specific process-dependent rates (Callaway, 1998; Klanderud, 2008), the possible effects of climate change (Root et al., 2003), and the development of models aiming to increase our understanding in future anticipation of the hydrological cycle following climate change (Vereecken et al., 2016), the effects of biocrusts on the hydrological processes are not in consensus, triggering ongoing discussions. The small-size organisms that constitute the crusts along with the close cell-soil association exert extra difficulties in clearly pinpointing at the exact hydrological mechanism. Not only that disagreement exists regarding some of the mechanisms, but even regarding the values involved, with reported differences of up to two orders of magnitude also from the very same research site, as is the case with dew.

Among the controversial issues are the use of dew as a possible water source for biocrusts and the effects of biocrusts on infiltration, runoff and evaporation. As far as dew is concerned, the reported values that presumably are available for biocrusts are of a wide range, even for the same research site, such as for the Hallamish dunefield in the Negev (Littmann and Veste, 2008). While one group of researchers reported daily values of up to 0.5 mm (Heusinkveld et al., 2006), another group reported maximum daily values of 0.1–0.3 mm (Veste et al., 2008), while a third group reported substantially lower values with an average value of only 0.034 mm (Kidron et al., 2002). As far as evaporation is concerned, while some researchers maintain that biocrusts impede evaporation, therefore playing a positive role upon plant growth (Eldridge et al., 2020), other maintain the opposite, i.e., an increase in evaporation and subsequently a decrease in soil moisture, resulting in a negative effect of biocrusts on the soil water regime and hence on plant growth and fecundity (Kidron, 2019).

While research on species-specific effects of biocrusts is still in its infancy, efforts are made to characterize the variable effects of the different crust types, mainly cyanobacterial, lichen- and moss-dominated crusts, which, may be considered as keystone groups for the biocrust microcosm. Similarly to the main species of vascular plants that disproportionally to their distribution primarily control the structure and function of the ecosystem, these keystone groups may largely determine numerous processes of the biocrust microcosm and among them hydrological processes.

During the current special issue, papers devoted to elucidate the impact of biological factors on the hydrological processes are presented. The papers include the effects of humans (1 paper), plants (3 papers) and biocrusts (6 papers). As for the effect of humans, Balashov et al. (2021) checked the possible effect of adding two types of biochars to soil on the soil moisture and N_2O emission of two soil types, reporting differences in accordance with the biochar type and quantity and in accordance with soil type.

As for the effect of plants, Zabret and Šraj (2021) and Jančo et al. (2021) examined the effect of trees on rainfall interception. Examining birch and pine trees in Slovenia, Jančo et al. (2021) found that rain duration and intensity largely control the interception, as well as the phenoseason, i.e., whether or not leaves are present on the tree canopy. Examining spruce trees in Slovakia, Jančo et al. (2021) measured the magnitude of the rain interception in relation to the crown architecture, i.e., the central crown zone near the stem, the crown periphery and the canopy gap. Leelamanie et al. (2021) examined the hydrophobic effect of three types of trees (Eucalyptus, Pine, Casuarina) planted in Sri Lanka. All granted high hydrophobicity to the soils, especially during the summer. All the above-mentioned papers have important consequences on infiltration and runoff.

Most of the special issue is devoted to research on biocrusts. While Muselli and Beysens (2021) focused on the occurrence of dew, all other five papers dealt with the effects of biocrusts on surface hydrology. Using meteorological parameters, Muselli and Beysens (2021) used an energy balance model developed by Beysens (2016) aiming to calculate dew yield. The authors used data gathered from 18 meteorological stations scattered throughout southern Africa to construct a map with dew distribution. By comparing the calculated dew data to rain precipitation, the authors proposed that dew yield may compensate for the decline in rain precipitation during the last decade (2010–2020), and may therefore explain the fact that no decrease in biocrust cover was reported following the decrease in rain precipitation.

Under greenhouse conditions, Thielen et al. (2021) investigated the effect of 5 species of mosses taken from forests of central Europe on the maximum water storage and evaporation. Moss structure was found to affect water storage and all mosses were found to retard evaporation. Factors that may affect infiltration and runoff were studied by Drahorad et al. (2021) and Guan and Liu (2021). Drahorad et al. (2021) investigated possible factors that may determine WR. The authors compared biocrusts from a temperate region in Slovakia and an arid region in the Negev. With mosses exhibiting higher WR than cyanobacterial crusts and the dunes in Slovakia exhibiting higher WR than that of the Negev, the authors conclude that WR is triggered by organic matter while diminishing by the higher amounts of calcium carbonate, dust, and subsequently higher pH of the Negev dunes. Moss-dominated biocrusts not only increase WR as found by these authors, but also increase water-holding capacity and subsequently decrease infiltration, as found by Guan and Liu (2021) in the Mu Us Desert in China. By using disc infiltrometer, Guan and Liu conducted infiltration experiments evaluating the various hydrological parameters which were found to be substantially affected by crust development.

The effect of different crust types on the flow length of runoff was studied by Lázaro et al. (2021) in the Tabernas Desert in Spain. Aiming to quantify the minimum runoff length (mRL), i.e., the effective contributing area in which runoff coefficient equals 1 of three crust types, cyanobacterial, early successional and late successional lichen crusts, the authors report on interesting results. Proposing that mRL may serve a proxy for RL, the authors found that while mRL was up to 3.3–4.0 m on a cyanobacterial biocrust, it was 2.2–7.5 m in the early successional lichen crust and only 1.0–1.5 m on late successional lichen crust, generally indicating a decrease in mRL with an increase in crust biomass.

Kidron (2021) presented a mini review that challenged some of the wide-spread views concerning the driving factors responsible for runoff generation over biocrusts in arid and semiarid regions. While WR was found to play an important role in temperate humid regions, the author claims that no conclusive data were yet reported on the involvement of WR in runoff in arid and semiarid regions. Other wide-spread views that explained runoff over biocrusts such as structure, texture, surface roughness are also challenged, claiming that they cannot explain runoff initiation which succeeds surface saturation, and is responsible in turn to infiltration-excess overland flow (also known as Hortonian overland flow, HOF). Extracellular polymeric substances (EPS) are suggested to play a major role in partial surface clogging and subsequently in runoff initiation - a prerequisite factor for HOF.

The combined efforts by ecologists and hydrologists, as manifested in this thematic issue, may help to increase our understanding regarding the interrelations between plants, biocrusts and hydrological processes. Obviously, as also manifested during this special volume, there are still issues in dispute and not in consensus. Bringing them to the forefront is a prerequisite step which may trigger additional research focusing on 'open' non-consensus issues, and may thus advance our understanding in ecosystem structure, function and management.

REFERENCES

Balashov, E., Buchkina, N.P., Šimanský, V., Horák, J., 2021. Effects of slow and fast pyrolysis biochar on N_2O emissions and water availability of two soils with high water-filled pore space. J. Hydrol. Hydromech., 69, 4, 467–474.

Belnap, J., Lange, O.L. (Eds.), 2003. Biological Soil Crusts: Structure, Function, and Management. Revised 2nd Printing. Springer Publisher, Berlin.

Beysens, D., 2016. Estimating dew yield worldwide from a few meteo data. Atmos. Res., 167, 146–155.

Callaway, R.M., 1998. Are positive interactions species-specific? Oikos, 82, 202–207.

Cerdà, A., 1997. The effect of patchy distribution of *Stipa tenacissima* L. on runoff and erosion. J. Arid Environ., 36, 37–51.

Chenu, C., 1993. Clay- or sand- polysaccharide associations as models for the interface between micro-organisms and soil: water related properties and microstructure. Geoderma, 56, 143–156.

Corenblit, D., Baas, A.C.W., Bornette, G., Darrozes, J., Delmotte, S., Francis, R.A., Gurnell, A.M., Julien, F., Naiman, R.J., Streiger, J., 2011. Feedbacks between geomorphology and biota controlling Earth surface processes and landforms: A review of foundation concepts and current understanding. Earth-Sci. Rev., 106, 307–331. https://doi.org/10.1016/j.earscirev.2011.03.002

Doerr, S.H., Shakesby, R.A., Walsh, R.P.D., 2000. Soil water repellency: its causes, characteristics and hydrogeomorphological significance. Earth-Sci. Rev., 51, 33–65. https://doi.org/10.1016/S0012-8252(00)00011-8

Drahorad, S.L., Felde, V.J.M.N.L., Ellerbrock, R.H., Henss, A., 2021. Water repellency decreases with increasing carbonate content and pH for different biocrust types on sand dunes. J. Hydrol. Hydromech., 69, 4, 369–377.

Ehlers, W., Goss, M.J., 2003. Water Dynamics in Plant Production. CABI Publishing. Wallingford, UK.

Eldridge, D.J., Reed, S., Travers, SK., Bowker, M.A., Maestre, F.T., Ding, J., Havrilla, C., Rodriguez-Caballero, E., Barger, N., Weber, B., Antoninka, A., Belnap, J., Chaudhary, B., Faist, A., Ferrenberg, S., Huber-Sannwald, E., Malam Issa, O., Zhao, Y., 2020. The pervasive and multifacetal influence

of biocrusts on water in the world's drylands. Glob. Change Biol., 26, 6003–6014. https://doi.org/10.1111/gcb.15232

Gillner, S., Vogt, J., Tharang, A., Dettmann, S., Roloff, A., 2015. Role of street trees in mitigating effects of heat and drought at highly sealed urban sites. Landscape Urban Plan., 143, 33–42. https://doi.org/10.1016/j.landurbplan.2015.06.005

Guan, H.J., Liu, X.Y., 2021. Biocrust effects on soil infiltrability in the Mu Us Desert: Soil hydraulic properties analysis and modeling. J. Hydrol. Hydromech., 69, 4, 378–386.

Harper, K.T., Marble, J.R., 1988. A role for nonvascular plants in management of arid and semiarid rangelands. In: Tuller, P.T. (Ed.): Applications of Plant Sciences to Rangeland Management and Inventory. Kluwer, Amsterdam, pp. 135–169.

Hazen, R.M., Papineau, D., Bleeker, W., Downs, R.T., Ferry, J.M., McCoy, T.J., Sverjensky, D.A., Yang, H., 2008. Mineral evolution. Am. Mineral., 93, 1693–1720.

Heusinkveld, B.G., Berkowicz, S.M., Jacobs, A.F.G., Holtslag, A.A.M., Hillen, W.C.A.M., 2006. An automated microlysimeter to study dew formation and evaporation in arid and semiarid regions. J. Hydrometeorol., 7, 825–832.

Jančo, M., Mezei, P., Kvas, A., Danko, M., Sleziak, P., Minďáš, J., Škvarenina, J., 2021. Effect of mature spruce forest on canopy interception in subalpine conditions during three growing seasons. J. Hydrol. Hydromech., 69, 4, 436–446.

Kidron, G.J., 2009. The Effect of shrub canopy upon surface temperatures and evaporation in the Negev Desert. Earth Surf. Process. Landf., 34, 123–132. https://doi.org/10.1002/esp.1706

Kidron, G.J., 2019. The dual effect of sand-covered biocrusts on annual plants: Increasing cover but reducing individual plant biomass and fecundity. Catena, 182, 104120. https://doi.org/10.1016/j.catena.2019.104120

Kidron, G.J., 2021. The role of biocrust-induced exopolymeric matrix in runoff generation in arid and semiarid zones – a mini review. J. Hydrol. Hydromech., 69, 4, 360–368.

Kidron, G.J., Yaalon, D.H., Vonshak, A., 1999. Two causes for runoff initiation on microbiotic crusts: hydrophobicity and pore clogging. Soil Sci., 164, 18–27.

Kidron, G.J., Herrnstadt, I., Barzilay, E., 2002. The role of dew as a moisture source for sand microbiotic crusts in the Negev Desert, Israel. J. Arid Environ., 52, 517–533. https://doi.org/10.1006/jare.2002.1014

Klanderud, K., 2008. Species-specific responses of an alpine plant community under simulated environmental change. J. Veg. Sci., 19, 363–372. https://doi.org/10.3170/2008-8-18376

Lange, B., Luescher, P., Germann, P.F., 2009. Significance of tree roots for preferential infiltration in stagnic soils. Hydrol. Earth Syst. Sci., 13, 1809–1821.

Lázaro, R., Calvo-Cases, A., Arnau-Rosalén, E., Rubio, C., Fuentes, D., López-Canfín, C., 2021. Defining minimum runoff length allows for discriminating biocrusts and rainfall events. J. Hydrol. Hydromech., 69, 4, 387–399.

Leelamanie, D.A.L., Piyaruwan, H.I.G.S., Jayasinghe, P.K.S.C., Senevirathne, P.A.N.R., 2021. Hydrophysical characteristics in water-repellent tropical Eucalyptus, Pine, and Casuarina plantation forest soils. J. Hydrol. Hydromech., 69, 4, 447–455.

Lichner, L., Hallett, P.D., Orfánus, T., Czachor, H., Rajkai, K., Šir, M., Tesař, M., 2010. Vegetation impact on the hydrology of an aeolian sandy soil in a continental climate. Ecohydrology, 3, 413–420. https://doi.org/10.1002/eco.153

Lichner, L., Hallett, P.D., Drongova, Z., Czachor, H., Kovacik, L., Mataix-Solera, J., Homolák, M., 2013. Algae influence the hydrophysical parameters of a sand soil. Catena, 108, 58–68. https://doi.org/10.1016/j.catena.2012.02.016

Littmann, T., Veste, M., 2008. Evapotranspiration, transpiration and dewfall. In: Breckle, S.-W, Yair, A.,Veste, M. (Eds.), Arid Dune Ecosystems: The Nizzana Sands in the Negev Desert, Ecological Studies 200, Springer, Berlin Heidelberg New York, pp. 183–200. https://doi.org/10.1007/978-3-540-75498-5_13

Miralles, D.G., Gash, J.H., Holmes, T.R.H., de Jeu, R.A.M., Dolman, A.J., 2010. Global canopy interception from satellite observations. J. Geophys. Res., 145, D16. https://doi.org/10.1029/2009JD013530

Muselli, M., Beysens, D. 2021. Mapping past, present and future dew and rain water resources for biocrust evolution in southern Africa. J. Hydrol. Hydromech., 69, 4, 400–420.

Or, D., Phutane, S., Dechesne, A., 2007. Extracellular polymeric substances affecting pore-scale hydrologic conditions for bacterial activity in unsaturated soils. Vadose Zone J., 6, 298–305. https://doi.org/10.2136/vzj2006.0080

Root, T.L., Price, J.T., Hall, K.R., Schneider, S.H., Rosenzweig, C., Pounds, J.A., 2003. Fingerprints of global warming on wild animals and plants. Nature, 421, 57–60.

Simonin, K.A., Santiago, L.S., Dawson, T.E., 2009. Fog interception by *Sequoia sempervirens* (D. Don) crowns decouples physiology from soil water deficit. Plant Cell Environ., 32, 882–892. https://doi.org/10.1111/j.1365-3040.2009.01967.x

Thielen, S.M., Gall, C., Ebner, M., Nebel, M., Scholten, T., Seitz, S., 2021. Water's path from moss to soil: A multi-methodological study on water absorption and evaporation of soil-moss combinations. J. Hydrol. Hydromech., 69, 4, 421–435.

Turbé, A., De Toni, A., Benito, P., Lavelle, P., Lavelle, P., Ruiz, N., van der Putten, W.H., Labouze, E., Mudgal, S., 2010. Soil biodiversity: Functions, threats and tools for policy makers. Technical Report 2010-049. European Communities. https://doi.org/10.2779/14571

Vereecken, H., Schnepf, A., Hopmans, J.W., Javaux, M., Or, D., Roose, T., Vanderborght, J., Young, M.H., Amelung, W., Aitkenhead, M., Allison, S.D., Assouline, S., Baveye, P., Berli, M., Brüggemann, N., Finke, P., Flury, M., Galser, T., Govers, G., Ghezzehei, T., Hallett, P., Hendricks Franssen, H.J., Heppell, J., Horn, R., Hulsman, J.A., Jacques, D., Jonard, F., Kollet, S., Lafolie, F., Lamorski, K., Leitner, D., McBratney, A., Minasny, B., Montzka, C., Nowak, W., Pachepsky, Y., Padarian, J., Romano, N., Roth, K., Rothfuss, Y., Rowe, E.C., Schwen, A., Šimůnek, J., Tiktak, A., Van Dam, J., van der Zee, S.E.A.T.M., Vogel, H.J., Vrugt, J.A., Wöhling, T., Young, I.M., 2016. Modeling soil processes: Review, key challenges, and new perspectives. Vadose Zone J., 15, 1–57. https://doi.org/10.2136/vzj2015.09.0131

Veste, M., Heusinkveld, B.G., Berkowicz, S.M., Breckle, S.-W., Littmann, T., Jacobs, A.F.G., 2008. Dew formation and activity of biological soil crusts. In: Breckle, S.-W., Yair, A., Veste, M. (Eds.). Arid Dune Ecosystems: The Nizzana Sands in The Negev Desert. Ecological Studies 200. Springer, Heidelberg, Germany, pp. 305–318. https://doi.org/10.1007/978-3-540-75498-5_21

Zabret, K., Šraj, M., 2021. Relation of influencing variables and weather conditions on the rainfall partitioning by birch and pine trees. J. Hydrol. Hydromech., 69, 4, 456–466.